Aus der Medizinischen Klinik III für Hämatologie, Onkologie und Palliativmedizin,
Universitätsmedizin Rostock

Direktor: Prof. Dr. med. Christian Junghanß

Etablierung & Charakterisierung individueller Modelle von Kopf-Hals-Tumoren für präklinische zielgerichtete Kombinationsstrategien

Inauguraldissertation
(Kumulative Promotionsschrift)
zur Erlangung des akademischen Grades:
Doktor der Medizinwissenschaften
Doctor rerum humanarum (Dr. rer. hum.)
der Universitätsmedizin Rostock

Vorgelegt von
Nina Schönwälder (geb. Irmscher) | geb. am 28.09.1995 in Bielefeld
aus Rostock

Rostock | 28.06.2022
https://doi.org/10.18453/rosdok_id00004309

Gutachter

Erstgutachter:	PD Dr. rer. nat. habil. Claudia Maletzki
Einrichtung:	Medizinischen Klinik III für Hämatologie, Onkologie und Palliativmedizin, Universitätsmedizin Rostock
Zweitgutachter:	PD Dr. med. habil. Annette Zimpfer
Einrichtung:	Institut für Pathologie, Universitätsmedizin Rostock
Drittgutachter:	Univ.-Prof. Dr. med. Chia-Jung Busch
Einrichtung:	Klinik und Poliklinik für Hals-, Nasen-, Ohrenkrankheiten, Kopf- und Halschirurgie, Universitätsmedizin Greifswald

Jahr der Einreichung: 2022
Jahr der Disputation: 2023

Inhaltsverzeichnis

Abbildungsverzeichnis

Abkürzungsverzeichnis

CalR	Calreticulin
CDK	Cyclin abhängigen Kinasen
CDKi	Cyclin abhängige Kinaseinhibitoren
ER	endoplasmatisches Retikulum
FDA	*US Food and Drug Administration*
HNSCC	Plattenepithelkarzinome des Kopf-Hals Bereiches (*head and neck squamous cell carcinoma*)
HPV	humanes Papillomavirus
IDO	Indoleamin 2,3-dioxygenase
KMO	Kynurenin-3-Monooxygenase
KYAT	Kynurenin-Aminotransferase
KYNU	Kynureninase
NGS	*Next Generation Sequencing*
NSG	NOD.Cg-Prkdc^{scid}Il2rg^{tm1Wjl}/SzJ
PBMC	mononukleäre Zellen des peripheren Blutes (*Peripheral Blood Mononuclear Cells,* PBMCs)
PDX	Patienten-abgeleitete Xenografts
Rb-Protein	Retinoblastom-Protein
TDO2	Tryptophan-2,3-Dioxygenase
5-FU	5-Fluoruracil

1. Einleitung

1.1 Plattenepithelkarzinome des Kopf-Hals Bereiches

Karzinome des Kopf-Hals Bereiches umfassen Tumoren der Mundhöhle, des Pharynx, des Larynx, der Speicheldrüsen, der nasalen Kavität und des paranasalen Sinus[1,2]. Der vorherrschende histologische Typ von Kopf-Hals-Tumoren sind Plattenepithelkarzinome (*head and neck squamous cell carcinoma*, HNSCC)[2]. Sie zeichnen sich durch eine hohe Heterogenität aus[3,4]. HNSCC ist die 7.-häufigste Ursache für krebsbedingte Sterblichkeit weltweit[2]. In Deutschland erkrankten 2016 mit 17,6 je 100.000 Einwohner mehr als doppelt so viele Männer als Frauen an einem Tumor im Mundhöhlen- oder Rachenbereich. Die Inzidenz für Männer in Mecklenburg-Vorpommern lag mit über 25 je 100.000 Einwohner sogar über dem deutschlandweiten Schnitt[5]. Die 5-Jahres-Überlebensrate in Deutschland schwankt, in Abhängigkeit des Geschlechts und dem Tumorstadium bei Diagnose, zwischen 36 % und 89 %[5].

Risikofaktoren für die Entstehung eines HNSCC sind Tabak- und Alkoholkonsum, sowie eine Infektion mit dem humanen Papillomavirus (HPV). HPV-Infektionen führen zur Entstehung von Tumoren im Oropharynx[3,6]. Neben der unterschiedlichen Lokalisation, zeigen HPV-assoziierte Tumoren im Vergleich zu nicht-HPV-assoziierten Tumoren auch eine unterschiedliche molekulare Signatur (z.B. *TP53*-mutiert vs. Wildtyp) und klinische Präsentation. Ferner weisen sie oftmals ein besseres Therapieansprechen auf, weshalb aktuell zwei distinkte HNSCC-Subtypen unterschieden werden[3,7,8]. Bei einem HPV-assoziierten HNSCC wird häufig das Protein p16 überexprimiert. Aufgrund dessen dient die Immunfärbung von p16 als Surrogatmarker für den HPV-Status[9,10]. Gemein ist beiden Subtypen der hypermutierte Phänotyp und die daraus resultierende hohe Tumormutationslast (*tumor mutational burden*)[11–13]. So unterscheidet sich die Mutationsrate nicht wesentlich zwischen HPV-negativen und -positiven Tumoren[14–16]. Während bei HPV-negativen Tumoren neben *TP53*-Mutationen auch *CDKN2A*-Deletionen dominieren, sind die karzinogenen Effekte von HPV sind auf die viralen Gene *E6* und *E7* zurückzuführen[14,17]. Das Onkoprotein E7 inaktiviert das Retinoblastom-Protein (Rb-Protein), welches die Aktivität der E2F-Transkriptionsfaktoren kontrolliert. Als Folge wird der G1-S-Phasenarrest unterbunden und eine Hyperproliferation der transformierten Zellen ermöglicht. Das Onkoprotein E6 interagiert mit dem Tumorsuppressor p53 und fördert dessen Degradation. Dies unterdrückt die p53-induzierte Apoptose, ermöglicht eine Replikation in Gegenwart von DNA-Schäden resultiert in chromosomaler Instabilität[3,18–20]. Es sind verschiedene Ansätze bekannt durch die sich Tumoren der Immunerkennung entziehen können. Der bekannteste ist die Hochregulation von PD-L1, welcher als Biomarker fungiert, aber auch Indoleamin 2,3-dioxygenase (IDO)[21–24]. IDO katabolisiert die Umwandlung von Tryptophan in Kynurenin in peripheren Geweben und ist

damit ein Schlüsselenzym entlang des Kynureninstoffwechsels. Neben IDO ist die Tryptophan-2,3-Dioxygenase (TDO2) ein weiteres Schlüsselenzym des Kynureninstoffwechsels, welches über die hepatische Route denselben Schritt katalysiert wie IDO. Kynurenin kann in unterschiedlichen Reaktionen über drei verschiedene Enzyme weiter verstoffwechselt werden. Entweder über die Kynurenin-3-Monooxygenase (KMO), durch eine der vier Kynurenin-Aminotransferase-Isoenzyme (KYAT1,2,3,4) oder durch die Kynureninase (KYNU). Der Kynureninstoffwechsel und das Immunsystem sind eng miteinander verbunden. So induziert Kynurenin zum Beispiel die Aktivierung von regulatorischen T-Zellen und myeloiden Suppressorzellen, welche die Funktionen von Effektor-T- Zellen und natürlichen Killerzellen unterdrücken und die Neovaskularisierung fördern[25–29].

1.2 Therapieoptionen für HNSCC

Die Therapie von Kopf-Hals-Tumoren ist von mehreren Faktoren abhängig. Bei der Wahl der Therapie berücksichtigt werden die Größe und Lage des Primärtumors, der Allgemeinzustand des Patienten, funktionelle und ästhetische Konsequenzen, sowie die Wahrscheinlichkeit des Behandlungserfolges. Grundsätzlich zur Therapie zugelassen sind die alleinige chirurgische Resektion, die alleinige Strahlentherapie, sowie eine Kombination aus Strahlentherapie mit Chemotherapie oder einer Kombination aus allen drei Behandlungsoptionen[30]. Insbesondere Cisplatin oder platinhaltige Kombinationen mit 5-FU, Taxanen oder Cetuximab finden dabei Anwendung[2,30,31]. Im Jahr 2016 hat die *US Food and Drug Administration* (FDA) die monoklonalen Antikörper gegen PD-1 Nivolumab und Pembrolizumab, für die Behandlung von platin-refraktären Patienten mit rezidiviertem/metastasiertem HNSCC zugelassen. 2019 folgte die Zulassung für die Erstlinienbehandlung von Patienten mit inoperablem rezidiviertem/metastasiertem HNSCC mit Pembrolizumab in Monotherapie oder in Kombination mit Platin und 5-FU[31]. Die Zulassung ist inzwischen auch in Deutschland erfolgt[30]. Etwa 58 % der Patienten werden erst im lokal fortgeschrittenen Stadium der Erkrankung vorstellig und haben eine schlechte Prognose[2]. Darüber hinaus haben alle bislang durchgeführten klinischen Studien zum Einsatz von Immuncheckpoint-Inhibitoren gezeigt, dass nicht alle Patienten von dieser innovativen Therapieform profitieren. So lag das objektive Ansprechen in der KEYNOTE-012 Studie zwischen 16 % und 24 %, in der KEYNOTE-055 Studie bei 16 %, in der CheckMate 141 Studie bei 13 % und in der KEYNOTE-040 Studie bei 14 %[32]. Damit ist diese neue Therapieoption zwar eine vielversprechende Alternative, aber immer noch nicht der erhoffte Durchbruch. Folglich müssen weitere Therapieoptionen identifiziert werden, um die Prognose der betroffenen Patienten langfristig zu verbessern. Die Entwicklung neuer Behandlungskonzepte erfolgt idealerweise in präklinischen Tumormodellen.

1.3 Präklinische Tumormodelle

Präklinische Modellsysteme sind wichtige Instrumente zur Verbesserung unseres Wissens über die Biologie von Tumoren. Sie helfen bei der Identifizierung wirksamer neuer Therapien und ermöglichen eine Annäherung an die humane *in vivo* Situation, um Daten von *bench-to-bedside* übertragen zu können. Im Idealfall bewahrt ein Modell den Phänotyp und die molekularen Merkmale in Kombination mit der komplexen und heterogenen Tumormikroumgebung, die mit Immun- und Stromazellen interagiert. Bislang gibt es aber kein ideales Modell, das all diese Merkmale abdeckt[33–35]. Es werden verschiedene Modellsysteme unterschieden, die grundlegend in *in vitro* bzw. *ex vivo*, *in vivo* und *in silico* Modelle unterteilt werden können[34–36]. Zu den *in vitro* / *ex vivo* Modellen zählen 2D- und 3D-Zellkulturen, wobei bei den 3D-Zellkulturen zwischen Sphäroiden und Organoiden unterschieden werden muss[34,35,37]. Weiterhin müssen immortalisierte Langzeitkulturen von primären, in niedriger Passage gehaltenen Zelllinien differenziert werden, da sie sich durch eine höhere biologische Relevanz auszeichnen[34,38]. Zu den bekanntesten *in vivo* Modellen gehören die Patienten-abgeleiteten Xenografts (*Patient-derived Xenografts*, PDX). Diese erhalten in frühen Passagen die Biologie und das molekulare Profil der humanen Tumoren[39–41]. Unter *in silico* Modellen werden mathematische Computer gestützte Methoden großer zellulärer Signaltransduktionsnetzwerke zur Vorhersage von Arzneimittelwirkungen und funktionellen Reaktionen auf der Grundlage patientenspezifischer *multi-Level-omics*-Profile verstanden[36,42]. Eine Übersicht der verschiedenen Modelle befindet sich in Abbildung 3 im Anhang.

1.4 Zielgerichtete Therapien

Ein besseres Verständnis der bei der Krebsentstehung beteiligten molekularen Mechanismen, wie der Dysregulation von Cyclin abhängigen Kinasen (CDKs) und der Überexpression von CDK/Cyclin Komplexen führte zur Entwicklung der Cyclin-abhängige Kinase-Inhibitoren (CDKis)[43–46]. Diese zeigen zytotoxische Effekte gegen verschiedene Tumorentitäten, einschließlich HNSCC[47–49]. CDKs spielen eine wichtige Rolle bei der Regulation des Zellzyklus. Ihre Aktivität während der einzelnen Zellzyklusphasen wird durch die die Oszillation von Cyclinen reguliert[44]. Neben ihrer bekanntesten Rolle im Zellzyklus sind sie aber auch bei der Transkription, beim Stoffwechsel oder bei der Selbsterneuerung von Stammzellen beteiligt[44,50]. Grundsätzlich sind global-wirkende von selektiven CDKis abzugrenzen. Dinaciclib inhibiert die CDK1, 2, 5 und 9 und zeigt damit ein globales Wirkspektrum[51]. THZ1 ist als Inhibitor der CDK7,12 und 13 beschrieben. Dieser CDKi beeinflusst die Phosphorylierung und Transkription der RNA-Polymerase 2 und wirkt ebenfalls relativ global[52,53]. Darüber hinaus gibt es drei selektive CDK4/6 Inhibitoren (CDK4/6i), die bereits von der FDA zugelassen sind. Palbociclib, Ribociclib und Abemaciclib werden aktuell zur Therapie des lokal fortgeschrittenen oder metastasierten Hormon-rezeptor-positiven Mammakarzinoms eingesetzt[54]. Obgleich alle

CDK4/6 Inhibitoren strukturell verwandt sind, ist deren Wirksamkeit und Nebenwirkungsprofil heterogen[55]. Abemaciclib zeigt im Vergleich zu Palbociclib und Ribociclib eine höhere Affinität für die CDK4 als für die CDK6[56–58]. Der Retinoblastom-Signalweg ist in gut 30 % aller HNSCC durch Deletion des *CDKN2A*-Gens (kodiert für p16) und eine Amplifikation des *CCND1*-Gens (kodiert für Cyclin *D*) verändert. Diese Aberrationen ermöglichen, durch Überwindung des G1-S-Phasencheckpoints im Zellzyklus, die dysregulierte Zellproliferation[59,60]. Weiterhin weisen, wie bereits erwähnt, ein Großteil der HPV-negativen Tumoren Mutationen im *TP53*-Gen auf (86 %)[16,60,61]. Dieses reguliert die Transkription zahlreicher nachgeschalteter Zielgene, die unter anderem am Zellzyklusstopp (wie z.B. p21), der Apoptose oder der DNA-Reparatur beteiligt sind. Durch Mutationen verliert p53 seine tumorsuppressive Funktion[60,62]. Vor diesem Hintergrund stellen CDKi einen vielversprechende Therapieoption für HNSCC dar. Dabei korreliert das Ansprechen auf CDK4/6i negativ mit dem HPV-Status, d.h. primär HPV-negative HNSCC sind sensitiv gegenüber dieser Substanzklasse[63]. Die höhere Anfälligkeit dieses Subtyps im Vergleich zu HPV-assoziierten HNSCC ist wahrscheinlich auf die bereits erwähnten Mutationen im Retinoblastom-Signalweg (*CCND1*-Amplifikation und Deletion des *CDKN2A*-Gens) zurückzuführen[64]. Umgekehrt überexprimieren HPV-bedingte Krebsarten p16, und haben durch das Onkogen E7 ein funktionell inaktiviertes Rb-Protein[65]. Das Vorhandensein des Rb-Proteins ist jedoch entscheidend für die therapeutische Wirkung von CDK4/6i und stellt einen bereits in anderen Tumorentitäten nachgewiesenen Biomarker dar[57,66,67]. Präklinische und klinische Arbeiten zeigen die Wirksamkeit von CDKis (primär CDK4/6i) bei HNSCC. Dabei wurden unter anderem zytostatische und radiosensibilisierende Effekte beobachtet, sowie ein Einfluss auf den Zellzyklus[63,68–70]. Dinaciclib und THZ1 sind bei HNSCC wenig erforscht. Präklinische Studien zu THZ1 zeigen jedoch auch hier antineoplastische Wirkung[71–73]. Kombinationstherapien gelten als ein vielversprechender Ansatz, um ein verbessertes Therapieansprechen bewirken zu können und der Entwicklung von Resistenzen vorzubeugen. Diese können aus konventionellen, zielgerichteten und immunbasierten Therapien bestehen[74–76]. Dabei ist jedoch das Timing der einzelnen Kombinationspartner ein nicht zu unterschätzender Faktor, wie die Studie von Robinson *et al.* zeigt. Ihre Studie beschreibt das Ansprechen auf Palbociclib bei chemo-naiven HNSCC-Zelllinien, aber eine intrinsische Resistenz bei vorheriger Applikation von Cisplatin[57,77]. In der Theorie sollten konventionelle Chemotherapeutika von einer ergänzenden CDKi-Behandlung profitieren, indem sie deren Wirkung ergänzen[78]. Bisherige Studien liefern jedoch widersprüchliche Ergebnisse[65]. Die Idee der Kombinationstherapie mit Immuncheckpoint-Inhibitoren ist, dass zielgerichtete Therapeutika ein schnelles Absterben der Tumorzellen induzieren, sodass es zur Freisetzung von Neoantigenen kommt und die Effektivität von Immuncheckpoint-Inhibitoren gesteigert wird[79,80]. Aber auch weitere Wirkmechanismen, wie

die Erhöhung der Stabilität des PD-L1-Proteins in Tumorzellen durch die Hemmung von CDK4/6 verdeutlichen die mechanistische Grundlage für Kombinationstherapien[81].

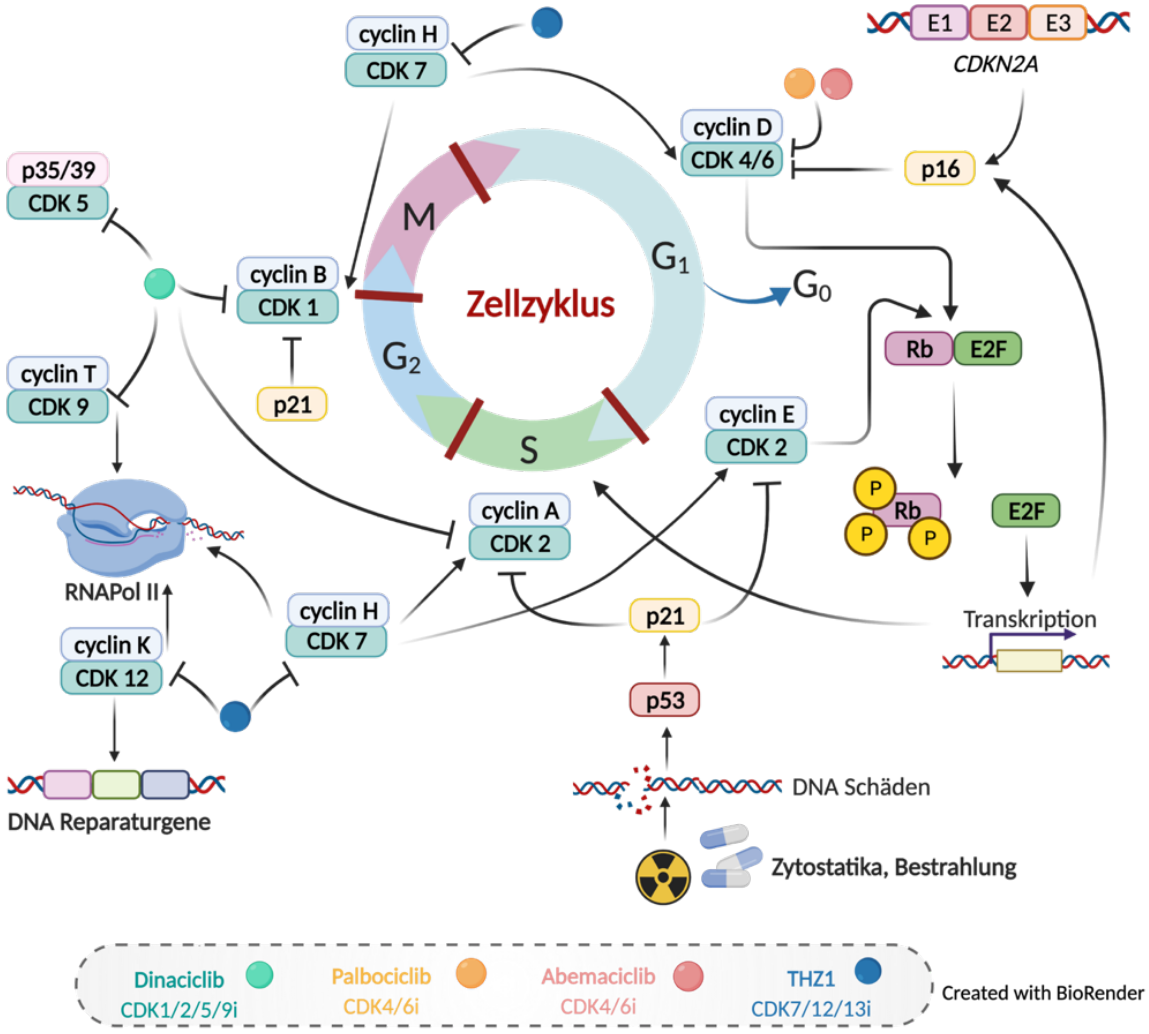

Abbildung 1: Zellzyklusregulierung und CDKis[61,82,83].
In Anlehnung an [57].

2. Fragestellung

Plattenepithelkarzinome des Kopf-Halses zeichnen sich durch ein hohes Maß an inter- und intratumoraler Heterogenität aus. Um die Heterogenität dieser Erkrankung abzubilden und innovative Therapiekonzepte zu entwickeln, werden gut charakterisierte präklinische Modelle benötigt.

Die vorliegende Arbeit beschäftigte sich mit der Etablierung Patienten-individueller Tumormodelle zur Erforschung neuer Behandlungsansätze für HNSCC-Patienten und der Identifikation geeigneter Biomarker zur Vorhersage eines Therapieansprechens. Auf Basis der erhobenen Befunde wurden verschiedene Kombinationsstrategien präklinisch validiert, um

Resistenzmechanismen zu überwinden. Folgende Fragestellungen wurden dazu näher betrachtet:

(I) Welchen Einfluss haben Therapeutika auf den Expressionsstatus von Genen des Kynureninstoffwechsel im Kontext eines Immun-Escape Mechanismus?
   a. Wirken Zytostatika und zielgerichtete Substanzen unterschiedlich?

(II) Zeigen CDKis eine Wirksamkeit gegenüber Kopf-Hals-Tumoren?
   a. Können Kombinationsansätze die Effekte verstärken?
   b. Welche molekularen Aberrationen liegen einer potenziellen Wirksamkeit zugrunde?

(III) Welche Erfolgsquote haben Patienten-individuelle Tumormodelle aus Biopsien und OP-Resektaten?
   a. Kann ein individuelles Therapieansprechen an diesen Modellen in der präklinischen Forschung erfolgen?

3. Methoden

Auf Basis der im nächsten Kapitel folgenden Ergebniszusammenfassung, sind in diesem Kapitel ausgewählte Methoden stichpunktartig aufgeführt. Eine ausführliche Beschreibung der durchgeführten Versuche befindet sich in den Originalpublikationen.

3.1 *In vitro* und *ex vivo* Kultur

verwendete Zelllinien: FADU, Detroit-562, Cal-33, PE/CA/PJ-15, UT-SCC-14, UT-SCC-15. FADU, Detroit-562, Cal-33, PE/CA/PJ-15 (*German collection of cell cultures* (Braunschweig, Deutschland), UT-SCC-14 und UT-SCC-15 (Prof. R. Grénman, Turku University Hospital, Turku, Finnland). HNSCC16 P1 M1, HNSCC46 P0 M2 und HNSCC48 P0 M1: selbst etabliert Kultivierung in Vollmedium: DMEM/HamsF12, + 10 % fetales Kälberserum (HNSCC48 P0 M1: Serumendkonzentration 15 %), 2 mmol/L Glutamin + Antibiotika. HNSCC-Tumorproben: Klinik und Poliklinik für Hals-Nasen-Ohrenheilkunde des Universitätsklinikums Rostock.

Die schriftliche Einwilligung der Patienten wurde gemäß der lokalen Ethikkommission (Referenznummer A2018-0003) und den Richtlinien für die Verwendung von menschlichem Material (Deklaration von Helsinki) eingeholt. Der Pathologe entnahm Tumorgewebe für die H&E Routinediagnostik und stellte makroskopisch vitales Tumorgewebe für Forschungszwecke zur Verfügung.

3.2 Ethische Erklärung – *in vivo* Versuche

Alle Tierversuche wurden vor Beginn durch das Landesamt für Landwirtschaft, Lebensmittelsicherheit und Fischerei Mecklenburg-Vorpommern, gemäß dem deutschen Tierschutzgesetz und der EU-Richtlinie 2010/63/EU genehmigt (Aktenzeichen: 7221.3-1-066/18 und 7221.3-1-032/19-4). Die Mäuse wurden in der zentralen Versuchstierhaltung der

Universitätsmedizin Rostock unter spezifisch pathogen-freien Bedingungen gezüchtet (Direktorin: Univ.-Prof. Dr. med. B. Vollmar). Alle Tiere erhielten *Enrichment* in Form von Maus-Iglus, Nistmaterial, Papierrollen und Holzstäbchen. Während des Versuchs wurden die Mäuse in Käfigen des Typs III bei einem 12-Stunden-Dunkel-Licht-Zyklus, einer Temperatur von 21 ± 2 °C und einer relativen Luftfeuchtigkeit von 60 ± 20 % mit Futter (Pellets, 10 mm) und Leitungswasser *ad libitum* gehalten. Zur Generierung von PDX Modellen wurden NOD.Cg-Prkdc^{scid}Il2rg^{tm1Wjl}/SzJ (NSG)-Mäuse verwendet und Tumorfragmente subkutan unter Ketamin/Xylazin-Narkose (90/6 mg/kg KG, i.p.) implantiert. Das Tumorwachstum wurde wöchentlich dokumentiert. Das Tumorvolumen wurde als (Länge × Breite^2)/2 berechnet. Nach Erreichen einer kritischen Tumorgröße von 1,5 cm³ wurden die Tiere euthanasiert, das Gewebe nativ und vital asserviert. Zelllinien-abgeleitete-Xenotransplantate wurden durch Injektion von 5 x 10^6 HNSCC-Zellen subkutan in die rechte Flanke weiblicher NSG-Mäuse (6-8 Wochen) erzeugt. Die Mäuse wurden euthanasiert, bevor die Tumoren 1,5 cm³ erreichten. *In vivo* Therapieansätze wurden mit HNSCC16 P1 M1 (NSG) durchgeführt oder UT-SCC-14 und UT-SCC-15 (NMRI Foxn1^{nu}). Ab einer Tumorgröße von ~50 mm^3 wurden die Tiere der Kontroll- oder der Behandlungsgruppe zugeführt.

3.3 Molekulare Analysen

- Isolierung der Gesamt-RNA mittels RNeasy Mini Kit von Qiagen; Isolierung Gesamt-DNA mittels AllPrep DNA/RNA/Protein Mini Kit von Qiagen
- Quantitative real-time PCR zum Nachweis von *IDO1*, *TDO2*, *KMO*, *KYAT1/2/3/4*, *KYNU*, *MYC*, *PDK2*, *SKP2* und *GAPDH*
- Illumina Cancer Hotspot Panel zum Nachweis genomischer Veränderungen (Institut für Pathologie)
- ZytoLight FISH Cytology zum Nachweis von *CDKN2A/B* und *CDK4* (Institut für Pathologie)

3.4 Zellbiologische & immunologische Methoden

- Radiosensitivität: 2 Gy und 14 Gy Einzelstrahlendosis an 5 aufeinanderfolgenden Tagen (Cs-137 γ-Bestrahlung; IBL 637, CIS Bio-International, Codolet, Frankreich)
- Bestimmung der Verdopplungszeit: $PDT = t \cdot ln(2)/\ln(N_X/N_0)$ (t = Inkubationszeit zwischen N_x und N_0, N_x = Gesamtmenge der Zellen am Ende des exponentiellen Wachstums und N_0 = Gesamtmenge der Zellen zu Beginn des exponentiellen Wachstums)
- Migrations - bzw. Wundheilungsversuch/Invasionsassay: Quantifizierung mittels WST-1
- Impedanzmessung: *Electric Cell-Substrate Impedance Sensingsystem* (ECIS Z; Applied Biophysics) (Unter Anleitung der Klinik und Poliklinik für Mund-, Kiefer-, und Plastische Gesichtschirurgie)
- Durchflusszytometrische Analysen:

- Charakterisierung des Tumormikromilieus: Immun-Panel, s. Publikation 4
- Apoptose-Nekrose: Yo-Pro 1 Iodid und Propidiumiodid
- Methuose: Alexa488 α-CD107a und Alexa594 α-Rab7a
- Immunogener Zelltod: α-CalR Primärantikörper/FITC-konjugierter Sekundärantikörper
- Phänotypisierung: FITC α-MHC I , PE/Cy7 α-CD274 und APC α-CD279
- Zellzyklus: 70 %iger Ethanol, TritonX-100, RNAse und Propidiumiodid
- Allogene Ko-Kultur: 5-(und-6)-Carboxyfluorescein-Diacetat, Succinimidyl-Ester-Färbung Tumorzellen, Dichtegradientenzentrifugation: Isolierung mononukleärer Zellen (*Peripheral Blood Mononuclear Cells*, PBMCs) + fluoreszierende Mikrosphären-Beads

- Immunfluoreszenz:
  - Nachweis von IDO1: α-IDO1 Primärantikörper/FITC-konjugierter Sekundärantikörper
  - Mitochondriale Aktivität: MitoTracker Red CMXRos
  - Reaktive Sauerstoffspezies: ROS Brite 670
  - Saure Kompartimente (Autophagie): Acridinorange und Calcein AM
  - Aktinfilamente: Alexa Fluor 488 Phalloidin oder Phalloidin-iFluor 594-Konjugat

3.5 Statistik

Die statistische Auswertung erfolgte mit GraphPad PRISM-Software, Version 5.02 oder 8.0.2. Alle Werte sind als Mittelwert ± SD (*in vitro*-Analyse) oder Mittelwert ± SEM (*in vivo*-Ansatz, mit Ausnahme von Publikation 3: Mittelwert ± SD) angegeben. Das Kriterium für Signifikanz wurde auf $p < 0,05$ festgelegt. Nach Prüfung auf Normalverteilung wurde eine einseitige ANOVA (*Bonferroni's multiple comparison* oder *Dunnett's multiple comparison*) oder ein T-Test durchgeführt. Wenn der Normalitätstest (Shapiro-Wilk Test) nicht erfolgreich war, wurde der Kruskal-Wallis- oder U-Test durchgeführt. Die nicht-parametrische Spearman Korrelation wurde verwendet, um Korrelationen zwischen einzelnen Parametern (zweiseitiger P-Wert) zu ermitteln. Die Kaplan-Meier-Überlebensanalyse wurde unter Anwendung des Log-Rank-Tests (Mantel-Cox) durchgeführt.

4. Ergebnisse

Die Ergebnisse der Arbeit werden anhand der vier folgenden Originalpublikationen in englischer Sprache präsentiert:

Publikation 1: Riess C, Schneider B, Kehnscherper H, Gesche J, **Irmscher N**, Shokraie F, Classen CF, Wirthgen E, Domanska G, Zimpfer A, Strüder D, Junghanss C,

Maletzki C (2020). Activation of the Kynurenine Pathway in Human Malignancies Can Be Suppressed by the Cyclin-Dependent Kinase Inhibitor Dinaciclib. *Frontiers in immunology*, 11, 55. (IF 2020 5,085)

Publikation 2: **Schoenwaelder N**, Salewski I, Engel N, Krause M, Schneider B, Müller M, Riess C, Lemcke H, Skorska A, Grosse-Thie C, Junghanss C, Maletzki C (2021). The Individual Effects of Cyclin-Dependent Kinase Inhibitors on Head and Neck Cancer Cells-A Systematic Analysis. *Cancers*, 13(10), 2396. (IF 2021 6,639)

Publikation 3: Strüder D, Momper T, **Irmscher N**, Krause M, Liese J, Schraven S, Zimpfer A, Zonnur S, Burmeister AS, Schneider B, Frerich B, Mlynski R, Große-Thie C, Junghanss C, Maletzki C. (2021). Establishment and characterization of patient-derived head and neck cancer models from surgical specimens and endoscopic biopsies. *Journal of Experimental & Clinical Cancer research*, 40(1), 246. (IF 2021 11,161)

Publikation 4: **Schoenwaelder N**, Krause M, Freitag T, Schneider B, Zonnur S, Zimpfer A, Becker AS, Salewski I, Strüder DF, Lemcke H, Grosse-Thie C, Junghanss C, Maletzki C. (2022). Preclinical Head and Neck Squamous Cell Carcinoma Models for Combined Targeted Therapy Approaches. *Cancers*, 18;14(10):2484. (IF 6,639)

Im Folgenden werden die wichtigsten Ergebnisse der Originalpublikationen in deutscher Sprache zusammengefasst. Die vollständigen Originalpublikationen befinden sich im Kapitel 8. Zusammenfassende Abbildungen der Ergebnisse befinden sich im Anhang (Abbildung 4 – Abbildung 7).

4.1 Publikation 1

In dieser Studie wurde der Expressionsstatus von Genen des Kynureninstoffwechsels bestimmt und Expressionsänderungen unter Standard- und zielgerichteter Therapie vergleichend analysiert, nachdem in Vorarbeiten in *dose-response-*Analysen und einem Apoptose-Nekrose-Assay die generelle Wirksamkeit von Dinaciclib an Zellkulturen von Kopf-Hals-Tumoren bestätigt wurde. *IDO1* ließ sich in geringen Mengen nachweisen, die *KYNU* und vor allem *TDO2* waren nahezu nicht nachweisbar. *KYAT2,3,4* waren im Gegensatz dazu höher exprimiert. Da Zelllinien die *in vivo*-Situation nicht immer ausreichend wiedergeben und IDO1 auch in Immunzellen induzierbar ist, wurde das Vorkommen von IDO1 in klinischen Resektionspräparaten untersucht. Dabei zeigte sich, das IDO1 bei einem geringen Teil tumorinfiltrierender Lymphozyten, jedoch nicht in den Tumorzellen vorkommt. *In vitro* konnte *IDO1* durch IFNγ Stimulation der Tumorzellen induziert werden. Durch diese *in vitro* Stimulation wird

die *in vivo* Situation einer entzündlichen Mikroumgebung nachgeahmt. Cetuximab war im Gegensatz zu Gemcitabin, 5-FU, Cisplatin und Dinaciclib die einzige IDO1-induzierende Substanz. Darüber hinaus induzierten sowohl die Zytostatika als auch Cetuximab mindestens eines der Kynureninstoffwechsel-assoziierten Gene, wie *KYAT1*, *KYAT2* und *KMO* ($p < 0,05$ *vs*. Kontrolle). Dies deutet auf eine Aktivierung dieses Signalwegs über verschiedene Effektoren hin. Interessanterweise wurde dieser Effekt durch die Zugabe von Dinaciclib zu den Zytostatika aufgehoben. Bemerkenswert ist, dass Dinaciclib sowohl allein, als auch in Kombination mit anderen Substanzen alle Kynureninstoffwechsel-assoziierten Gene supprimiert, was auf eine Hemmung des Tryptophankatabolismus hinweist. *IDO1* und weitere Gene des Kynureninstoffwechsels, wie *KYAT1*, *KYAT2* und *KMO* ließen sich durch Cetuximab, 5-FU und Gemcitabin induzieren. Umgekehrt supprimierte die zielgerichtete Therapie mit Dinaciclib den Kynureninstoffwechsel.

4.2 Publikation 2

Ausgehend von den Vorarbeiten in Publikation 1 wurde die Wirksamkeit von Dinaciclib und den CDKis Palbociclib und THZ1 in Kombination mit weiteren Substanzen an ausgewählten HNSCC Zelllinien untersucht. Dabei lag der Fokus der Kombinationspartner neben den CDKis auf den Zytostatika Cisplatin und 5-FU. Schwerpunkt der Arbeit war die Analyse der zugrunde liegenden Wirkmechanismen, um potenziell synergistische Effekte an ausgewählten Therapieschemata zu evaluieren. Die Arbeit zeigte die grundsätzliche Wirksamkeit von CDKis bei HNSCC auf und identifizierte teilweise synergistische Effekte zwischen diesen bei simultaner Applikation. Dinaciclib und THZ1 waren am effektivsten und zeigten noch stärkere Effekte im Kombination mit 5-FU. Die nachgewiesenen Effekte der verschiedenen getesteten Kombinationen umfassten einen apoptotischen und nekrotischen Zelltod sowie Methuose. Weiterhin wurden Auswirkungen auf die Impedanz, Aktinfasern und Motilitätseigenschaften der Tumorzellen nachgewiesen. Dinaciclib verursachte eine massive Ablösung der Zellen und induzierte den Zelltod. Nach THZ1 Behandlung war vermehrt die Bildung von Stressfasern zu beobachten. Weiterhin erhöhte Dinaciclib die mitochondriale Aktivität der Tumorzellen. Darüber hinaus wurde die Hochregulierung immunologisch relevanter Moleküle auf der Tumorzelloberfläche unter bestimmten CDKi-Wirkstoffkombinationen beobachtet. Hier hatten Dinaciclib und Palbociclib den größten Einfluss auf die Immunogenität, der sogar die Effekte der Standardmedikamente übertraf. Palbociclib, THZ1 und THZ1 + 5-FU induzierten zelllinienspezifisch einen G1-Phasenarrest. Schließlich bestätigte ein therapeutischer *in vivo*-Ansatz teilweise die zelllinien-basierten Ergebnisse. Eine wirksame Tumorwachstumskontrolle wurde durch die Kombinationstherapie Cisplatin + Dinaciclib erzielt. Die antitumoralen Effekte waren jedoch sehr individuell und bestätigen die Heterogenität dieser Tumorentität. Abschließend lässt sich festhalten, dass die therapeutische Wirksamkeit von CDKis bestätigt

wurde, sowie Wirkmechanismen aufgedeckt werden konnten. Besonders vielversprechend sind die immunmodulatorischen Effekte, welche in Analogie zu Befunden bei anderen Tumorentitäten das Potential einer Kombinationstherapie bestehend aus CDKis und Immuntherapie bestätigen.

4.3 Publikation 3

Die eingeschränkte Verfügbarkeit von Proben nicht-resektabler lokal fortgeschrittener oder metastasierender Tumoren erschwert die Generierung von PDX-Modellen aus diesen Geweben. In dieser Studie wurde unter Verwendung von endoskopischen Biopsien und chirurgischen HNSCC Resektaten die (I) Anwachsrate und Wachstumsgeschwindigkeit, (II) Histomorphologie und (III) Molekularpathologie vergleichend zwischen Primarien und PDX Geweben analysiert. Die Rekrutierung der Patienten und Asservierung von vitalem und nativen Tumorgewebe erfolgte im Rahmen der Etablierung einer HNSCC-Biobank am Standort Rostock. Alle Arbeiten erfolgten in enger Kooperation mit der Klinik und Poliklinik für Hals-Nasen-Ohrenheilkunde, Kopf- und Halschirurgie, dem Institut für Pathologie und der Klinik und Poliklinik für Mund-, Kiefer- und Plastische Gesichtschirurgie. Insgesamt wurden 50 Patienten (Männer:Frauen: 41:9) mit einem medianen Alter von 64 Jahren in die Studie eingeschlossen. Bei den meisten Patienten handelte es sich um Raucher (68%, ≥ 10 py), die keinen kritischen Alkoholkonsum (54 %) aufwiesen und im fortgeschrittenen Stadium vorstellig wurden (T4a/b). Die in der Studie eingeschlossenen Tumore befanden sich im Oropharynx, der Mundhöhle, im Kehlkopf und im Hypopharynx. Bei zwölf der eingeschlossenen Fälle wurde eine HPV-Infektion nachgewiesen (histologisch und molekular). Insgesamt wurden 23 endoskopische und 21 chirurgische Proben subkutan in NSG-Mäuse implantiert. Die Transplantation war in beiden Tumorproben erfolgreich (*Engraftment*rate 36,4 %). Bei den chirurgischen Resektaten war die *Engraftment*rate im Vergleich zu den Biopsien höher (52,4 vs. 21,7 %) und die *Engraftment*zeit kürzer ($p < 0,05$). Nach erfolgreichem *Engraftment* waren die Wachstumskinetiken vergleichbar. Weiterhin konnten vier PDX aus HPV-assoziierten HNSCC-Fällen generiert werden. Insgesamt hatten die klinischen Charakteristika der Patienten keinen signifikanten Einfluss auf die *Engraftment*rate. Der direkte Vergleich von Primärtumoren mit dem zugehörigen PDX bestätigte, dass sowohl das histomorphologische als auch das molekulare Profil im PDX erhalten blieb. Bei den HPV-negativen Tumoren dominierten *TP53*-Mutationen. Begleitende durchflusszytometrische Analysen an Primärtumoren zeigten eine heterogene Tumormikroumgebung zwischen HPV-positiven und -negativen Fällen, aber auch zwischen einzelnen Tumoren. Dies wurde auch durch immunhistochemische Analysen bestätigt. Interessanterweise identifizierten die durchflusszytometrischen Untersuchungen des Tumormikromilieus eine direkte positive Korrelation zwischen der Anzahl von $CD14^+CD163^+$ Makrophagen und dem *Engraftment* (Pearson r: -0,757; $p < 0,05$). Durch die Einbeziehung

von Biopsien nicht-resektabler HNSCC erweitert diese Studie die Verfügbarkeit von PDX-Modellen für die präklinische und translationale Forschung und erlaubt prospektive Studien zum individuellen Therapieansprechen.

4.4 Publikation 4

Ausgehend von den zuvor etablierten PDX Modellen wurde nachfolgend aus individuellen Modellen PDX-abgeleitete Zelllinien etabliert. Diese eignen sich besonders gut für die präklinische Wirkstofftestung. Neben der erfolgreichen Etablierung beschreibt diese Studie auch die umfassende zellbiologische und molekulare Charakterisierung der neuen Zelllinien. Unsere Arbeiten fokussieren weiterhin auf Kombinationsbehandlungen mit CDKis und klinisch zugelassenen Substanzen, sowie der Untersuchung der zugrunde liegenden Wirkmechanismen. Die Etablierung der Zelllinien erfolgte mittels Kollagenaseverdau nach vorheriger Passage in NSG-Mäusen mit geringfügigen Änderungen nach [84]. Wachsende Zellkulturen wurden in 25 cm^2-Zellkulturflaschen ausgesät, und die Serumkonzentration wurde schrittweise reduziert. Die Zelllinien zeigten eine unterschiedliche *in vitro* Wachstumskinetik, die sich mit dem Ki67-Status der Primarien deckte, sowie Unterschiede in der Morphologie, ihrem Invasionspotenzial und Radiosensitivität. Weiterhin unterschieden sich die ursprünglichen Tumoren in ihrem Tumormikromilieu hinsichtlich der Anzahl infiltrierender Lymphozyten, tumor-assoziierter Makrophagen und Checkpoint-Moleküle. Alle Zelllinien waren empfindlich gegenüber 5-FU und Cisplatin, sowie Dinaciclib und THZ1. Bei einer Zelllinie (HNSCC48 P0 M1) waren nach Behandlung mit Abemaciclib zytotoxische Effekte zu erkennen. Bei der Zelllinie HNSCC16 P1 M1, die primär nicht sensitiv gegenüber diesem CDK4/6i war, wurde nach Behandlung eine Hochregulierung der sauren Kompartimente beobachtet, sowie morphologisch eine geschwollene Struktur nachgewiesen. In weiterführenden Analysen wurden die Effekte mit molekularen Aberrationen korreliert, um potentielle Biomarker für das Ansprechen auf CDK4/6 Inhibitoren zu definieren. Mittels Cyto-FISH wurde bei der Zelllinie HNSCC48 P0 M1 eine partielle *CDKN2A*-Deletion festgestellt, die wahrscheinlich auf eine R58*-Mutation (Nachweis mittels *Next-Generation sequencing*) zurückzuführen ist. Außerdem wies diese Zelllinie eine Chromosom-12-Polysomie auf, die mit einem Anstieg der *CDK4*-spezifischen Kopienzahl einherging. Bei HNSCC16 P1 M1, nicht aber bei HNSCC46 P0 M2, konnten ebenfalls Polysomie-assoziierte *CDK4*-Zunahmen festgestellt werden. Diese erklären die beobachteten morphologischen Veränderungen unter Abemaciclib-Therapie. Cisplatin führte zu einer Herunterregulierung der Resistenz-assoziierten Gene *c-MYC* und *IDO1* in HNSCC16 P1 M1. Die Kombination von Cisplatin und Abemaciclib führte zu einer Hochregulierung von MHC I bin 2/3 Fällen und verstärkte die zytotoxischen Effekte der Monotherapie – insbesondere auch in HNSCC16 P1 M1, welche nur bedingt auf die Abemaciclib-Monotherapie angesprochen hat. Diese komplexen funktionellen

und molekularen Analysen an Patienten-individuellen HNSCC-Modellen identifizieren *CDK4*-Zugewinne als potenziellen Biomarker für die Vorhersage des Ansprechens auf Abemaciclib und beschreiben einen Ansatz zur Überwindung intrinsischer CDKi-Resistenz. Die etablierten Modelle repräsentieren HNSCC Tumoren unterschiedlicher Lokalisation und Mikroumgebung und sind ein idealer Ausgangspunkt, die Heterogenität von HNSCC weiter zu adressieren. In einem finalen, allogenen Ko-Kulturversuch zeigten sich vielversprechende Ergebnisse bei kombinierter Abemaciclib- und Pembrolizumab-Therapie. Diese müssen perspektivisch in einem autologen System bestätigt werden.

5. Diskussion

Die Prognose für HNSCC-Patienten ist weiterhin schlecht. Neue therapeutische Ziele konnten durch die Detektion molekularer Veränderungen im Genom der Tumoren identifiziert werden, jedoch ist die Umsetzung dieser in klinisch relevante, neue Behandlungsmöglichkeiten weiterhin anspruchsvoll[13,85–88]. Der Therapieerfolg für HNSCC-Patienten ist im Wesentlichen abhängig vom Tumorstadium zum Diagnosezeitpunkt, der Lokalisation und dem Alter des Patienten[89–91]. Über 50 % der Patienten werden erst im lokal fortgeschrittenen Stadium vorstellig und entwickeln häufig Rezidive und/oder Metastasen[2,92,93]. Eine weitere Herausforderung ist die intra- und intertumorale Heterogenität[3,94]. Die derzeitige Behandlungsstrategie von HNSCC basiert primär auf der Lokalisation und dem Tumorstadium und mit Ausnahme des HPV-Status haben zahlreiche molekulare und klinische Risikofaktoren keinen relevanten klinischen Nutzen[16,95]. Die Behandlung basiert maßgeblich auf der Systemtherapie mit Zytostatika bzw. Cetuximab[2,30,31]. Dabei gilt nach aktuellem Stand Cetuximab als einzige zugelassene, zielgerichtete Therapie mit moderatem *Outcome*[96–100]. Auch führten bislang durchgeführte klinische Studien zum Einsatz der Immuncheckpoint-Inhibitoren lediglich zu einem objektiven Ansprechen zwischen 13 und 24 %[32]. Die eingeschränkte Lebensqualität durch funktionelle und ästhetische Beeinträchtigungen, sowie die psychische Belastung sind weitere Faktoren, die bei ehemaligen HNSCC-Patienten zur zweithöchsten Selbstmordrate unter Krebsüberlebenden führen[101,102]. Da bisherige Anstrengungen zur Verbesserung der Prognose von HNSCC-Patienten in ihrer Wirksamkeit stark begrenzt sind und auch Überlebende weiterhin unter starken Einschränkungen leiden, besteht die dringende Notwendigkeit neue Therapieoptionen zu entwickeln. CDKis stellen dabei eine vielversprechende Option dar[13,16,59–62]. Sie werden in verschiedenen klinischen Studien zur Behandlung solider und hämatologischer Neoplasien untersucht (z.B. *NCT04169074*, *NCT04391595*, *NCT02897375*, *NCT04996160*). Bei lokal fortgeschrittenem oder metastasierten Brustkrebs sind CDK4/6is in Kombination mit einer endokrinen Therapie zugelassen[54,103–105]. Obwohl die Zulassung für HNSCC noch aussteht, sind erste präklinische Berichte vielversprechend[63,69–73].

Die Erkenntnis, dass eine hohe IDO1-Expression mit einer schlechteren Prognose bei Krebspatienten (inklusive HNSCC-Patienten) einhergeht, macht IDO1 zu einem vielversprechenden *Target*. Auch im Kontext von HNSCC laufen klinische Studien mit IDO-Inhibitoren[13,106]. Neben *IDO1* sind auch *TDO2, KMO, KYAT1,2,3,4* und *KYNU* am Kynureninstoffwechsel beteiligt[25–29]. In diesem werden biologisch aktive Metabolite gebildet, welche eine hohe Relevanz als Signalprotein zur Aufrechterhaltung der Immunregulierung und des zellulären Energiestoffwechsels haben. Eine IDO1 Blockade erscheint daher sinnvoll. Im Rahmen von Publikation 1 konnte gezeigt werden, dass der Kynureninstoffwechsel bei

HNSCC aktiv ist. In der Literatur ist das Vorkommen von IDO1 für HNSCC, unabhängig von der anatomischen Lage und dem HPV-Status beschrieben und gleichzeitig als Marker für die Progression von Plattenepithelkarzinomen deklariert[14,110,111]. Kynureninstoffwechsel-assoziierten Gene, wie *KYAT1*, *KYAT2* und *KMO* werden durch Zytostatika induziert. Cetuximab war die einzige *IDO1*-induzierende Substanz in Publikation 1. Die spezifischen biochemischen Mechanismen der Kynureninstoffwechsel-assoziierten Gene (wie *KYAT1*, *KYAT2* und *KMO*) sind in der Literatur kaum beschrieben. Die Induktion kann als ein möglicher Mechanismus der Therapieresistenz interpretiert werden, wie er bei HNSCC nach Standardtherapie häufiger beobachtet wird[112–114]. Eine mögliche Ursache ist die Sekretion proinflammatorischer Moleküle wie *High-Mobility-Group-Protein B1* durch absterbende Tumorzellen, die zu einer Immunaktivierung führen und somit den Kynureninstoffwechsel aktivieren[115–117]. Durch die Zugabe von Dinaciclib wurde der Effekt der Zytostatika aufgehoben. Bemerkenswert ist, dass dies unabhängig vom gewählten Kombinationspartner war und alle Kynureninstoffwechsel-assoziierten Gene supprimiert wurden. Dieses Ergebnis war unerwartet und ist in der Literatur nach aktuellem Stand noch nicht beschrieben. Diese Daten verdeutlichen das Potenzial von Dinaciclib. In Kombination mit der Standardtherapie könnte dieser CDKi die Immunfunktion wiederherstellen, der Resistenzentwicklung vorbeugen und so die Prognose von HNSCC-Patienten verbessern.

Zur Erweiterung der Verfügbarkeit von PDX-Modellen wurde in Anlehnung an vorangegangene Forschungen die Hypothese aufgestellt, dass endoskopische Biopsien vor einer Behandlung ausreichend vitales Tumorgewebe für das PDX-Wachstum in einem klinisch relevanten Zeitrahmen aufweisen[118–120]. In Publikation 3 wurde diese Hypothese in einem interdisziplinären Projekt bestätigt und PDX erfolgreich aus Biopsien und chirurgischen Resektaten etabliert. Die *Engraftment*rate war bei den Biopsien im Vergleich zu den chirurgischen Resektaten geringer. In der Literatur sind unterschiedliche Erfolgsquoten für verschiedene Tumorentitäten (3 - 90 %) beschrieben, wobei direkte Vergleiche höhere *Engraftment*raten für chirurgische Resektate zeigen[121–125]. Studien zu HNSCC-Tumorproben beschreiben widersprüchliche Ergebnisse[126,127]. Die Vergleichbarkeit zwischen verschiedenen Studien ist aufgrund einer fehlenden Standardisierung und unterschiedlicher Angaben stark limitiert. Eine Ursache für die geringere Erfolgsquote der Biopsien ist vermutlich die Entnahme aus den exophytischen Bereichen des Tumors. Insgesamt konnten vier PDX aus HPV-assoziierten HNSCC-Fällen generiert werden. Drei davon stammen aus Biopsien. In der Grundlagenforschung existiert eine Unterrepräsentation von HPV-assoziierten HNSCC-Modellen aufgrund eines Mangels an entsprechenden Modellen. Dies ist wahrscheinlich auf das langsamere *in vitro* Wachstum von HPV-assoziierten Tumorproben zurückzuführen, aber auch der Tatsache geschuldet, das bei diesen Tumoren weniger Primäroperationen

durchgeführt werden und somit weniger Probenmaterial für die Forschung zur Verfügung steht[128,129]. Die Möglichkeit der Generierung von PDX aus Biopsien ist für die präklinische Forschung HPV-assoziierter HNSCC somit von hoher Bedeutung. Biopsien ermöglichen weiterhin die Generierung von Tumormodellen aus rezidivierenden und metastasierten Tumoren, die nicht operativ entfernt werden können. Gleichzeitig ist der Bedarf an neuen Therapieoptionen insbesondere für diese Tumoren aber besonders hoch[2,92,93]. Auf Grundlage der in Publikation 3 etablierten HNSCC-PDX Modelle wurden in Publikation 4 drei HPV-negative PDX-abgeleitete Zelllinien etabliert, mit dem Ziel die intertumorale Heterogenität von HNSCC an Zelllinien in niedriger Passage zu untersuchen. Die Tumore wurden von Patienten in fortgeschrittenen Stadien reseziert. Diese Patienten haben typischerweise eine infauste Prognose[2,92,93]. Der direkte Vergleich zwischen Patiententumoren, PDX und der entsprechenden Zelllinie zeigte, dass das molekulare Profil in den untersuchten frühen Passagen erhalten blieb. Dies spiegelte das eines HPV-negativen HNSCC wieder. So wurden *TP53*-Mutationen in allen drei Fällen, sowie *SMAD4*- und *CDKN2A*-Mutationen bei HNSCC48 detektiert[17,60]. Während bei HNSCC16 P1 M1 und HNSCC46 P0 M2 die Allelfrequenz in den zugehörigen Proben über die „Passagen“ erhalten blieb oder anstieg, sank sie bei der HNSCC48 P0 M1 vorübergehend. Eine Zunahme der Allelfrequenz lässt sich wahrscheinlich auf die Anreicherung mutierter Zellklone und/oder das Auswachsen eines dominanten Klons in der Zellkultur zurückführen. Das beobachtete vorübergehende Absinken ist wahrscheinlich der intratumoralen Heterogenität geschuldet und offenbart eine Limitation der Studie und Zelllinien allgemein. Es kann angenommen werden, dass sich ein Subklon in dem für die PDX-Generierung von HNSCC48 P0 M1 verwendeten Gewebe nicht an die *in vitro* Bedingungen anpassen konnte. Solide Tumoren entstehen zunächst aus einem einzigen veränderten Zellklon mit anhaltender Proliferationsfähigkeit und der Fähigkeit, dem Immunsystem zu entkommen. Mit dem Fortschreiten der Erkrankung entwickeln sich Subklone, die zusätzliche genomische Aberrationen erwerben. Bei HNSCC wurden bis zu sechs verschiedene Subklone nachgewiesen[7,130]. Weiterhin ist nur etwa ein Drittel der somatischen Mutationen ubiquitär in jeder Tumorregion nachweisbar[130,131]. Zellkulturen können die *in vivo* Situation daher nur teilweise widerspiegeln. Diese Limitation soll in dieser Arbeit durch eine umfassende zellbiologische und molekulare Charakterisierung überwunden werden. Neben einer unterschiedlichen *in vitro* Wachstumskinetik, sowie Unterschiede in der Morphologie, dem Invasionspotenzial, der Radiosensitivität und dem Tumormikromilieu zeigten sich auch molekulare Unterschiede. Diese zeigten bei HNSCC48 P0 M1 eine partielle *CDKN2A*-Deletion in Verbindung mit einer Chromosom-9-Polysomie (Verhältnis des *CDKN2A*-Gens zu Zentromeren des Chromosoms 3:1) und eine Chromosom-12-Polysomie, die mit einem Anstieg der *CDK4*-spezifischen Kopienzahl einherging. Bei HNSCC16 P1 M1 entsprachen die *CDKN2A*-Zugewinne den Kopien von Chromosom 9 (n = 4-5/Zelle), während diese bei

HNSCC46 P0 M2 unverändert blieben und lediglich eine Chromosom-9-Polysomie vorlag. Im Gegensatz zur HNSCC46 P0 M2 zeigte die HNSCC16 P1 M1 Polysomie-assoziierte *CDK4*-Zugewinne. Eine solch detaillierte Charakterisierung von Tumormodellen trägt zur Identifizierung neuer Biomarker bei[132,133].

Ausgehend von der überzeugenden Wirkung von Dinaciclib in Publikation 1 an Langzeit-etablierten HNSCC Zelllinien wurden weitere CDKi bezüglich ihrer Wirksamkeit bei HNSCC in Publikation 2 und 4 untersucht. Diese Untersuchungen erfolgten unter anderem an den selbst etablierten PDX-abgeleiteten Zelllinien und zeigten vielversprechende Ergebnisse, insbesondere in Kombination mit konventioneller Therapie. Alle Zelllinien waren empfindlich gegenüber 5-FU und Cisplatin, sowie den global wirkenden CDKis Dinaciclib und THZ1 (Ergebnisse zu Dinaciclib in Publikation 4 nicht gezeigt). In Publikation 2 wurde zusätzlich der CDK4/6i Palbociclib getestet, während in Publikation 4 Abemaciclib näher untersucht wurde. Letzteres basiert auf der zunehmenden Beobachtung einer effektiven Immunmodulation[134,135]. Während in Publikation 2 alle Zelllinien sensitiv gegenüber Palbociclib waren, konnten in Publikation 4 nach Abemaciclib Behandlung nur bei der Zelllinie HNSCC48 P0 M1 zytotoxische Effekte nachgewiesen werden. Es wurden vielseitige Wirkungen spezifischer CDKi Mono- und Kombinationstherapien beobachtet. Zu diesen zählen der apoptotische/nekrotische Zelltod, sowie die Methuose und Autophagie, ein G1-Phasenarrest, Auswirkungen auf Aktinfasern und Motilitätseigenschaften, die mitochondriale Aktivität, sowie immunologisch relevante Oberflächenmoleküle. Dabei zeigten sich Kombinationstherapien mit klassischen Zytostatika einer CDKi Monotherapie überlegen. *In vitro* verstärkten 5-FU und Cisplatin die Effekte einer CDKi Monotherapie und *in vivo* führte die Kombination von Dinaciclib und Cisplatin zu einer wirksamen Kontrolle des Tumorwachstums. In einer aktuellen Übersichtsarbeit von 2022 kommen Ettl *et al.* zu dem Schluss, dass CDKis in Monotherapie weniger effektiv wirken, als in Kombination mit Chemo-, Radio- oder Immuntherapie. Sie führen weiter aus, dass diese Kombinationstherapien besonders vielversprechend für HNSCC-Patienten seien[136]. In der Literatur finden sich sowohl Studien, die über eine antagonistische Wirkung bei einer Kombinationstherapie bestehend aus Chemotherapie und CDK4/6i berichten, als auch aktuelle Studien die ein verbessertes Ansprechen beschreiben[137–145]. Eine weitere Rationale für die Kombination von CDKis mit konventioneller Chemotherapie basiert auf der Reduktion toxischer Nebenwirkung in der klinischen Anwendung. So ist die durch die Hemmung von CDK4/6 erzielte Myeloprotektion ein vielversprechender Ansatz[146,147]. Auch aktuelle präklinische Studien zur Kombinationstherapie bestehend aus den global wirkenden CDKis Dinaciclib und THZ1 mit klassischer Chemotherapie zeigen verstärkende Effekte[148–151]. Dinaciclib zeigte starke zytotoxische Effekte, die mechanistisch wahrscheinlich auf eine frühe Apoptose mit einem anschließenden Übergang zur Nekrose zurückzuführen

sind, wie auch von Hossain *et al.* beschrieben[152]. Im Einklang mit der starken Zytotoxizität verringerte sich die Impedanz unter Dinaciclib-Mono- und Kombinationstherapie massiv. Die Messung der Impedanz eignet sich zur Detektion von Veränderungen der Zell-Zell-Kontakte den Adhäsionseigenschaften der Zellen und ihrer Membranintegrität in Echtzeit[153]. Ein vergleichbarer, aber verzögerter Rückgang der Impedanz wurde ebenfalls unter THZ1 und 5-FU Kombinationstherapie erreicht. Die Verzögerung ist wahrscheinlich auf den Wirkmechanismus von 5-FU zurückzuführen und wurde auch beim Wundheilungsversuch beobachtet[154]. Interessant ist die Beobachtung, dass die THZ1 Monotherapie zu einem leichten Anstieg der Impedanz führte. Begleitet wurde dies von einer Umstrukturierung des kortikalen Aktins in Stressfasern. Stressfasern erhöhen die zelluläre Steifigkeit und verringern die Motilität[155,156]. Veränderungen in der Morphologie wurden auch unter Abemaciclib bei der HNSCC16 P1 M1 beobachtet. Die Zellen waren geschwollen und zeigten eine erhöhte Anzahl saurer Organellen, als ein erstes Indiz für Autophagie[157]. Vergleichbare Effekte wurden auch für Glioblastomzellen beschrieben[47]. In prospektiven Studien sollte der Einfluss von CDKis auf das Zytoskelett und die damit einhergehenden Folgen für zum Beispiel eine Erkennung durch Immunzellen oder die Metastasierung näher untersucht werden. Die bekannteste Reaktion auf die CDKi Behandlung ist die Veränderung des Zellzyklus. Der G1-Phasenstillstand nach Palbociclib Therapie war aufgrund der Wirkungsweise des CDK4/6i zu erwarten[158,159]. Die Dinaciclib-Mono- und Kombinationstherapie verstärkte die mitochondriale Aktivität. Für CDK4/6i sind verschiedene immunmodulatorische Effekte beschrieben. Dazu zählen unter anderem eine verstärkte Antigenpräsentation durch Tumorzellen (Hochregulierung von MHC I), die Sekretion proinflammatorischer Zytokine und Chemokine, die Aktivierung von Effektor-T-Zellen oder auch die Inhibition regulatorischer T-Zellen[160,161]. Ursächlich ist die Hochregulation von PD-L1 wahrscheinlich auf die Hemmung von CDK4 zurückzuführen, da CyclinD-CDK4 an der Vermittlung der Ubiquitinierung und des Abbaus von PD-L1 beteiligt ist[81]. Auch in dieser Arbeit wurde unter dem Einfluss einer CDKi Therapie ein Einfluss auf MHC I, PD-1, PD-L1 und Calreticulin (CalR) beschrieben. Verstärkt wurden die Effekte durch Kombination mit 5-FU oder Cisplatin. Dies macht die CDKis in Kombination mit Immuntherapie besonders interessant. Da die PD-L1 Proteinabundanz innerhalb der einzelnen Zellzyklusphasen fluktuiert, sollten in zukünftigen Analysen des Oberflächenmoleküls die Zellen zuvor synchronisiert werden, um Schwankungen in den Messungen zu vermeiden[81]. CDKis zeigen folglich verschiedenste Effekte auf HNSCC-Tumorzelllinien, die sich in Kombination mit klassischer Chemotherapie häufig noch verstärken lassen. Eine mögliche Erklärung für die beobachtete Zytotoxizität bei HNSCC48 P0 M1 ist die partielle Deletion von *CDKN2A* bei dieser Zelllinie. Im Gegensatz zur HNSCC46 P0 M2 zeigte die HNSCC16 P1 M1 und HNSCC48 P0 M1, wie bereits erwähnt, Polysomie-assoziierte *CDK4*-Zugewinne. Dies könnte ein mögliches molekulares Korrelat darstellen, warum die HNSCC16 P1 M1 zwar keine

zytotoxischen Effekte nach Abemaciclib Behandlung zeigte, jedoch durchaus morphologische Veränderungen. Vergleichbare Effekte waren bei der HNSCC46 P0 M2 nicht nachweisbar. Eine Resistenzentwicklung gegenüber der klinisch zugelassenen CDK4/6i gilt bei den meisten Patienten als unvermeidlich. Die zugrunde liegenden Mechanismen sind multifaktoriell und die Forschung in diesem Gebiet noch in der Entwicklung. Biomarker, die in der Lage sind, eine frühzeitige Resistenz zu erkennen oder die Wahrscheinlichkeit einer erfolgreichen Behandlung mit CDK4/6is vorherzusagen, müssen erst noch weiter identifiziert werden und stellen einen Bereich mit klinischem Bedarf dar. Dabei muss zwischen einer intrinsischen Resistenz, wie von uns beschrieben und einer extrinsischen Resistenz unterschieden werden[162,163]. Erste präklinischen Studien beim Mammakarzinom deuten auf einen Verlust des Rb-Proteins als Ursache für die Resistenz gegen CDK4/6i hin[57,66,67,164,165]. Weitere beschriebene extrinsische Resistenzmechanismen gegen CDK4/6i inkludieren Mutationen im Rb-Protein, die zu einer Aktivierung anderer Zellzyklusfaktoren wie E2F und der CyclinE/CDK2-Achse führen, eine Zunahme von CDK6, eine Hochregulierung des PI3K/mTOR-Signalweges, welche wiederum zu einer Hochregulierung von Cyclin D führt und eine Induktion von Autophagie[66,136,137,166,167].

Auf Grundlage der molekularen Analysen wird die Hypothese aufgestellt, dass die geschilderte Aberration in Form von *CDK4*-Zugenwinnen sich als Biomarker für ein individuelles Ansprechen auf Abemaciclib eignet. Bemerkenswert ist die Tatsache, dass die Abemaciclib-Resistenz bei HNSCC16 P1 M1 durch Zugabe von Cisplatin reversibel war. Dies verdeutlicht das Potenzial von Kombinationstherapien, besonders im Kontext von Resistenzen. Die Herausforderung, das Ansprechen auf Medikamente zu verbessern, wird teilweise auf die Hochregulierung von Genen zurückgeführt, die eine Resistenz vermitteln. Ein bekannter Marker ist *c-MYC* und war auch in den etablierten Zelllinien der Publikation 4 höher als in der angrenzenden normalen Mukosa[168]. In HNSCC16 P1 M1 führte Cisplatin zu einer Herunterregulierung der Resistenz-assoziierten Gene *c-MYC* und *IDO1* und in Kombination mit Abemaciclib war *IDO1* nicht mehr nachweisbar, während die Abemaciclib Monotherapie die *c-MYC* Genexpression leicht erhöhte. Eine frühere Studie zeigte für Abemaciclib den gegenteiligen Effekt bezüglich der *c-MYC* Genexpression nach Abemaciclib Behandlung, jedoch bei Schilddrüsenkrebs[169]. Diese Herunterregulierung in der Kombinationstherapie mit Cisplatin wurde auch bei der HNSCC46 P0 M2 für *IDO1* beobachtet, nachdem die Abemaciclib Monotherapie die Genexpression von *IDO1* erhöhte. In der Literatur finden sich dazu keine Daten.

Diese Arbeit zeigt, dass gut charakterisierte Tumormodelle bei der Identifizierung wirksamer Therapie (-kombinationen) hilfreich sind und eine wichtige Rolle bei der Detektion intrinsischer Resistenzmechanismen spielen. Sie verdeutlicht aber auch, dass vor dem Hintergrund der intertumoralen Heterogenität von HNSCC eine umfassende Charakterisierung notwendig ist,

um allgemeingültige Aussagen zwischen den untersuchten Zelllinien ziehen zu können bzw. unterschiedliche Ergebnisse erklärbar zu machen und potenzielle neue Marker zu identifizieren. Zudem liefert sie weitere Hinweise für das therapeutische Potenzial der CDKis und zeigt, dass diese mit klassischer Chemotherapie kombiniert werden können. Diese Erkenntnisse tragen zu unserem Verständnis bei, wie die Behandlung von HNSCC perspektivisch verbessert werden kann. Neben ihrer bekannten Funktion als Zellzyklusregulatoren wird immer deutlicher, dass CDKs auch bei anderen Prozessen, wie der Transkription, epigenetischer Regulation, Stoffwechsel, Selbsterneuerung von Stammzellen, neuronalen Funktionen und Dynamik des Zytoskeletts eine wichtige Rolle spielen, sodass bislang lediglich ein Teil des Potenzial des CDKis genauer erforscht ist [50,170]. Prospektive Studien sollten sich einerseits auf die Auswirkungen der CDKis auf Immunzellen konzentrieren, insbesondere aufgrund des Potenzials, die Immunogenität von Tumoren zu erhöhen. Ferner sollten Resistenzmechanismen stärker in den Fokus rücken. Besonders interessant ist in diesem Kontext die kürzlich veröffentlichte Publikation von Heckler *et al.,* in der beschrieben wird, dass Abemaciclib zu einer Anreicherung von $CD8^+$-Gedächtnisvorläuferzellen führt, die eine langfristig schützende Immunität vermitteln könnten[134]. In diesem Zusammenhang wurde in Kooperation mit der Klinik und Poliklinik für Mund-, Kiefer-, und Plastische Gesichtschirurgie, Rostock ein fluides Ko-Kultursystem für Tumor- und Immunzellen etabliert, welches die Simulation physiologischer Perfusion deutlich besser als in einem statischen System ermöglicht. Dieses ist für weiterführende immunologische Studien, insbesondere auch in einem autologen Setting, prädestiniert. Weitere aktuelle Arbeiten fokussieren sich auf extrinsische Resistenzmechanismen gegenüber CDKis. Hierzu konnten in begleitenden Arbeiten bereits CDKi resistente HNSCC Zelllinien etabliert werden. Diese komplexen Untersuchungen werden dazu beitragen, die Wirkmechanismen von CDKis gegenüber Tumor- und Immunzellen weiter aufzuklären, um perspektivisch die Wertigkeit dieser Therapieform für das HNSCC abschätzen zu können.

6. Zusammenfassung

In dieser Arbeit wurde zunächst an Langzeit-kultivierten Zelllinien die Wirksamkeit von ausgewählten CDKis beim HNSCC untersucht, verschiedene funktionelle Analysen durchgeführt und die Ergebnisse mit Angaben aus der Literatur verglichen. Dabei zeigte sich eine grundsätzliche Wirksamkeit von CDKis, die sich in Kombination mit klassischen Therapeutika, wie Cisplatin und 5-FU teilweise noch verstärken ließen. Neben den grundlegenden funktionellen Mechanismen, inklusive der Induktion von Apoptose/Nekrose, dem Zellzyklusarrest, der Verringerung der Invasivität, der strahleninduzierten DNA-Doppelstrangbrüche, dem Einfluss auf die Aktinfilamente, sowie den Mitochondrien, dem

endoplasmatischen Retikulum und der Vakuolisierung, lag der Fokus dabei auch auf den immunmodulatorischen Effekten. Diese umfassten sowohl die Suppression des Kynureninstoffwechsels, als auch die Induzierbarkeit der immunologisch relevanten Moleküle, MHC I und CalR.

Die Heterogenität von Kopf-Hals-Tumoren bedingt personalisierte Therapien, die für die präklinische Forschung gut charakterisierte Tumormodelle voraussetzen. Vor diesem Hintergrund wurde zunächst die Infrastruktur für eine Biobank aufgebaut. In diesem interdisziplinären Projekt, an dem verschiedene Kliniken der Universitätsmedizin Rostock beteiligt sind, wurde HNSCC Gewebe von endoskopischen Biopsien und OP-Resektaten eingeschlossen. Im Anschluss erfolgte die Etablierung und histomorphologische, sowie molekulare Charakterisierung individueller PDX Modelle. In einem nachfolgenden Ansatz wurden Zelllinien aus individuellen PDX-Modellen abgeleitet und umfassend *in vitro* charakterisiert. An diesen in niedriger Passage gehaltenen Zelllinien wurden erneut funktionelle Analysen mit dem Schwerpunkt CDKi und Zytostatika durchgeführt. Dabei bestätigte sich, dass CDKis unter Voraussetzung gewisser molekularer Aberrationen (*TP53* Mutation, *CDKN2A* Deletion, *CDK4* Zugewinne durch Chromosom 12 Polysomie) eine Wirksamkeit gegenüber HNSCC zeigen, aber Kombinationentherapien mit Zytostatika nötig sind, um die Effekte der zielgerichteten Substanzen zu verstärken. Weiterführende Studien sollten sich auf die Auswirkungen der CDKis auf die Immunzellen konzentrieren, insbesondere aufgrund des Potenzials von CDKi, die Tumorimmunogenität zu erhöhen. Außerdem sollte eine mögliche Resistenzentwicklung nach CDKi Behandlung untersucht werden, um frühzeitig zu intervenieren.

Zusammenfassung

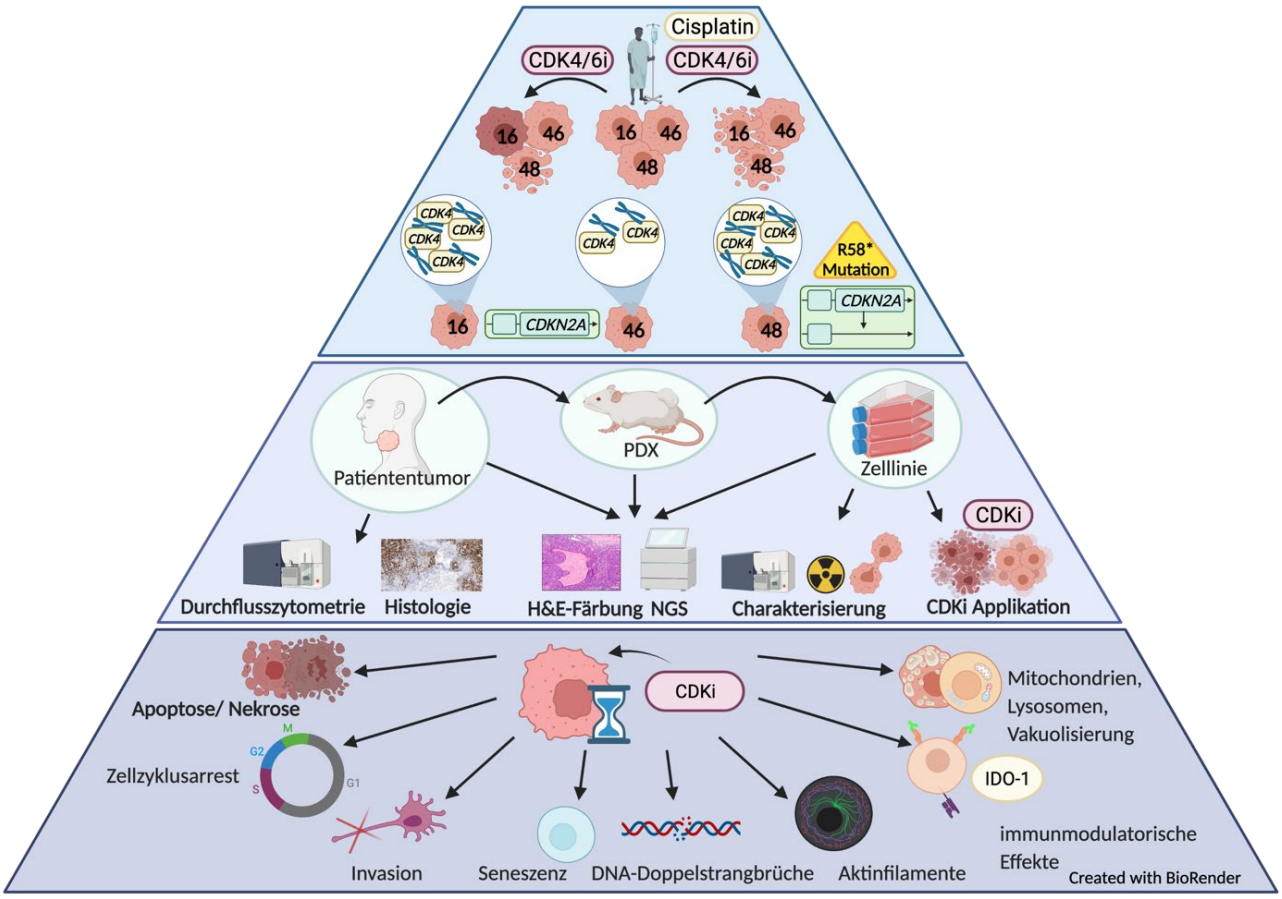

Abbildung 2: Schematische Darstellung der in dieser Arbeit erzielten Ergebnisse.

7. Literaturverzeichnis

1 Argiris A, Karamouzis M v., Raben D, Ferris RL. Head and neck cancer. The Lancet. 2008; **371**: 1695–1709.

2 Grünwald V, Chirovsky D, Cheung WY, Bertolini F, Ahn MJ, Yang MH *et al.* Global treatment patterns and outcomes among patients with recurrent and/or metastatic head and neck squamous cell carcinoma: Results of the GLANCE H&N study. *Oral Oncology* 2020; **102**. doi:10.1016/j.oraloncology.2019.104526.

3 Canning M, Guo G, Yu M, Myint C, Groves MW, Byrd JK *et al.* Heterogeneity of the head and neck squamous cell carcinoma immune landscape and its impact on immunotherapy. Frontiers in Cell and Developmental Biology. 2019; **7**: 52.

4 Keck MK, Zuo Z, Khattri A, Stricker TP, Brown CD, Imanguli M *et al.* Integrative Analysis of Head and Neck Cancer Identifies Two Biologically Distinct HPV and Three Non-HPV Subtypes. *Clinical Cancer Research* 2015; **21**: 870–881.

5 Robert Koch-Institut. Krebs in Deutschland | 2015/2016. *Robert Koch-Institut* 2019; **12**.www.krebsdaten.de. (accessed 12 Nov2021).

6 McDermott JD, Bowles DW. Epidemiology of Head and Neck Squamous Cell Carcinomas: Impact on Staging and Prevention Strategies. *Current Treatment Options in Oncology* 2019; **20**: 1–13.

7 Morris LGT, Chandramohan R, West L, Zehir A, Chakravarty D, Pfister DG *et al.* The molecular landscape of recurrent and metastatic head and neck cancers insights from a precision oncology sequencing platform. *JAMA Oncology* 2017; **3**: 244–255.

8 Puram S v., Rocco JW, America OC of N. Molecular Aspects of Head and Neck Cancer Therapy. *Hematology/oncology clinics of North America* 2015; **29**: 971.

9 Kühn JP, Schmid W, Körner S, Bochen F, Wemmert S, Rimbach H *et al.* Hpv status as prognostic biomarker in head and neck cancer—which method fits the best for outcome prediction? *Cancers* 2021; **13**. doi:10.3390/cancers13184730.

10 Huang SH, O'Sullivan B. Overview of the 8th Edition TNM Classification for Head and Neck Cancer. *Current treatment options in oncology* 2017; **18**. doi:10.1007/S11864-017-0484-Y.

11 Lin PC, Yeh YM, Hsu HP, Chan RH, Lin BW, Chen PC *et al.* Comprehensively exploring the mutational landscape and patterns of genomic evolution in hypermutated cancers. *Cancers* 2021; **13**: 4317.

12 Alexandrov LB, Nik-Zainal S, Wedge DC, Aparicio SAJR, Behjati S, Biankin A v. *et al.* Signatures of mutational processes in human cancer. *Nature* 2013; **500**: 415.

13 Fasano M, Perri F, Corte CM della, di Liello R, Scarpati GDV, Cascella M *et al.* Translational insights and new therapeutic perspectives in head and neck tumors. *Biomedicines* 2021; **9**. doi:10.3390/BIOMEDICINES9081045/S1.

14 Solomon B, Young RJ, Rischin D. Head and neck squamous cell carcinoma: Genomics and emerging biomarkers for immunomodulatory cancer treatments. Seminars in Cancer Biology. 2018; **52**: 228–240.

15 Seiwert TY, Zuo Z, Keck MK, Khattri A, Pedamallu CS, Stricker T *et al.* Integrative and Comparative Genomic Analysis of HPV-Positive and HPV-Negative Head and Neck Squamous Cell Carcinomas. *Clinical Cancer Research* 2015; **21**: 632–641.

16 Lawrence MS, Sougnez C, Lichtenstein L, Cibulskis K, Lander E, Gabriel SB *et al.* Comprehensive genomic characterization of head and neck squamous cell carcinomas. *Nature* 2015; **517**: 576.

17 Farah CS. Molecular landscape of head and neck cancer and implications for therapy. *Annals of Translational Medicine* 2021; **9**: 915–915.

18 Lu DW, El-Mofty SK, Wang HL. Expression of p16, Rb, and p53 proteins in squamous cell carcinomas of the anorectal region harboring human papillomavirus DNA. *Modern Pathology* 2003; **16**: 692–699.

19 Moody CA, Laimins LA. Human papillomavirus oncoproteins: pathways to transformation. *Nature Reviews Cancer 2010 10:8* 2010; **10**: 550–560.

20 Cho NH, Kim YT, Kim JW. Alteration of cell cycle in cervical tumor associated with human papillomavirus: cyclin-dependent kinase inhibitors. *Yonsei medical journal* 2002; **43**: 722–728.

21 Seliger B, Massa C, Yang B, Bethmann D, Kappler M, Eckert AW *et al.* Immune Escape Mechanisms and Their Clinical Relevance in Head and Neck Squamous Cell Carcinoma. *International Journal of Molecular Sciences* 2020; **21**: 1–17.

22 Moy JD, Moskovitz JM, Ferris RL. Biological mechanisms of immune escape and implications for immunotherapy in head and neck squamous cell carcinoma. European Journal of Cancer. 2017; **76**: 152–166.

23 Müller T, Braun M, Dietrich D, Aktekin S, Höft S, Kristiansen G *et al.* PD-L1: a novel prognostic biomarker in head and neck squamous cell carcinoma. *Oncotarget* 2017; **8**: 52889–52900.

24 de Meulenaere A, Vermassen T, Creytens D, Aspeslagh S, Deron P, Duprez F *et al.* Importance of choice of materials and methods in PD-L1 and TIL assessment in oropharyngeal squamous cell carcinoma. *Histopathology* 2018; **73**: 500–509.

25 Boros FA, Vécsei L. Immunomodulatory Effects of Genetic Alterations Affecting the Kynurenine Pathway. *Frontiers in Immunology* 2019; **10**: 2570.

26 Liu M, Wang X, Wang L, Ma X, Gong Z, Zhang S *et al.* Targeting the IDO1 pathway in cancer: from bench to bedside. *Journal of hematology & oncology* 2018; **11**. doi:10.1186/S13045-018-0644-Y.

27 Platten M, Wick W, van den Eynde BJ. Tryptophan catabolism in cancer: beyond IDO and tryptophan depletion. *Cancer research* 2012; **72**: 5435–5440.

28 Boros FA, Bohár Z, Vécsei L. Genetic alterations affecting the genes encoding the enzymes of the kynurenine pathway and their association with human diseases. *Mutation research Reviews in mutation research* 2018; **776**: 32–45.

29 Fiedorowicz M, Choragiewicz T, Thaler S, Schuettauf F, Nowakowska D, Wojtunik K *et al.* Tryptophan and Kynurenine Pathway Metabolites in Animal Models of Retinal and Optic Nerve Damage: Different Dynamics of Changes. *Frontiers in Physiology* 2019; **10**: 1254.

30 Leitlinienprogramm Onkologie der Arbeitsgemeinschaft der Wissenschaftlichen Medizinischen Fachgesellschaften, Deutsche Krebsgesellschaft, Deutsche Krebshilfe. S3-Leitlinie Diagnostik und Therapie des Mundhöhlenkarzinoms. 2021.https://www.leitlinienprogramm-onkologie.de/fileadmin/user_upload/Downloads/Leitlinien/Mundhoehlenkarzinom/Version_3/LL_Mundhoehlenkarzinom_Langversion_3.0.pdf (accessed 16 Nov2021).

31 Cohen EEW, Bell RB, Bifulco CB, Burtness B, Gillison ML, Harrington KJ *et al.* The Society for Immunotherapy of Cancer consensus statement on immunotherapy for the treatment of squamous cell carcinoma of the head and neck (HNSCC). *Journal for Immunotherapy of Cancer* 2019; **7**. doi:10.1186/S40425-019-0662-5.

32 Le X, Ferrarotto R, Wise-Draper T, Gillison M. Evolving Role of Immunotherapy in Recurrent Metastatic Head and Neck Cancer. *Journal of the National Comprehensive Cancer Network* 2020; **18**: 899–906.

33 Lum DH, Matsen C, Welm AL, Welm BE. Human Primary Tumorgraft Models: Comparisons with Traditional Oncology Pre-Clinical Models and The Clinical Relevance and Utility of Primary Tumorgrafts in Basic and Translational Oncology Research. *Current Protocols in Pharmacology* 2012; **CHAPTER**: Unit14.22.

34 Tinhofer I, Braunholz D, Klinghammer K. Preclinical models of head and neck squamous cell carcinoma for a basic understanding of cancer biology and its translation into efficient therapies. *Cancers of the Head & Neck* 2020; **5**: 9.

35 Sajjad H, Imtiaz S, Noor T, Siddiqui YH, Sajjad A, Zia M. Cancer models in preclinical research: A chronicle review of advancement in effective cancer research. *Animal Models and Experimental Medicine* 2021; **4**: 87–103.

36 Ogilvie LA, Kovachev A, Wierling C, Lange BMH, Lehrach H. Models of models: A translational route for cancer treatment and drug development. *Frontiers in Oncology* 2017; **7**: 219.

37 Białkowska K, Komorowski P, Bryszewska M, Miłowska K. Spheroids as a type of three-dimensional cell cultures—examples of methods of preparation and the most important application. *International Journal of Molecular Sciences* 2020; **21**: 1–17.

38 Richter M, Piwocka O, Musielak M, Piotrowski I, Suchorska WM, Trzeciak T. From Donor to the Lab: A Fascinating Journey of Primary Cell Lines. *Frontiers in Cell and Developmental Biology* 2021; **9**: 1869.

39 Lai Y, Wei X, Lin S, Qin L, Cheng L, Li P. Current status and perspectives of patient-derived xenograft models in cancer research. *Journal of Hematology & Oncology* 2017; **10**. doi:10.1186/S13045-017-0470-7.

40 Karamboulas C, Bruce JP, Hope AJ, Meens J, Huang SH, Erdmann N *et al.* Patient-Derived Xenografts for Prognostication and Personalized Treatment for Head and Neck Squamous Cell Carcinoma. *Cell reports* 2018; **25**: 1318-1331.e4.

41 Peng S, Creighton CJ, Zhang Y, Sen B, Mazumdar T, Myers JN *et al.* Tumor grafts derived from patients with head and neck squamous carcinoma authentically maintain the molecular and histologic characteristics of human cancers. *Journal of Translational Medicine* 2013; **11**: 1–11.

42 Hadjicharalambous M, Wijeratne PA, Vavourakis V. From tumour perfusion to drug delivery and clinical translation of in silico cancer models. *Methods* 2021; **185**: 82–93.

43 Jingwen B, Yaochen L, Guojun Z. Cell cycle regulation and anticancer drug discovery. *Cancer Biology & Medicine* 2017; **14**: 348.

44 Roskoski R. Cyclin-dependent protein serine/threonine kinase inhibitors as anticancer drugs. *Pharmacological Research* 2019; **139**: 471–488.

45 Sánchez-Martínez C, Lallena MJ, Sanfeliciano SG, de Dios A. Cyclin dependent kinase (CDK) inhibitors as anticancer drugs: Recent advances (2015–2019). Bioorganic and Medicinal Chemistry Letters. 2019; **29**. doi:10.1016/j.bmcl.2019.126637.

46 Giannone G, Tuninetti V, Ghisoni E, Genta S, Scotto G, Mittica G *et al.* Role of Cyclin-Dependent Kinase Inhibitors in Endometrial Cancer. *International Journal of Molecular Sciences* 2019; **20**. doi:10.3390/IJMS20092353.

47 Riess C, Koczan D, Schneider B, Linke C, del Moral K, Classen CF *et al.* Cyclin-dependent kinase inhibitors exert distinct effects on patient-derived 2D and 3D glioblastoma cell culture models. *Cell Death Discovery* 2021; **7**: 54.

48 Schoninger SF, Blain SW. The ongoing search for biomarkers of CDK4/6 inhibitor responsiveness in breast cancer. Molecular Cancer Therapeutics. 2020; **19**: 3–12.

49 Rahaman MH, Lam F, Zhong L, Teo T, Adams J, Yu M *et al.* Targeting CDK9 for treatment of colorectal cancer. *Molecular oncology* 2019; **13**: 2178–2193.

50 Lim S, Kaldis P. Cdks, cyclins and CKIs: roles beyond cell cycle regulation. *Development (Cambridge, England)* 2013; **140**: 3079–93.

51 Parry D, Guzi T, Shanahan F, Davis N, Prabhavalkar D, Wiswell D *et al.* Dinaciclib (SCH 727965), a novel and potent cyclin-dependent kinase inhibitor. *Molecular Cancer Therapeutics* 2010; **9**: 2344–2353.

52 Olson CM, Liang Y, Leggett A, Park WD, Li L, Mills CE *et al.* Development of a Selective CDK7 Covalent Inhibitor Reveals Predominant Cell-Cycle Phenotype. *Cell Chemical Biology* 2019; **26**: 792-803.e10.

53 Li B-B, Wang B, Zhu C-M, Tang D, Pang J, Zhao J *et al.* Cyclin-dependent kinase 7 inhibitor THZ1 in cancer therapy. *Chronic Diseases and Translational Medicine* 2019; **5**: 155.

54 Sobhani N, Fassl A, Mondani G, Generali D, Otto T. Targeting Aberrant FGFR Signaling to Overcome CDK4/6 Inhibitor Resistance in Breast Cancer. Cells. 2021; **10**. doi:10.3390/cells10020293.

55 George MA, Qureshi S, Omene C, Toppmeyer DL, Ganesan S. Clinical and Pharmacologic Differences of CDK4/6 Inhibitors in Breast Cancer. *Frontiers in Oncology* 2021; **11**. doi:10.3389/FONC.2021.693104.

56 Goel S, Decristo MJ, Watt AC, Brinjones H, Sceneay J, Li BB *et al.* CDK4/6 inhibition triggers anti-tumor immunity. *Nature* 2017; **548**: 471.

57 Riess C, Irmscher N, Salewski I, Strüder D, Classen CF, Große-Thie C *et al.* Cyclin-dependent kinase inhibitors in head and neck cancer and glioblastoma—backbone or add-on in immune-oncology? *Cancer and Metastasis Reviews* 2020. doi:10.1007/s10555-020-09940-4.

58 Parylo S, Vennepureddy A, Dhar V, Patibandla P, Sokoloff A. Role of cyclin-dependent kinase 4/6 inhibitors in the current and future eras of cancer treatment. *Journal of Oncology Pharmacy Practice* 2019; **25**: 110–129.

59 Pickering CR, Zhang J, Yoo SY, Bengtsson L, Moorthy S, Neskey DM *et al.* Integrative genomic characterization of oral squamous cell carcinomaidentifies frequent somatic drivers. *Cancer discovery* 2013; **3**: 770–781.

60 Zhou G, Liu Z, Myers JN. TP53 Mutations in Head and Neck Squamous Cell Carcinoma and Their Impact on Disease Progression and Treatment Response. *Journal of cellular biochemistry* 2016; **117**: 2682.

61 Leemans CR, Snijders PJF, Brakenhoff RH. The molecular landscape of head and neck cancer. *Nature Reviews Cancer 2018 18:5* 2018; **18**: 269–282.

62 Levine AJ, Oren M. The first 30 years of p53: growing ever more complex. *Nature reviews Cancer* 2009; **9**: 749.

63 Göttgens EL, Bussink J, Leszczynska KB, Peters H, Span PN, Hammond EM. Inhibition of CDK4/CDK6 Enhances Radiosensitivity of HPV Negative Head and Neck Squamous Cell Carcinomas. *International Journal of Radiation Oncology Biology Physics* 2019; **105**: 548–558.

64 Shapiro GI. Cyclin-dependent kinase pathways as targets for cancer treatment. *Journal of clinical oncology : official journal of the American Society of Clinical Oncology* 2006; **24**: 1770–1783.

65 Billard-Sandu C, Tao YG, Sablin MP, Dumitrescu G, Billard D, Deutsch E. CDK4/6 inhibitors in P16/HPV16-negative squamous cell carcinoma of the head and neck. *European archives of oto-rhino-laryngology : official journal of the European Federation of Oto-Rhino-Laryngological Societies (EUFOS) : affiliated with the German Society for Oto-Rhino-Laryngology - Head and Neck Surgery* 2020; **277**: 1273–1280.

66 Condorelli R, Spring L, O'Shaughnessy J, Lacroix L, Bailleux C, Scott V *et al.* Polyclonal RB1 mutations and acquired resistance to CDK 4/6 inhibitors in patients with metastatic breast cancer. *Annals of oncology : official journal of the European Society for Medical Oncology* 2018; **29**: 640–645.

67 Herrera-Abreu MT, Palafox M, Asghar U, Rivas MA, Cutts RJ, Garcia-Murillas I *et al.* Early Adaptation and Acquired Resistance to CDK4/6 Inhibition in Estrogen Receptor-Positive Breast Cancer. *Cancer research* 2016; **76**: 2301–2313.

68 Adkins D, Ley J, Neupane P, Worden F, Sacco AG, Palka K *et al.* Palbociclib and cetuximab in platinum-resistant and in cetuximab-resistant human papillomavirus-unrelated head and neck cancer: a multicentre, multigroup, phase 2 trial. *The Lancet Oncology* 2019; **20**: 1295–1305.

69 Billard-Sandu C, Tao YG, Sablin MP, Dumitrescu G, Billard D, Deutsch E. CDK4/6 inhibitors in P16/HPV16-negative squamous cell carcinoma of the head and neck. European Archives of Oto-Rhino-Laryngology. 2020; **277**: 1273–1280.

70 van Caloen G, MacHiels JP. Potential role of cyclin-dependent kinase 4/6 inhibitors in the treatment of squamous cell carcinoma of the head and neck. *Current opinion in oncology* 2019; **31**: 122–130.

71 Yuan J, Jiang YY, Mayakonda A, Huang M, Ding LW, Lin H *et al.* Super-Enhancers Promote Transcriptional Dysregulation in Nasopharyngeal Carcinoma. *Cancer research* 2017; **77**: 6614–6626.

72 Ge H, Yao Y, Jiang Y, Wu X, Wang Y. Pharmacological inhibition of CDK7 by THZ1 impairs tumor growth in p53-mutated HNSCC. *Oral diseases* 2021. doi:10.1111/ODI.13783.

73 Zhang W, Ge H, Jiang Y, Huang R, Wu Y, Wang D *et al.* Combinational therapeutic targeting of BRD4 and CDK7 synergistically induces anticancer effects in head and neck squamous cell carcinoma. *Cancer Letters* 2020; **469**: 510–523.

74 Gotwals P, Cameron S, Cipolletta D, Cremasco V, Crystal A, Hewes B *et al.* Prospects for combining targeted and conventional cancer therapy with immunotherapy. *Nature Reviews Cancer 2017 17:5* 2017; **17**: 286–301.

75 Ahn R, Ursini-Siegel J. Clinical Potential of Kinase Inhibitors in Combination with Immune Checkpoint Inhibitors for the Treatment of Solid Tumors. *International Journal of Molecular Sciences* 2021; **22**: 1–23.

76 Dasari S, Bernard Tchounwou P. Cisplatin in cancer therapy: Molecular mechanisms of action. *European Journal of Pharmacology* 2014; **740**: 364–378.

77 Robinson AM, Rathore R, Redlich NJ, Adkins DR, VanArsdale T, van Tine BA *et al.* Cisplatin exposure causes c-Myc-dependent resistance to CDK4/6 inhibition in HPV-negative head and neck squamous cell carcinoma. *Cell death & disease* 2019; **10**: 867.

78 Deep G, Agarwal R. New combination therapies with cell-cycle agents. Current Opinion in Investigational Drugs. 2008; **9**: 591–604.

79 Colli LM, Machiela MJ, Zhang H, Myers TA, Jessop L, Delattre O *et al.* Landscape of combination immunotherapy and targeted therapy to improve cancer management. *Cancer research* 2017; **77**: 3666.

80 Vanneman M, Dranoff G. Combining Immunotherapy and Targeted Therapies in Cancer Treatment. *Nature reviews Cancer* 2012; **12**: 237.

81 Zhang J, Bu X, Wang H, Zhu Y, Geng Y, Nihira NT *et al.* Cyclin D-CDK4 kinase destabilizes PD-L1 via cullin 3-SPOP to control cancer immune surveillance. *Nature* 2018; **553**: 91–95.

82 Matthews HK, Bertoli C, de Bruin RAM. Cell cycle control in cancer. *Nature Reviews Molecular Cell Biology 2021* 2021; : 1–15.

83 Zhao R, Choi BY, Lee MH, Bode AM, Dong Z. Implications of Genetic and Epigenetic Alterations of CDKN2A (p16INK4a) in Cancer. *EBioMedicine* 2016; **8**: 30–39.

84 Oppel F, Shao S, Schürmann M, Goon P, Albers AE, Sudhoff H. An Effective Primary Head and Neck Squamous Cell Carcinoma In Vitro Model. *Cells* 2019; **8**: 555.

85 Shibata H, Saito S, Uppaluri R. Immunotherapy for Head and Neck Cancer: A Paradigm Shift From Induction Chemotherapy to Neoadjuvant Immunotherapy. *Frontiers in Oncology* 2021; **11**: 3533.

86 Guo W, Chen X, Zhu L, Wang Q. A six-mRNA signature model for the prognosis of head and neck squamous cell carcinoma. *Oncotarget* 2017; **8**: 94528.

87 Olivier M, Asmis R, Hawkins GA, Howard TD, Cox LA. The Need for Multi-Omics Biomarker Signatures in Precision Medicine. *International Journal of Molecular Sciences* 2019; **20**. doi:10.3390/IJMS20194781.

88 Gong W, Xiao Y, Wei Z, Yuan Y, Qiu M, Sun C *et al.* Toward the use of precision medicine for the treatment of head and neck squamous cell carcinoma. *Oncotarget* 2017; **8**: 2141.

89 Cadoni G, Giraldi L, Petrelli L, Pandolfini M, Giuliani M, Paludetti G *et al.* Prognostic factors in head and neck cancer: a 10-year retrospective analysis in a single-institution in Italy. *Acta Otorhinolaryngologica Italica* 2017; **37**: 458.

90 Szturz P, van Laer C, Simon C, van Gestel D, Bourhis J, Vermorken JB. Follow-Up of Head and Neck Cancer Survivors: Tipping the Balance of Intensity. *Frontiers in Oncology* 2020; **10**: 688.

91 Stromberger C, Yedikat B, Coordes A, Tinhofer I, Kalinauskaite G, Budach V *et al.* Prognostic Factors Predict Oncological Outcome in Older Patients With Head and Neck Cancer Undergoing Chemoradiation Treatment. *Frontiers in Oncology* 2021; **10**: 3253.

92 Ionna F, Bossi P, Guida A, Alberti A, Muto P, Salzano G *et al.* Recurrent/Metastatic Squamous Cell Carcinoma of the Head and Neck: A Big and Intriguing Challenge Which May Be Resolved by Integrated Treatments Combining Locoregional and Systemic Therapies. *Cancers* 2021; **13**. doi:10.3390/CANCERS13102371.

93 Magnes T, Melchardt T, Weiss L, Mittermair C, Neureiter D, Klieser E *et al.* Prognostic score in patients with recurrent or metastatic carcinoma of the head and neck treated with cetuximab and chemotherapy. *PLOS ONE* 2017; **12**: e0180995.

94 Mroz EA, Rocco JW. Intra-tumor heterogeneity in head and neck cancer and its clinical implications. *World Journal of Otorhinolaryngology - Head and Neck Surgery* 2016; **2**: 60.

95 Galot R, le Tourneau C, Guigay J, Licitra L, Tinhofer I, Kong A *et al.* Personalized biomarker-based treatment strategy for patients with squamous cell carcinoma of the head and neck: EORTC position and approach. *Annals of Oncology* 2018; **29**: 2313–2327.

96 Taberna M, Oliva M, Mesía R. Cetuximab-containing combinations in locally advanced and recurrent or metastatic head and neck squamous cell carcinoma. *Frontiers in Oncology* 2019; **9**: 383.

97 Gebre-Medhin M, Brun E, Engström P, Cange HH, Hammarstedt-Nordenvall L, Reizenstein J *et al.* ARTSCAN III: A Randomized Phase III Study Comparing Chemoradiotherapy With Cisplatin Versus Cetuximab in Patients With Locoregionally Advanced Head and Neck Squamous Cell Cancer. *Journal of clinical oncology : official journal of the American Society of Clinical Oncology* 2021; **39**: 38–47.

98 Lau A, Yang W fa, Li KY, Su Y xiong. Systemic Therapy in Recurrent or Metastatic Head and Neck Squamous Cell Carcinoma- A Systematic Review and Meta-Analysis. *Critical Reviews in Oncology/Hematology* 2020; **153**: 102984.

99 Xiang M, Holsinger FC, Colevas AD, Chen MM, Le QT, Beadle BM. Survival of patients with head and neck cancer treated with definitive radiotherapy and concurrent cisplatin or concurrent cetuximab: A Surveillance, Epidemiology, and End Results-Medicare analysis. *Cancer* 2018; **124**: 4486–4494.

100 Agulnik M. New approaches to EGFR inhibition for locally advanced or metastatic squamous cell carcinoma of the head and neck (SCCHN). *Medical Oncology* 2012; **29**: 2481–2491.

101 Johnson DE, Burtness B, Leemans CR, Lui VWY, Bauman JE, Grandis JR. Head and neck squamous cell carcinoma. *Nature Reviews Disease Primers 2020 6:1* 2020; **6**: 1–22.

102 Osazuwa-Peters N, Simpson MC, Zhao L, Boakye EA, Olomukoro SI, Deshields T *et al.* Suicide risk among cancer survivors: Head and neck versus other cancers. *Cancer* 2018; **124**: 4072–4079.

103 CHMP. Ibrance, INN - palbociclib. www.ema.europa.eu/contact (accessed 14 Dec2021).

104 CHMP. Kisqali, INN - ribociclib. www.ema.europa.eu/contact (accessed 14 Dec2021).

105 CHMP. Verzenios (Abemaciclib) Übersicht über Verzenios und Gründe für die Zulassung in der EU. www.ema.europa.eu/contact (accessed 14 Dec2021).

106 Mitchell TC, Hamid O, Smith DC, Bauer TM, Wasser JS, Olszanski AJ *et al.* Epacadostat Plus Pembrolizumab in Patients With Advanced Solid Tumors: Phase I Results From a Multicenter, Open-Label Phase I/II Trial (ECHO-202/KEYNOTE-037). *Journal of clinical oncology : official journal of the American Society of Clinical Oncology* 2018; **36**: 3223–3230.

107 Badawy AA-B. Kynurenine Pathway of Tryptophan Metabolism: Regulatory and Functional Aspects. *International journal of tryptophan research : IJTR* 2017; **10**: 1178646917691938.

108 Song X, Si Q, Qi R, Liu W, Li M, Guo M *et al.* Indoleamine 2,3-Dioxygenase 1: A Promising Therapeutic Target in Malignant Tumor. *Frontiers in Immunology* 2021; **0**: 5520.

109 Pallotta MT, Orabona C, Volpi C, Vacca C, Belladonna ML, Bianchi R *et al.* Indoleamine 2,3-dioxygenase is a signaling protein in long-term tolerance by dendritic cells. *Nature Immunology 2011 12:9* 2011; **12**: 870–878.

110 Bates AM, Hernandez MPG, Lanzel EA, Qian F, Brogden KA. Matrix metalloproteinase (MMP) and immunosuppressive biomarker profiles of seven head and neck squamous cell carcinoma (HNSCC) cell lines. *Translational cancer research* 2018; **7**: 533.

111 Seppälä M, Halme E, Tiilikainen L, Luukkainen A, Laranne J, Rautiainen M *et al.* The expression and prognostic relevance of indoleamine 2,3-dioxygenase in tongue squamous cell carcinoma. *Acta oto-laryngologica* 2016; **136**: 729–735.

112 Ortiz-Cuaran S, Bouaoud J, Karabajakian A, Fayette J, Saintigny P. Precision Medicine Approaches to Overcome Resistance to Therapy in Head and Neck Cancers. *Frontiers in Oncology* 2021; **11**: 104.

113 Kanno Y, Chen CY, Lee HL, Chiou JF, Chen YJ. Molecular Mechanisms of Chemotherapy Resistance in Head and Neck Cancers. *Frontiers in Oncology* 2021; **11**. doi:10.3389/FONC.2021.640392.

114 Picon H, Guddati AK. Mechanisms of resistance in head and neck cancer. *American Journal of Cancer Research* 2020; **10**: 2742.

115 Showalter A, Limaye A, Oyer JL, Igarashi R, Kittipatarin C, Copik AJ *et al.* Cytokines in Immunogenic Cell Death: Applications for Cancer Immunotherapy. *Cytokine* 2017; **97**: 123.

116 Strasser B, Becker K, Fuchs D, Gostner JM. Kynurenine pathway metabolism and immune activation: Peripheral measurements in psychiatric and co-morbid conditions. *Neuropharmacology* 2017; **112**: 286–296.

117 Loretz N, Becker C, Hochstrasser S, Metzger K, Beck K, Mueller J *et al.* Activation of the kynurenine pathway predicts mortality and neurological outcome in cardiac arrest patients: A validation study. *Journal of Critical Care* 2022; **67**: 57–65.

118 Kimple RJ, Harari PM, Torres AD, Yang RZ, Soriano BJ, Yu M *et al.* Development and Characterization of HPV-Positive and HPV-Negative Head and Neck Squamous Cell Carcinoma Tumorgrafts. *Clinical Cancer Research* 2013; **19**: 855–864.

119 Klinghammer K, Raguse JD, Plath T, Albers AE, Joehrens K, Zakarneh A *et al.* A comprehensively characterized large panel of head and neck cancer patient-derived xenografts identifies the mTOR inhibitor everolimus as potential new treatment option. *International Journal of Cancer* 2015; **136**: 2940–2948.

120 Facompre ND, Rajagopalan P, Sahu V, Pearson AT, Montone KT, James CD *et al.* Identifying predictors of HPV-related head and neck squamous cell carcinoma progression and survival through patient-derived models. *International Journal of Cancer* 2020; **147**: 3236–3249.

121 Choi S il, Jeon AR, Kim MK, Lee YS, Im JE, Koh JW *et al.* Development of Patient-Derived Preclinical Platform for Metastatic Pancreatic Cancer: PDOX and a Subsequent Organoid Model System Using Percutaneous Biopsy Samples. *Frontiers in Oncology* 2019; **9**: 875.

122 Hermans E, van der Merwe SW, Depreeuw J, Dekervel J, Radaelli E, Roskams T *et al.* Successful application of endoscopic ultrasound-guided fine needle biopsy to establish

pancreatic patient-derived tumor xenografts: a pilot study. *Endoscopy* 2016; **48**: 1016–1022.

123 Wang Z, Fu S, Zhao J, Zhao W, Shen Z, Wang D *et al.* Transbronchoscopic patient biopsy-derived xenografts as a preclinical model to explore chemorefractory-associated pathways and biomarkers for small-cell lung cancer. *Cancer Letters* 2019; **440–441**: 180–188.

124 Dong Y, Manley BJ, Becerra MF, Redzematovic A, Casuscelli J, Tennenbaum DM *et al.* Tumor Xenografts of Human Clear Cell Renal Cell Carcinoma But Not Corresponding Cell Lines Recapitulate Clinical Response to Sunitinib: Feasibility of Using Biopsy Samples. *European Urology Focus* 2017; **3**: 590–598.

125 Roife D, Kang Y, Wang L, Fang B, Swisher SG, Gershenwald JE *et al.* Generation of patient-derived xenografts from fine needle aspirates or core needle biopsy. *Surgery* 2017; **161**: 1246–1254.

126 Lilja-Fischer JK, Ulhøi BP, Alsner J, Stougaard M, Thomsen MS, Busk M *et al.* Characterization and radiosensitivity of HPV-related oropharyngeal squamous cell carcinoma patient-derived xenografts. *Acta Oncologica* 2019; **58**: 1489–1494.

127 Kang HN, Kim JH, Park AY, Choi JW, Lim SM, Kim J *et al.* Establishment and characterization of patient-derived xenografts as paraclinical models for head and neck cancer. *BMC Cancer* 2020; **20**. doi:10.1186/S12885-020-06786-5.

128 Facompre ND, Sahu V, Montone KT, Harmeyer KM, Nakagawa H, Rustgi AK *et al.* Barriers to generating PDX models of HPV-related head and neck cancer. *The Laryngoscope* 2017; **127**: 2777–2783.

129 Zhao M, Sano D, Pickering CR, Jasser SA, Henderson YC, Clayman GL *et al.* Assembly And Initial Characterization Of A Panel Of 85 Genomically Validated Cell Lines From Diverse Head And Neck Tumor Sites. *Clinical cancer research : an official journal of the American Association for Cancer Research* 2011; **17**: 7248.

130 Lee MY, Allen CT. Mechanisms of resistance to T cell-based immunotherapy in head and neck cancer. *Head and Neck* 2020; : 1–12.

131 Gerlinger M, Rowan AJ, Horswell S, Larkin J, Endesfelder D, Gronroos E *et al.* Intratumor Heterogeneity and Branched Evolution Revealed by Multiregion Sequencing. *New England Journal of Medicine* 2012; **366**: 883–892.

132 Budach V, Tinhofer I. Novel prognostic clinical factors and biomarkers for outcome prediction in head and neck cancer: a systematic review. The Lancet Oncology. 2019; **20**: e313–e326.

133 Sahni S, Nahm C, Krisp C, Molloy MP, Mehta S, Maloney S *et al.* Identification of Novel Biomarkers in Pancreatic Tumor Tissue to Predict Response to Neoadjuvant Chemotherapy. *Frontiers in Oncology* 2020; **10**: 237.

134 Heckler M, Ali LR, Clancy-Thompson E, Qiang L, Ventre KS, Lenehan P *et al.* Inhibition of CDK4/6 Promotes CD8 T-cell Memory Formation. *Cancer Discovery* 2021; **11**: 2564–2581.

135 Schaer DA, Beckmann RP, Dempsey JA, Huber L, Forest A, Amaladas N *et al.* The CDK4/6 Inhibitor Abemaciclib Induces a T Cell Inflamed Tumor Microenvironment and Enhances the Efficacy of PD-L1 Checkpoint Blockade. *Cell Reports* 2018; **22**: 2809–2817.

136 Ettl T, Schulz D, Bauer RJ. The Renaissance of Cyclin Dependent Kinase Inhibitors. *Cancers* 2022; **14**: 293.

137 Arora M, Bogenberger JM, Abdelrahman AM, Yonkus J, Alva-Ruiz R, Leiting JL *et al.* Synergistic combination of cytotoxic chemotherapy and cyclin-dependent kinase 4/6 inhibitors in biliary tract cancers. *Hepatology (Baltimore, Md)* 2022; **75**: 43–58.

138 Franco J, Witkiewicz AK, Knudsen ES. CDK4/6 inhibitors have potent activity in combination with pathway selective therapeutic agents in models of pancreatic cancer. *Oncotarget* 2014; **5**: 6512–6525.

139 Dean JL, McClendon AK, Knudsen ES. Modification of the DNA damage response by therapeutic CDK4/6 inhibition. *The Journal of biological chemistry* 2012; **287**: 29075–29087.

140 McClendon AK, Dean JL, Rivadeneira DB, Yu JE, Reed CA, Gao E *et al.* CDK4/6 inhibition antagonizes the cytotoxic response to anthracycline therapy. *Cell Cycle* 2012; **11**: 2747.

141 Iyengar M, O'Hayer P, Cole A, Sebastian T, Yang K, Coffman L *et al.* CDK4/6 inhibition as maintenance and combination therapy for high grade serous ovarian cancer. *Oncotarget* 2018; **9**: 15658–15672.

142 Gao Y, Shen J, Choy E, Mankin H, Hornicek F, Duan Z. Inhibition of CDK4 sensitizes multidrug resistant ovarian cancer cells to paclitaxel by increasing apoptosiss. *Cellular oncology (Dordrecht)* 2017; **40**: 209–218.

143 Cao J, Zhu Z, Wang H, Nichols TC, Lui GYL, Deng S *et al.* Combining CDK4/6 inhibition with taxanes enhances anti-tumor efficacy by sustained impairment of pRB-E2F pathways in squamous cell lung cancer. *Oncogene 2019 38:21* 2019; **38**: 4125–4141.

144 Salvador-Barbero B, Álvarez-Fernández M, Zapatero-Solana E, el Bakkali A, Menéndez M del C, López-Casas PP *et al.* CDK4/6 Inhibitors Impair Recovery from Cytotoxic Chemotherapy in Pancreatic Adenocarcinoma. *Cancer Cell* 2020; **37**: 340-353.e6.

145 Kumarasamy V, Ruiz A, Nambiar R, Witkiewicz AK, Knudsen ES. Chemotherapy impacts on the cellular response to CDK4/6 inhibition: distinct mechanisms of interaction and efficacy in models of pancreatic cancer. *Oncogene 2019 39:9* 2019; **39**: 1831–1845.

146 He S, Roberts PJ, Sorrentino JA, Bisi JE, Storrie-White H, Tiessen RG *et al.* Transient CDK4/6 inhibition protects hematopoietic stem cells from chemotherapy-induced exhaustion. *Science Translational Medicine* 2017; **9**. doi:10.1126/SCITRANSLMED.AAL3986/SUPPL_FILE/AAL3986_SM.PDF.

147 Dhillon S. Trilaciclib: First Approval. *Drugs 2021 81:7* 2021; **81**: 867–874.

148 Xu L, Li L, Zhang J, Cai W, Zhao S, Liu S. Accumulated cytotoxicity of CDK inhibitor dinaciclib with first-line chemotherapy drugs in salivary adenoid cystic carcinoma cells. *Odontology* 2020; **108**: 300–311.

149 Kuo K-L, Lin W-C, Liu S-H, Hsu F-S, Kuo Y, Liao S-M *et al.* THZ1, a covalent CDK7 inhibitor, enhances gemcitabine-induced cytotoxicity via suppression of Bcl-2 in urothelial carcinoma. *American journal of cancer research* 2021; **11**: 171–180.

150 Danilov A v., Hu S, Orr B, Godek K, Mustachio LM, Sekula D *et al.* Dinaciclib Induces Anaphase Catastrophe in Lung Cancer Cells via Inhibition of Cyclin-Dependent Kinases 1 and 2. *Molecular cancer therapeutics* 2016; **15**: 2758–2766.

151 Chen XX, Xie FF, Zhu XJ, Lin F, Pan SS, Gong LH *et al.* Cyclin-dependent kinase inhibitor dinaciclib potently synergizes with cisplatin in preclinical models of ovarian cancer. *Oncotarget* 2015; **6**: 14926–14939.

152 Md Sakib Hossain D, Javaid S, Cai M, Zhang C, Sawant A, Hinton M *et al.* Dinaciclib induces immunogenic cell death and enhances anti- PD1–mediated tumor suppression. *Journal of Clinical Investigation* 2018; **128**: 644–654.

153 Anwer S, Szaszi K. Measuring Cell Growth and Junction Development in Epithelial Cells Using Electric Cell-Substrate Impedance Sensing (ECIS). *Bio-protocol* 2020; **10**. doi:10.21769/BIOPROTOC.3729.

154 Zhang N, Yin Y, Xu SJ, Chen WS. 5-Fluorouracil: Mechanisms of resistance and reversal strategies. Molecules. 2008; **13**: 1551–1569.

155 Northcott JM, Dean IS, Mouw JK, Weaver VM. Feeling stress: The mechanics of cancer progression and aggression. *Frontiers in Cell and Developmental Biology* 2018; **6**: 1–12.

156 Brückner BR, Nöding H, Skamrahl M, Janshoff A. Mechanical and morphological response of confluent epithelial cell layers to reinforcement and dissolution of the F-actin cytoskeleton. *Progress in Biophysics and Molecular Biology* 2019; **144**: 77–90.

157 Murugan S, Amaravadi RK. Methods for studying autophagy within the tumor microenvironment. In: *Advances in Experimental Medicine and Biology*. Springer New York LLC, 2016, pp 145–166.

158 Maskey RS, Wang F, Lehman E, Wang Y, Emmanuel N, Zhong W *et al.* Sustained mTORC1 activity during palbociclib-induced growth arrest triggers senescence in ER+ breast cancer cells. *Cell Cycle* 2020. doi:10.1080/15384101.2020.1859195.

159 Yu Y, Liao H, Xie R, Zhang Y, Zheng R, Chen J *et al.* Overexpression of miRNA-3613-3p Enhances the Sensitivity of Triple Negative Breast Cancer to CDK4/6 Inhibitor Palbociclib. *Frontiers in Oncology* 2020; **10**. doi:10.3389/fonc.2020.590813.

160 Petroni G, Formenti SC, Chen-Kiang S, Galluzzi L. Immunomodulation by anticancer cell cycle inhibitors. *Nature reviews Immunology* 2020; **20**: 669.

161 Goel S, Decristo MJ, Watt AC, Brinjones H, Sceneay J, Li BB *et al.* CDK4/6 inhibition triggers anti-tumor immunity. *Nature* 2017; **548**: 471.

162 McCartney A, Migliaccio I, Bonechi M, Biagioni C, Romagnoli D, de Luca F *et al.* Mechanisms of Resistance to CDK4/6 Inhibitors: Potential Implications and Biomarkers for Clinical Practice. *Frontiers in Oncology* 2019; **9**: 666.

163 Garrido-Castro AC, Goel S. CDK4/6 Inhibition in Breast Cancer: Mechanisms of Response and Treatment Failure. *Current breast cancer reports* 2017; **9**: 26.

164 Dean JL, McClendon AK, Hickey TE, Butler LM, Tilley WD, Witkiewicz AK *et al.* Therapeutic response to CDK4/6 inhibition in breast cancer defined by ex vivo analyses of human tumors. *http://dx.doi.org/104161/cc21195* 2012; **11**: 2756–2761.

165 Witkiewicz AK, Knudsen ES. Retinoblastoma tumor suppressor pathway in breast cancer: Prognosis, precision medicine, and therapeutic interventions. *Breast Cancer Research* 2014; **16**: 1–12.

166 Herrera-Abreu MT, Palafox M, Asghar U, Rivas MA, Cutts RJ, Garcia-Murillas I *et al.* Early Adaptation and Acquired Resistance to CDK4/6 Inhibition in Estrogen Receptor–Positive Breast Cancer. *Cancer Research* 2016; **76**: 2301–2313.

167 Li Z, Razavi P, Li Q, Toy W, Liu B, Ping C *et al.* Loss of the FAT1 Tumor Suppressor Promotes Resistance to CDK4/6 Inhibitors via the Hippo Pathway. *Cancer Cell* 2018; **34**: 893-905.e8.

168 Alexa-Stratulat T, Pešić M, Gašparović AČ, Trougakos IP, Riganti C. What sustains the multidrug resistance phenotype beyond ABC efflux transporters? Looking beyond the tip of the iceberg. *Drug Resistance Updates* 2019; **46**: 100643.

169 Abutorabi ES, Irani S, Yaghmaie M, Ghaffari SH. Abemaciclib (CDK4/6 Inhibitor) Blockade Induces Cytotoxicity in Human Anaplastic Thyroid Carcinoma Cells. *Reports of Biochemistry & Molecular Biology* 2020; **8**: 438.

170 Bendris N, Lemmers B, Blanchard JM. Cell cycle, cytoskeleton dynamics and beyond: the many functions of cyclins and CDK inhibitors. Cell Cycle. 2015; **14**: 1786–1798.

frontiers in Immunology

ORIGINAL RESEARCH
published: 14 February 2020
doi: 10.3389/fimmu.2020.00055

Activation of the Kynurenine Pathway in Human Malignancies Can Be Suppressed by the Cyclin-Dependent Kinase Inhibitor Dinaciclib

*Christin Riess[1,2,3], Björn Schneider[4], Hanna Kehnscherper[3], Julia Gesche[3], Nina Irmscher[3], Fatemeh Shokraie[1], Carl Friedrich Classen[1], Elisa Wirthgen[1], Grazyna Domanska[5], Annette Zimpfer[4], Daniel Strüder[6], Christian Junghanss[3] and Claudia Maletzki[3]**

[1] University Children's Hospital, Rostock University Medical Centre, Rostock, Germany, [2] Institute for Medical Microbiology, Virology, and Hygiene, Rostock University Medical Centre, Rostock, Germany, [3] Medical Clinic III - Hematology, Oncology, Palliative Care, Department of Internal Medicine, Rostock University Medical Center, Rostock, Germany, [4] Institute of Pathology, Rostock University Medical Center, University of Rostock, Rostock, Germany, [5] Institute of Immunology and Transfusion Medicine, University of Greifswald, Greifswald, Germany, [6] Department of Otorhinolaryngology, Head and Neck Surgery "Otto Koerner", Rostock University Medical Center, Rostock, Germany

OPEN ACCESS

Edited by:
Ignacio Melero,
University of Navarra, Spain

Reviewed by:
Benjamin Heng,
Macquarie University, Australia
Michael Platten,
German Cancer Research Center (DKFZ), Germany

***Correspondence:**
Claudia Maletzki
claudia.maletzki@med.uni-rostock.de

Specialty section:
This article was submitted to Cancer Immunity and Immunotherapy, a section of the journal Frontiers in Immunology

Received: 16 September 2019
Accepted: 09 January 2020
Published: 14 February 2020

Citation:
Riess C, Schneider B, Kehnscherper H, Gesche J, Irmscher N, Shokraie F, Classen CF, Wirthgen E, Domanska G, Zimpfer A, Strüder D, Junghanss C and Maletzki C (2020) Activation of the Kynurenine Pathway in Human Malignancies Can Be Suppressed by the Cyclin-Dependent Kinase Inhibitor Dinaciclib. Front. Immunol. 11:55. doi: 10.3389/fimmu.2020.00055

Indoleamine 2,3-dioxygenase (IDO) and tryptophan 2,3-dioxygenase (TDO2) are the key enzymes of tryptophan (TRP) metabolism in the kynurenine pathway (KP). Both enzymes function as indicators of immunosuppression and poor survival in cancer patients. Direct or indirect targeting of either of these substances seems thus reasonable to improve therapy options for patients. In this study, glioblastoma multiforme (GBM) as well as head and neck squamous cell carcinomas (HNSCC) were examined because of their different mechanisms of spontaneous and treatment-induced immune escape. Effects on gene expression and protein levels were examined. Accompanying assessment of TRP metabolites from treated GBM cell culture supernatants was conducted. Our results show a heterogeneous and inversely correlated expression profile of TRP-metabolizing genes among GBM and HNSCC cells, with low, but inducible *IDO1* expression upon IFNγ treatment. *TDO2* expression was higher in GBM cells, while genes encoding kynurenine aminotransferases were mainly confined to HNSCC cells. These data indicate that the KP is active in both entities, with however different enzymes involved in TRP catabolism. Upon treatment with Temozolomide, the standard of care for GBM patients, *IDO1* was upregulated. Comparable, although less pronounced effects were seen in HNSCC upon Cetuximab and conventional drugs (i.e., 5-fluorouracil, Gemcitabine). Here, *IDO1* and additional genes of the KP (*KYAT1*, *KYAT2*, and *KMO*) were induced. Vice versa, the novel yet experimental cyclin-dependent kinase inhibitor Dinaciclib suppressed KP in both entities. Our comprehensive data imply inhibition of the TRP catabolism by Dinaciclib, while conventional chemotherapeutics tend to activate this pathway. These data point to limitations of conventional therapy and highlight the potential of targeted therapies to interfere with the cells' metabolism more than anticipated.

Keywords: targeted therapy, solid tumor models, tryptophan metabolites, IDO1, chemotherapy

INTRODUCTION

Tumor cells release immunosuppressive factors that shape a tolerogenic environment and enable progression and invasion. Indoleamine 2,3-dioxygenase (IDO1) is an intracellular monomeric, immune-checkpoint molecule that degrades the essential amino acid l-tryptophan along the kynurenine pathway (KP) (1, 2). Like other immune checkpoints, including programmed cell death protein 1 and cytotoxic T-lymphocyte-associated protein 4, IDO suppresses the hosts' antitumor immunity by inducing apoptosis in T- and natural killer cells (3). As a direct consequence of this, many cancer and cancer-associated cells express *IDO1* (mesenchymal stromal cells, myeloid-derived suppressor cells, dendritic cells, endothelial cells, tumor-associated macrophages, and fibroblasts) (3–6). *IDO1* is influenced by interferon-γ (IFNγ) (7–9), nitric oxide (10), pro- [interleukin (IL)-1β, tumor necrosis factor α] and anti-inflammatory (IL4, IL10, transforming growth factor β) cytokines. *IDO1* activity inhibits T-cell activation and proliferation and even mediates regulatory T-cell recruitment to the tumor microenvironment, provoking local immune tolerance. In head and neck squamous cell carcinomas (HNSCCs), *IDO1* inversely correlates with programmed cell death protein ligand 1, which constitutes an important prognostic biomarker for immune-checkpoint inhibition (11). The increased IDO1 activation decreases intratumoral TRP levels, resulting in tumor starvation and increase in kynurenine (KYN) metabolites (which are toxic to lymphocytes) (12). This immune exhaustion may be further boosted by conventional chemotherapeutics, leading to decreased efficacy. Therefore, *IDO1* overexpression in the tumor microenvironment intimately impairs patients' outcome and may serve as a future prognostic predictor and drug target (13–18).

In the KP, most studies focused on IDO1 because this molecule is amenable to pharmacological intervention (19–22), and a couple of specific and global IDO inhibitors [including natural compounds (17, 23, 24)] already entered clinical trials, mostly reporting safe application and efficacy (stable disease at best outcome) (25). Current trials are evaluating the efficacy of IDO1 inhibitors in combination with chemotherapy, radiotherapy, and other immunotherapies including cytotoxic T-lymphocyte-associated protein 4 blockade (11, 22). The latter is based on the observation of an enhanced lytic ability of tumor-antigen-specific T cells upon IDO1 inhibition and decreased numbers of local immunosuppressive cells such as regulatory T cells and myeloid-derived suppressor cells (20, 26). The efficacy and toxicity data from recent clinical trials with IDO1 inhibitors is reviewed in Yentz and Smith (27). In most cases, however, overall survival was not significantly improved, leaving the future role for this combination therapy in question (28). More key enzymes are involved in TRP metabolism: tryptophan 2.3-dioxygenase (TDO2), a member of the oxidoreductases family, catalyzes the same initial step of the KP as IDO1 (2). Thus, TDO2 has been shown to be constitutively and highly expressed in various cancer cells such as malignant glioma and HNSCC (29, 30). More importantly, TDO2 also has immunomodulatory functions by promoting immune tolerance. This, in turn, promotes survival, growth, invasion, and metastasis and decreases patients' survival (just like *IDO1*) (13, 22, 31, 32).

In this study, we performed a comprehensive analysis on the expression status of genes belonging to the KP. HNSCC and glioblastoma multiforme (GBM) were picked as prime examples for different spontaneous and treatment-induced immune escape mechanisms. Therefore, expression changes were determined under standard and targeted therapy, and results were compared among each other.

Abbreviations: CDKi, cyclin-dependent kinase inhibitor; GBM, glioblastoma multiforme; HNSCC, head and neck squamous cell carcinoma; IDO1, indoleamine 2,3-dioxygenase; IFN, interferon; KYAT, kynurenine aminotransferase; KP, kynurenine pathway; PBMC, peripheral blood mononuclear cells; SCC, squamous cell carcinoma; TDO2, tryptophan 2,3-dioxygenase.

MATERIALS AND METHODS

Tumor Cell Lines and Culture Conditions

Patient-derived GBM cell lines ($N = 13$; HROG02, HROG04, HROG05, HROG06, HROG10, HROG15, HROG24, HROG36, HROG38, HROG52, HROG63, HROG73, HROG75) and HNSCC cell lines ($N = 6$; FADU, Detroit-562, Cal-33, PE/CA/PJ-15, UT-SCC-14, UT-SCC-15) were either established and basically characterized in our lab or originally obtained from the German collection of cell cultures (DSMZ; Braunschweig, Germany). UT-SCC14 and UT-SCC15 cells were kindly provided by Prof. R. Grenman [University of Turku, Finland (33)]. All cells were routinely cultured in our lab and maintained in full medium: Dulbecco's modified Eagle Medium/HamsF12 supplemented with 10% fetal calf serum, glutamine (2 mmol/L), and antibiotics (medium and supplements were purchased from PAA, Cölbe, Germany). For functional analysis, cell lines from each tumor entity were chosen, and all subsequent experiments were performed with these lines only.

IFNγ Stimulation

Cells were cultured in six-well plates or ibidi chamber slides, incubated overnight and treated with IFNγ (50 ng/ml, Immunotools, Friesoythe, Germany) for 24 and 72 h, respectively. Thereafter, cells were harvested and further processed.

Cytostatic Drugs and Targeted Substance

Cytostatics used in this study included 5-fluorouracil (5-FU) (2.5 μM), Cisplatin (0.2 μM), Gemcitabine (0.0002 μM), and Cetuximab (0.34 μM) for HNSCC, as well as Temozolomide (10 μM, TMZ) for GBM (pharmacy of the University Hospital Rostock). CDKi Dinaciclib (10 or 100 nM) was used as experimental targeted drug. All substances were used in doses below the IC_{50} as determined before.

Apoptosis/Necrosis Assay

A Yo-Pro-1/PI-based assay for discriminating early apoptotic, late apoptotic, and necrotic cells was applied as described before (34).

Hemolysis Assay

Hemolytic activity of Dinaciclib was determined by hemoglobin release from whole blood cells after 2 h of incubation. Briefly,

whole blood of healthy donors ($N = 5$) was seeded in 96-well plates and treated with increasing Dinaciclib doses (ranging from 1, 5, and 10 μM). Negative controls were left untreated, and positive controls (=maximum lysis) were treated with 1% sodium dodecyl sulfate. Following the incubation period, cell-free supernatants were transferred into a new 96-well plate, and absorption was measured on a plate reader at 560 nm (reference wave length, 750 nm). Hemolytic activity was quantified according to the following formula and corrected for spontaneous hemolysis (=untreated controls):

$$\%\text{Hemolysis} = ((OD_{560nm}\text{sample} - OD_{560nm}\text{buffer})/OD_{560nm}\text{max} - OD_{560nm}\text{buffer}) \times 100$$

In addition, peripheral blood mononuclear cells' (PBMC) viability ($N = 5$) were determined by Calcein AM staining. This was done upon 24 h incubation at the above-mentioned doses. Fluorescence measurement and quantification were done as described (34).

IDO1 Immunofluorescence

Tumor cells were treated with 50 ng/ml of IFNγ (Immunotools), TMZ, Cetuximab, or Dinaciclib for 24 h in chamber slides, respectively. Cells were washed with phosphate-buffered saline, fixed in 4% paraformaldehyde w/o methanol (Thermo Scientific, Darmstadt, Germany) for 20 min, washed again, followed by cell permeabilization in 0.3% Triton X−100/5% normal bovine serum in phosphate-buffered saline for 60 min. Cells were then incubated overnight at 4°C in monoclonal rabbit IDO1 primary antibody (1:100; Cell Signaling Technology, Frankfurt/Main, Germany). Cells were washed, labeled with fluorochrome-conjugated secondary antibody using goat antirabbit secondary antibody (1:250, Boster Biological Technology, Pleasanton CA, USA), and incubated in the dark for 2 h. Cell nuclei were stained with 4′,6-diamidino-2-phenylindole (DAPI), and cells were analyzed with a Zeiss LSM-780 Confocal Laser Microscope (Zeiss, Jena, Germany). Quantification of staining intensity was done using the ImageJ software. Therefore, channels were split into red, green, and blue. Subsequently, integrated density profiles of the same size were measured in the green channel.

IDO1 Immunohistochemistry on Patients' Tumor Samples

Primary antibody against IDO1 (rabbit IgG, clone D5J4E, Cell Signaling Technology, dilution 1:200) was used. All samples were pretreated for 20 min at 97°C and pH 6.9. Standard immunoperoxidase technique was applied using an automated immunostainer (DAKO link) with diaminobenzidine as chromogen. IDO1 expression was defined as cytoplasmatic and membranous staining in >1% inflammatory cells.

Quantification of Tryptophan, Kynurenine, and Kynurenic Acid in Cell Culture Supernatant by Liquid Chromatography Tandem Mass Spectrometry System

The basis for the measurement was the method of Fuertig et al. which was adapted to the system used here (35).

Sample Preparation

Cell culture supernatant was mixed 1:1 with internal standards [10 μM D5-kynurenic acid (Buchem BV, Apeldoorn, Netherlands), 10 μM D5-phenylalanine (Cambridge Isotope Laboratories, Inc. Andover, MA, United States), 5 μM D4-kynurenine (Cambridge Isotope Laboratories), 10 μM D5-tryptophan (Sigma Aldrich, Hamburg, Germany), 10 μM D3-quinolinic acid (Buchem BV), 5.5 nM 15N5-8-hydroxy-2-deoxyguanosine (Cambridge Isotope Laboratories)], and with 10 μl of mobile phase (0.4% formic acid, 1% acetonitrile in water). Reagents were gently shaken on a mixer, and 150 μl of ice-cold methanol was added. Samples were incubated overnight at −20°C to allow protein precipitation. On the following day, samples were centrifugated at 0°C and 18,000×*g* for 15 min. Supernatants were transferred to a new tube, and the liquid phase was removed by evaporation at 30°C among vacuum. Solid samples were stored until measurement at −20°C. Afterwards, dried extracts were reconstituted in 100 μl of acidified mobile phase. Samples were incubated at 40°C (1 h), centrifuged (4°C, 18,000×*g*, 5 min), and clear supernatant (100 μl) was transferred onto a 96-well plate.

Liquid Chromatography Tandem Mass Spectrometry

Measurements were performed on an AB Sciex 5500 QTrap™ mass spectrometer (AB SCIEX, Darmstadt, Germany) with electrospray ionization in positive mode combined with a high-performance liquid chromatography system (Agilent 1260 Infinity Binary LC, Santa Clara, United States) including a degasser unit, column oven, autosampler, and a binary pump. Twenty microliters of the supernatant was injected and separated using a VisionHT C18 column (100 × 2.1 mm; particle size, 3 μm; Grace, MD, United States). To prevent contamination, a precolumn (VisionHT C18, Guard 5 × 2 mm) was used additionally. The temperature of the column oven was set at 15°C. The flowrate was set to 0.4 ml/min, and the sample was separated in a total run time of 11 min using solution A (water + 0.1% formic acid + 0.01% trifluoroacetic acid) and solution B (MeOH + 0.1% formic acid + 0.01% trifluoroacetic acid) with the following gradient: 0–2.8 min, 97% A, 3% B; 2.8–3.3 min, 70% A, 30% B; 3.3–4.4, 40% A, 60% B; 4.5–5.0 min, 40% A, 60% B; 5.0–5.5, 5% A, 95% B; 5.5–6.9 min, 5% A, 95% B; 6.9–7.0 min, 97% A, 3% B; 7.0–11.0 min, 97% A, 3% B.

The eluate between 0.5 and 9 min was introduced into the mass spectrometer and analyzed in MRM mode. The ion spray voltage (IS) was 4,000 V, the curtain gas flow was 40.0 psi, and the ion source temperature were set at 550°C.

Internal standards were used for metabolite quantification (**Table 1**). Data analysis, including peak integration and concentration determination, was performed with Analyst software (Version 1.5.1, AB Sciex, Darmstadt, Germany).

RNA Isolation, cDNA Synthesis, and Quantitative Real-Time PCR

Total RNA was isolated with RNeasy Mini Kit (Qiagen, Hilden, Germany) according to the manufacturers' instructions. RNA was reverse transcribed into complementary DNA (cDNA) from

1 μg RNA using 1 μl dNTP mix (10 mM), oligo (dT)15 primer (50 ng/μl), 1 μl reverse transcriptase (100 U), and 4 μl 5× reverse transcription buffer complete (all purchased from Bioron GmbH, Ludwigshafen, Germany). Final reaction volume was 20 μl (filled with RNAse free water). cDNA synthesis conditions were as follows: 70°C for 10 min, 45°C for 120 min, and 70°C for 10 min. Target cDNA levels of human cell lines were analyzed by quantitative real-time PCR using TaqMan Universal PCR Master Mix and self-designed TaqMan gene expression assays either labeled with 6-FAM-3′ BHQ-1 or 5′ HEX−3′ BHQ-1 to be used as duplex: *IDO1*, *TDO2*, *KMO*, *HAAO*, *KYAT1/2/3/4*, *KYNU*, *QPRT*, and *GAPDH* or *ß-actin* were used as housekeeping genes. Reaction was performed in the light cycler Viia7 (Applied Biosystems, Foster City, USA) with the following PCR conditions: 95°C for 10 min, 40 cycles of 15 s at 95°C, and 1 min at 60°C. All reactions were run in triplicates. The messenger RNA (mRNA) levels of target genes were normalized to *GAPDH/β-actin*. Reactions were performed in triplicate wells and repeated four times. The general expression level of each sample was considered by calculating $2^{-\Delta CT}$ ($\Delta Ct = Ct_{target} - Ct_{Housekeeping\ genes}$).

TABLE 1 | Internal standards.

Analyte	Q1 mass (m/z)	Q3 mass (m/z)	CE (V)	DP (V)
Tryptophan	205.1	118.0	28.0	39.0
d5-Tryptophan	210.1	122.1	37.0	31.0
Kynurenine	209.1	94.1	19.6	41.0
d4-Kynurenine	213.1	140.1	21.0	39.0
Kynurenic acid	190.1	162.0	24.0	65.0
d5-Kynurenic acid	195.1	167.1	24.0	65.0

Statistical Analysis

All values are reported as mean ± SD. After proving the assumption of normality, differences between controls and treated cells were determined using the unpaired Student's *t*-test. If normality failed, the non-parametric Mann-Whitney *U*-test was applied. Statistical evaluation was performed using GraphPad PRISM software, version 5.02 (GraphPad Software, San Diego, CA, USA). In case of multiple comparisons, two- or one-way ANOVA on ranks (Bonferroni's multiple comparison test) was used. The criterion for significance was taken to be $p < 0.05$.

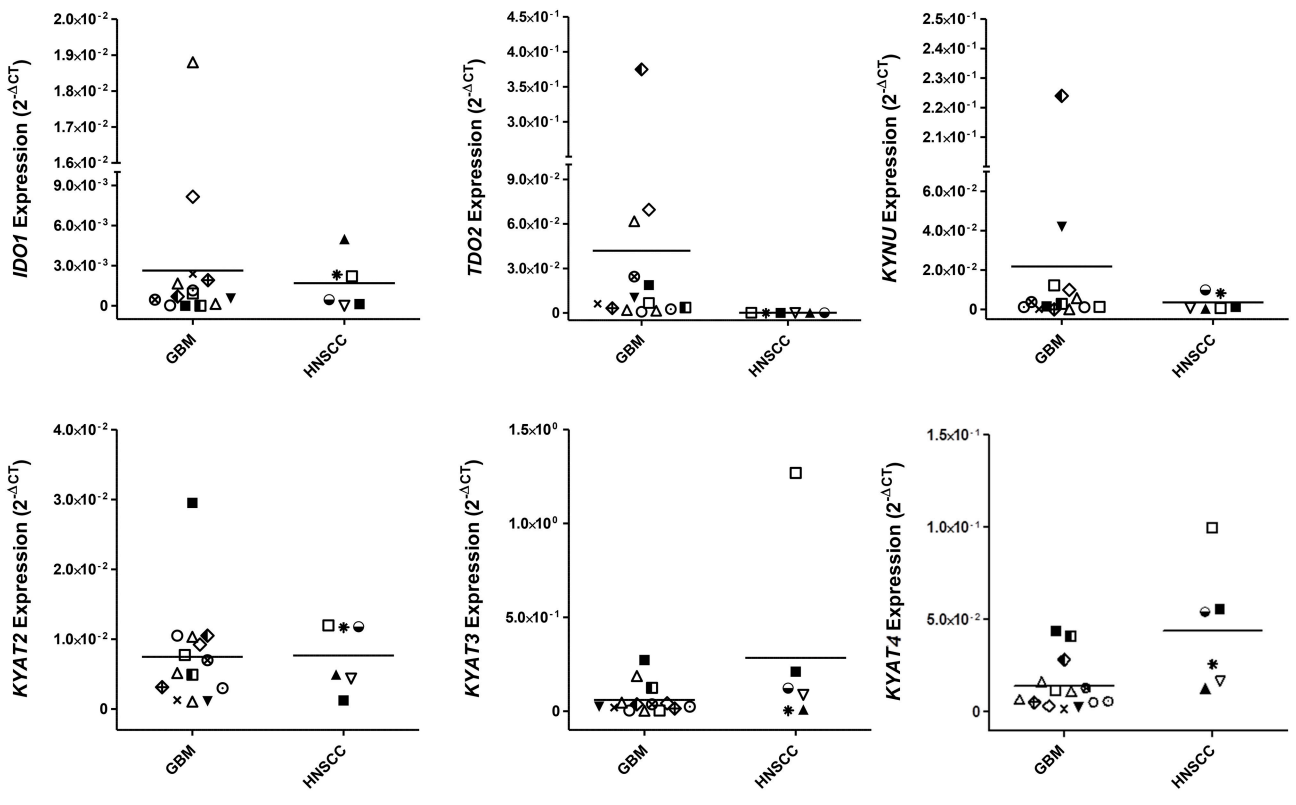

FIGURE 1 | Relative messenger RNA (mRNA) expression of IDO1, TDO2, KYNU, KYAT2, KYAT3, and KYAT4 in glioblastoma multiforme (GBM) and head and neck squamous cell carcinoma cells (HNSCC). The graphs indicate the mRNA expression normalized to the housekeeping genes ($2^{-\Delta}$CT). GBM ($N = 13$, HROG02, HROG04, HROG05, HROG06, HROG10, HROG15, HROG24, HROG36, HROG38, HROG52, HROG63, HROG73, HROG75) and HNSCC cell lines [$N = 6$; FADU, Detroit-562, Cal-33, PE/CA/PJ-15, UT-SCC14, UT-SCC-15 (33)].

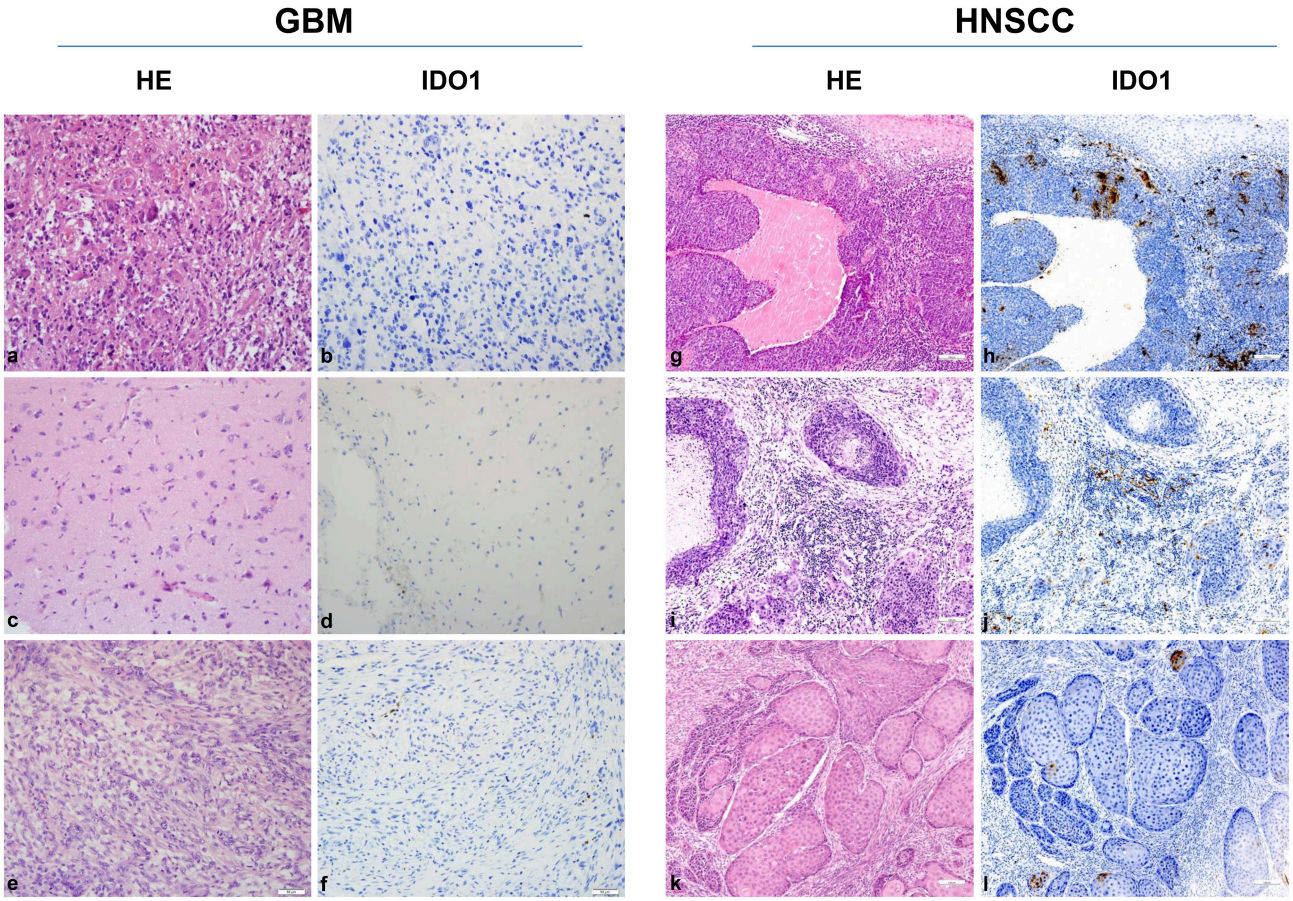

FIGURE 2 | IDO1 immunohistochemistry. Representative images of primary glioblastoma multiforme (GBM) [HROG36 **(a,b)**, HROG63 **(c,d)**, and HROG73 **(e,f)**] and head and neck squamous cell carcinoma (HNSCC) [HNSCC06 **(g,h)**, HNSCC02 **(i,j)**, HNSCC01 **(k,l)**] samples. Left panel: Routine HE staining. Right panel: Note the focal IDO1 expression on tumor-infiltrating lymphocytes exclusively in HNSCC cases. HNSCC case 1 **(g,h)**: tonsil ($HPV^{positive}$); case 2 **(i,j)**: mouth base ($HPV^{negative}$, relapse); case 3 **(k,l)**: larynx ($HPV^{negative}$). Pictures were taken at 20× and 10× magnification, respectively.

RESULTS

Basal IDO1 and Related Genes in GBM and HNSCC Cell Lines

While IDO1 itself is not the only mechanism by which tumors can resist immune-mediated killing, we studied the expression status of different KP-related genes on a panel of human GBM and HNSCC cell lines. These experiments revealed not only differences between both entities but also a heterogeneous profile of all tested genes among cell lines (**Figure 1**). *IDO1* was differently expressed by most glioma samples (11/13) analyzed. In general, *IDO1* was only detectable at very low levels (**Figure 1**). *TDO2*, the other rate-limiting enzyme of the KP (36), was constitutively expressed by all glioma samples, and expression was even higher in comparison to *IDO1*. Generally, expression status for *TDO2* and kynurenine hydrolase (*KYNU*) was higher in GBM, while HNSCC expressed more kynurenine aminotransferases (*KYAT*) (**Figure 1**). Hence, these data indicate that the KP is active in both entities, with however different enzymes being involved in TRP catabolism.

Still, tumor cell lines grown *in vitro* not necessarily represent the *in vivo* situation; we therefore analyzed the IDO1 abundance in clinical resection specimens (**Figure 2**). In GBM, IDO1 was detectable in one of three cases (representative images are shown in **Figure 2**). By contrast, HNSCC samples presented with IDO1 but only on a small fraction of tumor-infiltrating lymphocytes (**Figure 2**). Although not analyzed systematically, the only $HPV^{positive}$ case in this small cohort showed highest IDO1 abundance, nicely reflecting the tumors' immunogenicity (11, 37).

Gene Expression and Protein Changes Upon IFNγ Stimulation

IDO1 is an IFNγ-inducible enzyme. Upon stimulation, the KP is activated to induce immunosuppression. *In vitro* stimulation with IFNγ mimics the *in vivo* situation of an inflammatory microenvironment. Hence, upon immune-mediated inflammation, IDO1-negative tumor cells may upregulate *IDO1* as resistance mechanism.

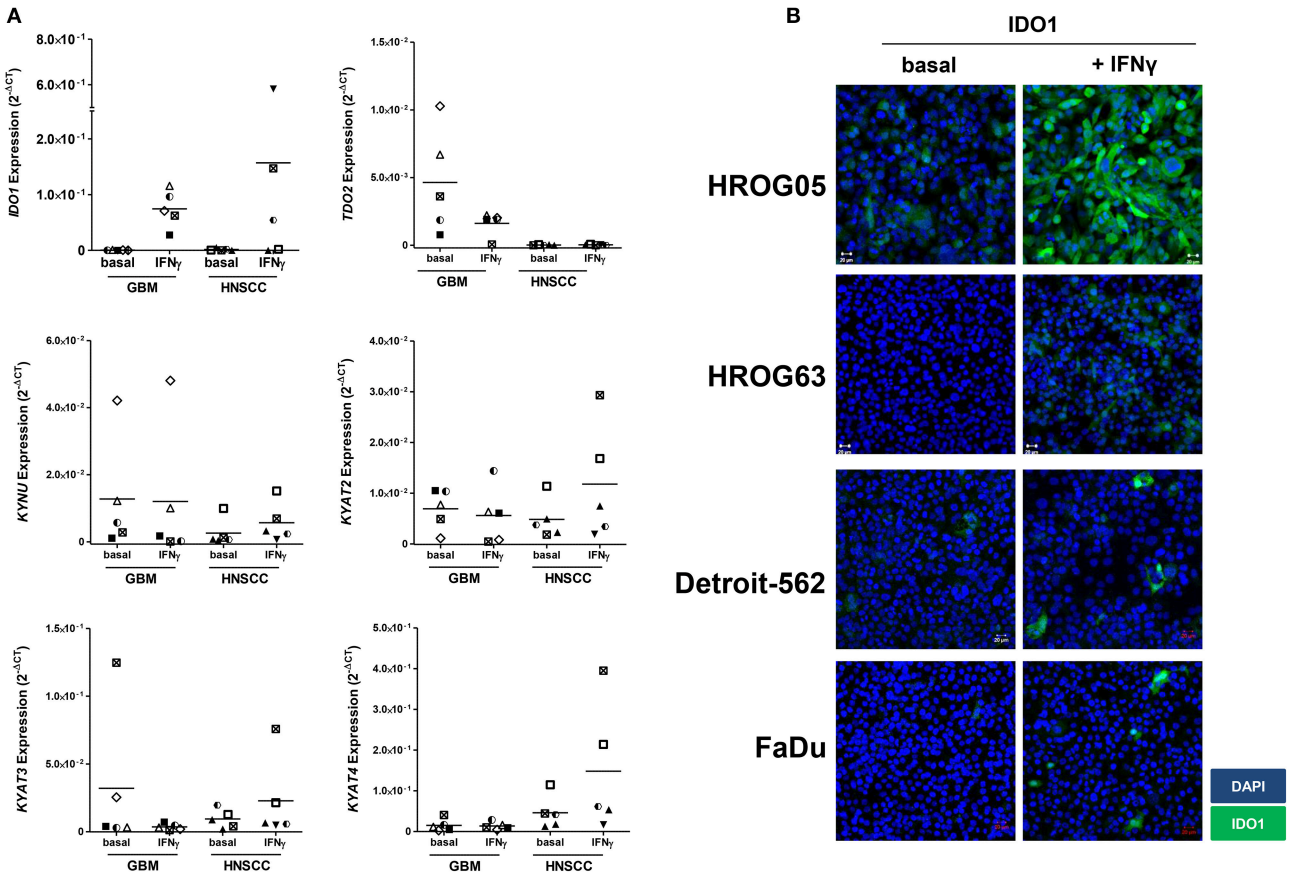

FIGURE 3 | Relative messenger RNA (mRNA) expression of *IDO1, TDO2, KYNU, KYAT2, KYAT3*, and *KYAT4* as well as IDO1 protein abundance following interferon-γ (IFNγ) stimulation in glioblastoma multiforme (GBM) and head and neck squamous cell carcinoma (HNSCC) cells. The cell cultures were either untreated or treated with IFNγ (50 ng/ml) for 24 h. **(A)** The graphs indicate the mRNA expression normalized to the housekeeping genes ($2^{-\Delta}$CT). GBM $N = 5$ cell lines (HROG02, HROG05, HROG52, HROG63, HROG75); HNSCC, $N = 4$ cell lines (FADU, Detroit-562, Cal-33, PE/CA/PJ-15). **(B)** IDO1 immunofluorescence in selected cell lines. Cell nuclei were stained with DAPI, and IDO1 was depicted by monoclonal rabbit IDO1 primary antibody (1:100; Cell Signaling Technology), followed by secondary antibody (1:250, Boster Biological Technology Pleasanton, CA, United States) labeling. Cells were analyzed with a Zeiss LSM-780 Confocal Laser Microscope. Original magnification 20×.

Using five individual GBM cell lines, *IDO1* expression was inducible in all cases (**Figure 3A**). Upregulation of *IDO1* was high on protein levels in HROG05 cells and marginal in HROG63 (**Figure 3B**). *TDO2* and *KYAT3* were suppressed upon IFNγ stimulation in three of five samples and hardly detectable in one cell line, supporting data from a recent publication (38). *KYNU* was not affected by IFNγ stimulation (**Figure 3A**).

Just as in GBM, *IDO1* was inducible in HNSCC cells (**Figure 3A**). Immunofluorescence revealed focal expression of singular cells with different intensity (**Figure 3B**). Of note, IFNγ stimulation even induced upregulation of *KYAT1*, *KYAT2*, *KYAT3*, and *KYAT4* (**Figure 3A** and data not shown), most likely constituting a compensatory mechanism as described before in experimental autochthonous tumor models (39).

Interference With the KP of Cytostatic and Targeted Therapies

Next, we examined whether cytostatic and targeted drugs have an influence on the KP. For GBM, TMZ was chosen, and for HNSCC, 5-FU, Cisplatin, Gemcitabine, as well as Cetuximab were used. As a targeted yet still experimental agent, the potent and specific CDKi Dinaciclib was applied to cells of both entities.

Before this experiment, drug doses were carefully tested in dose-response analyses (data not shown) along with discrimination of apoptosis and necrosis. Generally, drugs used in this study tended to induce necrosis, while apoptosis, if present, was only detectable at early time points. Exemplary results for the HNSCC cell line Detroit-562 are given in **Supplementary Figures 1A,B**. While cytostatics are well-known to affect normal cells' viability, the impact of the CDKi Dinaciclib on immune and red blood cells is less clear. We therefore performed a hemolysis and leukocyte viability assay. In this experiment, no toxicity was seen against normal cells (**Supplementary Figure 1C**). Even at high concentrations, Dinaciclib impaired cellular viability/integrity only marginally (**Supplementary Figure 1C**).

TMZ is an oral alkylating agent that methylates DNA at the O^6 position of guanine causing cell cycle arrest at G2/M. It is used as standard of care for GBM. However, acquired resistance, a process not fully understood, leads to

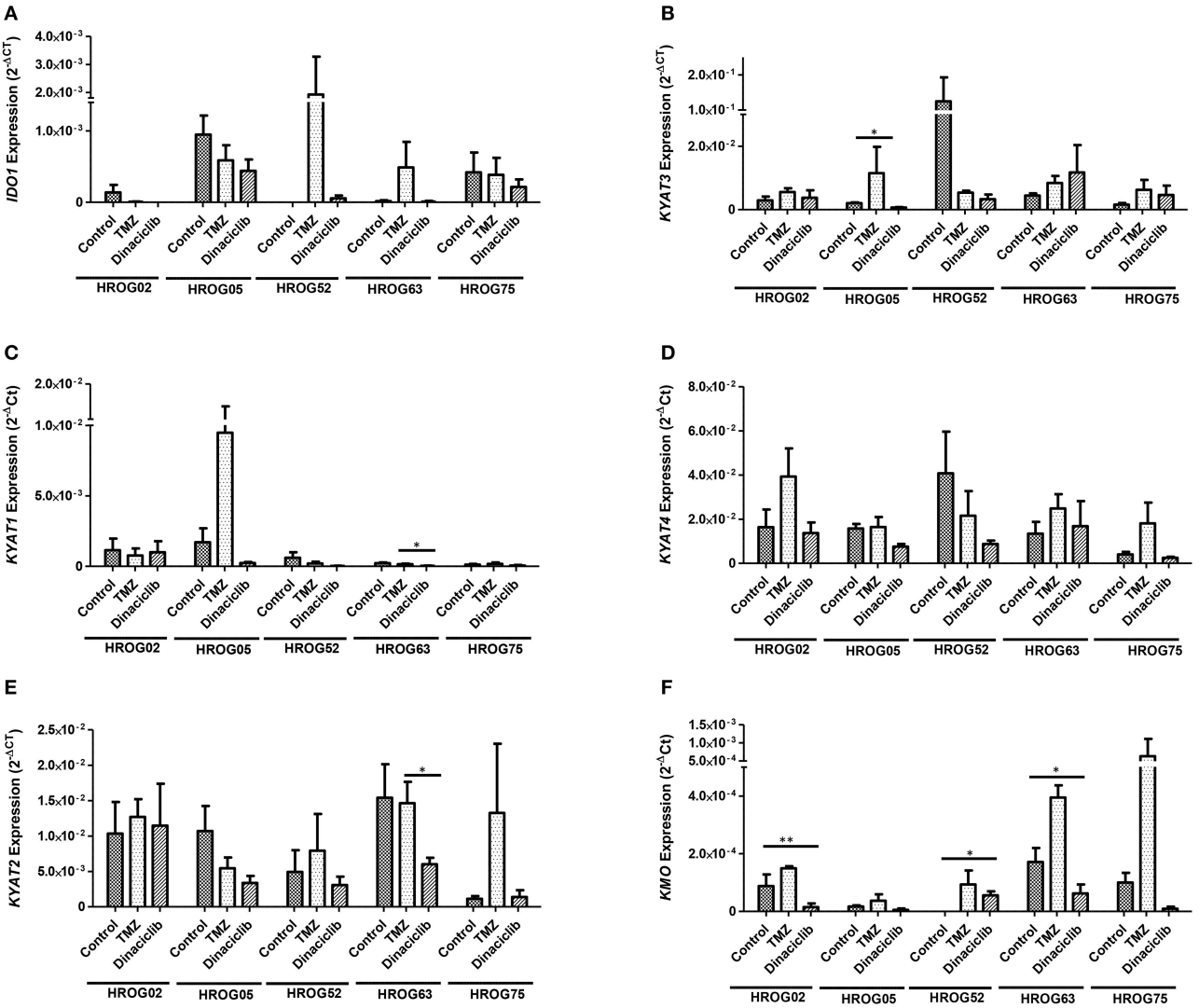

FIGURE 4 | Relative messenger RNA (mRNA) expression of *IDO1, KYAT1, KYAT2, KYAT3*, *KYAT4,* and KMO upon cytostatic drugs and targeted therapy in glioblastoma multiforme (GBM) cells. Graphs indicate the mRNA expression of selected kynurenine pathway (KP)-related genes normalized to the housekeeping genes ($2^{-\Delta}$CT). Results show data of three independent experiments. *$p < 0.05$; **$p < 0.01$ vs. control. Two-way ANOVA.

major limitations in treatment. Here, TMZ downregulated *IDO1* in three of five GBM cell lines but led to increased expression in HROG52 and HROG63—a paired GBM cell line established from the very same patient (primary lesion and upon relapse) (**Figure 4**). Gene expression of *KYAT2*, *KYAT4*, and *KMO* was heterogeneous. Generally, there was a trend toward higher expression of those genes but with cell-line-specific differences (e.g., *KYAT3*: $p < 0.05$ vs. control in HROG05 cells; **Figure 4**). *KYNU* expression was not affected by TMZ (data not shown). Interestingly, the combination of IFNγ and TMZ that mimics the *in vivo* situation led to similar or even stronger *IDO1* upregulation compared to IFNγ alone in two out of four glioma samples (**Figure 5**). Adding Dinaciclib to either IFNγ or TMZ lowered the mRNA expression of *IDO1* massively. Other KP-related genes like *TDO2* and *KYAT1-4* were similarly downregulated (**Figure 5**). **Supplementary Table for Figure 5** provides a detailed statistical analysis of each cell line in relation to the individual treatment regimens.

In HNSCC cells, Cetuximab was the only *IDO1*-inducing substance (exemplary results for Detroit-562 cells are given in **Figure 6**). Beyond that, the cytostatics as well as Cetuximab induced at least one of the KP-related genes ($p < 0.05$ vs. control), implicating activation of this pathway *via* different effectors. By adding Dinaciclib to cytostatic drugs, this effect was abrogated, even in the presence of IFNγ (**Figure 6** and data not shown). Of note, Dinaciclib alone as well as in combination with other substances effectively suppressed all KP-related genes, implying inhibition of the TRP catabolism by this CDKi.

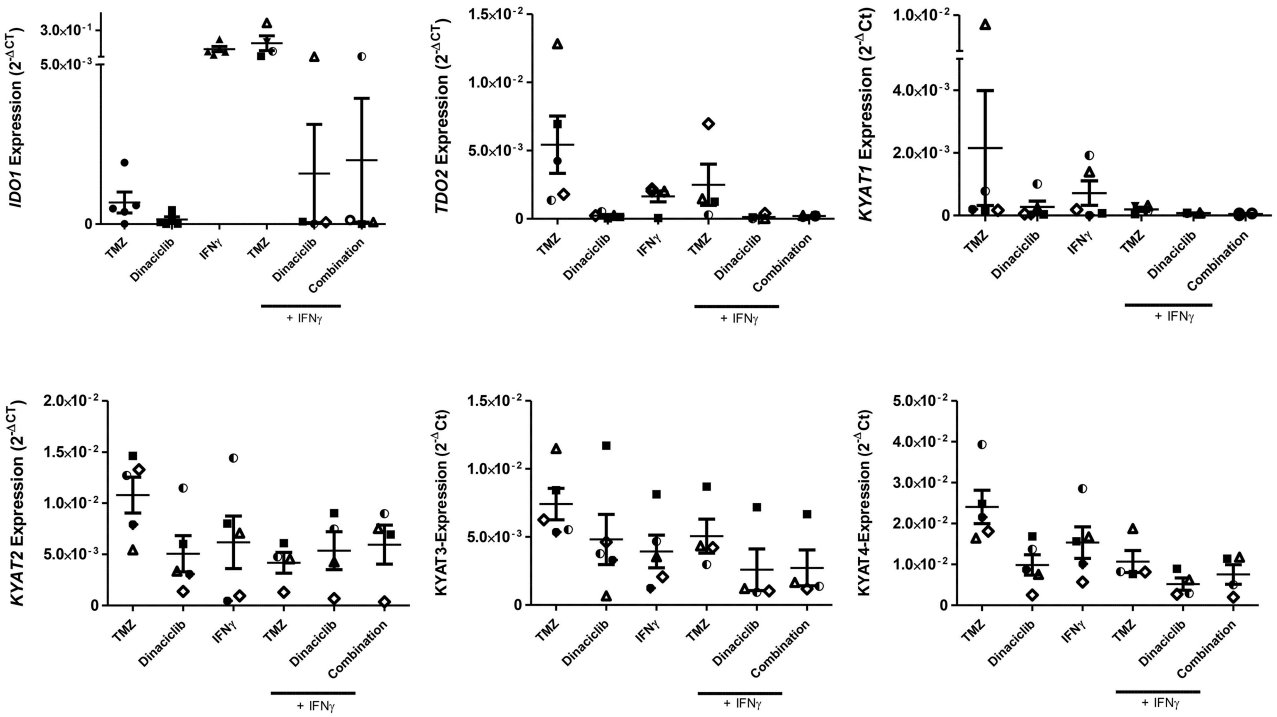

FIGURE 5 | Relative messenger RNA (mRNA) expression of *IDO1, TDO2, KYAT1, KYAT2, KYAT3*, and *KYAT4* upon concomitant treatment with interferon-γ (IFNγ) and cytostatic drugs in glioblastoma multiforme (GBM) cells. The cell cultures ($N = 5$, HROG02, HROG05, HROG52, HROG63, HROG75) were either left untreated or treated with IFNγ (50 ng/ml) for 24 h. Treatments were performed simultaneously, i.e., IFNγ ± TMZ, and/or Dinaciclib. Graphs indicate the mRNA expression of selected KP-related genes normalized to the housekeeping genes ($2^{-\Delta}$CT). Results show data of three independent experiments. A statistical report is given in **Supplementary Table for Figure 5**.

Dinaciclib Blocks IFNγ-Induced IDO1 Expression in GBM and HNSCC Cells

Considering the active downregulation of KP-related genes by Dinaciclib, we investigated whether this CDKi is able to inhibit or reverse IFNγ-induced IDO1 upregulation in GBM and HNSCC cells on a protein level. TMZ and Cetuximab were included as active inductors of *IDO1* and associated KP-related genes.

IFNγ and selected drugs were added simultaneously for 72 h. Dinaciclib effectively blocked IFNγ-induced IDO1 protein in both entities, while TMZ alone as well as the combination with IFNγ strongly enhanced IDO1 protein level (**Figure 7**). Hence, mRNA expression data were nicely confirmed.

When Dinaciclib was combined with IFNγ and TMZ, the IDO1-inducing stimulus of these latter substances was far too strong to be suppressed (**Figure 7**). However, the low number of residual cells in this combination hints toward additive or even synergistic effects independent from IDO1 (**Figures 7A,B**).

While IDO1 was highly inducible in GBM cells only, we then determined protein level upon IFNγ-prestimulation approaching the *in vivo* situation. The cytotoxic effect of Dinaciclib was preserved; however, levels of IDO1 enzyme were not significantly altered (**Supplementary Figures 2A,B**). Comparable results were obtained for TMZ. Virtually, all residual cells showed positive staining; still there was a trend toward lower intensity in monotherapy and in combination (**Supplementary Figure 2B**).

Taken together, the CDKi Dinaciclib is able to block IFNγ-mediated and thus most likely even chemotherapy-induced *IDO1* upregulation in GBM and HNSCC cells. However, blunt interference with this TRP-metabolizing enzyme is unlikely.

Treatment Induced Influence on KP-Related Metabolites

Our data revealed IDO1 induction by TMZ, which is reversible by Dinaciclib. Thus, we examined the influence on KP-related metabolites in GBM cell lines.

TRP, KYN, and the downstream metabolite kynurenic acid (KYNA) were quantified by MS using cell culture supernatants of GBM cell lines (**Figures 8A,B**). TRP was catabolized after 24 h from all cell lines among all treatment regimens. Adding TMZ or Dinaciclib in monotherapy marginally affected TRP consumption as well as KYN and KYNA production. Stimulation with either IFNγ or a combination of TMZ resulted in greatly enhanced TRP depletion and increased KYN levels, although to varying degrees in the different cell lines (**Figure 8A**). Small amounts of KYNA were produced constitutively and to a greater extent after IFNγ mono- and TMZ combination in all cell lines (**Figure 8A**). In contrast, KYNA level remained unchanged upon Dinaciclib in combination with IFNγ, confirming immunofluorescence results (please see **Figure 7** for details). The same was true for the KYN/TRP ratio, being only

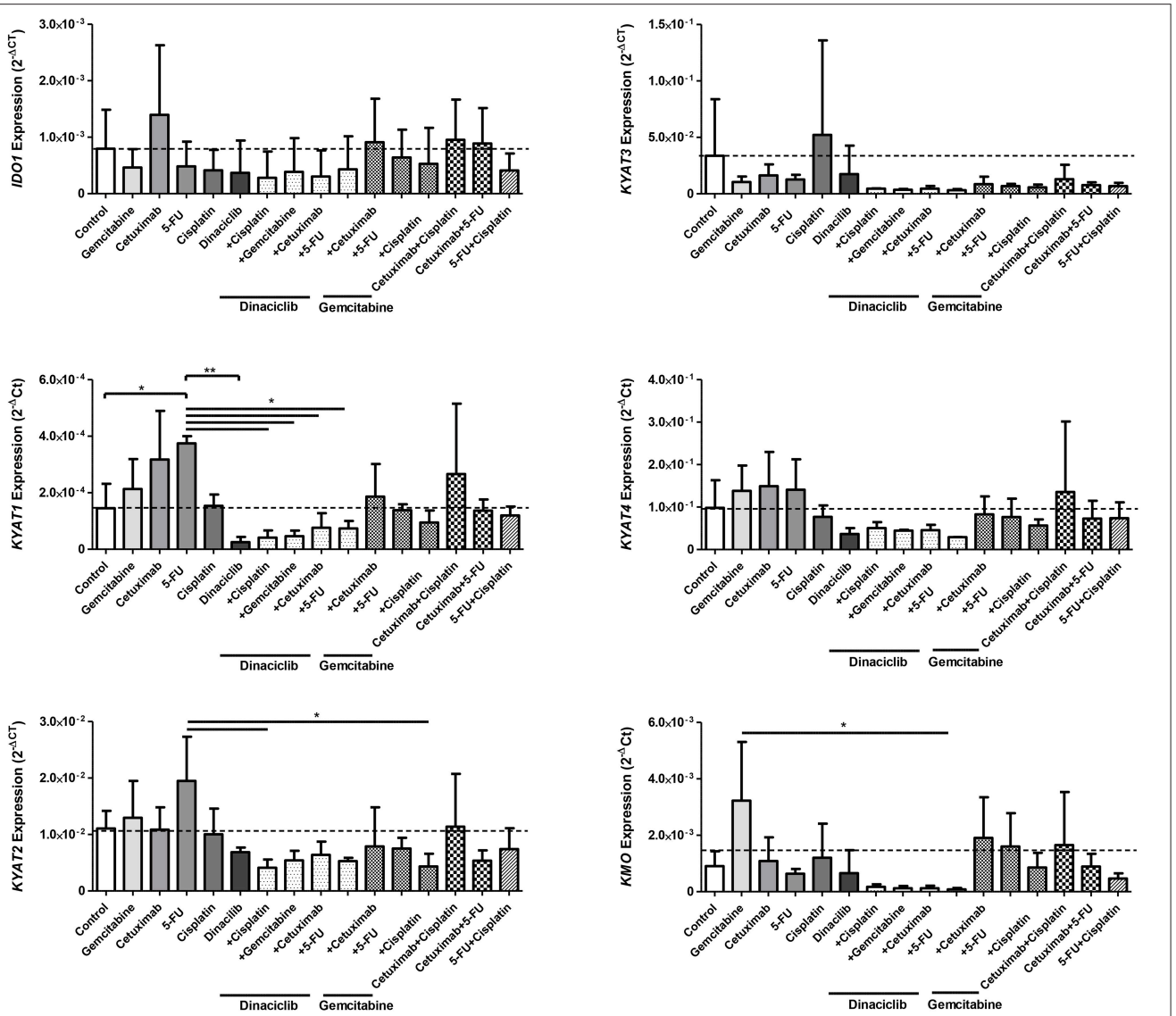

FIGURE 6 | Relative messenger RNA (mRNA) expression of *IDO1, KYAT1, KYAT2, KYAT3*, *KYAT4,* and KMO upon cytostatic drugs and targeted therapy in head and neck squamous cell carcinoma (HNSCC) cells. Graphs indicate the mRNA expression of selected KP-related genes normalized to the housekeeping genes ($2^{-\Delta}$CT). Results show data of three independent experiments using HNSCC cell line Detroit-562. *$p < 0.05$; **$p < 0.01$. One-way ANOVA (Bonferroni's multiple comparison test).

affected in samples treated with IFNγ as well as the combination of IFNγ and TMZ (**Figure 8B**).

These data underline our gene and protein expression data. The CDKi Dinaciclib is directly or indirectly capable of blocking the KP. TMZ particularly in combination with the proinflammatory cytokine IFNγ accelerates TRP consumption accompanied by KYN and KYNA production in GBM cells.

DISCUSSION

The finding that high *IDO1* expression is associated with shorter survival in cancer patients made IDO1 a promising target either by specific inhibitors or indirectly by immunomodulation. A recent study described dramatically suppressed tumor growth upon *IDO1* knockdown by increasing the number of $CD4^+$ and $CD8^+$ T cells in murine GBM models (9). However, the exact mechanisms underlying IDO1 and thus TRP metabolism along the KP remain unclear. Therefore, we focused on the expression of *IDO1* and *IDO*-related KP genes and their potential involvement in immune evasion in experimental models of HNSCC and GBM.

We were able to show that the KP is active in both entities, with different enzymes involved in TRP catabolism. Of note, basal *IDO1* expression was low and inversely correlated with *TDO2*. In the only prior study on primary GBM cultures, similar results were described with constitutive *TDO2* expression in

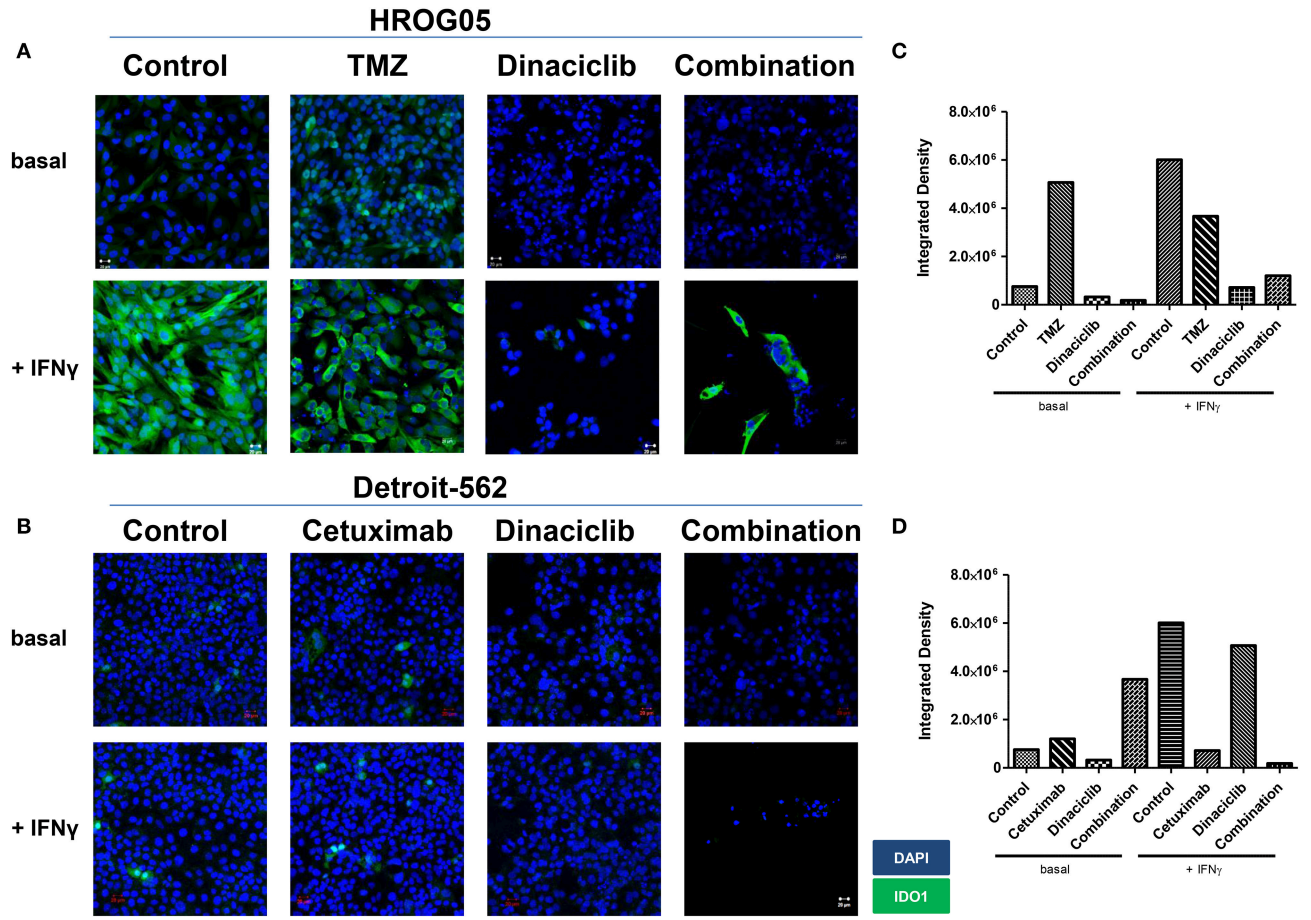

FIGURE 7 | Indoleamine 2,3-dioxygenase (IDO1) protein abundance in selected glioblastoma multiforme (GBM) and head and neck squamous cell carcinoma (HNSCC) cells upon cytostatic drugs and targeted therapy. The cell cultures [**(A)** GBM: HROG05; **(B)** HNSCC: Detroit-562] were either left untreated or treated with IFNγ (50 ng/ml) for 24 h. Treatments were performed simultaneously, i.e., IFNγ ± TMZ, Cetuximab, and/or Dinaciclib. Cell nuclei were stained with DAPI. Original magnification 20×. **(C,D)** Quantification was done to score staining intensity in untreated and treated HROG05 and Detroit-562 cells. This was carried out using ImageJ software as described in Material and Methods.

most GBM cell cultures (29). In here, TDO2 likely promotes tumor growth by suppressing antitumor immune responses (2, 31). KP products are considered as therapeutic targets because *IDO1* and other genes of the TRP metabolism are not expressed in healthy brain tissue, but gradually increase with GBM dedifferentiation (low vs. high grade GBM). In HNSCC, different results on *IDO1* are documented, and expression is heterogeneous among different HNSCC cell lines. Of note, IDO1 abundance of primary resection specimen and cultured cells seems to be independent from anatomical site and HPV status (40). Still, IDO1 is a useful marker for progression of in oral squamous cell carcinoma (41). In esophageal squamous cell carcinoma, progression and metastasis correlates with strong inflammation at the tumors' invasive front and disturbed TRP metabolism (42). These cumulative data highlight the biological relevance of the KP in malignancies and may explain why IDO1 is barely detectable upon long-term *in vitro* culture. By mimicking the inflamed microenvironment and thus taking a step closer to the *in vivo* situation, IFNγ was added as strong IDO1 inductor (43). While GBM cells responded with the expected *IDO1* upregulation on mRNA expression and protein level as well as accelerated TRP consumption, this molecule was barely inducible in HNSCC cells. It is conceivable that this is due to the duration of *in vitro* culture. GBM cells were established recently and thus used in defined low passages (<P40), whereas half of the HNSCC cell lines were long-term cultures with more or less unknown passage [Detroit-562 as well as UT-SCC14 and UT-SCC15 (44) are the only exceptions; <P40]. Cell lines may acquire additional mutations overtime changing their protein expression. Another *in vitro* limitation is that experiments were conducted without immunological pressure. *In vivo* studies are desirable to verify the results.

Indirect effects of TRP metabolism include interference with other biological functions like migration, angiogenesis, and cell growth regulation (18, 40). To investigate the influence of anticancer drugs on TRP catabolism, we performed a comprehensive analysis using conventional chemotherapy (TMZ, 5-FU, Cisplatin, Gemcitabine) and targeted drugs

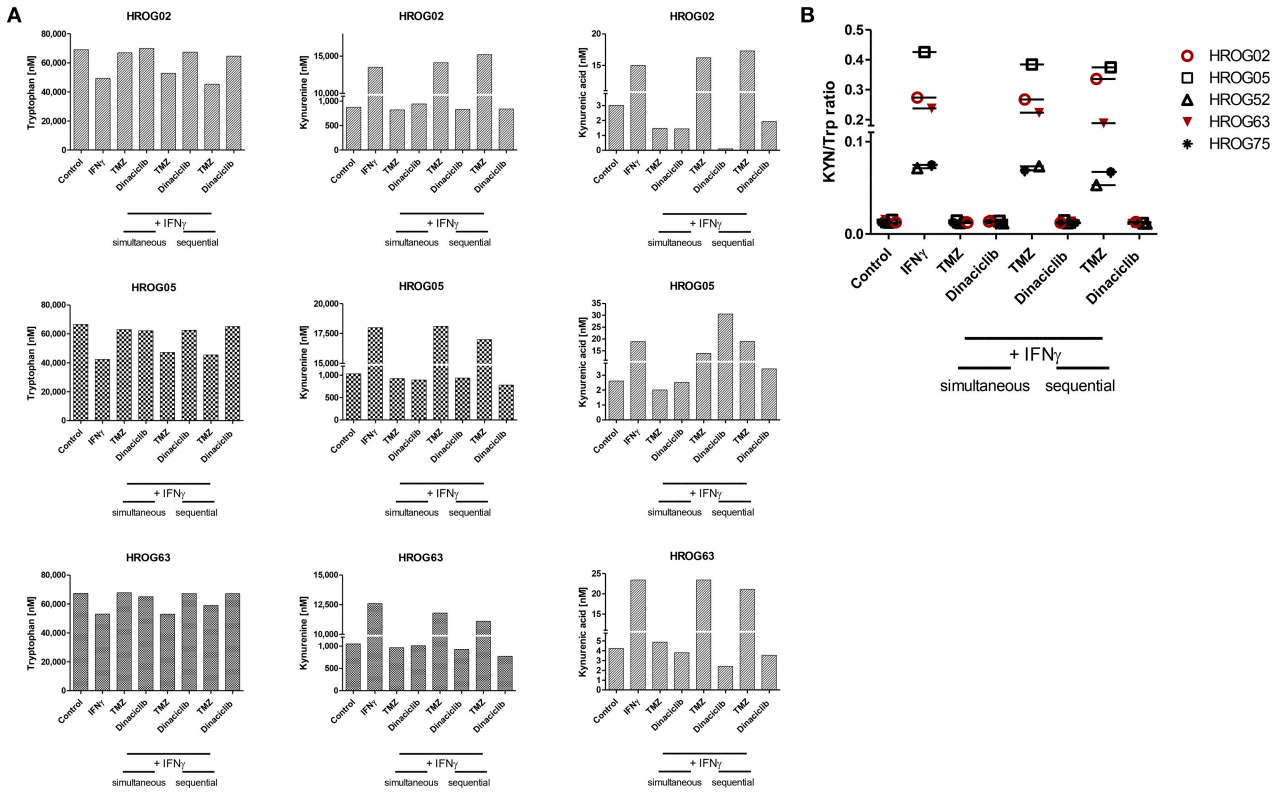

FIGURE 8 | Indoleamine 2,3-dioxygenase (IDO) protein abundance in glioblastoma multiforme (GBM) and head and neck squamous cell carcinoma (HNSCC) cells as well as kynurenine pathway (KP) metabolite levels in GBM cells upon cytostatic drugs and targeted therapy. Treatments were performed sequentially, i.e., interferon-γ (IFNγ) pretreatment for IDO1 induction, followed by Temozolomide (TMZ) and/or Dinaciclib. **(A)** KP metabolites changed upon TMZ but not Dinaciclib treatment. The combination of TMZ and IFNγ accelerates tryptophan (TRP) consumption accompanied by kynurenine (KYN) and kynurenic acid (KYNA) production **(B)**. KYN/TRP ratios in GBM cells were determined dividing KYN values by TRP values. Results show data of a single measurement.

(Cetuximab, Dinaciclib). The KP-related gene expression and metabolites were determined in residual cells. In GBM, the standard of care drug TMZ was applied either with or without IFNγ stimulation. While this substance affected *IDO1* on the expression level, the amount of the resulting protein increased. This may be explained by either increased protein's half-life due to a reduced rate of degradation or the preferential translation during cellular stress. In previous studies, exposure of several cultured human malignant glioma cell lines, primary neurons, and a neuroblastoma cell line to IFNγ reduced TRP levels in culture medium accompanied by increased *IDO1* expression and KYN production (29, 45). Our results confirm these data, and in addition, we were able to demonstrate that IFNγ stimulation in combination with TMZ stimulated KYN and KYNA production and TRP catabolism in GBM cell cultures. The increase in TRP catabolism and KYN production (KYN/TRP ratio) is widely used as indirect indicator of the cumulative activities of TDO2, IDO1, and IDO-2 (38, 46). The KP in brain tumors is likely triggered by IFNγ from immediate surrounding tissue (29, 47, 48). Thus, *IDO1* expression in brain tumor cells is likely to be triggered when IFNγ is produced from activated T cells and/or microglia and neurons. Furthermore, gliomas and glioneuronal tumors have an elevated tryptophan uptake and catabolism *in vivo* (49). Given our observation on a further enhanced KP activity upon TMZ treatment, this might provide an explanation of (acquired) drug resistance and final relapse. Hence, IDO1 blocking agents should be investigated in TMZ-tailored therapeutic approaches.

In HNSCC cells, KP activation was different. KP-related genes were exclusively induced by standard drugs, and only Cetuximab induced *IDO1*. Additional upregulated genes involved kynurenine aminotransferases, responsible for synthesizing a neuroprotectant, and KMO. While the specific biochemical activity of these molecules and biological relevance in cancer is barely examined, we interpret this result as one possible mechanism of resistance upon therapy—a finding quite common after conventional chemotherapy and usually also being associated with poor response toward neoadjuvant therapy in other entities (50).

Mechanistically, this can be attributed to the secretion of proinflammatory substances, such as prostaglandin E2 or high-mobility group protein B1 by dying tumor cells, secondary contributing to KP activation. By accumulating TRP, toxic metabolites of tumor cells actively shape an immunosuppressive microenvironment. Breaking down this shield is one of the main objectives in pharmacological inhibition of KP. Questions remain why most inhibitors failed in clinical trials, and mechanisms are

only just beginning to become clear. A fact worth mentioning is the functional redundancy of IDO1, IDO-2, and TDO2 (51), augmenting the risk of mechanistic bypass.

Dinaciclib is a potent and specific CDK inhibitor of CDK1, CDK2, CDK5, and CDK9. Preclinical studies showed that this inhibitor is capable of decelerating tumor growth in numerous cancer entities via cell cycle arrest and apoptosis induction (52, 53). In our study, Dinaciclib was the only KP-inhibiting substance tested here. Of note, impairment of the KP was independent from the combination partner, and this CDKi effectively suppressed IFNγ-induced *IDO1* upregulation after simultaneous treatment. While this result was completely unexpected and has—to the best of our knowledge—not been described previously, our data do not support the idea of blunt interference with the KP. GBM cells with strong *IDO1* expression showed only marginally reduced IDO1 protein level after Dinaciclib treatment. This effect might be boosted after long or repeated treatment cycles. In line with these findings, several preclinical studies already proposed synergistic effects of selective and unselective IDO1 inhibitors when administered in conjunction with chemo- and/or radiotherapy (4). This may finally have impact for second- or third-line immunotherapeutic approaches. Therefore, the late KYN/TRP index is indeed a relevant clinical benchmark providing prognostic value for GBM patients (54).

Summarizing our findings, we provide evidence for the relevance of TRP catabolism in malignancies especially in the context of standard therapy. The CDKi Dinaciclib was identified as indirect KP inhibitor. Lastly, specific KP inhibition may increase the efficacy of standard drugs by restoring immune function and thus improve patients' outcome.

DATA AVAILABILITY STATEMENT

The datasets generated for this study are available on request to the corresponding author.

AUTHOR CONTRIBUTIONS

CR performed experiments, analyzed data, and participated in manuscript writing. BS and AZ performed immunohistochemistry and analysis, and provided images. HK, JG, NI, and FS performed experiments and analyzed data. GD performed LC-MS analyses. CC and CJ participated in paper finalization and critically revised the manuscript. DS and EW critically revised the manuscript. CM designed study, the outline of the manuscript, performed data interpretation, and wrote the manuscript.

FUNDING

CM was supported by grants from the Deutsche Forschungsgemeinschaft (MA5799/2-1 and MA5799/2-2).

ACKNOWLEDGMENTS

The authors are also grateful to Susanne Neumeister and Dr. Ann-Kristin Henning from the Institute of Clinical Chemistry and Laboratory Medicine, University of Greifswald, for assisting with the quantification of TRP metabolites.

SUPPLEMENTARY MATERIAL

The Supplementary Material for this article can be found online at: https://www.frontiersin.org/articles/10.3389/fimmu.2020.00055/full#supplementary-material

Supplementary Figure 1 | Quantitative analysis of cell death in Detroit-562 HNSCC cells upon cytostatic drugs and targeted therapy. The cells were treated with the given substances for 24 and 72 h. Thereafter, cells were harvested and stained with Yo-Pro-1 to detect early and late apoptotic cells, as well as propidium iodide for necrosis determination. Apoptosis/necrosis discrimination was done on a flow cytometer (BD FACSVerse™) as described in material and methods. **(A)** Quantitative analysis of cell death after 24 and 72 h, respectively. $*p < 0.05$ vs. control; $**p < 0.01$ vs. control. *t*-test. **(B)** Representative dot plots showing elevated numbers of necrotic cells upon treatment. **(C)** Hemolysis and viability of PBMC upon treatment with Dinaciclib. Therefore, whole blood and PBMC were cultured in the presence of increasing Dinaciclib concentrations (1, 5, and 10 μM) for 2 and 24 h, respectively. Hemolytic activity was determined from cell-free supernatants (red blood cell lysis), Calcein AM was used for quantifying viability of PBMC. Mean + SD, $N = 5$ individual donors.

Supplementary Figure 2 | IDO1 protein abundance in HROG05 GBM cells upon cytostatic drugs and targeted therapy. The cells were pretreated with IFNγ (50 ng/ml) for 24 h. Thereafter TMZ, Dinaciclib and the combination of both substances was added to see whether IFNγ-induced upregulation of IDO1 is reversible. **(A)** None of these substances downregulated IDO1 in the sequential setting. Cell nuclei were stained with DAPI. Original magnification 20x. **(B)** Quantification was done to score staining intensity in untreated and treated HROG05 cells. This was carried out by using ImageJ software as described in material and methods.

Supplementary Table for Figure 5 | Statistical analysis of individual treatment regimens, depicted for each cell line, and genes analyzed.

REFERENCES

1. Liu M, Wang X, Wang L, Ma X, Gong Z, Zhang S, et al. Targeting the IDO1 pathway in cancer: from bench to bedside. *J Hematol Oncol.* (2018) 11:100. doi: 10.1186/s13045-018-0644-y
2. Platten M, Wick W, Van den Eynde BJ. Tryptophan catabolism in cancer: beyond IDO and tryptophan depletion. *Cancer Res.* (2012) 72:5435–40. doi: 10.1158/0008-5472.CAN-12-0569
3. Gajewski TF, Schreiber H, Fu Y-X. Innate and adaptive immune cells in the tumor microenvironment. *Nat Immunol.* (2013) 14:1014–22. doi: 10.1038/ni.2703
4. Muller AJ, DuHadaway JB, Donover PS, Sutanto-Ward E, Prendergast GC. Inhibition of indoleamine 2,3-dioxygenase, an immunoregulatory target of the cancer suppression gene Bin1, potentiates cancer chemotherapy. *Nat Med.* (2005) 11:312–9. doi: 10.1038/nm1196
5. Moon YW, Hajjar J, Hwu P, Naing A. Targeting the indoleamine 2,3-dioxygenase pathway in cancer. *J Immunother Cancer.* (2015) 3:51. doi: 10.1186/s40425-015-0094-9
6. Munn DH, Mellor AL. IDO in the tumor microenvironment: inflammation, counter-regulation, and tolerance. *Trends Immunol.* (2016) 37:193–207. doi: 10.1016/j.it.2016.01.002

7. Avril T, Saikali S, Vauleon E, Jary A, Hamlat A, De Tayrac M, et al. Distinct effects of human glioblastoma immunoregulatory molecules programmed cell death ligand-1 (PDL-1) and indoleamine 2,3-dioxygenase (IDO) on tumour-specific T cell functions. *J Neuroimmunol.* (2010) 225:22–33. doi: 10.1016/j.jneuroim.2010.04.003
8. Wainwright DA, Chang AL, Dey M, Balyasnikova IV, Kim CK, Tobias A, et al. Durable therapeutic efficacy utilizing combinatorial blockade against IDO, CTLA-4, and PD-L1 in mice with brain tumors. *Clin Cancer Res.* (2014) 20:5290–301. doi: 10.1158/1078-0432.CCR-14-0514
9. Hanihara M, Kawataki T, Oh-Oka K, Mitsuka K, Nakao A, Kinouchi H. Synergistic antitumor effect with indoleamine 2,3-dioxygenase inhibition and temozolomide in a murine glioma model. *J Neurosurg.* (2016) 124:1594–601. doi: 10.3171/2015.5.JNS141901
10. Badawy AAB. Kynurenine pathway of tryptophan metabolism: regulatory and functional aspects. *Int J Tryptophan Res.* (2017) 10:1178646917691938. doi: 10.1177/1178646917691938
11. Solomon B, Young RJ, Rischin D. Head and neck squamous cell carcinoma: genomics and emerging biomarkers for immunomodulatory cancer treatments. *Semin Cancer Biol.* (2018) 52:228–40. doi: 10.1016/j.semcancer.2018.01.008
12. Acovic A, Gazdic M, Jovicic N, Harrell CR, Fellabaum C, Arsenijevic N, et al. Role of indoleamine 2,3-dioxygenase in pathology of the gastrointestinal tract. *Therap Adv Gastroenterol.* (2018) 11:1756284818815334. doi: 10.1177/1756284818815334
13. Sordillo PP, Sordillo LA, Helson L. The kynurenine pathway: a primary resistance mechanism in patients with glioblastoma. *Anticancer Res.* (2017) 37:2159–71. doi: 10.21873/anticanres.11551
14. Zamanakou M, Germenis AE, Karanikas V. Tumor immune escape mediated by indoleamine 2,3-dioxygenase. *Immunol Lett.* (2007) 111:69–75. doi: 10.1016/j.imlet.2007.06.001
15. Ma W-J, Wang X, Yan W-T, Zhou Z-G, Pan Z-Z, Chen G, et al. Indoleamine-2,3-dioxygenase 1/cyclooxygenase 2 expression prediction for adverse prognosis in colorectal cancer. *World J Gastroenterol.* (2018) 24:2181–90. doi: 10.3748/wjg.v24.i20.2181
16. Brandacher G, Perathoner A, Ladurner R, Schneeberger S, Obrist P, Winkler C, et al. Prognostic value of indoleamine 2,3-dioxygenase expression in colorectal cancer: effect on tumor-infiltrating T cells. *Clin Cancer Res.* (2006) 12:1144–51. doi: 10.1158/1078-0432.CCR-05-1966
17. Jeong Y-I, Kim SW, Jung ID, Lee JS, Chang JH, Lee C-M, et al. Curcumin suppresses the induction of indoleamine 2,3-dioxygenase by blocking the Janus-activated kinase-protein kinase Cdelta-STAT1 signaling pathway in interferon-gamma-stimulated murine dendritic cells. *J Biol Chem.* (2009) 284:3700–8. doi: 10.1074/jbc.M807328200
18. Platten M, von Knebel Doeberitz N, Oezen I, Wick W, Ochs K. Cancer immunotherapy by targeting IDO1/TDO and their downstream effectors. *Front Immunol.* (2014) 5:673. doi: 10.3389/fimmu.2014.00673
19. Uyttenhove C, Pilotte L, Theate I, Stroobant V, Colau D, Parmentier N, et al. Evidence for a tumoral immune resistance mechanism based on tryptophan degradation by indoleamine 2,3-dioxygenase. *Nat Med.* (2003) 9:1269–74. doi: 10.1038/nm934
20. Fox E, Oliver T, Rowe M, Thomas S, Zakharia Y, Gilman PB, et al. Indoximod: an immunometabolic adjuvant that empowers T cell activity in cancer. *Front Oncol.* (2018) 8:370. doi: 10.3389/fonc.2018.00370
21. Beatty GL, O'Dwyer PJ, Clark J, Shi JG, Bowman KJ, Scherle PA, et al. First-in-human phase I study of the oral inhibitor of indoleamine 2,3-dioxygenase-1 epacadostat (INCB024360) in patients with advanced solid malignancies. *Clin Cancer Res.* (2017) 23:3269–76. doi: 10.1158/1078-0432.CCR-16-2272
22. Platten M, Nollen EAA, Röhrig UF, Fallarino F, Opitz CA. Tryptophan metabolism as a common therapeutic target in cancer, neurodegeneration and beyond. *Nat Rev Drug Discov.* (2019) 18:379–401. doi: 10.1038/s41573-019-0016-5
23. Kanai M, Yoshimura K, Asada M, Imaizumi A, Suzuki C, Matsumoto S, et al. A phase I/II study of gemcitabine-based chemotherapy plus curcumin for patients with gemcitabine-resistant pancreatic cancer. *Cancer Chemother Pharmacol.* (2011) 68:157–64. doi: 10.1007/s00280-010-1470-2
24. Maletzki C, Scheinpflug P, Witt A, Klar E, Linnebacher M. Targeting immune-related molecules in cancer therapy: a comprehensive *in vitro* analysis on patient-derived tumor models. *Biomed Res Int.* (2019) 2019:4938285. doi: 10.1155/2019/4938285
25. Vacchelli E, Aranda F, Eggermont A, Sautes-Fridman C, Tartour E, Kennedy EP, et al. Trial watch: IDO inhibitors in cancer therapy. *Oncoimmunology.* (2014) 3:e957994. doi: 10.4161/21624011.2014.957994
26. Schafer CC, Wang Y, Hough KP, Sawant A, Grant SC, Thannickal VJ, et al. Indoleamine 2,3-dioxygenase regulates anti-tumor immunity in lung cancer by metabolic reprogramming of immune cells in the tumor microenvironment. *Oncotarget.* (2016) 7:75407–24. doi: 10.18632/oncotarget.12249
27. Yentz S, Smith D. Indoleamine 2,3-dioxygenase (IDO) inhibition as a strategy to augment cancer immunotherapy. *BioDrugs.* (2018) 32:311–7. doi: 10.1007/s40259-018-0291-4
28. Long GV, Dummer R, Hamid O, Gajewski TF, Caglevic C, Dalle S, et al. Epacadostat plus pembrolizumab versus placebo plus pembrolizumab in patients with unresectable or metastatic melanoma (ECHO-301/KEYNOTE-252): a phase 3, randomised, double-blind study. *Lancet Oncol.* (2019) 20:1083–97. doi: 10.1016/S1470-2045(19)30274-8
29. Adams S, Teo C, McDonald KL, Zinger A, Bustamante S, Lim CK, et al. Involvement of the kynurenine pathway in human glioma pathophysiology. *PLoS ONE.* (2014) 9:e112945. doi: 10.1371/journal.pone.0112945
30. Ball HJ, Jusof FF, Bakmiwewa SM, Hunt NH, Yuasa HJ. Tryptophan-catabolizing enzymes—party of three. *Front Immunol.* (2014) 5:485. doi: 10.3389/fimmu.2014.00485
31. Pilotte L, Larrieu P, Stroobant V, Colau D, Dolusic E, Frederick R, et al. Reversal of tumoral immune resistance by inhibition of tryptophan 2,3-dioxygenase. *Proc Natl Acad Sci USA.* (2012) 109:2497–502. doi: 10.1073/pnas.1113873109
32. Abdel-Magid AF. Targeting the inhibition of tryptophan 2,3-dioxygenase (TDO-2) for cancer treatment. *ACS Med Chem Lett.* (2017) 8:11–3. doi: 10.1021/acsmedchemlett.6b00458
33. Jamieson SM, Tsai P, Kondratyev MK, Budhani P, Liu A, Senzer NN, et al. Evofosfamide for the treatment of human papillomavirus-negative head and neck squamous cell carcinoma. *JCI Insight.* (2018) 3:122204. doi: 10.1172/jci.insight.122204
34. Maletzki C, Klier U, Marinkovic S, Klar E, Andrä J, Linnebacher M. Host defense peptides for treatment of colorectal carcinoma-a comparative *in vitro* and *in vivo* analysis. *Oncotarget.* (2014) 5:4467–79. doi: 10.18632/oncotarget.2039
35. Fuertig R, Ceci A, Camus SM, Bezard E, Luippold AH, Hengerer B. LC-MS/MS-based quantification of kynurenine metabolites, tryptophan, monoamines and neopterin in plasma, cerebrospinal fluid, and brain. *Bioanalysis.* (2016) 8:1903–17. doi: 10.4155/bio-2016-0111
36. Opitz CA, Litzenburger UM, Sahm F, Ott M, Tritschler I, Trump S, et al. An endogenous tumour-promoting ligand of the human aryl hydrocarbon receptor. *Nature.* (2011) 478:197–203. doi: 10.1038/nature10491
37. Guo T, Califano JA. Molecular biology and immunology of head & neck cancer. *Surg Oncol Clin N Am.* (2015) 24:397–407. doi: 10.1016/j.soc.2015.03.002
38. Adam I, Dewi DL, Mooiweer J, Sadik A, Mohapatra SR, Berdel B, et al. Upregulation of tryptophanyl-tRNA synthethase adapts human cancer cells to nutritional stress caused by tryptophan degradation. *Oncoimmunology.* (2018) 7:e1486353. doi: 10.1080/2162402X.2018.1486353
39. Smith C, Chang MY, Parker KH, Beury DW, DuHadaway JB, Flick HE, et al. IDO is a nodal pathogenic driver of lung cancer and metastasis development. *Cancer Discov.* (2012) 2:722–35. doi: 10.1158/2159-8290.CD-12-0014
40. Bates AM, Gomez Hernandez MP, Lanzel EA, Qian F, Brogden KA. Matrix metalloproteinase (MMP) and immunosuppressive biomarker profiles of seven head and neck squamous cell carcinoma (HNSCC) cell lines. *Transl Cancer Res.* (2018) 7:533–42. doi: 10.21037/tcr.2018.05.09
41. Seppala M, Halme E, Tiilikainen L, Luukkainen A, Laranne J, Rautiainen M, et al. The expression and prognostic relevance of indoleamine 2,3-dioxygenase in tongue squamous cell carcinoma. *Acta Otolaryngol.* (2016) 136:729–35. doi: 10.3109/00016489.2016.1152631
42. Cheng J, Jin H, Hou X, Lv J, Gao X, Zheng G. Disturbed tryptophan metabolism correlating to progression and metastasis of esophageal squamous cell carcinoma. *Biochem Biophys Res Commun.* (2017) 486:781–7. doi: 10.1016/j.bbrc.2017.03.120

43. Grant RS, Naif H, Espinosa M, Kapoor V. IDO induction in IFN-gamma activated astroglia: a role in improving cell viability during oxidative stress. *Redox Rep.* (2000) 5:101–4. doi: 10.1179/135100000101535357
44. Tonlaar N, Galoforo S, Thibodeau BJ, Ahmed S, Wilson TG, Yumpo Cardenas P, et al. Antitumor activity of the dual PI3K/MTOR inhibitor, PF-04691502, in combination with radiation in head and neck cancer. *Radiother Oncol.* (2017) 124:504–12. doi: 10.1016/j.radonc.2017.08.001
45. Miyazaki T, Moritake K, Yamada K, Hara N, Osago H, Shibata T, et al. Indoleamine 2,3-dioxygenase as a new target for malignant glioma therapy. Laboratory investigation. *J Neurosurg.* (2009) 111:230–7. doi: 10.3171/2008.10.JNS081141
46. Suzuki Y, Suda T, Asada K, Miwa S, Suzuki M, Fujie M, et al. Serum indoleamine 2,3-dioxygenase activity predicts prognosis of pulmonary tuberculosis. *Clin Vaccine Immunol.* (2012) 19:436–42. doi: 10.1128/CVI.05402-11
47. Guillemin GJ, Smythe G, Takikawa O, Brew BJ. Expression of indoleamine 2,3-dioxygenase and production of quinolinic acid by human microglia, astrocytes, and neurons. *Glia.* (2005) 49:15–23. doi: 10.1002/glia.20090
48. Adams S, Braidy N, Bessede A, Brew BJ, Grant R, Teo C, et al. The kynurenine pathway in brain tumor pathogenesis. *Cancer Res.* (2012) 72:5649–57. doi: 10.1158/0008-5472.CAN-12-0549
49. Juhasz C, Chugani DC, Muzik O, Wu D, Sloan AE, Barger G, et al. *In vivo* uptake and metabolism of alpha-[11C]methyl-L-tryptophan in human brain tumors. *J Cereb Blood Flow Metab.* (2006) 26:345–57. doi: 10.1038/sj.jcbfm.9600199
50. Li F, Wei L, Li S, Liu J. Indoleamine-2,3-dioxygenase and Interleukin-6 associated with tumor response to neoadjuvant chemotherapy in breast cancer. *Oncotarget.* (2017) 8:107844–58. doi: 10.18632/oncotarget.22253
51. Muller AJ, Manfredi MG, Zakharia Y, Prendergast GC. Inhibiting IDO pathways to treat cancer: lessons from the ECHO-301 trial and beyond. *Semin Immunopathol.* (2019) 41:41–8. doi: 10.1007/s00281-018-0702-0
52. Parry D, Guzi T, Shanahan F, Davis N, Prabhavalkar D, Wiswell D, et al. Dinaciclib (SCH 727965), a novel and potent cyclin-dependent kinase inhibitor. *Mol Cancer Ther.* (2010) 9:2344–53. doi: 10.1158/1535-7163.MCT-10-0324
53. Lin SF, Lin JD, Hsueh C, Chou TC, Wong RJ. A cyclin-dependent kinase inhibitor, dinaciclib in preclinical treatment models of thyroid cancer. *PLoS ONE.* (2017) 12:e172315. doi: 10.1371/journal.pone.0172315
54. Zhai L, Dey M, Lauing KL, Gritsina G, Kaur R, Lukas RV, et al. The kynurenine to tryptophan ratio as a prognostic tool for glioblastoma patients enrolling in immunotherapy. *J Clin Neurosci.* (2015) 22:1964–8. doi: 10.1016/j.jocn.2015.06.018

Conflict of Interest: The authors declare that the research was conducted in the absence of any commercial or financial relationships that could be construed as a potential conflict of interest.

cancers

MDPI

Article

The Individual Effects of Cyclin-Dependent Kinase Inhibitors on Head and Neck Cancer Cells—A Systematic Analysis

Nina Schoenwaelder [1,*], Inken Salewski [1], Nadja Engel [2], Mareike Krause [1], Björn Schneider [3], Michael Müller [4], Christin Riess [1,5], Heiko Lemcke [6,7,8], Anna Skorska [6,7,8], Christina Grosse-Thie [1], Christian Junghanss [1] and Claudia Maletzki [1]

1 Department of Internal Medicine, Medical Clinic III—Hematology, Oncology, Palliative Medicine, University Medical Center Rostock, 18057 Rostock, Germany; Inken.salewski@med.uni-rostock.de (I.S.); mareike.krause@uni-rostock.de (M.K.); Christin.riess@med.uni-rostock.de (C.R.); christina.grosse-thie@med.uni-rostock.de (C.G.-T.); christian.junghanss@med.uni-rostock.de (C.J.); claudia.maletzki@med.uni-rostock.de (C.M.)
2 Department of Oral and Maxillofacial Surgery, Facial Plastic Surgery, University Medical Center Rostock, 18057 Rostock, Germany; Nadja.Engel@med.uni-rostock.de
3 Institute of Pathology, University Medical Center Rostock, Strempelstr.14, 18057 Rostock, Germany; bjoern.schneider@med.uni-rostock.de
4 Core Facility for Cell Sorting & Cell Analysis, Laboratory for Clinical Immunology, University Medical Center Rostock, 18057 Rostock, Germany; Michael.Mueller2@med.uni-rostock.de
5 University Children's Hospital, Rostock University Medical Centre, 18057 Rostock, Germany
6 Department of Cardiac Surgery, Reference and Translation Center for Cardiac Stem Cell Therapy (RTC), University Medical Center Rostock, 18057 Rostock, Germany; Heiko.Lemcke@med.uni-rostock.de (H.L.); anna.skorska@med.uni-rostock.de (A.S.)
7 Department of Cardiology, University Medical Center Rostock, 18059 Rostock, Germany
8 Department Life, Light & Matter, Faculty of Interdisciplinary Research, University Rostock, 18059 Rostock, Germany
* Correspondence: nina.schoenwaelder@med.uni-rostock.de; Tel.: +49-381-494-5764

Simple Summary: This study examined the therapeutic potential of a combined therapy approach, based on clinical approved drugs (5-FU, Cisplatin, cetuximab) and cyclin-dependent kinase inhibitors (CDKi, dinaciclib, palbociclib, THZ1). We identified individual effects on head and neck squamous cell carcinoma cells, including induction of apoptosis/necrosis, and senescence as well as reduced invasiveness. Besides, we describe the relevance of the sequential timing of each combination partner to achieve synergistic effects. Another interesting finding of our study is the upregulation of immunologically relevant molecules on the tumor cell surface under certain CDKi-drug combinations. Here, dinaciclib and palboclicb had highest impact on immunogenicity, which even exceeded effects of the standard drugs. Finally, a therapeutic in vivo approach partially confirmed cell line-based results. Here, effective tumor growth control was seen when cisplatin was combined with dinaciclib. However, antitumoral effects were highly individual and nicely confirm the heterogeneity of this tumor entity.

Abstract: Cyclin-dependent kinase inhibitors (CDKi´s) display cytotoxic activity against different malignancies, including head and neck squamous cell carcinomas (HNSCC). By coordinating the DNA damage response, these substances may be combined with cytostatics to enhance cytotoxicity. Here, we investigated the influence of different CDKi´s (palbociclib, dinaciclib, THZ1) on two HNSCC cell lines in monotherapy and combination therapy with clinically-approved drugs (5-FU, Cisplatin, cetuximab). Apoptosis/necrosis, cell cycle, invasiveness, senescence, radiation-induced γ-H2AX DNA double-strand breaks, and effects on the actin filament were studied. Furthermore, the potential to increase tumor immunogenicity was assessed by analyzing Calreticulin translocation and immune relevant surface markers. Finally, an in vivo mouse model was used to analyze the effect of dinaciclib and Cisplatin combination therapy. Dinaciclib, palbociclib, and THZ1 displayed anti-neoplastic activity after low-dose treatment, while the two latter substances slightly enhanced radiosensitivity. Dinaciclib decelerated wound healing, decreased invasiveness, and induced MHC-I, accompanied by high amounts of surface-bound Calreticulin. Numbers of early and late apoptotic

Citation: Schoenwaelder, N.; Salewski, I.; Engel, N.; Krause, M.; Schneider, B.; Müller, M.; Riess, C.; Lemcke, H.; Skorska, A.; Grosse-Thie, C.; et al. The Individual Effects of Cyclin-Dependent Kinase Inhibitors on Head and Neck Cancer Cells—A Systematic Analysis. *Cancers* **2021**, *13*, 2396. https://doi.org/10.3390/cancers13102396

Academic Editor: Samuel C. Mok

Received: 1 March 2021
Accepted: 11 May 2021
Published: 15 May 2021

cells increased initially (24 h), while necrosis dominated afterward. Antitumoral effects of the selective CDKi palbociclib were weaker, but combinations with 5-FU potentiated effects of the monotherapy. Additionally, CDKi and CDKi/chemotherapy combinations induced MHC I, indicative of enhanced immunogenicity. The in vivo studies revealed a cell line-specific response with best tumor growth control in the combination approach. Global acting CDKi's should be further investigated as targeting agents for HNSCC, either individually or in combination with selected drugs. The ability of dinaciclib to increase the immunogenicity of tumor cells renders this substance a particularly interesting candidate for immune-based oncological treatment regimens.

Keywords: targeted therapy; combination strategies; immunogenic cell death; xenograft model

1. Introduction

Mammalian cell cycle is controlled by cyclin dependent kinases (CDKs) [1]. In tumors, CDKs are dysregulated and CDK/cyclin complexes frequently overexpressed [2–4]. Tumor cells bypass the CDK4/6-Rb axis because it is critical for cell cycle entry and cell proliferation [5]. The knowledge about these mutations is a chance to identify molecular targets for pharmacological interventions [6]. Indeed, several CDK inhibitors (CDKi's) been developed for cancer treatment. Additionally to the highly selective and FDA-approved CDKi's palbociclib, ribociclib, and abemaciclib, multi- and pan-CDKi's are now entering clinical trials. These include, among others, dinaciclib that targets CDK1, CDK2, CDK5, and CDK9 [7,8], and THZ1, which is active against CDK7, CDK12, and CDK13 [9,10].

Advances in understanding of pathobiology and molecular characteristics have contributed to the introduction of novel therapy approaches. Still, the treatment of solid tumors remains challenging. Additionally to intrinsic resistance mechanisms, the development or outgrowth of single subclones after therapy promotes immune escape and complicates precision medicine.

Head and neck cancers are paradigmatic for tumor heterogeneity. They can be found in the oral cavity, pharynx, larynx, salivary glands, nasal cavity, and paranasal sinuses [11]. The predominant histological type of head and neck tumors is squamous cell carcinomas (HNSCC) [11]. HNSCC is the 7th most common cancer worldwide [11–13]. Risk factors include tobacco, alcohol, and human papillomavirus (HPV) infection. The latter drives tumor formation in the oropharynx with distinct clinical, histopathological, and molecular characteristics [14,15]. Around 58% of the patients present with loco-regionally advanced disease at diagnosis and this patient cohort has a poor prognosis [11]. Hence, the implementation of targeted therapies in standard treatment schedules constitutes a promising and urgently needed approach for improving treatment and outcome. In 2019, a multicenter, multigroup, phase 2 trial reported promising activity outcomes in patients with platinum-resistant or cetuximab-resistant HPV-unrelated HNSCC receiving palbociclib and cetuximab [16]. Though combination strategies are promising, the sequential timing of each combination partner remains debatable [17–19]. To move forward, we here employed simultaneous and sequential combination strategies of clinically approved therapeutics and CDKi's for treating HNSCC with the aim to identify the best strategy.

2. Results

2.1. CDKi Treatment Impairs Viability and Exerts Synergistic Effects in Combination Therapy

UT-SCC-14 and UT-SCC-15 were used as in vitro cell culture models, since these cells are representative for primary and recurrent HNSCC. Both cell lines were susceptible to standard drugs and CDKi's in clinically relevant doses (below 1 μM for CDKi's and $\leq$90 μg/mL for cytostatic drug), as determined in preliminary experiments. For combination experiments, standard drugs 5-Fluorouracil (5-FU), Cisplatin, and cetuximab as well as CDKi's (dinaciclib, palbociclib, THZ1) were applied in doses below the IC_{50} (Figure 1A,B; cetuximab is the only exceptions, here IC_{50} doses were used). The time course of treatment

CDKi's (dinaciclib, palbociclib, THZ1) were applied in doses below the IC_{50} (Figure 1A,B; cetuximab is the only exceptions, here IC_{50} doses were used). The time course of treatment considered each cell lines' doubling times and attempted to mimic the in vivo situation. Therefore, cells received two treatment cycles of 72 h.

In a first series, simultaneous combinations were applied (Figure 1B). Notably, dual CDKi treatment was synergistic or additive in UT-SCC-14 and partially in UT-SCC-15 cells as determined by biomass quantification. Here, combinations of dinaciclib with palbociclib or THZ1 were synergistic (Figure 1B). CDKi/drug combinations were mainly antagonistic. The only exception was seen for Cisplatin in conjunction with dinaciclib (UT-SCC-14) and cetuximab with dinaciclib or THZ1 (UT-SCC-15).

A **1 x 72 h treatment**

drug	UT-SCC-14	UT-SCC-15
	Biomass in relation to control [%]	
5-FU	72	92
Cisplatin	71	106
cetuximab	45	74

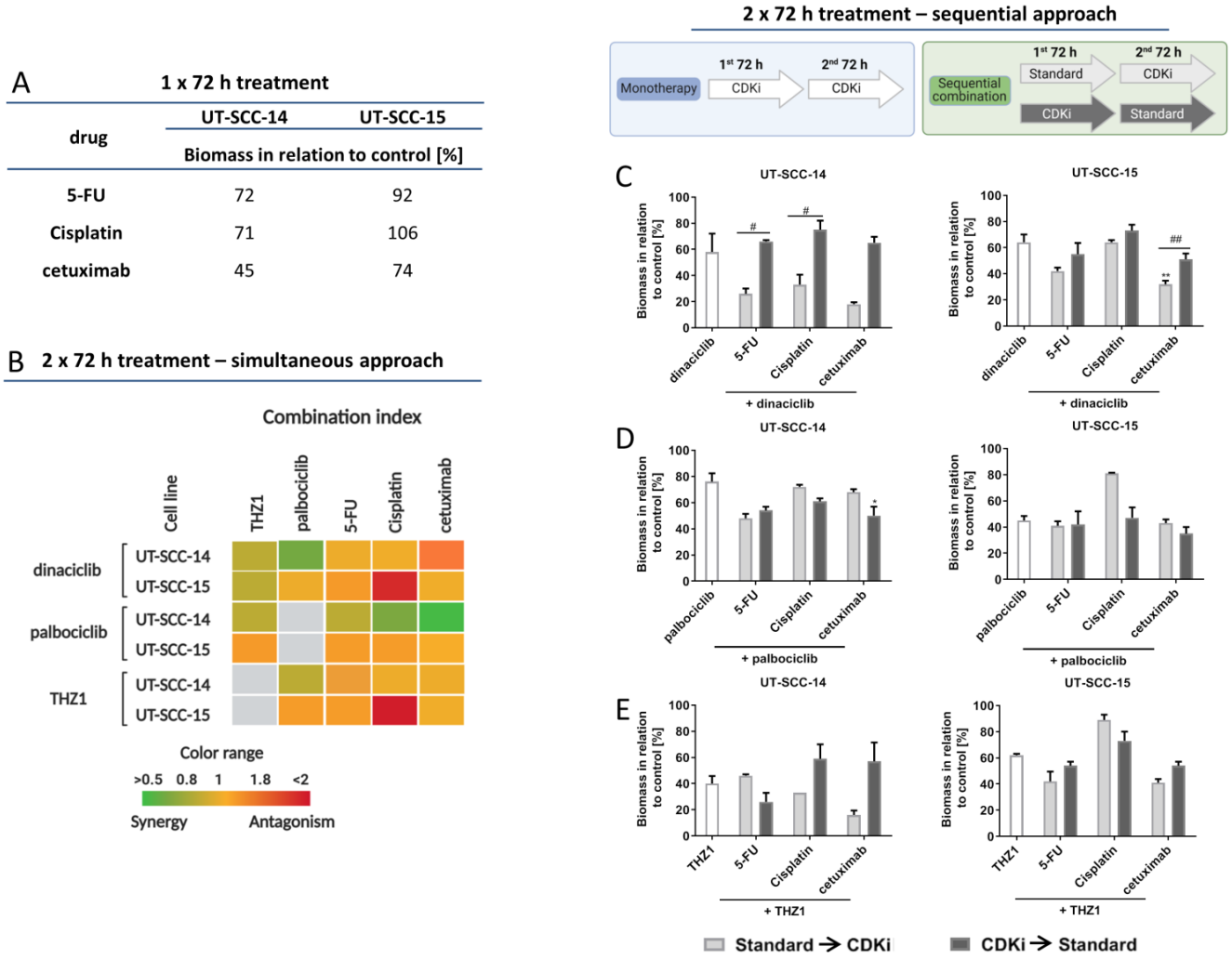

Figure 1. Simultaneous and sequential treatment schedules. (**A**) Biomass quantification after monotherapy with 5-FU, Cisplatin, and cetuximab (1 × 72 h). Doses used here were determined before using classical dose response curve analysis. Read out was done by crystal violet staining and biomass in relation to untreated controls quantified. In (**B**) the Bliss Independence model was used to calculate potential synergistic effects. The green color indicates a synergistic and red color an antagonistic effect of the simultaneous combinations. (**C**–**E**) Sequential treatment: (**C**) dinaciclib [0.005 µM], (**D**) palbociclib [1 µM], and (**E**) THZ1 [UT-SCC14: 0.02 µM; UT-SCC-15: 0.005 µM] in comparison to 2 × 72 h CDKi monotherapy (first bar of each graph). Drug doses were as follows: 5-FU [0.32 µg/mL], Cisplatin [UT-SCC14: 0.5 µg/mL; UT-SCC-15: 0.05 µg/mL], cetuximab [0.5 µg/mL]. Mann Whitney U-test (*n* = 3–4 independent experiments) # $p \leq 0.05$, ## $p < 0.01$ vs. 1st CDKi; Kruskal Wallis test ($n = 3$–4 independent experiments) * $p < 0.05$, ** $p < 0.01$ vs. monotherapy. The 1 × 72 h monotherapy with 5-FU, Cisplatin or Cetuximab confirms that the potential enhancing effect of sequential combination therapy is not due to the single administration of these substances but the effect of the 2 × 72 h CDKi monotherapy (in the left bar) is actually enhanced.

In a first series, simultaneous combinations were applied (Figure 1B). Notably, dual CDKi treatment was synergistic or additive in UT-SCC-14 and partially in UT-SCC-15 cells as determined by biomass quantification. Here, combinations of dinaciclib with palbociclib or THZ1 were synergistic (Figure 1B). CDKi/drug combinations were mainly antagonistic. The only exception was seen for Cisplatin in conjunction with dinaciclib (UT-SCC-14) and cetuximab with dinaciclib or THZ1 (UT-SCC-15).

To test if the effect of a 2 × 72 h CDKi monotherapy can be boosted, sequential combinations were performed (Figure 1C–E). The first bar of each graph shows CDKi monotherapy, followed by the sequential combination treatments. CDKi were either given before or after standard therapy. The sequential treatment with dinaciclib (Figure 1C) revealed higher biomass reduction in both cell lines when standard therapy was given first. There was a strong reduction for all three combinations in UT-SCC-14 and UT-SCC-15. The sequential treatment with palbociclib yielded opposite results (Figure 1D). Here, palbociclib pretreatment prior to Cisplatin or cetuximab was better than the other way around. The order of 5-FU application had no leverage. For the sequential combination with THZ1 (Figure 1E), cell line-specific responses were seen. UT-SCC-14 cells' viability was more affected when 5-FU was given first and second THZ1. Comparable effects were seen after THZ1/Cisplatin treatment in UT-SCC-15 cells. Still, the other combinations were only effective when the standard drug was given before.

The aforementioned findings nicely confirm the heterogeneous response pattern of HNSCC.

2.2. CDKi's Induce Apoptotic and Necrotic Cell Death and Mediate Calreticulin Translocation

To investigate the effects of different treatments on the two cell lines, an apoptosis-necrosis assay was performed on selected treatment schedules (Figure 2A,B). Cells were simultaneously treated with CDKi's and drugs (5-FU, Cisplatin) for 24 and 72 h (Figure 2A,B). Short-term dinaciclib monotherapy mainly induced early apoptotic and necrotic cell death. The other monotherapies had minor or no impact on cell viability. After 72 h, overall cell death was higher in treated cells, but with individual differences. Dinaciclib alone or in combination induced necrosis, THZ1 and its combinations triggered apoptosis or a mixed form of apoptosis and necrosis (Figure 2A,B). Additionally to the induced cell death, senescence was studied, since this is a common response to CDK inhibition (Figure S1). These experiments revealed senescence induction by specific CDKi's (e.g., dinaciclib) or its combination with standard drugs (e.g., 5-FU). However, senescence was not the dominating cellular response here, suggesting a minor role. UT-SCC-14 cells clumped together, especially under dinaciclib monotherapy and combination therapy, while UT-SCC-15 cell clusters were disrupted. The combination of THZ1 and 5-FU had similar effects to dinaciclib.

Then, the ability to induce immunogenic cell death was measured after 72 h by detecting calreticulin (CalR) on the tumor cells' surface (Figure 2C). The proportion of CalR positive cells and the mean fluorescence intensity signal (MFI) (Figure 2D) were recorded. Dinaciclib induced CalR translocation in monotherapy and combination therapy significantly. Notably, the combination of THZ1 and 5-FU likewise induced CalR translocation. While these findings already hint towards immune stimulating properties, we additionally checked for immunologically relevant markers (Figure 3A,B). The abundance of HLA-ABC (MHC class I) and PD-1 on tumor cells was examined. A significant increase in MHC class I was seen after dinaciclib monotherapy and combination therapy as well as upon palbociclib treatment of UT-SCC-14 cells (Figure 3A). The MHC class I abundance changed marginally in UT-SCC-15 cells irrespective of the treatment schedule used (Figure 3B). This was, however, likely because of the high basal MHC class I abundance, which was about 80%. Still, dinaciclib and their combinations tended to upregulate MHC class I, finally yielding ~100%. PD-1 was upregulated by certain treatments. This did, however, not reach statistical significance (Figure 3A,B).

death, senescence was studied, since this is a common response to CDK inhibition (Figure S1). These experiments revealed senescence induction by specific CDKi's (e.g., dinaciclib) or its combination with standard drugs (e.g., 5-FU). However, senescence was not the dominating cellular response here, suggesting a minor role. UT-SCC-14 cells clumped together, especially under dinaciclib monotherapy and combination therapy, while UT-SCC-15 cell clusters were disrupted. The combination of THZ1 and 5-FU had similar effects to dinaciclib.

Cancers **2021**, *13*, x 5 of 20

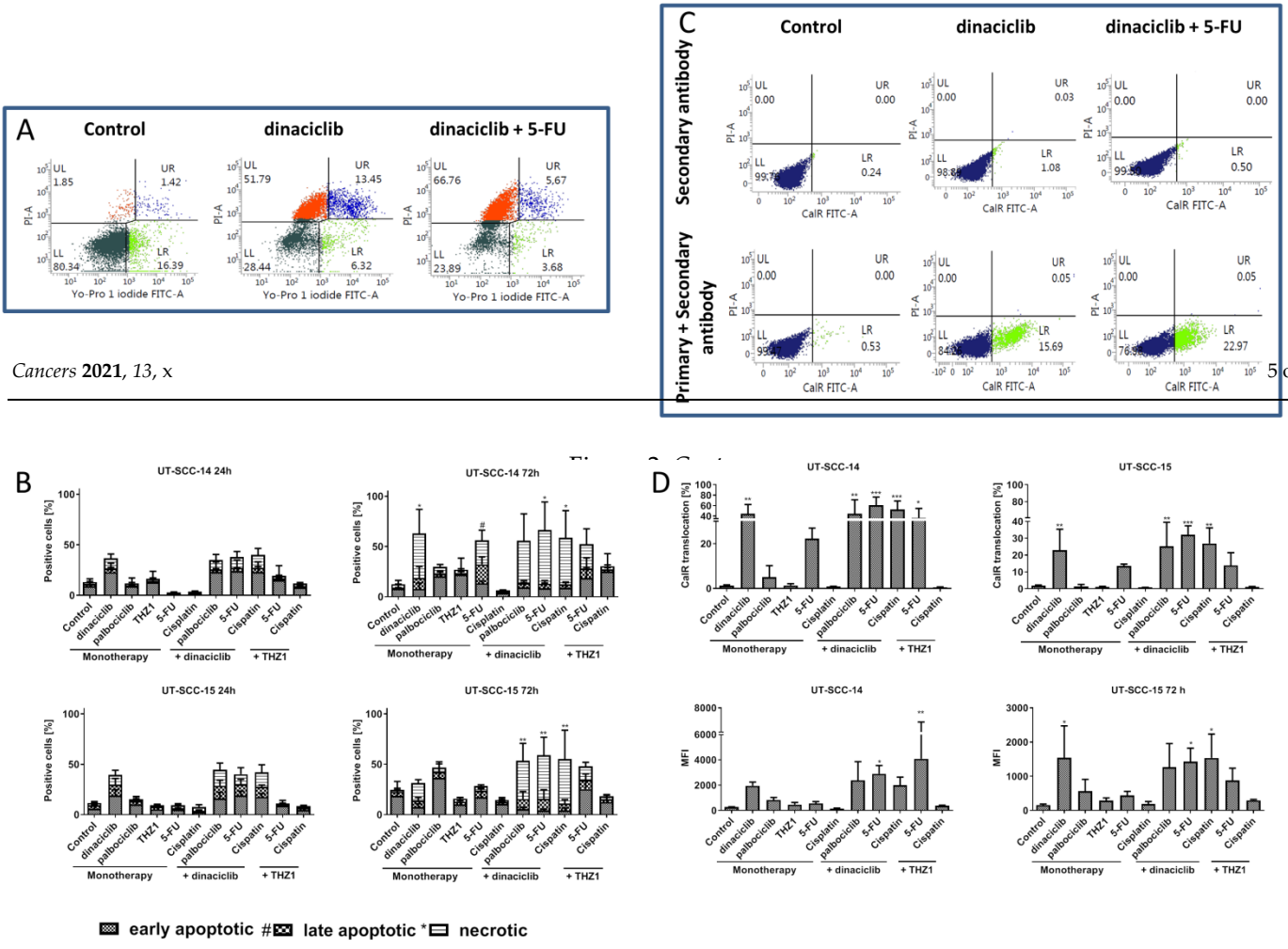

Figure 2. Apoptosis/necrosis assay and detection of immunogenic cell death (ICD). For (**A**,**B**) apoptosis/necrosis assay, cells were stained with Yo-Pro 1 iodide and PI. Cells that were positive for Yo-Pro 1 iodide were defined as early apoptotic, cells that were positive for PI were defined as necrotic, and double positive cells were defined as late apoptotic. Apoptosis/necrosis assay was done after 24 h and 72 h. (**A**) Representative dots plots showing distribution of viable and dead cells (either apoptotic or necrotic). (**B**) Quantitative analysis of apoptotic and necrotic cells subdivided into early apoptotic (Yo-Pro1$^+$/PI$^-$), late apoptotic (Yo-Pro1$^+$/PI$^+$) and necrotic ((Yo-Pro1$^-$/PI$^+$). (**C**,**D**)) ICD was detected after 72 h treatment by staining CalR on the cell surface. In both assays, 10,000 events were measured and the percentage of cells showing CalR translocation and the mean fluorescence intensity (MFI) of CalR$^+$ cells are provided. Drug doses were as follows: dinaciclib [0.02 µM], palbociclib [1 µM], THZ1 [UT-SCC-14: 0.2 µM; UT-SCC-15: 0.005 µM], 5-FU [90 µg/mL], Cisplatin [0.1 µg/mL]. (**B**) Kruskal Wallis Test (n = 4–5 independent experiments) late apoptotic # $p < 0.05$ vs. control; necrotic * $p < 0.05$, ** $p < 0.01$ vs. control (**D**) 1way ANOVA (n = 3–4 independent experiments) * $p \leq 0.05$, ** $p \leq 0.01$, *** $p \leq 0.001$ vs. control.

Then, the ability to induce immunogenic cell death was measured after 72 h by detecting calreticulin (CalR) on the tumor cells' surface (Figure 2C). The proportion of CalR positive cells and the mean fluorescence intensity signal (MFI) (Figure 2D) were recorded. Dinaciclib induced CalR translocation in monotherapy and combination therapy significantly. Notably, the combination of THZ1 and 5-FU likewise induced CalR translocation. While these findings already hint towards immune stimulating properties, we additionally checked for immunologically relevant markers (Figure 3A,B). The abundance of HLA-ABC (MHC class I) and PD-1 on tumor cells was examined. A significant increase in MHC class I was seen after dinaciclib monotherapy and combination therapy as well as upon palbociclib treatment of UT-SCC-14 cells (Figure 3A). The MHC class I abundance changed marginally in UT-SCC-15 cells irrespective of the treatment schedule used (Figure 3B). This was, however, likely because of the high basal MHC class I abundance, which was about 80%. Still, dinaciclib and their combinations tended to upregulate MHC class I, finally yielding ~100%. PD-1 was upregulated by certain treatments. This did, however, not reach statistical significance (Figure 3A,B).

2.3. CDKi Induce Cell Cyclce Arrest

Cancers **2021**, *13*, x 6 of 20

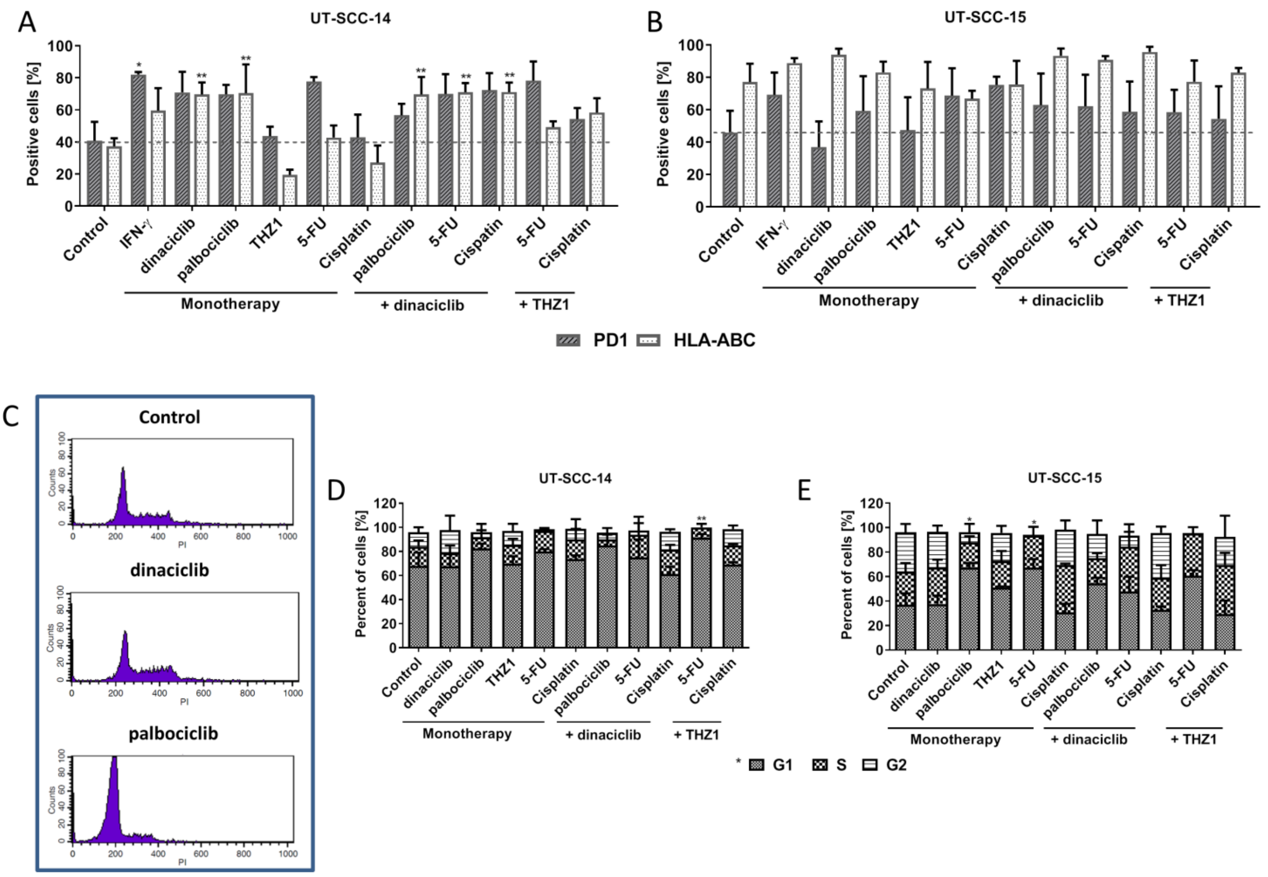

Figure 3. Phenotyping and cell cycle analysis. Phenotyping of **(A)** UT-SCC-14 and **(B)** UT-SCC-15 cells using multi-color flow cytometry. Therefore, cells were stained after 48 h treatment with test substances using the following antibodies: anti-HLA-ABC antibody (MHC I) and anti-CD279 (PD-1). Drug doses were as follows: IFN-γ [50 ng/mL]; dinaciclib [0.02 μM]; palbociclib [1 μM]; THZ1 [UT-SCC14: 0.02 μM; UT-SCC-15: 0.005 μM]; 5-FU [90 μg/mL]; Cisplatin [0.1 μg/mL]. 1 way ANOVA ($n \geq 3$ independent experiments) * $p < 0.05$, ** $p < 0.01$, vs. control. **(C–E)** Cell cycle analysis. Ethanol-fixed cells were stained with PI. **(C)** Representative histograms showing distribution of cell cycle phases in control cells and upon therapy. **(D,E)** Quantitative cell cycle analysis showing amounts of cells in G1, S, and G2 phase. Drug doses were as follows: dinaciclib [0.005 μM]; palbociclib [1 μM]; THZ1 [UT-SCC14: 0.02 μM; UT-SCC-15: 0.005 μM]; 5-FU [90 μg/mL]; Cisplatin [0.1 μg/mL]. 1way ANOVA ($n = 3$ independent experiments) * $p < 0.05$, ** $p < 0.01$ vs. control.

2.3. CDKi Induce Cell Cycle Arrest

Due to the mode of action of CDKi's, cell cycle analysis was done on residual tumor cells (typically below 50%, Figure 3C–E). Representative histograms for all treatments are given in Figure S4. The number of residual cells after dinaciclib treatment was low. In these, tumor cell cycle distribution was quite similar to controls. In UT-SCC-14 cells, a G1 arrest was only seen after combined THZ1 and 5-FU therapy ($p < 0.05$ vs. control), while the remaining cells treated with palbociclib. With regard to the UT-SCC-15 cells, significant changes after palbociclib- and THZ1- based combinations with 5-FU. By contrast,

2.4. CDKi's Have Minor Impact on Double-Strand Breaks and Radiosensitivity

Treatment-induced double-strand breaks (DSBs) were determined by fluorescence microscopy using γ-H2AX (Figure 4). H2AX is phosphorylated by kinases after DNA double-strand breaks on serine 139. CDKi monotherapy or combination therapy itself had minor impacts on γ-H2AX foci, which were hardly detectable (Figure 4). To test if the applied regimens may enhance radiosensitivity, we then checked for irradiation-induced DSBs using 2 Gy (Figure 4B). Indeed, numbers of γ-H2AX-positive cells increased, with

highest amounts in cells treated with palbociclib. With regard to the combinations, γ-H2AX foci were primarily seen in palbociclib-or THZ1- based combinations with 5-FU. By contrast, such radiosensitizing effects were not seen in combinations with dinaciclib and may thus constitute a specific consequence of palbociclib or THZ1 treatment.

Cancers **2021**, *13*, x 7 of 20

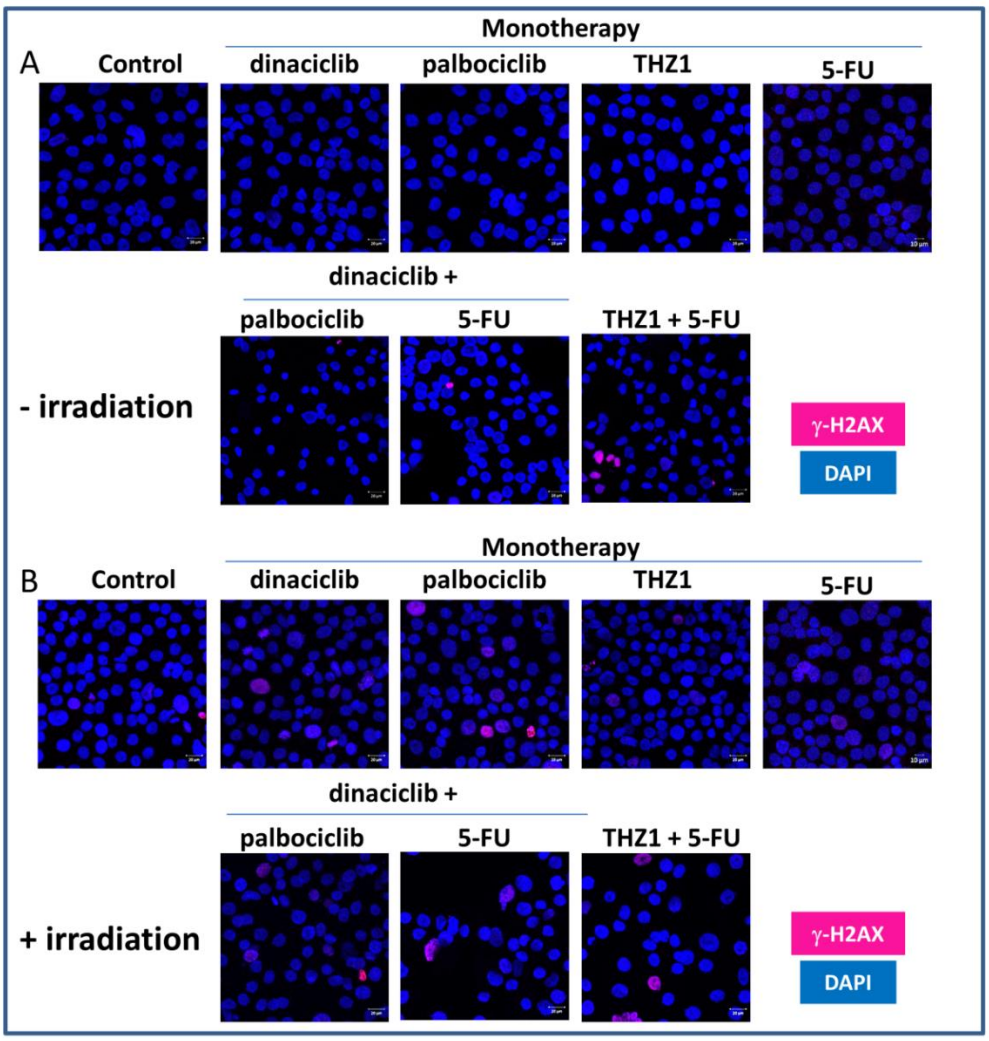

Figure 4. γ-H2AX staining of UT-SCC-14 cells. In order to detect a potential radiosensitizing effect of the test substances, cells were treated 24 h with selected monotherapy and combination therapies and then irradiated with 2 Gy using an IBL637. (**A**,**B**) We had three control groups. The first was completely untreated, the second was treated with the test substances but not irradiated, and the third was only irradiated but not treated with the test substances. Drug doses were as follows: dinaciclib [0.005 µM]; palbociclib [1 µM]; THZ1 [0.02 µM]; 5-FU [0.32 µg/mL]; γ-H2AX staining was performed 6 h after irradiation. Cell nuclei were stained with DAPI. Images were taken on a Zeiss LSM-780 Confocal Laser Microscope.

2.5. CDKi's Remodel the Actin Filament

Live cell monitoring via impedance measurements is particularly suitable for studying alterations in the cell monolayer, in the adhesion properties, and in the membrane integrity in real time. While the impedance increased over time in untreated control cells, dinaciclib treatment massively reduced impedance (Figure 5A,B). For palbociclib treated UT-SCC-14 cells, the measured impedance slightly decreased after 48 h, while THZ1 monotherapy slightly increased impedance (Figure 5A). Notably, the combination of THZ1 and 5-FU caused a delayed impedance breakdown in both cell lines. Here, impedance increased within the first 20 h. Thereafter, the impedance stagnated for approximately 3 h, and then decreased for the next 48 h until no impedance was detectable. Dinaciclib in conjunction with cytostatics (Cisplatin, 5-FU) induced a complete and irreversible breakdown.

Cancers **2021**, *13*, x 8 of 20

within the first 20 h. Thereafter, the impedance stagnated for approximately 3 h, and then decreased for the next 48 h until no impedance was detectable. Dinaciclib in conjunction with cytostatics (Cisplatin, 5-FU) induced a complete and irreversible breakdown.

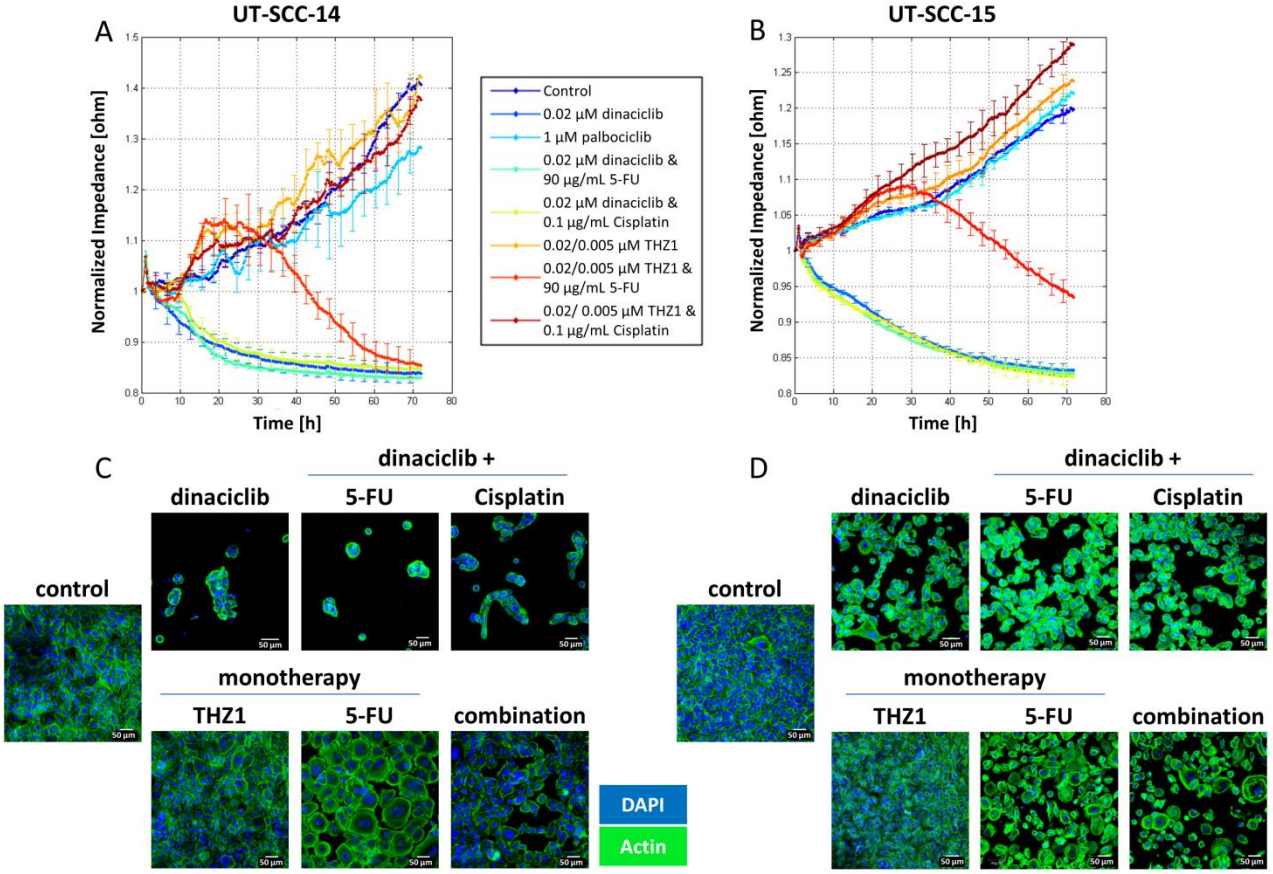

Figure 5. Impedance measurement and cytoskeletal staining. (**A**,**C**) UT-SCC-14 and (**B**,**D**) UT-SCC-15 cells. Cells were seeded in a 96-well ECIS array plate with 20 interdigitated electrodes/well and treated with selected test substances to investigate the impact of the treatment schedules. Drug doses were as follows: dinaciclib [0.02 µM]; palbociclib [1 µM]; THZ1 [UT-SCC14: 0.02 µM; UT-SCC-15: 0.005 µM]; 5-FU [90 µg/mL]; Cisplatin [0.1 µg/mL]. Impedance was monitored in real-time. The analysis of cell-cell contacts was performed by 4000 kHz using ECIS Software. Then, actin staining was performed with phalloidin green. Cell nuclei were stained with DAPI. Analysis was performed with a Zeiss LSM-780 Confocal Laser Microscope. Original magnification 200×.

Figure 5. Impedance measurement and cytoskeletal staining. (**A**,**C**) UT-SCC-14 and (**B**,**D**) UT-SCC-15 cells. Cells were seeded in a 96-well ECIS array plate with 20 interdigitated electrodes/well and treated with selected test substances to investigate the impact of the treatment schedules. Drug doses were as follows: dinaciclib [0.02 µM]; palbociclib [1 µM]; THZ1 [UT-SCC14: 0.02 µM; UT-SCC-15: 0.005 µM]; 5-FU [90 µg/mL]; Cisplatin [0.1 µg/mL]. Impedance was monitored in real-time. The analysis of cell-cell contacts was performed by 4000 kHz using ECIS Software. Then, actin staining was performed with phalloidin green. Cell nuclei were stained with DAPI. Analysis was performed with a Zeiss LSM-780 Confocal Laser Microscope. Original magnification 200×.

To confirm the impedance data, actin fibers were stained 72 h after treatment (Figure 5C,D). Untreated UT-SCC-14 cells form a typical monolayer with a cortically formed cytoskeleton and less stress fibers within the cells. Dinaciclib itself caused massive cell detachment and consequently cell death. Nearly all UT-SCC-14 cells were detached after dinaciclib treatment, while some UT-SCC-15 cells remained attached and spread. Cytostatics (Cisplatin, 5-FU) intensified actin abundance in both cell lines.

To confirm the impedance data, actin fibers were stained 72 h after treatment (Figure 5C,D). Untreated UT-SCC-14 cells form a typical monolayer with a cortically formed cytoskeleton and less stress fibers within the cells. Dinaciclib itself caused massive cell detachment and consequently cell death. Nearly all UT-SCC-14 cells were detached after dinaciclib treatment, while some UT-SCC-15 cells remained attached and spread. Cytostatics (Cisplatin, 5-FU) intensified actin abundance in both cell lines.

THZ1 strengthened the formation of stress fibers in both cell lines that increases cellular stiffness and changes the motility properties [20]. This finding adds to the higher impedance under THZ1 treatment compared to the untreated control. THZ1 in combination with 5-FU caused higher cytotoxic effects, so most cells were detached.

THZ1 strengthened the formation of stress fibers in both cell lines that increases cellular stiffness and changes the motility properties [20]. This finding adds to the higher impedance under THZ1 treatment compared to the untreated control. THZ1 in combination with 5-FU caused higher cytotoxic effects, so most cells were detached.

2.6. Influence on Mitochondria, Lysosomes, the Endoplasmatic Reticulum and Vacuole Formation

2.6. Influence on Mitochondria, Lysosomes, the Endoplasmatic Reticulum and Vacuole Formation

CDKi-based treatments induced cytoplasmic vacuole formation. Hence, we checked the influence of the treatment schedules on mitochondria, lysosomes, and endoplasmatic reticulum (ER) (Figure 6). In both cell lines, mitochondrial activity increased after dinaciclib monotherapy and combination therapy (Figure 6). Monotherapy with palbociclib, THZ1, or Cisplatin induced lysosome formation, but only in UT-SCC-14 cells. An effect of

CDKi-based treatments induced cytoplasmic vacuole formation. Hence, we checked the influence of the treatment schedules on mitochondria, lysosomes, and endoplasmatic reticulum (ER) (Figure 6). In both cell lines, mitochondrial activity increased after dinaciclib monotherapy and combination therapy (Figure 6). Monotherapy with palbociclib, THZ1, or Cisplatin induced lysosome formation, but only in UT-SCC-14 cells. An effect of

Cancers **2021**, *13*, x 9 of 20

monotherapy and combination therapy (Figure 6). Monotherapy with palbociclib, THZ1, or Cisplatin induced lysosome formation, but only in UT-SCC-14 cells. An effect of the treatments on the ER could not be demonstrated. After 5-FU treatment, the mitochondrial activity of UT-SCC-15 cells slightly increased that was reversed by THZ1. Cisplatin monotherapy had opposite effects that were neutralized by the combination partners (Figure 6B).

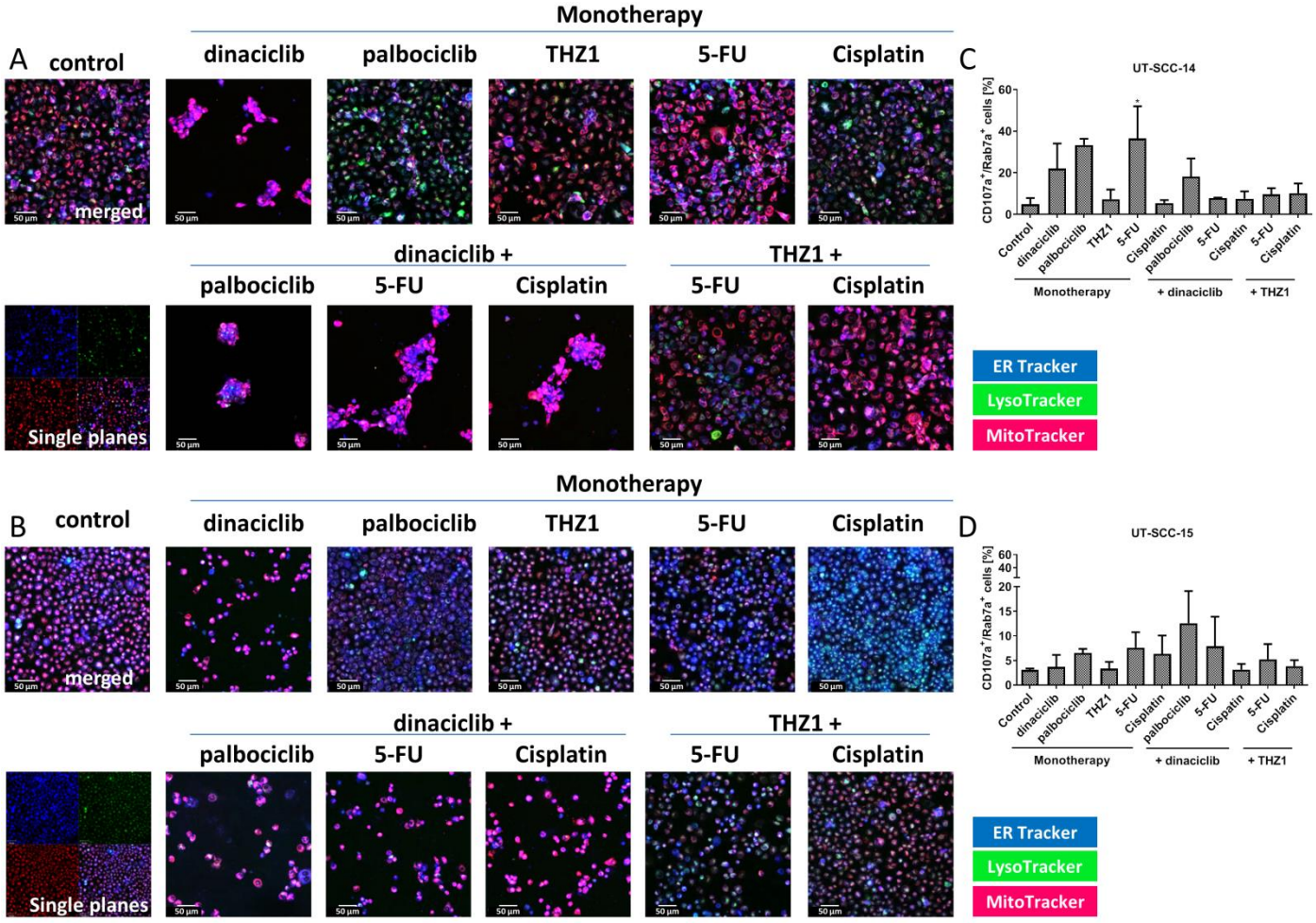

Figure 6. Influence on mitochondria, lysosomes, ER, and vacuole formation (**A**,**C**) UT-SCC-14 and (**B**,**D**) UT-SCC-15 cells. (**A**,**C**) To investigate the effect of the test substances on the mitochondrial activity, the lysosome formation, and the ER, cells were treated for 72 h with test substances and stained with MitoTracker (red), LysoTracker (green), and ER-Tracker (blue). Drug doses were as follows: dinaciclib [0.02 µM]; palbociclib [1 µM]; THZ1 [UT-SCC14: 0.02 µM; UT-SCC-15: 0.005 µM]; 5-FU [90 µg/mL]; Cisplatin [0.1 µg/mL]. Representative merged images are shown. For the control, a separated fluorescent image is shown. Analysis was performed with a ZEISS Elyra 7 Confocal Laser Microscope. (**C**,**D**) Cells were stained for CD107a and Rab7a as a hint for vacuole formation and measured via flow cytometry. The percentage of CD107a and Rab7a positive cells are shown. Drug doses were as follows: dinaciclib [0.02 µM]; palbociclib [1 µM]; THZ1 [UT-SCC14: 0.02 µM; UT-SCC-15: 0.005 µM]; 5-FU [90 µg/mL]; Cisplatin [0.1 µg/mL]. 1way ANOVA (n = 3 independent experiments) * $p < 0.05$ vs. control.

Cells were stained for specific late endo-lysosomal markers CD107a (LAMP1) and Rab7a to confirm observed findings (Figure 6C,D). The GTPase Rab7a [21] is primarily associated with late endosomes and lysosomes [22]. Typically showing higher numbers of late endo-lysosomal markers after treatment, in detail dinaciclib, palbociclib, and 5-FU monotherapy resulted in the highest increase of positive cells ($p < 0.05$, Palbociclib and 5-FU vs. control) (Figure 6C). The combination could not boost effects. In UT-SCC-15 cells, highest numbers of CD107a$^+$/Rab7a$^+$ cells were detected after dual CDK inhibition (palbociclib + dinaciclib) (Figure 6D), implying that lysosomal formation plays a minor role here.

(Figure 6C). The combinations could not boost effects. In UT-SCC-15 cells, highest numbers of $CD107a^+/Rab7a^+$ cells were detected after dual CDK inhibition (palbociclib + dinaciclib) (Figure 6D), implying that lysosomal formation plays a minor role here.

2.6.1. CDKi's Reduce Invasiveness and Migratory Potential

An assay was performed to explore the migration potential of cells to a cell free space under treatment. The cell line UT-SCC-14 filled the scratch within 24 h; the same was true for THZ1 and 5-FU monotherapy and combination therapy (Figure S2A). The toxic activity of dinaciclib induced cell death within 72 h and an accordingly incomplete scratch closure. Adding THZ1 to dinaciclib delayed migration, so the scratch was filled after 48 h. Using an invasion assay, the ability of cells to escape from the toxic environment was then investigated. For this experiment, selective treatments were included based on the obtained results shown before. The invasive cells from treatment medium were put in relation to invasive cells from control medium. CDKi treatment with dinaciclib significantly reduced invasiveness (Figure S2B). Effects were even stronger when two CDKi's were combined (dinaciclib + THZ1), but not by adding 5-FU. Still, these data confirm the potential of CDKi's to interfere with cellular invasion.

2.6.2. In Vivo Results

Finally, a xenograft mouse model was used to test if in vitro results can be transferred in vivo. For this proof-of-concept study, dinaciclib and Cisplatin were chosen as therapeutics and given alone or in combination (Figure 7A). We decided to use this combination, since dinaciclib had strong antitumoral effects in all previous analyses and Cisplatin is the accepted standard of care for HNSCC patients.

UT-SCC-14 xenografts showed a poor treatment response. Monotherapy had no influence on tumor growth and the combination was only able to decelerate growth (Figure 7B). In contrast, UT-SCC-15 xenograft growth was significantly reduced under therapy (Figure 7B). Dinaciclib and its combination with Cisplatin decreased the tumor volume to a minimum, the latter even stopped tumor growth until the experimental endpoint (two months follow-up). As a consequence of the better treatment response, mice challenged with UT-SCC-15 lived longer compared to those harboring UT-SCC-14 xenografts (Figure 7C). The outcome was best in the combination with a median survival of 63 days (vs. control 42 days, $p < 0.05$). As for dinaciclib monotherapy, mice had to be euthanized mostly because of tumor ulcerations. Hence, the poorer survival in both cases is not justified by the tumor volume as an endpoint but due to ethical aspects. Histology of residual tumors confirmed the different treatment responses. UT-SCC-14 xenografts presented with initial necrosis that increased after dinaciclib treatment (Figure 7D). After Cisplatin therapy, beginning necrosis with initial inflammatory reaction was visible, but also vital tumor tissue. In the combination, keratinized squamous cell carcinoma containing degenerated cells was found. In addition, neutrophilic infiltration was observed. The UT-SCC-15 xenograft sections of control mice showed characteristics of a keratinizing squamous cell carcinoma with developing necrosis. After dinaciclib treatment, degenerated and early apoptotic cells became prominent with surrounding necrosis. Cisplatin monotherapy primarily induced necrosis. The dark spot in the center of the image is degenerated keratinized squamous epithelium. Necrosis was dominating in the combination with some swollen cells, indicative of early cell damage in the initial stage.

Cancers **2021**, *13*, x 11 of 20

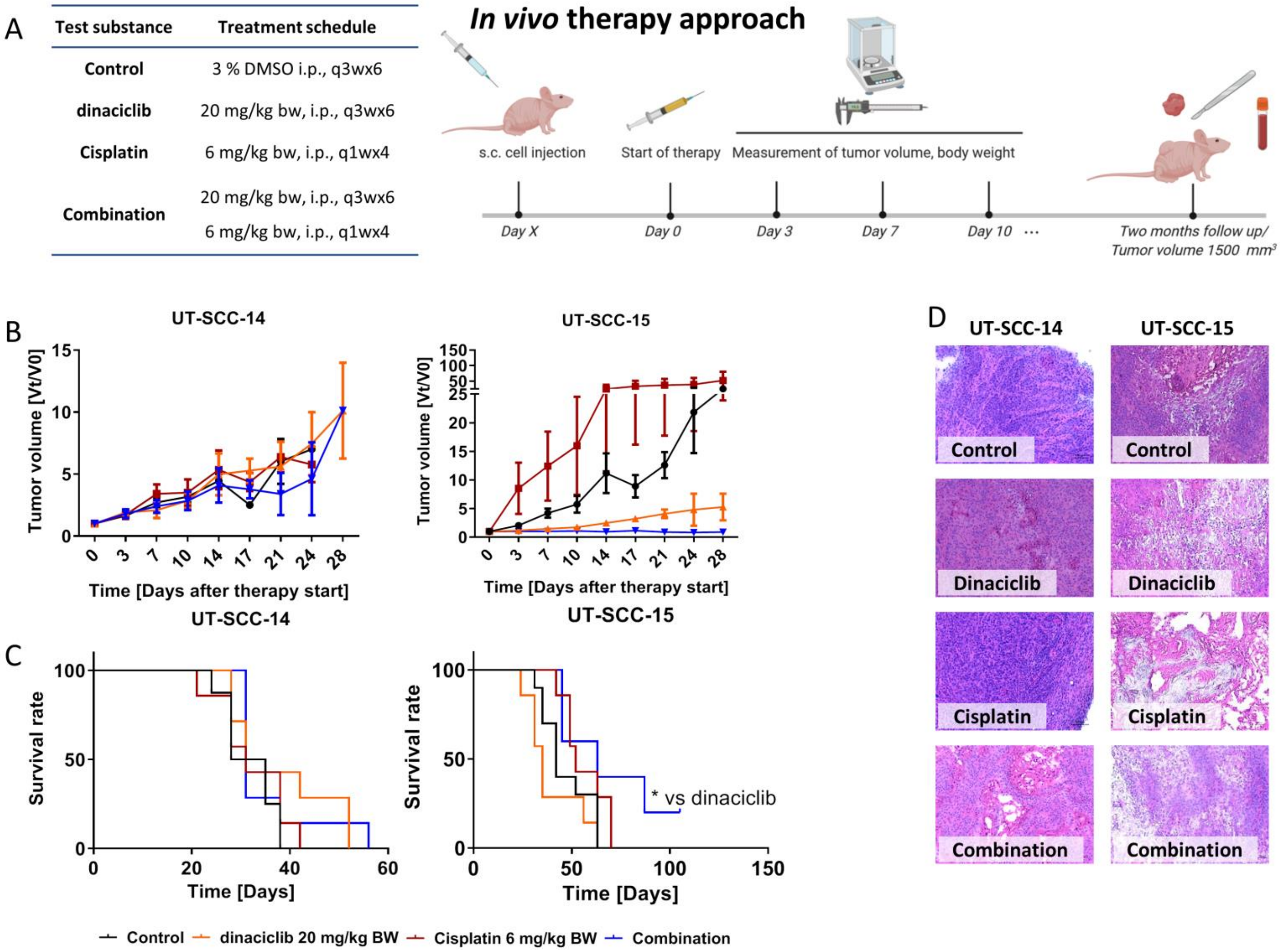

Figure 7. In vivo therapy approach. (**A**) Schematic overview over the treatment protocol with given doses of the test substances. (**B**) Tumor growth curve. Tumor volume was calculated as tumor volume at day × (Vt) divided through the tumor volume at the therapy start (V0). (**C**) Kaplan-Meier survival curve and Log-rank (Mantel-Cox) test. UT-SCC-14: control (*n* = 8 mice); Cisplatin/dinaciclib/combination (*n* = 7 mice/group); UT-SCC-15: control (*n* = 10 mice); Cisplatin/dinaciclib (*n* = 7 mice/group); combination (*n* = 5 mice); * $p < 0.05$ vs. dinaciclib. (**D**) Representative images of the HE stained tumors of each treatment group. Magnification 20×, Scale bar.

3. Discussion

CDKi's are being applied in clinical trials to treat solid and hematological malignancies (e.g., *NCT04169074*, *NCT04391595*, *NCT03981614*, and *NCT01627054*). For locally advanced or metastatic breast cancer, the CDK4/6 inhibitors palbociclib, ribociclib, and abemaciclib are FDA approved in combination with endocrine therapy [22,23]. Though approval for HNSCC is still pending, first preclinical and clinical reports are promising [16,24,25].

Our study adds another piece of evidence and identifies the CDK4/6 inhibitor palbociclib as well as the global acting CDKi's dinaciclib and THZ1 as promising candidates for HNSCC treatment. We additionally describe the strong dependency on (a) the combination partner and (b) the temporal order of applying each substance to reach therapeutic effects. Notably, simultaneous dual CDKi treatment, but not the combination with standard drugs, worked synergistically in our settings. The sequential application yielded heterogeneous results, depending on the CDKi used for combination. In theory, chemotherapeutic drugs should benefit from prior CDKi treatment by completing their effects [26,27]. However, this was only seen here when the CDK4/6 inhibitor palbociclib was used as first treatment, confirming findings from a recent study in which intrinsic resistance was reported when Cisplatin was given before palbociclib because of drug-induced *c-Myc*

Cisplatin was given before palbociclib because of drug-induced *c-Myc* and *Cyclin E* upregulation [19]. Though not analyzed in detail here, comparable molecular alterations can be anticipated. Besides direct antitumoral effects, another argument for applying specific CDKi's in the first-line is the protection of normal hematopoietic stem and progenitor cells via transient G1 cell cycle arrest induction and the maintenance of antitumor immunity to boost the patient's tolerability towards chemotherapy [28]. This "positive" side effect was recently observed in phase II trials on patients with small-cell lung cancer receiving the CDK4/6 inhibitor trilaciclib [28,29]. Hence, a favorable outcome can indeed be speculated if CDK4/6 inhibitors are applied in the first-line. For the more global acting CDKi's, such beneficial responses are very unlikely. Instead, leukopenia and neutropenia were reported as direct consequences of the complex mode of action, including interference with RNA polymerase II binding [30–32]. These systemic toxicities constitute a major limitation and clinicians will have to cope with this challenge. With regard to the sequential application applied here, first-line chemotherapy was superior to second-line chemotherapy. This regimen was comparable to or even better than two cycles of dinaciclib or THZ1 monotherapy. Mechanistically, effects were due to early apoptosis with a shift to necrosis afterward. Quite in line with this, Hossain et al. also observed apoptosis induction by short-term dinaciclib treatment [33]. Notably, THZ1, had a minor impact on apoptosis, though this was described in literature in an nM range and thus was comparable to doses used here [34]. This might be best explained by some kind of delayed apoptosis induction but not intrinsic apoptosis resistance of our HNSCC cells. In support of this, the specific CDK4/6 inhibitor palbociclib triggered apoptosis in both cell lines, confirming recent observations [35]. Senescence, another CDKi-induced cellular stress response, was also seen here; however, it was not as profound as described in the literature [36]. Hence, senescence may either play a minor role in HNSCC or it was an early event and thus undetectable after two rounds of treatment. The strong cytotoxicity of dinaciclib and certain CDKi/drug combinations argue in favor of the latter.

Quite in line with this, impedance reduced massively under dinaciclib monotherapy and combination therapy that was accompanied by remarkable changes in cell shape and cytoskeletal organization. This, in turn, may impair cell-cell contacts via adhesion molecules, electrical coupling, and passage through gap junctions [37]. A comparable, but delayed impedance breakdown was achieved when THZ1 was combined with 5-FU, likely because of the 5-FU's mechanism of action [38]. Such a delayed effect under 5-FU treatment was also seen in the wound healing assay. Conversely, THZ1 monotherapy slightly increased impedance, accompanied by re-organization of cortical actin into stress fibers. These stress fibers increase the cellular stiffness and reduce the motility [20,39,40]. We therefore propose the identified shift in actin organization as main response towards drugs applied in this study that has to be addressed in more detail prospectively. By performing a direct comparison of the two cell culture models used here, it is obvious that the cell line UT-SCC-15, established from a nodal recurrence of a primary tongue carcinoma [41], shows more cortical actin than intracellular stress fibers. In the UT-SCC-14 cells, it is exactly the other way around. The cortical actin filaments are important to create tension, leading to gradients that generate changes in the shape which are important during cell migration, cell division, and tissue morphogenesis [42]. Also, we hypothesize that the remodeling of the actin filament makes the cells more vulnerable to immune cells. A prerequisite—among others—for this is the induction of immunogenic cell death (ICD) in tumor cells to activate phagocytes [33,43,44]. Actually, we observed increased Calreticulin (CalR) translocation upon combined THZ1/5-FU treatment. While this effect was not visible under monotherapy, we suggest this treatment regimen as a promising strategy for immunotherapeutic approaches. Notably, dinaciclib was similarly able to induce CalR translocation and upregulation of the immunologically relevant marker MHC class I to an extent comparable to THZ1/5-FU combination therapy. This makes dinaciclib particularly interesting in the context of immunotherapy, as hypothesized before [33,45]. Hossain et al. treated murine CT26 colon cancer cells for 24 h with different dinaciclib

concentrations (0.05 µM–25 µM) and identified a linear increase in CalR translocation. The readout in this study was the mean fluorescence intensity, which was around 1200 after treatment with 0.05 µM dinaciclib [33]. In our work, a concentration of 0.02 µM dinaciclib yielded an MFI around 2000 for UT-SCC-14 and an MFI of around 1500 for UT-SCC-15 cells. Though the MFI is not directly comparable among different studies, it still confirms previous findings. Additionally to this, the observed upregulation of MHC class I enhances antigen presentation and ultimately stimulates $CD8^+$-T-cells to finally promote antitumor immunity [46].

Radiotherapy is the mainstay of therapy for HNSCC patients and can be combined with immunotherapy. While radiotherapy itself has the potential to reprogram the tumor microenvironment, several drugs including CDKi's have been identified as radiosensitizers [24,47,48]. However, the CDKi´s used here had a minor impact on double-strand breaks and radiosensitivity. Radiosensitization, if any, was seen after combining palbociclib or THZ1 with 5-FU. Wang et al. reported palbociclib-induced DNA damage in an p53-independent manner and repressed DNA damage repair ability via RAD51 downregulation [35]. THZ1 inhibits CDK7, CDK12, and CDK13 [49] and was described as radiosensitizer in a study on medulloblastomas [50]. Genes involved in homologous recombination such as Brca2, Rad51, and Rad50 were downregulated, accompanied by increased γH2AX-foci post irradiation [50]. Another study likewise confirmed increased amounts of γ-H2AX foci upon THZ1 treatment [51]. Hence, THZ1 has the potential to sensitize to radiation and impair recovery from radiation-induced DNA damage. The fact that another target of THZ1, CDK12, selectively controls the expression of genes involved in the DNA damage response, supports this theory [52]. The question remains why such effects were undetectable in our study. Apart from the radiation dose (2Gy), the time is a critical factor for detecting or missing a clear radiation response. Hence, it is conceivable that we have simply missed certain effects.

Another common response towards CDKi treatment is cell cycle alteration. Palbociclib induced a G1 phase arrest that complies with its mode of action and has been described in the literature [53–55]. Combined THZ1 and 5-FU therapy yielded comparable results in both cell lines that can be explained as follows: 5-FU limits the availability of thymidylate and inhibits the DNA synthesis [56,57]. THZ1 impairs CDK2 activity via inhibition of CDK7 [58,59]. CDK2 is required for the transition from G1 to S phase, blocking this CDK thus holds the cell cycle [49]. This has profound biological effects. In a very recent study on patient-derived glioblastoma models, we described the CDKi-induced loss of mitochondrial function in pioneering work, characterized by a multivacuolar phenotype and signs of early-methuosis [60]. Methuosis, a non-apoptotic cell death phenotype, is defined by the accumulation of large fluid-filled cytoplasmic vacuoles that originate from macropinosomes [61]. With regard to the HNSCC cells used here, dinaciclib monotherapy and combination therapy strengthened the mitochondrial activity. However, methuosis did not seem to play a major role, as late endosomes and vacuoles markers CD107a and Rab7a exclusively increased under CDKi or 5-FU monotherapy. Hence, CDKi's have indeed different effects on individual tumor cells.

In a final in vivo proof-of-concept experiment, dinaciclib and Cisplatin were chosen based on the following criteria: Dinaciclib has complex effects on HNSCC tumor cells, including growth inhibition, prevention of migration/invasion, and cytotoxicity. Besides, dinaciclib is a potent ICD inducer and a promising candidate for combined immunotherapies. Cisplatin is a well-known cytostatic drug approved as 1st line HNSCC treatment and widely applied in the clinic [11,62,63]. Additionally, preclinical reports on combined dinaciclib-Cisplatin application are promising, as recently shown for a subcutaneous ovarian cancer xenograft model in nude mice [64]. Here, the combination approach was likewise superior to either single treatment and most effective in suppressing UT-SCC-15 growth. While this cell line was established from a nodal recurrence, it is tempting to speculate that advanced tumors may even benefit more from this regimen than lower-stage tumors. However, this has to be tested on a larger series of (matched) tumor samples. However, the

accelerated growth of UT-SCC-15 xenografts under Cisplatin monotherapy is worth mentioning. Intrinsic resistance is unlikely, since these cells showed good sensitivity in vitro. Also, acquired resistance can be excluded because tumors grew constantly under treatment. Comparable effects were not reported in the literature. We can therefore only assume that outcomes may be improved by changing the treatment schedule (i.e., dose, application route, and the number of injections). Still, the complex interaction of tumor, normal stromal, and immune cells influences outcomes—a major contributing factor that can only partially be considered in vitro [65].

To sum up these findings, we provide another piece of evidence for the therapeutic activity of CDKi's, their complex mode of action, and the rationale to combine targeted agents with "conventional" drugs or even immune-restoring approaches to succeed in the long run.

4. Materials and Methods

4.1. Tumor Cell Lines and Culture Conditions

Two patient-derived cell lines: UT-SCC-14 and UT-SCC-15, were used. The UT-SCC-14 was established from a primary tumor of the tongue and the UT-SCC-15 derived from a nodal recurrence of the same origin. Both cell lines are HPV negative. Cells were maintained in full medium: DMEM/HamsF12 supplemented with 10% fetal calf serum (FCS), glutamine (2 mmol/L) and antibiotics (medium and antibiotics were purchased from Pan Biotech, Aidenbach, Germany, FCS from Sigma-Aldrich, Darmstadt, Germany and glutamine from Biochrom, Berlin, Germany) and kept in low passages.

4.2. Cytostatic Drugs and Targeted Substances

The approved cytostatic drugs 5-FU (50 mg/mL) and Cisplatin (1 mg/mL), the approved therapeutic antibody cetuximab (5 mg/mL) and the targeted substances dinaciclib, palbociclib, and THZ1 (all 10 mM) were used. 5-FU, Cisplatin and cetuximab were purchased from the pharmacy of the University Hospital Rostock, dinaciclib and palbociclib from Selleckchem, Munich, Germany, and THZ1 from Hycultec, Beutelsbach, Germany.

4.3. Dose Response Curves and Combination Therapy

For dose response curves, cells were seeded in 96 well plates in three technical replicates per cell line and incubated for 24 h at 37 °C and 5% CO_2. Afterwards, cells were treated for 2 × 72 h in monotherapy with the different test substances in concentrations ranging between 0.05 µg/mL and 1 mg/mL for approved drugs and 1 nM and 1 µM for CDKi's. Thereafter, various combinations were tested in simultaneous and sequential settings. Doses used for combinations were as follows: 5-FU [0.32 µg/mL or 90 µg/mL], Cisplatin [0.05 µg/mL, 0.5 µg/mL, or 0.1 µg/mL], cetuximab [0.5 µg/mL], dinaciclib [0.005 µM or 0.02 µM], palbociclib [1 µM], and THZ1 [0.02 µM or 0.005 µM] depending on the treatment duration of each substance (1 × 72 h or 2 × 72 h). Readout was done by crystal violet staining. In sequential combination therapy, two different approaches were applied. Firstly, the cells were treated with the standard therapy for 72 h and the CDKi's afterwards, and secondly, the administration was done in reverse order. To rule out the possibility that the single 72-h administration of the approved therapeutics is responsible for the potentially stronger effect, they were tested in monotherapy for 72 h. Potential synergistic or additive effects between the substances in a 2 × 72 h simultaneous combination approach were analyzed with the Bliss Independence model.

4.4. γ-H2AX Staining

Tumor cells were treated for 24 h in Chamber Slides with selected concentrations and combinations of the test substances and then irradiated with 2 Gy (Cs-137 γ-irradiation; IBL 637, CIS Bio-International, Codolet, France). γ-H2AX staining was performed 6 h after irradiation. Cells were washed with phosphate-buffered saline (PBS), fixed in 4% paraformaldehyde w/o methanol (Thermo Scientific, Darmstadt, Germany) for 30 min,

washed again, followed by cell permeabilization in 0.5% Triton X−100 (Sigma-Aldrich, Darmstadt, Germany) for 15 min. After blocking the unspecific binding sites with 1% bovine serum albumin (Serva, Heidelberg, Germany), cells were incubated with the monoclonal γ-H2AX antibody (1:100; BioLegend, San Diego, CA, USA) over night at 4 °C. Cells were washed and nuclei stained with 4′,6-diamidino-2-phenylindole (DAPI) (AAT Bioquest, Sunnyvale, CA, USA). Analysis was performed with a ZEISS Elyra 7 Confocal Laser Microscope (Zeiss, Jena, Germany).

4.5. Apoptosis-Necrosis Assay, Phenotyping, and Immunogenic Cell Death

Apoptosis-necrosis was determined after 24 and 72 h treatment, phenotyping was done after 48 h, and determination of immunogenic cell death (ICD) was recorded after 72 h treatment. Cells were analyzed on a Flow Cytometer (BD FACSVerse™, BD Pharmingen, San Jose, CA, USA). Data analysis was done using the BD FACSuite software (BD Pharmingen).

For Apoptosis-necrosis, cells were stained for 20 min at room temperature with 0.2 μM Yo-Pro 1 iodide (Thermo Scientific, Ex/Em 491/509 nm; blue laser 488 nm) and 20 μg/mL Propidiumiodide (PI) (Sigma-Aldrich, Darmstadt, Germany; Ex/Em: 535⁄617 nm; blue laser 488 nm). PI was added shortly before flow cytometry. For phenotyping, cells were stained for 30 min at 4 °C with FITC anti-HLA-ABC antibody (MHC I) (1:50; ImmunoTools, Friesoythe, Germany) and APC anti-CD279 (PD-1) (1:50; both from BioLegend, blue (488 nm) and red (633 nm) laser). ICD was detected by staining translocated CalR on the cell surface. Cells were incubated for 30 min at 4 °C with the polyclonal rabbit CalR primary antibody (1:50; Abgent, San Diego, CA, USA). Cells were washed and labeled with FITC-conjugated secondary antibody (donkey anti rabbit, 1:50; BioLegend), and incubated again for 30 min at 4 °C. In order to exclude non-specific binding of the FITC-labeled secondary antibody, control cells were additionally stained with the secondary antibody without using the primary antibody. For CalR quantification, the number of cells that were positive for the secondary antibody was subtracted from the CalR+ secondary antibody stained cells.

4.6. Cell Cycle Assay

Cell cycle was determined after 48 h of treatment. Cells were harvested, counted, and resuspended with 1 mL ice cold 70% ethanol. Cells were incubated overnight at −20 °C, washed again, and incubated with 0.5 mL 0.25% TritonX-100 for 15 min on ice. Cells were washed and resuspended in RNAse A (100 μg/mL), supplemented with PI (20 μg/mL). After 30 min incubation on ice, cells were analyzed on a Flow Cytometer (FACSCalibur, BD, San Jose, CA, USA). Data analysis was done using BD FlowJo software (BD Pharmingen, San Diego, CA, USA).

4.7. Influence on Mitochondria, Lysosomes, ER, and Vacuole Formation

The influence on mitochondria, lysosomes, and the ER was examined with immunofluorescence staining. Cells were seeded in Chamber Slides and stained after 72 h treatment. Then, cells were washed and the staining with MitoTracker Red CMXRos (20 nM, CellSignaling Technology, Danvers, MA, USA) and ER-Tracker Blue-White DPX (1 μM, Invitrogen) was done simultaneously for 35 min at 37 °C. Cells were washed and stained with LysoTracker DND-26 (50 nM, CellSignaling Technology) for 2 min at room temperature. Analysis was performed on a ZEISS Elyra 7 Confocal Laser Microscope (Zeiss).

Additionally, vacuole formation was analyzed after 72 h treatment using specific antibodies. Cells were harvested and incubated with Alexa488 anti-CD107a antibody (Biolegend, 1:50 in 0.1% BSA) for 30 min at 4 °C. Then, cells were washed and resuspended in 0.5 mL FluorFix™ Buffer (Biolegend) for 20 min at room temperature. Afterwards, cells were washed twice with 1× intracellular staining perm wash buffer and incubated with Alexa594 anti-Rab7a antibody (Biolegend, 1:50 in 0.1% BSA) for 30 min at room temperature. The reaction was stopped with PBS and washed before cells were resuspended

in 200 µL PBS (+2 mM EDTA). Cells were analyzed by flow cytometry on a Flow Cytometer (FACSAriaII, BD, blue (488nm) and yellow-green (561 nm) laser). Data analysis was performed using BD FACSDiva software (BD).

4.8. Senescence

Senescence-associated β-galactosidase (SA-β-gal, Cell Signaling Technology, Cambridge, UK) was analyzed after 72 h of treatment. Cells were washed and fixed. After a second washing step, cells were stained with a Galactosidase Staining Solution. Therefore, cells were incubated at 37 °C overnight in a dry incubator and checked for senescence the following day under a microscope. To analyze the number of senescent cells, ImageJ was used.

4.9. Impedance Measurement and Actin Staining

Impedance was measured with a commercial Electric Cell-Substrate Impedance Sensing system (ECIS Zθ; Applied Biophysics, New York, NY, USA) equipped with a 96-well array station (Applied Biophysics) to monitor time and frequency dependent complex impedance, Z (t, f). Cells were grown on a 96-well ECIS array plate with 20 interdigitated electrodes/well (96W20idf PET; ibidi GmbH, Gräfelfing, Germany). Prior to cell seeding, electrodes were stabilized with serum-free media overnight in the incubator with high humidity at 37 °C and 5% CO_2. Impedance measurements were performed directly in the treatment medium in the incubator, allowing real-time monitoring of all impedance alterations at 11 frequencies (0.0625, 0.125, 0.25, 0.5, 1, 2, 4, 8, 16, 32, and 64 kHz) in a 180-s interval. 24 h after cell seeding, treatment was added for 72 h. Analysis of cell-cell contacts was performed by 4000 kHz using ECIS Software (Applied Biophysics).

To confirm the results of the impedance measurement, the actin filament was stained with phalloidin (1:300; Invitrogen, Darmstadt, Germany). Therefore, cells were treated for 72 h in Chamber Slides, fixed, permeabilized, stained, and analyzed as described for γ-H2AX.

4.10. Wound Healing and Invasion Assay

A wound healing assay was done in 12-well plates. After formation of a confluent cell layer, a defined scratch was set. Medium was removed, cells were washed with cell culture media, and the corresponding treatment based on the most promising simultaneous combinations was added. Scratch closure was documented by light microscopy routinely during the following 72 h.

For the invasion assay, inserts (8.0 µm translucent; Greiner bio-one, Frickenhausen, Germany) were coated with 70 µL Matrigel (1:25 in serum free media; Corning, NY, USA) and cells seeded in serum free, treatment containing media. The inserts were placed in a 24-well plate containing 750 µL media with 10% FCS and incubated for 72 h. Invasiveness was analyzed by WST-1 assay. The inserts were placed into a new 24-well plate containing WST-1 in serum free media. WST-1 containing medium without cells served as a blank. After 2.5 h of incubation, absorption was measured at a wavelength of 450 nm.

4.11. In Vivo Study

4.11.1. Ethical Statement

The German local authority approved all animal experiments: Landesamt für Landwirtschaft, Lebensmittelsicherheit und Fischerei Mecklenburg-Vorpommern (7221.3-1-066/18), under the German animal protection law and the EU Guideline 2010/63/EU. Mice were bred in the animal facility of the University Medical Center in Rostock under specific pathogen-free conditions. All animals received enrichment in the form of mouse-igloos (ANT Tierhaltungsbedarf, Buxtehude, Germany), nesting material (shredded tissue paper, Verbandmittel GmbH, Frankenberg, Deutschland), paper roles (75 × 38 mm, H 0528–151, ssniff-Spezialdiäten GmbH), and wooden sticks (40 × 16 × 10 mm, Abedd, Vienna, Austria). During the experiment, mice were kept in type III cages (Zoonlab GmbH, Castrop-Rauxel,

Germany) at 12-h dark:light cycle, the temperature of 21 ± 2 °C, and relative humidity of 60 ± 20% with food (pellets, 10 mm, ssniff-Spezialdiäten GmbH, Soest, Germany) and tap water ad libitum.

4.11.2. Experimental Protocol

Xenografts were generated by injecting 5×10^6 cells of UT-SCC-14 or UT_SCC-15 (in 50 µL PBS) subcutaneously in the right flank of 6–8 weeks old female NMRI Foxn1^{nu} mice. Two weeks later, mice bearing tumors of ~50 mm^3 were allocated to treatment groups (Figure 7). Tumor diameters were measured with caliper every three to four days. Tumor volumes were calculated as (length × width^2)/2. Mice were euthanized before tumors reached 1500 mm^3. Tumors were embedded in Cryomatrix (Thermo Scientific, Darmstadt, Germany) and used for HE staining.

4.12. Statistics

All values are expressed as mean ± SD (in vitro analysis) or mean ± SEM (in vivo therapy approach). Differences between controls and treated cells were determined by using one-way *ANOVA* (Bonferroni's Multiple Comparison Test) after proving the assumption of normality (Shapiro-Wilk test). If normality failed, the Kruskal Wallis test was applied. This information is given in the figure captions. Kaplan-Meier survival analysis was done by applying the log rank (Mantel Cox) test. Statistical evaluation was performed using GraphPad PRISM software, version 8.0.2 (GraphPad Software, San Diego, CA, USA). The criterion for significance was set to $p < 0.05$.

5. Conclusions

Cyclin-dependent kinase inhibitors (CDKi) have broad therapeutic potential. Here, we show that CDKi's can be combined with standard cytostatic drugs and that dual CDK inhibition is at least as successful as CDKi/drug combinations. These findings contribute to our understanding of how the treatment of HNSCC can be improved prospectively. The complex effects exerted by specific CDKi-combinations include apoptotic and necrotic cell death as well as methuosis, an uncommon form of cell death, associated with vacuolization of macropinosome and endosome compartments. Dinaciclib and THZ1 were most effective and even better in combination with 5-FU. Another novel finding is the impact on actin fibers and motility properties of tumor cells by specific CDKi's. Prospective studies should focus on the effects on immune cells—especially because of the CDKi's potential to increase tumor immunogenicity.

Supplementary Materials: The following are available online at https://www.mdpi.com/article/10.3390/cancers13102396/s1. Figure S1: Senescence, Figure S2: Scratch-Assay and Invasiveness UT-SCC-14., Figure S3: Influence on mitochondria, lysosomes, ER, and vacuole formation. Figure S4: Cell cycle analysis.

Author Contributions: Conceptualization, N.S. and C.M.; methodology, N.S., I.S., N.E., M.K., M.M., B.S., and C.R.; validation, N.S., C.M.; formal analysis, N.S.; investigation, N.S., I.S.; resources, C.M., C.J., N.E., and H.L.; data curation, N.S., N.E., M.K.; writing—original draft preparation, N.S., I.S.; writing—review and editing, C.M., C.G.-T., A.S.; visualization, N.S., C.M.; supervision, C.M.; project administration, C.M. All authors have read and agreed to the published version of the manuscript.

Funding: This research received no external funding.

Institutional Review Board Statement: The study was conducted according to the guidelines of the Declaration of Helsinki, and approved by the German local authority Ethics Committee) Landesamt für Landwirtschaft, Lebensmittelsicherheit und Fischerei Mecklenburg-Vorpommern, under the German animal protection law and the EU Guideline 2010/63/EU (protocol code: 7221.3-1-066/18 and date of approval: 15 January 2019).

Informed Consent Statement: Not applicable.

Data Availability Statement: The data presented in this study are available in this article (and supplementary material).

Acknowledgments: The patient-derived cell lines UT-SCC-14 and UT-SCC15 were kindly provided by Reidar Grénman (Turku University Hospital, Turku, Finland).

Conflicts of Interest: The authors declare no conflict of interest.

References

1. Schafer, K.A. The Cell Cycle: A review. *Vet. Pathol.* **1998**, *35*, 461–478. [CrossRef]
2. Jingwen, B.; Yaochen, L.; Guojun, Z. Cell cycle regulation and anticancer drug discovery. *Cancer Biol. Med.* **2017**, *14*, 348. [CrossRef] [PubMed]
3. Roskoski, R. Cyclin-dependent protein serine/threonine kinase inhibitors as anticancer drugs. *Pharmacol. Res.* **2019**, *139*, 471–488. [CrossRef] [PubMed]
4. Sánchez-Martínez, C.; Lallena, M.J.; Sanfeliciano, S.G.; de Dios, A. Cyclin dependent kinase (CDK) inhibitors as anticancer drugs: Recent advances (2015–2019). *Bioorgan. Med. Chem. Lett.* **2019**, *29*, 126637. [CrossRef] [PubMed]
5. Asghar, U.; Witkiewicz, A.K.; Turner, N.C.; Knudsen, E.S. The history and future of targeting cyclin-dependent kinases in cancer therapy. *Nat. Rev. Drug Discov.* **2015**, *14*, 130–146. [CrossRef]
6. Patel, V.; Jakus, J.; Harris, C.M.; Ensley, J.F.; Robbins, K.C.; Yeudall, W.A. Altered expression and activity of G1/S cyclins and cyclin-dependent kinases characterize squamous cell carcinomas of the head and neck. *Int. J. Cancer* **1997**, *73*, 551–555. [CrossRef]
7. Parry, D.; Guzi, T.; Shanahan, F.; Davis, N.; Prabhavalkar, D.; Wiswell, D.; Seghezzi, W.; Paruch, K.; Dwyer, M.P.; Doll, R.; et al. Dinaciclib (SCH 727965), a novel and potent cyclin-dependent kinase inhibitor. *Mol. Cancer Ther.* **2010**, *9*, 2344–2353. [CrossRef] [PubMed]
8. Paruch, K.; Dwyer, M.P.; Alvarez, C.; Brown, C.; Chan, T.Y.; Doll, R.J.; Keertikar, K.; Knutson, C.; McKittrick, B.; Rivera, J.; et al. Discovery of dinaciclib (SCH 727965): A potent and selective inhibitor of cyclin-dependent kinases. *ACS Med. Chem. Lett.* **2010**, *1*, 204–208. [CrossRef]
9. Schoninger, S.F.; Blain, S.W. The Ongoing Search for Biomarkers of CDK4/6 Inhibitor Responsiveness in Breast Cancer. *Mol. Cancer Ther.* **2020**, *19*, 3–12. [CrossRef] [PubMed]
10. Greber, B.J.; Perez-Bertoldi, J.M.; Lim, K.; Iavarone, A.T.; Toso, D.B.; Nogales, E. The cryoelectron microscopy structure of the human CDK-activating kinase. *Proc. Natl. Acad. Sci. USA* **2020**, *117*, 22849–22857. [CrossRef] [PubMed]
11. Grünwald, V.; Chirovsky, D.; Cheung, W.Y.; Bertolini, F.; Ahn, M.J.; Yang, M.H.; Castro, G.; Berrocal, A.; Sjoquist, K.; Kuyas, H.; et al. Global treatment patterns and outcomes among patients with recurrent and/or metastatic head and neck squamous cell carcinoma: Results of the GLANCE H&N study. *Oral Oncol.* **2020**, *102*, 104526. [PubMed]
12. Bray, F.; Ferlay, J.; Soerjomataram, I.; Siegel, R.L.; Torre, L.A.; Jemal, A. Global cancer statistics 2018: GLOBOCAN estimates of incidence and mortality worldwide for 36 cancers in 185 countries. *CA. Cancer J. Clin.* **2018**, *68*, 394–424. [CrossRef]
13. Gebre-Medhin, M.; Brun, E.; Engström, P.; Haugen Cange, H.; Hammarstedt-Nordenvall, L.; Reizenstein, J.; Nyman, J.; Abel, E.; Friesland, S.; Sjödin, H.; et al. ARTSCAN III: A Randomized Phase III Study Comparing Chemoradiotherapy With Cisplatin Versus Cetuximab in Patients With Locoregionally Advanced Head and Neck Squamous Cell Cancer. *J. Clin. Oncol.* **2021**, *39*, 38–47. [CrossRef] [PubMed]
14. McDermott, J.D.; Bowles, D.W. Epidemiology of Head and Neck Squamous Cell Carcinomas: Impact on Staging and Prevention Strategies. *Curr. Treat. Options Oncol.* **2019**, *20*, 1–13. [CrossRef] [PubMed]
15. Salakova, M.; Koslabova, E.; Grega, M.; Smahelova, J.; Klozar, J.; Vencalek, O.; Tachezy, R. Mucosal and skin HPV types in tumour-free tonsils and tonsillar tumours. *Neoplasma* **2018**, *65*, 278–286. [CrossRef]
16. Adkins, D.; Ley, J.; Neupane, P.; Worden, F.; Sacco, A.G.; Palka, K.; Grilley-Olson, J.E.; Maggiore, R.; Salama, N.N.; Trinkaus, K.; et al. Palbociclib and cetuximab in platinum-resistant and in cetuximab-resistant human papillomavirus-unrelated head and neck cancer: A multicentre, multigroup, phase 2 trial. *Lancet Oncol.* **2019**, *20*, 1295–1305. [CrossRef]
17. Yoon, N.; Vander Velde, R.; Marusyk, A.; Scott, J.G. Optimal Therapy Scheduling Based on a Pair of Collaterally Sensitive Drugs. *Bull. Math. Biol.* **2018**, *80*, 1776–1809. [CrossRef] [PubMed]
18. Li, Y.F.; Chang, L.; Li, W.H.; Xiao, M.Y.; Wang, Y.; He, W.J.; Xia, Y.X.; Wang, L.; Chen, Y. Radiotherapy concurrent versus sequential with endocrine therapy in breast cancer: A meta-analysis. *Breast* **2016**, *27*, 93–98. [CrossRef]
19. Robinson, A.M.; Rathore, R.; Redlich, N.J.; Adkins, D.R.; VanArsdale, T.; Van Tine, B.A.; Michel, L.S. Cisplatin exposure causes c-Myc-dependent resistance to CDK4/6 inhibition in HPV-negative head and neck squamous cell carcinoma. *Cell Death Dis.* **2019**, *10*, 867. [CrossRef]
20. Northcott, J.M.; Dean, I.S.; Mouw, J.K.; Weaver, V.M. Feeling stress: The mechanics of cancer progression and aggression. *Front. Cell Dev. Biol.* **2018**, *6*, 1–12. [CrossRef]
21. Humphries, W.H.; Szymanski, C.J.; Payne, C.K. Endo-lysosomal vesicles positive for rab7 and lamp1 are terminal vesicles for the transport of dextran. *PLoS ONE* **2011**, *6*, e26626. [CrossRef]
22. Shah, A.; Bloomquist, E.; Tang, S.; Fu, W.; Bi, Y.; Liu, Q.; Yu, J.; Zhao, P.; Palmby, T.R.; Goldberg, K.B.; et al. FDA approval: Ribociclib for the treatment of postmenopausal women with hormone receptor-positive, HER2-negative advanced or metastatic breast cancer. *Clin. Cancer Res.* **2018**, *24*, 2999–3004. [CrossRef]

23. Groenland, S.L.; Martínez-Chávez, A.; van Dongen, M.G.J.; Beijnen, J.H.; Schinkel, A.H.; Huitema, A.D.R.; Steeghs, N. Clinical Pharmacokinetics and Pharmacodynamics of the Cyclin-Dependent Kinase 4 and 6 Inhibitors Palbociclib, Ribociclib, and Abemaciclib. *Clin. Pharmacokinet.* **2020**, *59*, 1501–1520. [CrossRef] [PubMed]
24. Göttgens, E.L.; Bussink, J.; Leszczynska, K.B.; Peters, H.; Span, P.N.; Hammond, E.M. Inhibition of CDK4/CDK6 Enhances Radiosensitivity of HPV Negative Head and Neck Squamous Cell Carcinomas. *Int. J. Radiat. Oncol. Biol. Phys.* **2019**, *105*, 548–558. [CrossRef]
25. Billard-Sandu, C.; Tao, Y.G.; Sablin, M.P.; Dumitrescu, G.; Billard, D.; Deutsch, E. CDK4/6 inhibitors in P16/HPV16-negative squamous cell carcinoma of the head and neck. *Eur. Arch. Oto-Rhino-Laryngol.* **2020**, *277*, 1273–1280. [CrossRef] [PubMed]
26. Deep, G.; Agarwal, R. New combination therapies with cell-cycle agents. *Curr. Opin. Investig. Drugs* **2008**, *9*, 591–604.
27. Shah, M.A.; Schwartz, G.K. Cell cycle-mediated drug resistance: An emerging concept in cancer therapy. *Clin. Cancer Res.* **2001**, *7*, 2168–2181. [PubMed]
28. Weiss, J.M.; Csoszi, T.; Maglakelidze, M.; Hoyer, R.J.; Beck, J.T.; Domine Gomez, M.; Lowczak, A.; Aljumaily, R.; Rocha Lima, C.M.; Boccia, R.V.; et al. Myelopreservation with the CDK4/6 inhibitor trilaciclib in patients with small-cell lung cancer receiving first-line chemotherapy: A phase Ib/randomized phase II trial. *Ann. Oncol.* **2019**, *30*, 1613–1621. [CrossRef] [PubMed]
29. Hart, L.L.; Ferrarotto, R.; Andric, Z.G.; Beck, J.T.; Subramanian, J.; Radosavljevic, D.Z.; Zaric, B.; Hanna, W.T.; Aljumaily, R.; Owonikoko, T.K.; et al. Myelopreservation with Trilaciclib in Patients Receiving Topotecan for Small Cell Lung Cancer: Results from a Randomized, Double-Blind, Placebo-Controlled Phase II Study. *Adv. Ther.* **2021**, *38*, 350–365. [CrossRef]
30. Mitri, Z.; Karakas, C.; Wei, C.; Briones, B.; Simmons, H.; Ibrahim, N.; Alvarez, R.; Murray, J.L.; Keyomarsi, K.; Moulder, S. A phase 1 study with dose expansion of the CDK inhibitor dinaciclib (SCH 727965) in combination with epirubicin in patients with metastatic triple negative breast cancer. *Invest. New Drugs* **2015**, *33*, 890–894. [CrossRef] [PubMed]
31. Kumar, S.K.; LaPlant, B.; Chng, W.J.; Zonder, J.; Callander, N.; Fonseca, R.; Fruth, B.; Roy, V.; Erlichman, C.; Stewart, A.K.; et al. Dinaciclib, a novel CDK inhibitor, demonstrates encouraging single-agent activity in patients with relapsed multiple myeloma. *Blood* **2015**, *125*, 443–448. [CrossRef]
32. Riess, C.; Irmscher, N.; Salewski, I.; Strüder, D.; Classen, C.F.; Große-Thie, C.; Junghanss, C.; Maletzki, C. Cyclin-dependent kinase inhibitors in head and neck cancer and glioblastoma—backbone or add-on in immune-oncology? *Cancer Metastasis Rev.* **2020**, *40*, 153–171. [CrossRef] [PubMed]
33. Md Sakib Hossain, D.; Javaid, S.; Cai, M.; Zhang, C.; Sawant, A.; Hinton, M.; Sathe, M.; Grein, J.; Blumenschein, W.; Pinheiro, E.M.; et al. Dinaciclib induces immunogenic cell death and enhances anti- PD1–mediated tumor suppression. *J. Clin. Investig.* **2018**, *128*, 644–654. [CrossRef] [PubMed]
34. Zhang, Y.; Zhou, L.; Bandyopadhyay, D.; Sharma, K.; Allen, A.J.; Kmieciak, M.; Grant, S. The covalent CDK7 inhibitor THz1 potently induces apoptosis in multiple myeloma cells in vitro and in vivo. *Clin. Cancer Res.* **2019**, *25*, 6195–6205. [CrossRef]
35. Wang, T.H.; Chen, C.C.; Leu, Y.L.; Lee, Y.S.; Lian, J.H.; Hsieh, H.L.; Chen, C.Y. Palbociclib induces DNA damage and inhibits DNA repair to induce cellular senescence and apoptosis in oral squamous cell carcinoma. *J. Formos. Med. Assoc.* **2020**. [CrossRef]
36. Wagner, V.; Gil, J. Senescence as a therapeutically relevant response to CDK4/6 inhibitors. *Oncogene* **2020**, *39*, 5165–5176. [CrossRef] [PubMed]
37. Dominiak, A.; Chełstowska, B.; Olejarz, W.; Nowicka, G. Communication in the cancer microenvironment as a target for therapeutic interventions. *Cancers* **2020**, *12*, 1232. [CrossRef]
38. Zhang, N.; Yin, Y.; Xu, S.J.; Chen, W.S. 5-Fluorouracil: Mechanisms of resistance and reversal strategies. *Molecules* **2008**, *13*, 1551–1569. [CrossRef]
39. Brückner, B.R.; Nöding, H.; Skamrahl, M.; Janshoff, A. Mechanical and morphological response of confluent epithelial cell layers to reinforcement and dissolution of the F-actin cytoskeleton. *Prog. Biophys. Mol. Biol.* **2019**, *144*, 77–90. [CrossRef]
40. Shannon, S.; Jia, D.; Entersz, I.; Beelen, P.; Yu, M.; Carcione, C.; Carcione, J.; Mahtabfar, A.; Vaca, C.; Weaver, M.; et al. Inhibition of glioblastoma dispersal by the MEK inhibitor PD0325901. *BMC Cancer* **2017**, *17*, 121. [CrossRef]
41. Yaromina, A.; Zips, D.; Thames, H.D.; Eicheler, W.; Krause, M.; Rosner, A.; Haase, M.; Petersen, C.; Raleigh, J.A.; Quennet, V.; et al. Pimonidazole labelling and response to fractionated irradiation of five human squamous cell carcinoma (hSCC) lines in nude mice: The need for a multivariate approach in biomarker studies. *Radiother. Oncol.* **2006**, *81*, 122–129. [CrossRef] [PubMed]
42. Chugh, P.; Paluch, E.K. The actin cortex at a glance. *J. Cell Sci.* **2018**, *131*, 1–9. [CrossRef]
43. Gardai, S.J.; McPhillips, K.A.; Frasch, S.C.; Janssen, W.J.; Starefeldt, A.; Murphy-Ullrich, J.E.; Bratton, D.L.; Oldenborg, P.A.; Michalak, M.; Henson, P.M. Cell-surface calreticulin initiates clearance of viable or apoptotic cells through trans-activation of LRP on the phagocyte. *Cell* **2005**, *123*, 321–334. [CrossRef]
44. Kroemer, G.; Galluzzi, L.; Kepp, O.; Zitvogel, L. Immunogenic Cell Death in Cancer Therapy. *Ann. Rev. Immunol.* **2013**, *31*, 51–72. [CrossRef]
45. Riess, C.; Schneider, B.; Kehnscherper, H.; Gesche, J.; Irmscher, N.; Shokraie, F.; Classen, C.F.; Wirthgen, E.; Domanska, G.; Zimpfer, A.; et al. Activation of the Kynurenine Pathway in Human Malignancies Can Be Suppressed by the Cyclin-Dependent Kinase Inhibitor Dinaciclib. *Front. Immunol.* **2020**, *11*, 55. [CrossRef]
46. Li, B.B.; Khan, N.; Ubellacker, J.M.; Xie, S.; Metzger-filho, O.; Roberts, T.M.; Kim, H.; Mcallister, S.S.; Jean, J. CDK4/6 inhibition triggers anti-tumor immunity. *Nature* **2017**, *548*, 471–475.
47. Wang, J.; Yang, T.; Xu, G.; Liu, H.; Ren, C.; Xie, W.; Wang, M. Cyclin-dependent kinase 2 promotes tumor proliferation and induces radio resistance in glioblastoma. *Transl. Oncol.* **2016**, *9*, 548–556. [CrossRef] [PubMed]

48. Xie, X.; Zheng, W.; Chen, T.; Lin, W.; Liao, Z.; Liu, J.; Ding, Y. CDK4/6 inhibitor palbociclib amplifies the radiosensitivity to nasopharyngeal carcinoma cells via mediating apoptosis and suppressing DNA damage repair. *Onco. Targets. Ther.* **2019**, *12*, 11107–11117. [CrossRef] [PubMed]
49. Olson, C.M.; Liang, Y.; Leggett, A.; Park, W.D.; Li, L.; Mills, C.E.; Elsarrag, S.Z.; Ficarro, S.B.; Zhang, T.; Düster, R.; et al. Development of a Selective CDK7 Covalent Inhibitor Reveals Predominant Cell-Cycle Phenotype. *Cell Chem. Biol.* **2019**, *26*, 792–803.e10. [CrossRef]
50. Veo, B.; Danis, E.; Pierce, A.; Wang, D.; Fosmire, S.; Sullivan, K.D.; Joshi, M.; Khanal, S.; Dahl, N.; Karam, S.; et al. Transcriptional control of DNA repair networks by CDK7 regulates sensitivity to radiation in Myc-driven medulloblastoma. *Cell Rep.* **2021**, *35*, 109013. [CrossRef]
51. Pessina, F.; Giavazzi, F.; Yin, Y.; Gioia, U.; Vitelli, V.; Galbiati, A.; Barozzi, S.; Garre, M.; Oldani, A.; Flaus, A.; et al. Functional transcription promoters at DNA double-strand breaks mediate RNA-driven phase separation of damage-response factors. *Nat. Cell Biol.* **2019**, *21*, 1286–1299. [CrossRef] [PubMed]
52. Krajewska, M.; Dries, R.; Grassetti, A.V.; Dust, S.; Gao, Y.; Huang, H.; Sharma, B.; Day, D.S.; Kwiatkowski, N.; Pomaville, M.; et al. CDK12 loss in cancer cells affects DNA damage response genes through premature cleavage and polyadenylation. *Nat. Commun.* **2019**, *10*, 1757. [CrossRef]
53. Maskey, R.S.; Wang, F.; Lehman, E.; Wang, Y.; Emmanuel, N.; Zhong, W.; Jin, G.; Abraham, R.T.; Arndt, K.T.; Myers, J.S.; et al. Sustained mTORC1 activity during palbociclib-induced growth arrest triggers senescence in ER+ breast cancer cells. *Cell Cycle* **2020**, *20*, 65–80. [CrossRef]
54. Yu, Y.; Liao, H.; Xie, R.; Zhang, Y.; Zheng, R.; Chen, J.; Zhang, B. Overexpression of miRNA-3613-3p Enhances the Sensitivity of Triple Negative Breast Cancer to CDK4/6 Inhibitor Palbociclib. *Front. Oncol.* **2020**, *10*, 2541. [CrossRef] [PubMed]
55. Vijayaraghavan, S.; Karakas, C.; Doostan, I.; Chen, X.; Bui, T.; Yi, M.; Raghavendra, A.S.; Zhao, Y.; Bashour, S.I.; Ibrahim, N.K.; et al. CDK4/6 and autophagy inhibitors synergistically induce senescence in Rb positive cytoplasmic cyclin e negative cancers. *Nat. Commun.* **2017**, *8*, 15916. [CrossRef]
56. Focaccetti, C.; Bruno, A.; Magnani, E.; Bartolini, D.; Principi, E.; Dallaglio, K.; Bucci, E.O.; Finzi, G.; Sessa, F.; Noonan, D.M.; et al. Effects of 5-Fluorouracil on Morphology, Cell Cycle, Proliferation, Apoptosis, Autophagy and ROS Production in Endothelial Cells and Cardiomyocytes. *PLoS ONE* **2015**, *10*, e0115686. [CrossRef]
57. Tokunaga, E.; Oda, S.; Fukushima, M.; Maehara, Y.; Sugimachi, K. Differential growth inhibition by 5-fluorouracil in human colorectal carcinoma cell lines. *Eur. J. Cancer* **2000**, *36*, 1998–2006. [CrossRef]
58. Schachter, M.M.; Fisher, R.P. The CDK-activating kinase Cdk7. *Cell Cycle* **2013**, *12*, 3239–3240. [CrossRef] [PubMed]
59. Higashi, H.; Suzuki-Takahashi, I.; Saitoh, S.; Segawa, K.; Taya, Y.; Okuyama, A.; Nishimura, S.; Kitagawa, M. Cyclin-dependent kinase-2 (Cdk2) forms an inactive complex with cyclin D1 since Cdk2 associated with cyclin D1 is not phosphorylated by Cdk7-cyclin-H. *Eur. J. Biochem.* **1996**, *237*, 460–467. [CrossRef]
60. Riess, C.; Koczan, D.; Schneider, B.; Linke, C.; del Moral, K.; Classen, C.F.; Maletzki, C. Cyclin-dependent kinase inhibitors exert distinct effects on patient-derived 2D and 3D glioblastoma cell culture models. *Cell Death Discov.* **2021**, *7*, 54. [CrossRef]
61. Maltese, W.A.; Overmeyer, J.H. Methuosis: Nonapoptotic cell death associated with vacuolization of macropinosome and endosome compartments. *Am. J. Pathol.* **2014**, *184*, 1630–1642. [CrossRef]
62. Ghosh, S. Cisplatin: The first metal based anticancer drug. *Bioorg. Chem.* **2019**, *88*, 102925. [CrossRef] [PubMed]
63. Dasari, S.; Bernard Tchounwou, P. Cisplatin in cancer therapy: Molecular mechanisms of action. *Eur. J. Pharmacol.* **2014**, *740*, 364–378. [CrossRef] [PubMed]
64. Chen, X.X.; Xie, F.F.; Zhu, X.J.; Lin, F.; Pan, S.S.; Gong, L.H.; Qiu, J.G.; Zhang, W.J.; Jiang, Q.W.; Mei, X.L.; et al. Cyclin-dependent kinase inhibitor dinaciclib potently synergizes with cisplatin in preclinical models of ovarian cancer. *Oncotarget* **2015**, *6*, 14926–14939. [CrossRef] [PubMed]
65. Egeblad, M.; Nakasone, E.S.; Werb, Z. Tumors as organs: Complex tissues that interface with the entire organism. *Dev. Cell* **2010**, *18*, 884–901. [CrossRef] [PubMed]

Journal of Experimental & Clinical Cancer Research

RESEARCH

Open Access

Establishment and characterization of patient-derived head and neck cancer models from surgical specimens and endoscopic biopsies

Daniel Strüder[1], Theresa Momper[2], Nina Irmscher[2], Mareike Krause[2], Jan Liese[3], Sebastian Schraven[1], Annette Zimpfer[4], Sarah Zonnur[4], Ann-Sophie Burmeister[2], Björn Schneider[4], Bernhard Frerich[3], Robert Mlynski[1], Christina Große-Thie[2], Christian Junghanss[2] and Claudia Maletzki[2*]

Abstract

Background: Head and neck squamous cell carcinoma (HNSCC) is heterogeneous in etiology, phenotype and biology. Patient-derived xenografts (PDX) maintain morphology and molecular profiling of the original tumors and have become a standard "Avatar" model for human cancer research. However, restricted availability of tumor samples hindered the widespread use of PDX. Most PDX-projects include only surgical specimens because reliable engraftment from biopsies is missing. Therefore, sample collection is limited and excludes recurrent and metastatic, non-resectable cancer from preclinical models as well as future personalized medicine.

Methods: This study compares the PDX-take rate, -growth, histopathology, and molecular characteristics of endoscopic specimens with surgical specimens. HNSCC samples ($n = 55$) were collected ad hoc, fresh frozen and implanted into NOD.Cg-Prkdc^{scid}Il2rg^{tm1Wjl}/SzJ mice.

Results: Engraftment was successful in both sample types. However, engraftment rate was lower (21 *vs.* 52%) and growth delayed (11.2 *vs.* 6.7 weeks) for endoscopic biopsies. Following engraftment, growth kinetic was similar. Comparisons of primary tumors and corresponding PDX models confirmed preservation of histomorphology (HE histology) and molecular profile (Illumina Cancer Hotspot Panel) of the patients' tumors. Accompanying flow cytometry on primary tumor specimens revealed a heterogeneous tumor microenvironment among individual cases and identified M2-like macrophages as positive predictors for engraftment. Vice versa, a high PD-L1 expression (combined positive score on tumor/immune cells) predicted PDX rejection.

Conclusion: Including biopsy samples from locally advanced or metastatic lesions from patients with non-surgical treatment strategies, increases the availability of PDX for basic and translational research. This facilitates (pre-) clinical studies for individual response prediction based on immunological biomarkers.

Keywords: Primary cancer, HPV positive and negative, Individual tumor models, Immune cell infiltration, Recurrence, Metastasis, Non-resectable, Endoscopic biopsy, Head and neck squamous cell carcinoma

*Correspondence: claudia.maletzki@med.uni-rostock.de
[2] Department of Internal Medicine, Medical Clinic III - Hematology, Oncology, Palliative Medicine, Rostock University Medical Center, Schillingallee 70, 18057 Rostock, Germany
Full list of author information is available at the end of the article

Background

Head and neck squamous cell cancer (HNSCC) is the 7th most common cancer worldwide and associated with a poor outcome [1–5]. Despite aggressive surgery, radiation- and chemotherapy, ~ 50% of patients die, while survivors suffer from pain, dysphagia and dysphonia [6]. Today, recurrence, and treatment response are difficult to predict, because of inter- and intratumoral heterogeneity in etiology, phenotype, and biology. Preclinical models must represent this heterogeneity to identify predictive biomarkers and develop effective personalized medicine.

Patient-derived xenografts (PDX), generated by implantation of human cancer tissue into immunodeficient mice, are considered as the gold standard for preclinical cancer research [7–11]. In early passages, PDXs faithfully recapitulate the original tumors' cellular, molecular and histopathological structures as well as drug response and clinical outcome [8, 12]. Thus, PDX provide an excellent platform for translational research on biomarkers and drug development (including setup of clinical trials) [12–15].

However, the restricted availability of tumor samples hinders widespread use of PDX in HNSCC. The PDX take rate for surgical HNSCC-specimens (50–75%) is comparable to other solid tumors (lung ~ 30–60%, CRC 70%, pancreas ~ 50%) [14–21], but the availability of suitable specimens is limited. In early stage tumors, the pathologist needs most of the surgery specimen for tumor staging and margin controls, while advanced (metastatic) disease is mostly treated with chemo-, immune- or radiation therapy (without surgery). Therefore, PDX from surgery specimens exclude recurrent and advanced (metastatic) HNSCC from preclinical models and personalized medicine.

In lung-, gastrointestinal-, pancreatic-, bladder- and skin cancer PDX-projects, the lack of surgical specimens has led to the use of endoscopic- and needle biopsies [15, 22, 23]. Engraftment rates were lower for biopsies (33–60%) *vs.* surgery specimens (40–100%), but PDX formation from minimally invasive procedures was possible. For HNSCC, endoscopic PDX sampling appears technically suitable, because of exophytic tumor growth and diagnostic sampling from both the vital margin and the necrotic center of the lesion. Two recent HNSCC studies regularly used biopsies for PDX formation [24, 25]. Lilja-Fischer et al. reported a biopsy take rate of 33% in oropharyngeal cancer [24] while Kang et al. observed 100% engraftment efficacy for biopsies in a small and defined patient cohort [26]. Therefore, HNSCC PDX biopsy engraftment appears to be feasible. However, take rate, time to engraftment and contributing factors of endoscopic biopsies for HNSCC PDX formation remain unclear.

In this study, we describe a practical and straightforward method to establish p16 positive and negative PDX models using endoscopic and surgical tumor samples. Performing a side-by-side comparison, we show that the engraftment rate was lower for biopsies, but PDX had similar growth kinetics once established. With this setup, a PDX library was created including clinical characteristics, pathological analysis as well as molecular and immunological data of the tumor microenvironment.

Materials and methods

Tumor sample preparation

HNSCC samples were donated from consecutive patients undergoing an endoscopic biopsy or surgery at a University Medical Center from 06/2018 through 01/2020. Patients with pathologically proven or suspicion of HNSCC and the following characteristics were eligible: 1) HNSCC of the oral cavity, oropharynx, hypopharynx, larynx and neck lymph node metastases; 2) size of the tumor > 2 cm; 3) primary disease or recurrence; 4) > 18 years of age. Written informed consent was obtained according to the local Ethics Committee (reference number A2018-0003) and the guidelines for the use of human material. Blood sampling (2 × 7.5 ml Heparin) was performed prior to endoscopy/surgery. Endoscopic biopsies were sampled using endoscopic scissors as required for the routine diagnostic procedure. Surgery specimens were obtained by open (e.g. pharyngotomy, laryngectomy) or transoral approach (e.g. laser, radio frequency).

Immediately after dissection, the samples were sent to the Institute of Pathology (in room temperature NaCl 0.9%) for instantaneous H&E section. The pathologist removed tumor tissue for routine diagnostics, necrotic/fibrotic areas and provided macroscopically vital tumor tissue for the experimental laboratory. All specimens of at least $5 \times 5 \times 5$ mm^3 were accepted and processed within 120 min of ischemia time using a clean bench. Tumor samples were cut into fragments of $3 \times 3 \times 3$ mm^3 and split: Two pieces were snap frozen and stored in liquid nitrogen for molecular analysis. The remaining fragments were frozen viable (FCS, 10% DMSO) and stored at -80 °C for xenografting (Fig. 1).

Ethical statement

All animal experiments were approved by the local governmental authority (approval number: 7221.3-1-066/18), in accordance with the governmental animal protection law and the EU Guideline 2010/63/EU. For in vivo engraftment, six-week-old female NOD.Cg-Prkdc^{scid}Il2rg^{tm1}Wjl (NSG, Charles River Laboratories, Lyon, France) mice were used as recipients. Mice were bred in the local animal core facility under specific pathogen-free

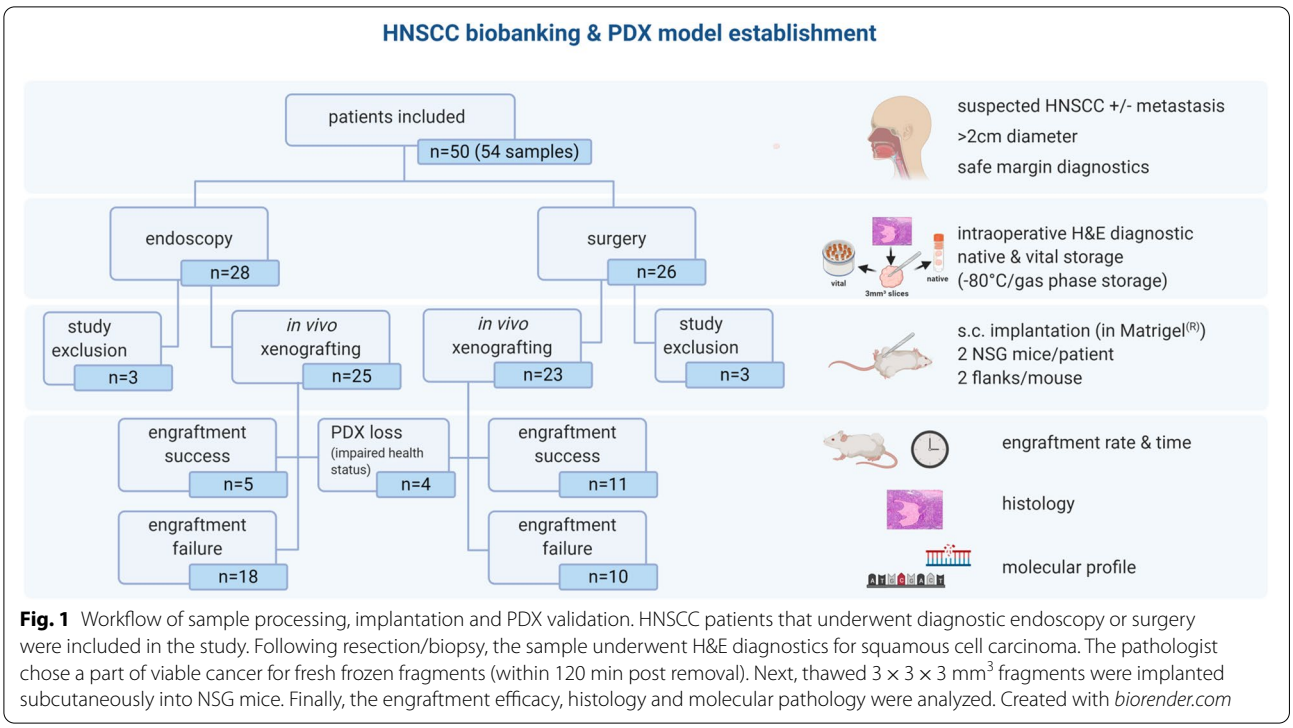

Fig. 1 Workflow of sample processing, implantation and PDX validation. HNSCC patients that underwent diagnostic endoscopy or surgery were included in the study. Following resection/biopsy, the sample underwent H&E diagnostics for squamous cell carcinoma. The pathologist chose a part of viable cancer for fresh frozen fragments (within 120 min post removal). Next, thawed 3 × 3 × 3 mm^3 fragments were implanted subcutaneously into NSG mice. Finally, the engraftment efficacy, histology and molecular pathology were analyzed. Created with *biorender.com*

conditions. During the experiment, mice were kept in type III cages (Zoonlab GmbH, Castrop-Rauxel, Germany) at 12-h dark:light cycle, the temperature of 21 ± 2 °C, and relative humidity of 60 ± 20% with food (pellets, 10 mm, ssniff-Spezialdiäten GmbH, Soest, Germany) and tap water ad libitum. During their whole lifetime, all animals received enrichment as mouse-igloos (ANT Tierhaltungsbedarf, Buxtehude, Germany), nesting material (shredded tissue paper, Verbandmittel GmbH, Frankenberg, Deutschland, paper roles (75 × 38 mm, H 0528–151, ssniff-Spezialdiäten GmbH), and wooden sticks (40 × 16 × 10 mm, Abedd, Vienna, Austria).

PDX generation

After melting of the frozen samples, DMSO was removed and the tumor fragments were embedded in Matrigel (Corning® Matrigel® Basement Membrane Matrix, Wiesbaden, Germany) for 10 min. Meanwhile, the NSG-mice were anesthetized using Ketamin/Xylazin (dose: 90/6 mg/kg bw). After verification of sufficient anesthesia, both hind flanks were shaved, iodine disinfected and incised (3 mm). Tumor fragments were implanted subcutaneously and wounds were closed using simple interrupted sutures (Ethicon 6–0, Johnson & Johnson GmbH, Neuss, Germany) followed by iodine disinfection. Mice were placed under a heating lamp during recovery from anaesthesia and received analgesia (Metamizol 1250 mg/l, in drinking water) (pre- and) post-surgery to reduce pain.

After recovery, the flank tumors were measured weekly using a caliper. If no tumor growth occurred for 6 months, mice were euthanized. When flank tumors grew and reached a maximum size of 1.5 × 1.5 × 1.5 cm^3, euthanasia and tissue collection was performed. The tumor was minced as described for the primary sample. Briefly, two fragments were used for molecular and histological analysis and the remaining fragments were viable frozen for further passaging. Tumor nomenclature was as followed: HNSCC [serial number] P [passage P0/P1] M [mouse M1/M2]. The patients' serial numbers are maintained throughout all PDX passages.

Histology and immunohistochemistry of patient tumor tissue and PDX

Morphology of patient tumor tissue and their corresponding PDX models was studied by an expert pathologist. Histopathology of primary tumors and PDX followed standard protocols for HNSCC staging including HE staining and immunohistochemistry; antibodies: anti-CD8 (Clone C8/144B, Dako, Hamburg, Germany, anti-p16 (clone: G175-405, BD Bioscience, Heidelberg, Germany), anti-Ki-67 (Clone Mib-1, Dako), anti-PD-L1 (Clone 22C3, Dako).

Molecular pathology

Nucleic acids and proteins were isolated from snap frozen primary tumors and PDX [mean weight: 16.6 mg].

Simultaneous purification of DNA, RNA, and protein (from the same tissue sample) was performed using AllPrep DNA/RNA/Protein Mini Kit (Qiagen, Hilden, Germany) Isolation was executed according to the manufacturers' instructions: (I) tissue disruption and homogenization; (II) RNA isolation; (III) protein isolation; and (IV) gDNA isolation. Isolated nucleic acids and proteins were stored at -80 °C. gDNA samples were used to detect genomic alterations using the Illumina Cancer Hotspot Panel (Illumina, Berlin, Germany) covering mutations in 50 different genes with an iSeq100 sequencing system (Illumina) according to the manufacturer's protocols. For human papilloma virus (HPV) testing, a commercially available kit was used (VisionArray HPV Chip 1.0, Zyto-Vision, Bremerhaven, Germany) and applied according to the manufacturer's instructions.

Multi-color flow cytometry

Surface marker expression on single tumor cell suspensions was assessed by multi-color flow using a panel of human-specific conjugated antibodies (mAb, 1 µg each): anti-CD3 FITC (clone OKT-3), anti-CD4 PE (clone IT4), anti-CD8 PE (clone MEM-31), anti-CD56 PE (clone MEM-188), anti-CD16 APC (clone 3G8), anti-CD274 PECy7 (clone 29E.2A3), anti-CD70 FITC (clone 113–16), anti-CD14 FITC (clone 63D3), anti-CD204 PE (clone 7C9C20), anti-CD169 APC (clone 7–239), anti-CD163 PECy7 (clone GHI/61). Whole blood and tumor samples were stained for 30 min (4 °C). Afterwards, erythrocytes were lysed using 155 mM NH_4Cl (MERCK Millipore, Darmstadt, Germany), 10 mM $KHCO_3$ (MERCK Millipore), and 0.1 mM EDTA (Applichem, Darmstadt, Germany). Negative controls were stained with the appropriate isotypes (Biolegend) or left unstained. Cells were washed, resuspended in PBS and analyzed by flow cytometry on a FACSVerse Cytometer (BD Pharmingen). Data analysis was performed using BD FACSuite software (BD Pharmingen).

Statistics

Statistical evaluation was performed using GraphPad PRISM software, version 5.02 (GraphPad, San Diego, USA). Values are reported as the mean ± SD. After proving the assumption of normality, differences between biopsies and surgery specimens were calculated using the unpaired Student's t-test. If normality failed, the non-parametric Mann–Whitney *U* test was applied. Multiple comparisons were done using one way ANOVA on ranks (Bonferroni's Multiple Comparison Test). Spearman nonparametric correlation was used to calculate correlations between individual parameters (two-tailed *P* value). The criterion for significance was taken to be $p < 0.05$.

Results

Patient and sample characteristics

Fifty patients were included (male:female: 41:9) with high performance status (ECOG 1.06 ± 0.88) with a median age of 64.0 years (range 46 to 82) (Table 1 and Fig. 1). Most patients were smokers (68%, ≥ 10 py), without critical alcohol consumption (54%). The majority of patients presented with locally advanced disease (T4a/4b) and four with a recurrence after (chemo)-radiation. Tumors were localized in the oropharynx ($n = 19$), oral cavity ($n = 17$), larynx ($n = 11$) and hypopharynx ($n = 5$) (Table 1). Neck metastases were collected from four patients (primary + related metastasis: HNSCC40/40II/40III and HNSCC45/46; metastasis only: HNSCC08 and HNSCC48). One case was a HNSCC lymph node metastasis of unknown primary (CUP) (HNSCC37). Thirteen of the tumors were $p16^+$ (determined by p16 immunoreactivity, representative images of $p16^+$ and $p16^-$ cases are given in Fig. 2). To analyze whether p16 positivity is the result of HPV infection, molecular HPV testing was done (Supplementary Table 1). HPV was confirmed in 12 cases, whereas one case (HNSCC26) was finally classified as $p16^+/HPV^-$.

Table 1 Characteristics of the 50 study participants (Σ = 56 samples)

Group characteristics	Surgery Σ *n* = 26		Biopsy Σ *n* = 28	
	%	*n*	%	*n*
Female	15	4	18	5
Male	85	22	82	23
Age [years]	64.8	± 9.4	64.5	± 8.1
Performance status [ECOG]	1.0	± 0.7	1.1	± 1.0
Noxae				
Smoking [> 10 py]	73	19	68	19
Alcohol [> 1 drink/d]	58	15	32	9
Localization	38	10		
Oral cavity	23	6	25	7
Oropharnyx	12	3	46	13
Hypopharynx	27	7	7	2
Larynx			18	5
CUP			4	1
p16 status				
Positive	15	4	32	9
Negative	85	22	68	19
G1/G2/G3 [%]	6/73/21		5/70/25	
T1/T2/T3/T4 [%]	13/27/30/30		-/17/29/54*	
N0/N1/N2/N3 [%]	56/30/5/9		15/35/60/0*	

Values depict absolute/relative numbers and mean ± SD. Chi-square test was performed to analyze homogeneity of surgery *vs*. biopsy groups (*$p < 0.05$)

Abbreviations: *py* pack years, *CUP* cancer of unknown primary, *G1/2/3* grading

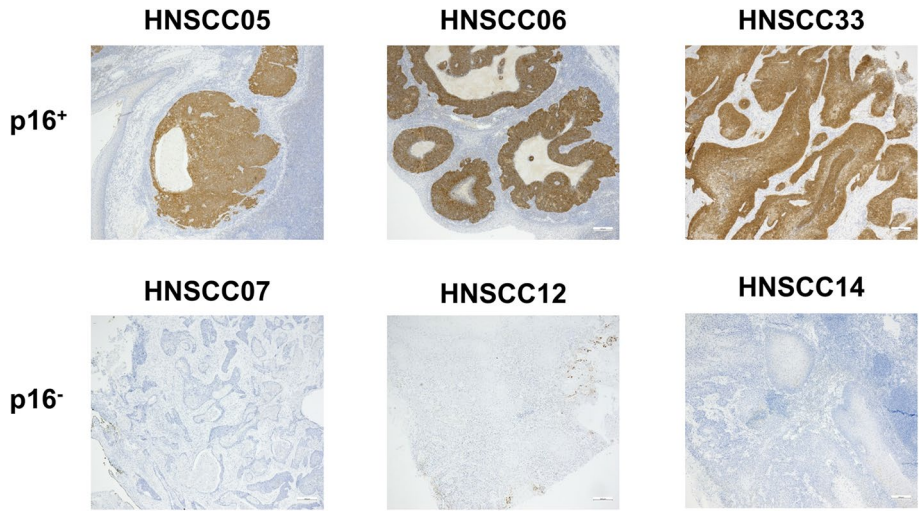

Fig. 2 Immunohistochemistry of p16. Representative images of $p16^+$ and $p16^-$ cases are shown (5 × magnification). Immunohistochemistry was done as described in material & methods using clone: G175-405

The mean sample size of the tumor piece was 1.2 ± 1.6 cm^3. In some cases of endoscopic biopsies, several pieces were obtained. Biopsy samples were smaller than surgical specimens (mean size: 0.9 cm^3 *vs.* 1.3 cm^3). The ischemia time was the same for biopsies and surgery samples (< 120 min, mean: 89.5 ± 33.6 min).

Detailed information on clinical follow-up, including adjuvant treatment, is summarized in Table 1. So far, four patients died because of progressive disease (HNSCC21, HNSCC31, HNSCC48, and HNSCC51).

PDX engraftment rate of biopsies and surgical specimens

Fourty eight cryopreserved individual HNSCC tumors were implanted subcutaneously into NSG mice (Table 1). Six HNSCC cases did not undergo PDX engraftment because of limitations in tumor quantity/quality and unspecific tumor type (CUP). Additional four HNSCC cases were lost because of impaired health of laboratory animals. Finally, 44 cases were included in data acquisition: 23 biopsy samples and 21 surgery samples.

Engraftment was obtained in 16 cases, yielding an overall efficacy of 36.4%. The engraftment rate was higher for surgical specimens (52.4 *vs.* 21.7%) and engraftment time was shorter (6.9 ± 2.4 *vs.* 10.6 ± 3.8 weeks; $p < 0.05$; Fig. 3A). After successful engraftment, PDX had comparable growth kinetics: Surgical specimens reached the maximum size in 9.5 ± 4.8 weeks and biopsies in 12.2 ± 4.6 weeks (Fig. 3A). Some aggressive cases grew in several flanks/implantation sites, while other cases did not engraft at all (Fig. 3B). Therefore, the positive flank related engraftment rate was 59.7% (Table 2). Again, the number of individual PDX/tumor was higher for surgical specimens (77.3%, Fig. 3B). Still, positive engraftment was seen in 37.5% of biopsy samples.

Notably, four PDX were established from $p16^+$/HPV-driven HNSCC cases (HNSCC06, HNSCC26, HNSCC42, and HNSCC54); three of them were taken from biopsies. Hence, the p16 status did not impact engraftment efficacy. Additional clinical parameters such as age, smoking, tumor localization, TNM stage and grade did not correlate with the engraftment. The same was true for the sampling related factors ischemia time and sample size (Table 3).

Serial passaging of the first seven established PDX models into P1 NSG mice was successful. All PDX grew after passaging and showed growth acceleration (time to tumor resection: 11.4 weeks vs. P0: 13.8 weeks) (Fig. 3C).

Histomorphology is preserved in PDX

All PDX closely resembled their primaries (Fig. 4). Tumor architecture, growth pattern, cytological features and stromal architecture were principally preserved. Besides, tumor differentiation (i.e., poor, moderate, or well) largely matched between patients and PDX models (Fig. 4). The PDX reflected intratumoral and intertumoral heterogeneity. Sometimes there were minor differences in tumor morphology (degree of keratinization) between individual mice: HNSCC13 P0 M1 showed strong keratinization, whereas in HNSCC13 P0 M2 the number of keratinizing areas was moderate (Fig. 5).

Regarding the biopsies and surgical specimens, no differences in preservation of morphology could be detected.

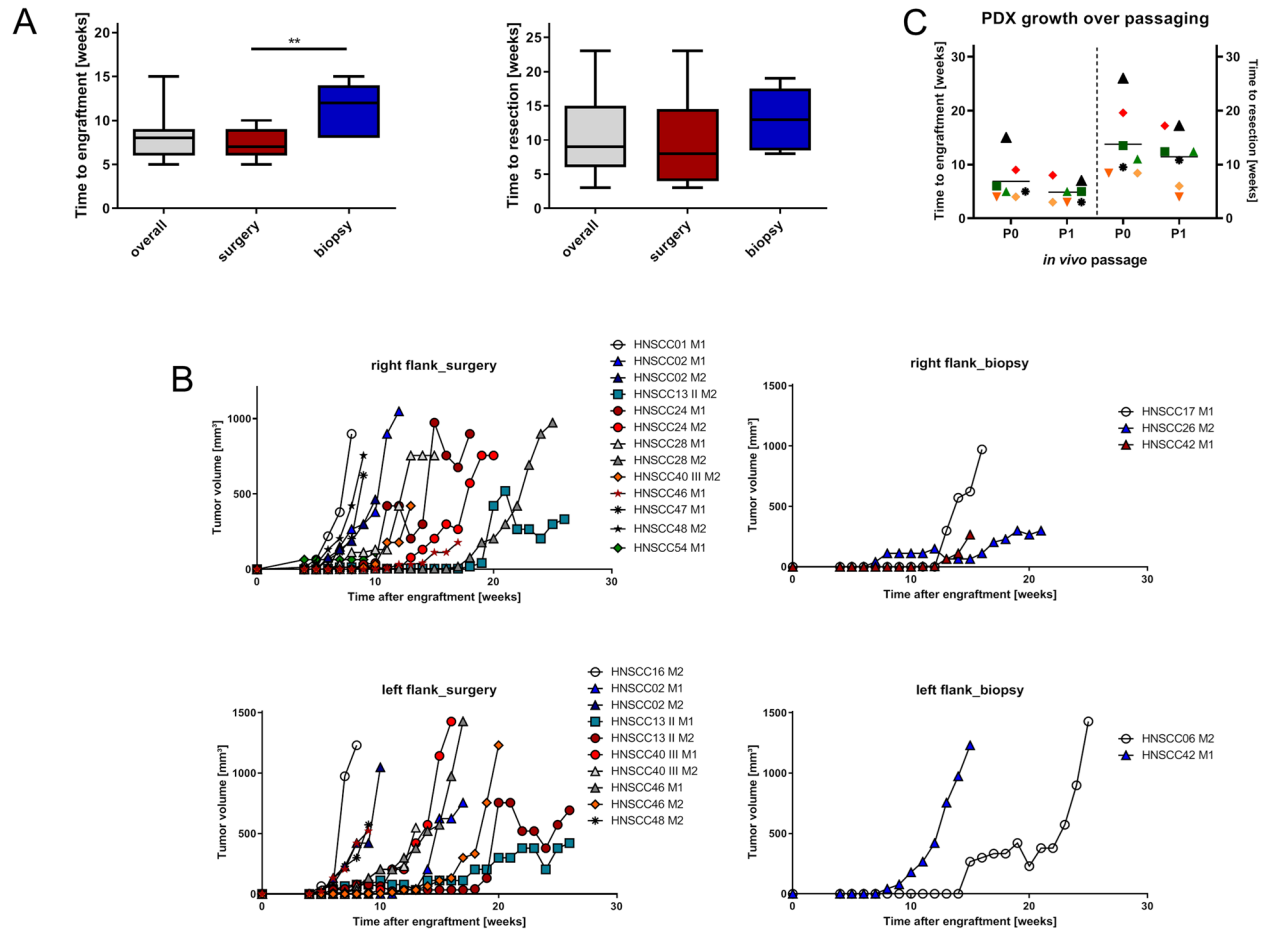

Fig. 3 PDX formation, success rate, and growth kinetic in NSG mice. **A** Boxplots depicting the time from implantation to engraftment (appearance of palpable tumor in the flanks) and the time from the engraftment to resection when tumors reached maximum sizes [1500 mm^3]. Whiskers show the minimum and maximum. $^{**}p < 0.01$, unpaired t-test (two tailed). **B** Growth curves of the individual PDX: Each line represents a PDX grown in P0 in one mouse. M – mouse. **C** Growth acceleration after passaging: Scatterplot depicting the time from implantation to engraftment and resection for the initial implantation (= P0) and after cryopreservation and replantation into NSG mice (= P1). Each dot is representative for an individual HNSCC case using the same symbol and color for P0 and P1

Table 2 Overview on engraftment efficacy in NSG mice comparatively shown for biopsies and surgical specimen

Analyzed parameter	N	%
PDX engraftment [total]	16/44	36.36
Biopsies	5/23	21.73
Surgical resection specimen	11/21	52.38
Positive flanks [total]	43/72	59.72[a]
Biopsies	9/24	37.50[a]
Surgical resection specimen	34/44	77.30[a]

[a] taken from a total of two mice/case each implanted with two tumor fragments (left and right flank)

Table 3 Correlation analysis for PDX formation of HNSCC cases between biopsies and surgical specimen

Spearman correlation	*p* Value	Correlation coefficient[a]
Sample type	0.912	0.016
Sample size	0.300	-0.154
Age	0.887	0.021
Ischemia time	0.808	0.036
Ki-67 index	0.770	-0.043

[a] 1 = perfect positive correlation; -1 = perfect negative correlation; 0 = no correlation

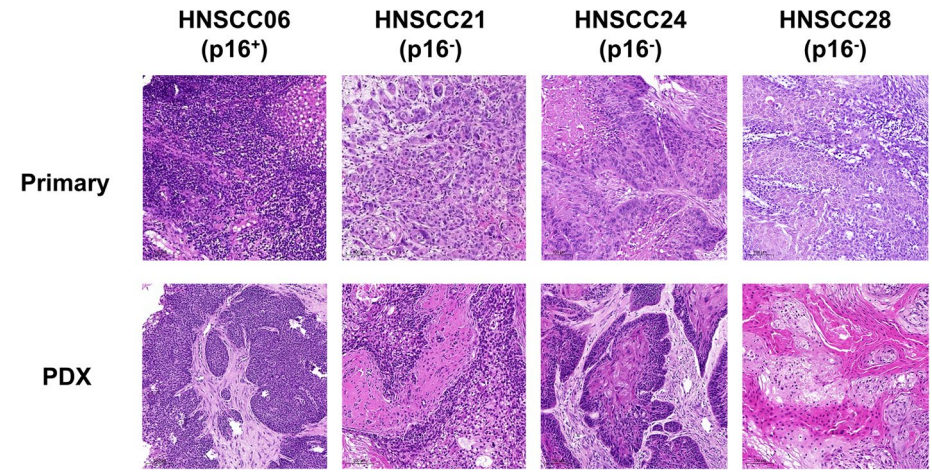

Fig. 4 Histology of matched primary tumors and PDX models. HE histology represents maintenance of HNSCC tumor morphology following xenografting

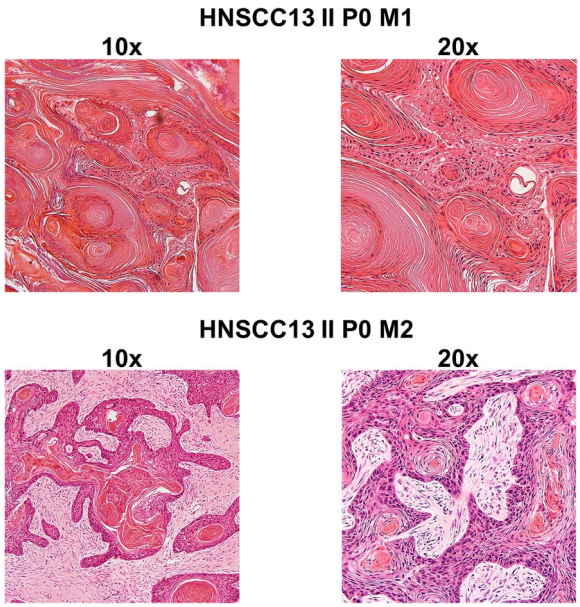

Fig. 5 Intratumoral heterogeneity. HE staining of two individual PDX from case HNSCC13. Both PDX models preserve keratinization of the patient tumor. While HNSCC13 P0 M1 had strong keratinization, the corresponding PDX HNCCC13 P0 M2 had only few keratinizing areas

Tumor microenvironment of patient tumors and PDX

Immunohistochemistry and flow cytometry revealed correlations between PDX engraftment, PD-L1 expression, and macrophage infiltration (Fig. 6). Immunohistological quantification of PD-L1 using the combined positive score (PD-L1 positivity in tumor and tumor-infiltrating immune cells), showed a trend towards better engraftment for low combined positive score (CPS $\leq$ 10); whereas cases with high CPS were more likely to be rejected (CPS [yes] *vs.* CPS [no]: 18.22 vs. 33.41; Pearson r: -0.109] (Fig. 6A).

The leukocyte infiltration of the tumor microenvironment was quantified by flow cytometry. Twenty five cases were analyzed ($p16^-$: 16 cases; $p16^+$: 9 cases). Leukocytic infiltration was heterogeneous (Fig. 6B), but $p16^+$ tumors showed a characteristic infiltration pattern. We identified high infiltration with $CD3^+CD4^+$ helper ($p < 0.01$ *vs.* $p16^-$ tumors) and $CD3^+CD8^+$ cytotoxic T cells, along with elevated numbers of $CD3^+CD274^+$ T cells. $CD14^+CD163^+$ and $CD14^+CD204^+$ macrophages were less frequent in $p16^+$ cases. $CD16^+CD56^+$ natural killer (NK) cells were heterogeneous irrespective of the p16 status.

Correlation of the innate immune cell compartment with PDX engraftment showed that engraftment was more frequent in cases with high numbers of $CD14^+CD163^+$ macrophages (Pearson r: -0.757; $p < 0.05$) and low numbers of $CD14^+CD204^+$ macrophages.

Molecular pathology is preserved in PDX

The mutational profile was studied in 13 patient samples and corresponding PDX. The overall number of genomic alterations in the cancer hotspot panel was low: *TP53* (61.5%) and *KDR* (38.4%) were the most affected genes. The direct comparison of the molecular fingerprint identified few discrepancies in most commonly affected genes (Fig. 7). In the PDX of HNSCC02, a *KRAS* mutation (c.114 T > C; variant allele frequency (VAF): 7.3%) and *SMARCB1* mutation (VAF: 5.2%) was detected. Vice versa, the patient tumor sample harbored an *EGFR* mutation (c.2361G > A; VAF: 30.5%) that was lost in the PDX. In HNSCC01, a *KRAS* mutation (c.114 T > C, VAF: 32.7%) was exclusively seen in the PDX. It can be assumed that intratumoral heterogeneity explains these findings best.

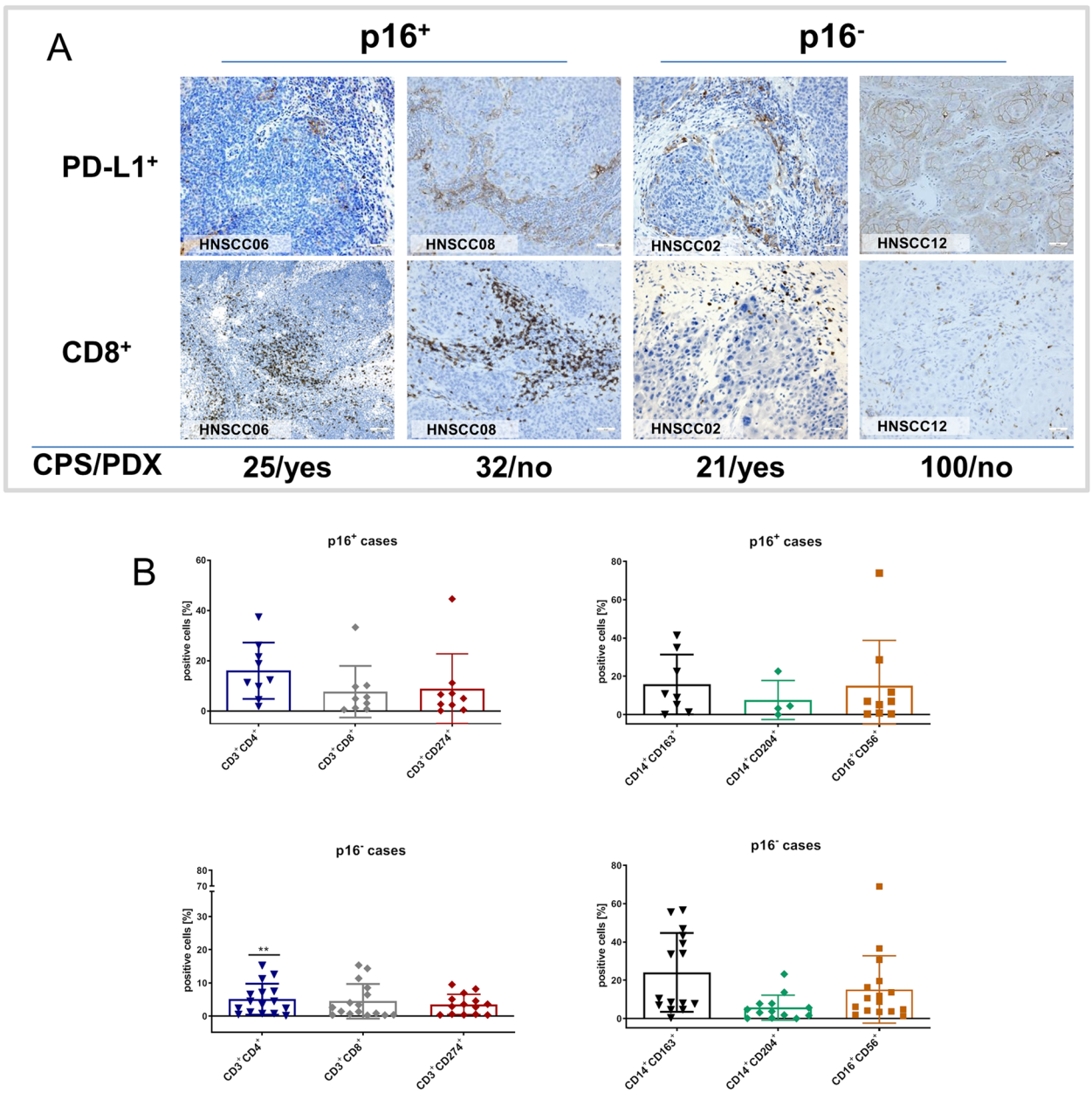

Fig. 6 Tumor microenvironment phenotyping by flow cytometry and immunohistochemistry of $p16^+$ and $p16^-$ HNSCC. **A** Scatterplot depicting the percentage number of positive cells stained with the appropriate monoclonal antibodies followed by flow cytometric analysis and measuring 50,000 events in a live gate. Data analysis was performed using BD FACSuite software. HNSCC cases were separated according to the p16 status (i.e. $p16^+$ of $p16^-$). The number of tumor-infiltrating macrophages ($CD14^+CD163^+$ and $CD14^+CD204^+$) correlated with engraftment success. $^{**}p < 0.01$ $p16^+$ tumors vs. $p16^-$ tumors; Mann Whitney *U* test. **B** Representative images showing PD-$L1^+$ tumor and immune cells as well as infiltrating $CD8^+$ cells in primary tumors. Tumor resection specimens were stained with the appropriate antibodies as stated in material & methods. The combined positive score (CPS) was calculated considering PD-L1 positivity in tumor and tumor-infiltrating immune cells. Additional information on engraftment success is given in the lower part (PDX – patient derived xenograft)

Discussion

Patient-derived xenografts (PDX) maintain morphology and molecular profiling of the original tumors, thus providing a platform for the examination of disease biology, biomarkers, and novel therapeutic agents. However, restricted availability of tumour samples hindered the widespread use of PDX. In line with previous research on different cancer entities [7, 10, 27–29], we hypothesized

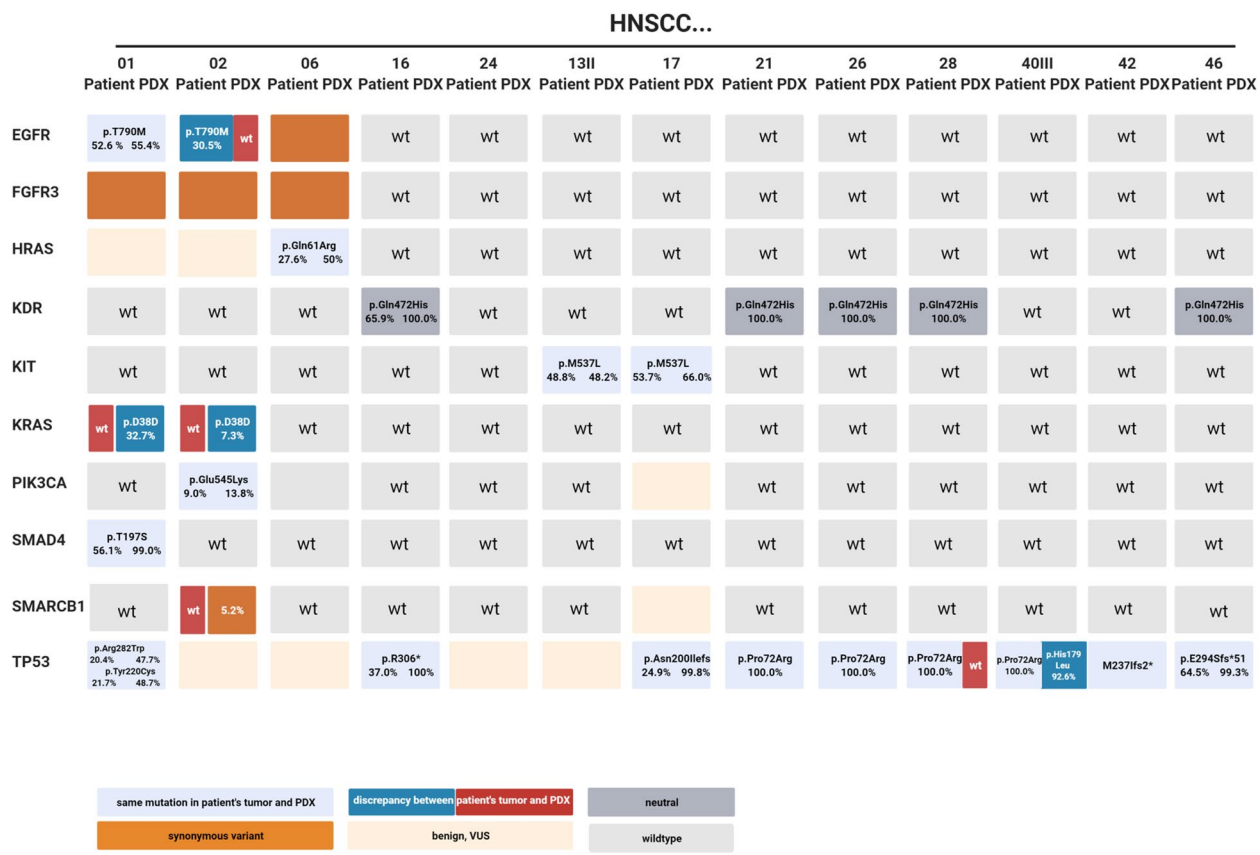

Fig. 7 Molecular profile of matched primary tumors and PDX models. Nucleic acids were isolated from snap frozen samples and stored at -80 °C. Purified gDNA samples were than used to detect genomic alterations using the Illumina Cancer Hotspot Panel (Illumina, Berlin, Germany) covering mutations in 50 different genes with an iSeq100 sequencing system (Illumina) according to the manufacturer's protocols. The specific mutations along with the variant allele frequency are depicted in the boxes. Differences between primary patients' samples and matched PDX are highlighted. Mutations were classified in the following categories: non-synonymous—variant is given in the box (in case of the same mutation in the primary and PDX: light blue, difference between primary and PDX: red/blue); synonymous: orange; benign, VUS: light-orange; neutral: grey. The latter is defined as "passenger" mutation that does not play a role in HNSCC; wt – wildtype: light grey. Created with *biorender.com*

that (pre-treatment) endoscopic biopsies contain sufficient viable tumor for PDX growth, in a clinically relevant time frame [21, 30].

Therefore, a comparative analysis on engraftment efficacy of tumor biopsies and surgical specimens was conducted. While both biopsy and surgery specimens were suitable for PDX formation in vivo, the engraftment rate was substantially lower for biopsies.

Recently, PDX engraftment from biopsies has been tested for many cancer entities. The success rates were 3 to 90% using fine- and core needle laparoscopic biopsies [15, 22, 23, 31, 32]. In line with our findings, direct comparisons with surgery sampling showed mainly lower biopsy engraftment rates. For HNSCC, Lilja-Fischer et al. implanted mainly HPV^{+} oropharyngeal cancer biopsies with a success rate of 33%, which is similar to our biopsy engraftment [24]. In conflict with these results, Kang et al. reported a superior HNSCC biopsy engraftment of 100% compared to 16% of surgery samples, yet in a very small patient cohort [25]. However, both groups did not specify whether the biopsies were diagnostic tonsillectomies, lymph node metastasis extirpations or endoscopic biopsies. Take rates approaching 100% are more typical for metastatic lymph node biopsies, which are not part of routine HNSCC diagnostics. Reviewing the present results in the scope of previous research, we expect engraftment rates of ~ 30% for biopsies and 50–70% for surgical specimens in HNSCC. However, comparisons of engraftment rates are impaired by limited standardization: Depending on the authors, the engraftment rate has been reported after one, two or three passages. More differences comprise the mouse strain (complex immunodeficient vs. athymic), the number of animals/tumor and the implantation technique (orthotopic vs. subcutaneous vs. kidney capsule vs. muscle). More standards are highly desirable to reduce laboratory animal expenditure.

A critical factor for engraftment efficacy is tissue ischemia and cryopreservation of tumor samples prior to engraftment that impair viability and thus PDX formation [33–37]. Tissue ischemia has been controlled by pathological diagnostics, processing, and viable freezing within 120 min. Immediate tissue transfer into mice is supposed to enable the highest yield of viable cells, but it also requires a complex infrastructure including timing of surgery, availability of laboratory personnel and accessibility to mice at a specific age (usually < 3 month). We therefore decided to cryopreserve fresh frozen tumor samples prior to engraftment and our engraftment efficacy was comparable to previous research using direct implantation. The standardized cryopreservation enables implantation of several tumor samples simultaneously and re-implantation of frozen backup samples if initial PDX formation fails. Freezing also facilitates reanimation of early passaged tumors at later time points. To date, all individual PDX cases were cryopreserved in P0 and seven have been replanted into NSG mice. All of them grew successfully in P1.

Additional to the higher engraftment rate, surgery samples showed an accelerated in vivo growth. After tumor formation, the growth kinetics was the same in both groups. Handling time, specimen size, p16 status, Ki-67 index, patients' clinical characteristics and implantation ($3 \times 3 \times 3$ mm^3 fragments) did not differ between the study groups. As sampling quality does not appear to be the primary reason, it can only be speculated on the underlying causes for impaired biopsy engraftment. One plausible explanation may be sampling of less proliferating tumor cells in biopsies because of intratumoral heterogeneity [32]. Likewise, the tumor microenvironment at the invasive margin may have played a role, too. Biopsies are usually taken from exophytic tumor areas to avoid bleeding and tumor cell dispersion: These areas are exposed to air, toxins and microorganisms. Also, basal proliferating areas remain untouched. In contrast, PDX of surgical specimens originate from central areas of the tumor to ensure safe pathological margin diagnostics. If the surgery samples are large and margins safe (e.g. laryngectomy) (I) viable cells from the cancer invasion front may be selected and (II) specific areas (center vs. margin) of the tumor may be punched to consider heterogeneity.

To improve engraftment rates, orthotopic implantation of HNSCC biopsy pieces might provide a good alternative. Also, metastasis and accurate mimicry of the original tumors' environment can be anticipated. Another way to increase the number of PDX models from biopsies is a preselection of the tumor type (e.g. focusing only on highly malignant/aggressive cases) or ex vivo enrichment of tumor cells via tumor-surface antigen-based sorting/separation (such as EpCAM or cancer-initiating/stem cells), followed by co-implantation with non-malignant stromal cells. Finally, grafting of three-dimensional patient-derived tumor organoids or even circulating tumor cells is increasingly applied in preclinical research and may help to ameliorate success rates prospectively [38].

Even though surgery samples have many advantages, including non-resectable advanced cancer biopsy samples in preclinical models is crucial. Since these tumors are usually treated by radiation or chemotherapy, drug response prediction would be highly desirable. Additionally, 75% of the $p16^+$ PDX originated from biopsies in this study. HPV-related HNSCC PDX underline the importance of biopsy xenografting in cancer entities, which are mostly treated by irradiation therapy. Improvement of biopsy engraftment could also enable repetitive PDX generation from pre-therapeutic endoscopy, surgery, post-radiation endoscopy and cancer recurrence to study cancer progression and clonal selection.

Previous studies described an association of clinical and pathological features between tumors with rapid and slow PDX growth. In pancreatic cancer, for instance, rapid growth was significantly associated with male gender and lymph node metastases [21]. Likewise, rapid PDX growth was associated with a poor outcome in melanoma and HNSCC patients [10, 30]. A recent study described an association of tumor mutational burden and reduced $E7/p16^{INK4A}$ levels with $p16^+$ HNSCC PDX and organoid engraftment [27]. Hence, successful and rapid PDX establishment is suspected to be predictive for increased risk of recurrence and poor outcome. Since the biobank has been established recently, survival rates could not be calculated. However, previous data on the correlation of PDX engraftment and patient outcome can be confirmed at least partially: One PDX was established from a chemoradiation refractory patient (HNSCC48) who deceased shortly after salvage surgery. This PDX grew rapidly and growth accelerated after serial passaging.

Another important factor in HNSCC research is the tumor microenvironment, since HNSCC naturally shows high immune cell infiltration. Fuji et al., described the impact of the tumor microenvironment on engraftment efficacy of colorectal cancer specimens and concluded that tumor-infiltrating lymphocytes can inhibit engraftment by exerting suppressive effects on tumor growth [39]. The tumor microenvironment was scanned with immunohistochemistry and flow cytometry in the present work. Both methods confirmed increased immune activity in $p16^+$ tumors as part of the immune response to the viral infection compared to $p16^-$ tumors. Regarding the influence of the TME on PDX growth, immunohistochemistry revealed that low CPS scores were associated

with high engraftment rates. Flow cytometric TME analysis identified (tumor associated) $CD14^+CD163^+$ and $CD14^+CD204^+$ macrophages as critical determinants for PDX propagation. Both subtypes are strongly associated with the M2-like phenotype. In breast and lung cancer, circulating $CD14^+CD204^+$ cells are representative for an advanced tumor stage and contribute to metastasis [40, 41]. In esophageal cancer, the high infiltration of $CD163^+$ macrophages is significantly associated with chemoresistance [42]. Because of the value of tumor microenvironment analysis for PDX engraftment and biomarker identification, flow cytometry could become a method of choice for quantitative examination of the immune infiltration. Flow cytometry is timesaving and measures multiple cell types simultaneously in small tumor samples (compared with immunohistochemistry). A major constraint of flow cytometric tumor microenvironment phenotyping is the lack of spatially resolved measurements regarding leukocyte localization within the tumor and its interaction with different cell types, such as tumor cells and cancer-associated fibroblasts. A very recent study integrated histomorphological patterns of immune cell infiltration and mRNA expression data of immune genes in HNSCC. In this study, the status of tumor-infiltrating lymphocytes in the intra-epithelial and stromal compartment was identified as non-redundant biomarker in HNSCC that should be evaluated separately [43]. In the present study, immunohistochemistry was combined with flow cytometry and it suggests the latter as an important add-on tool for tumor microenvironment analysis in preclinical models.

Finally, this work has several limitations. One major limitation is the partial molecular characterization using the 50 gene comprising Illumina Cancer Hotspot Panel. However, HNSCC is characterized by heterogeneous (epi-)genetic alterations and several comprehensive studies did not find reliable molecular biomarkers for PDX engraftment. As the focus was on the tumor microenvironment; applying flow cytometry and immunohistochemistry could identify macrophages differentiation and PD-L1 immune status as potential biomarkers for PDX engraftment. A second limitation relates to tumor heterogeneity: Implantation, histology and cancer sequencing were performed from one sample. Joining punches from different areas may preserve heterogeneity in future studies. Next, the PDX suffer from a selection bias in favor of advanced cancer. However, most HNSCC cancers are already advanced on diagnosis and most T1/2 lesions are sufficiently treated by transoral surgery. Therefore, advanced disease models are more valuable for preclinical research. Still, the results on implantation of specimens from small biopsies may also enhance research on PDX from early-stage lesions.

This study has implications for HNSCC PDX-based research: We have established and characterized new $p16^+$ and $p16^-$ in vitro and in vivo models from primary, recurrent and metastasized HNSCC. The new PDX represent morphology and molecular alterations of the patients' tumors. Using endoscopic biopsies, this new PDX models comprise advanced disease patients that were not eligible for surgery. In this context, the correlation between PDX growth and clinical outcome could lead to the identification of clinical biomarkers.

Even though the engraftment rate is lower, PDX from biopsies are essential to include aggressive recurrent and metastasized carcinomas -that cannot be treated by surgery- in preclinical research. Since PDX engraftment from biopsies is feasible, routine implantation of endoscopic biopsies should be implemented in HNSCC research projects. As a result, biopsy PDX might play a crucial role in personalized therapy for HNSCC patients in advanced tumor stage.

Conclusion

This study describes the successful establishment of patient-derived xenograft models from head and neck cancers obtained from endoscopic biopsies and surgery resection specimens. Additionally to the higher engraftment efficacy of the latter compared to the former, intratumoral M2-like macrophages as well as a low PD-L1 expression on tumor and immune cells were identified as independent positive predictors for engraftment. Vice versa, the p16 status had no impact on engraftment efficacy. Finally, PDX models from both sources were successfully transferred and expanded thus broadening the resources for preclinical drug response analyses.

Abbreviations

CUP: Cancer of unknown primary; HNSCC: Head and neck squamous cell carcinoma; HPV: Human papilloma virus; PDX: Patient-derived xenografts; VAF: Variant allele frequency.

Supplementary Information

The online version contains supplementary material available at https://doi.org/10.1186/s13046-021-02047-w.

Additional file 1: Supplementary Table 1. Patient characteristics and clinical information

Acknowledgements

The authors thank Ms. Ilona Klamfuss and Ms. Chantal von Hoersten for breeding NSG mice.

Authors' contributions

DS – recruited patients and participated in study design, performed in vivo experiments, participated in data analysis and manuscript writing; TM, NI – processed tumor material, performed in vivo experiments, isolated nucleic

acids, carried out flow cytometry, and participated in data analysis; MK—processed tumor material, performed flow cytometry, and cryopreservation of primary and PDX material; JL, SS – recruited and informed patients; AZ, SZ – performed histopathological examinations and participated in immunohistochemical data analysis; AB – participated in histopathological examinations; BS – performed NGS analysis and data interpretation; BF, RM, CGT, CJ – critically revised the manuscript; CM—conceived of the study, performed in vivo experiments, analyzed data, performed statistical analysis, and wrote the manuscript. All authors read and approved the final manuscript.

Funding
The study was supported by a grant from the Rostock University Medical Center in the framework of the FORUN program 2019. Open Access funding enabled and organized by Projekt DEAL.

Availability of data and materials
All data generated or analyzed during this study are included in this published article [and its supplementary information files].

Declarations

Ethics approval and consent to participate
All procedures performed in studies involving human participants were in accordance with the ethical standards of the institutional and/or national research committee and with the 1964 Helsinki declaration and its later amendments or comparable ethical standards. Informed consent was obtained from all individual participants involved in the study. Written informed consent was obtained according to the local Ethics Committee (reference number A2018-0003).
All animal experiments were approved by the local governmental authority (approval number: 7221.3-1-066/18), in accordance with the governmental animal protection law and the EU Guideline 2010/63/EU. All applicable international, national, and/or institutional guidelines for the care and use of animals were followed.

Consent for publication
Not applicable.

Competing interests
The authors declare that they have no competing interests.

Author details
[1]Department of Otorhinolaryngology, Head and Neck Surgery "Otto Koerner", Rostock University Medical Center, Rostock, Germany. [2]Department of Internal Medicine, Medical Clinic III - Hematology, Oncology, Palliative Medicine, Rostock University Medical Center, Schillingallee 70, 18057 Rostock, Germany. [3]Department of Oral and Maxillofacial Surgery, Facial Plastic Surgery, Rostock University Medical Center, Rostock, Germany. [4]Institute of Pathology, Rostock University Medical Center, Rostock, Germany.

Received: 9 March 2021 Accepted: 16 July 2021
Published online: 06 August 2021

References

1. Malone E, Siu LL. Precision medicine in head and neck cancer: myth or reality? Clin Med Insights Oncol. 2018;12:117955491877958. https://doi.org/10.1177/1179554918779581.
2. Guo T, Califano JA. Molecular biology and immunology of head & neck cancer. Surg Oncol Clin N Am. 2015;24(3):397–407. https://doi.org/10.1016/j.soc.2015.03.002.
3. Specenier P, Vermorken JB. Optimizing treatments for recurrent or metastatic head and neck squamous cell carcinoma. Expert Rev Anticancer Ther. 2018;18(9):901–15. https://doi.org/10.1080/14737140.2018.1493925.
4. Dang RP, Le VH, Miles BA, et al. Clinical outcomes in patients with recurrent or metastatic human papilloma virus-positive head and neck cancer. Anticancer Res. 2016;36(4):1703–9.
5. Billard-Sandu C, Tao YG, Sablin MP, Dumitrescu G, Billard D, Deutsch E. CDK4/6 inhibitors in P16/HPV16-negative squamous cell carcinoma of the head and neck. Eur Arch Oto-Rhino-Laryngol. 2020;277(5):1273–80. https://doi.org/10.1007/s00405-020-05891-2.
6. Ordonez R, Otero A, Jerez I, Medina JA, Lupianez-Perez Y, Gomez-Millan J. Role of radiotherapy in the treatment of metastatic head and neck cancer. Onco Targets Ther. 2019;12:677–83. https://doi.org/10.2147/OTT.S181697.
7. Lai Y, Wei X, Lin S, Qin L, Cheng L, Li P. Current status and perspectives of patient-derived xenograft models in cancer research. J Hematol Oncol. 2017;10(1):106. https://doi.org/10.1186/s13045-017-0470-7.
8. Peng S, Creighton CJ, Zhang Y, et al. Tumor grafts derived from patients with head and neck squamous carcinoma authentically maintain the molecular and histologic characteristics of human cancers. J Transl Med. 2013;11:198. https://doi.org/10.1186/1479-5876-11-198.
9. Byrne AT, Alférez DG, Amant F, et al. Interrogating open issues in cancer precision medicine with patient-derived xenografts. Nat Rev Cancer. 2017;17(4):254–68. https://doi.org/10.1038/nrc.2016.140.
10. Karamboulas C, Bruce JP, Hope AJ, et al. Patient-derived xenografts for prognostication and personalized treatment for head and neck squamous cell carcinoma. Cell Rep. 2018;25(5):1318-1331.e4. https://doi.org/10.1016/j.celrep.2018.10.004.
11. Byrne AT, Alférez DG, Amant F, et al. Interrogating open issues in cancer precision medicine with patient-derived xenografts. Nat Rev Cancer. 2017;17(4):254–68. https://doi.org/10.1038/nrc.2016.140.
12. Woo XY, Giordano J, Srivastava A, et al. Conservation of copy number profiles during engraftment and passaging of patient-derived cancer xenografts. Nat Genet. 2021;53(1):86–99. https://doi.org/10.1038/s41588-020-00750-6.
13. Lipner MB, Marayati R, Deng Y, et al. Metformin treatment does not inhibit growth of pancreatic cancer patient-derived xenografts. PLoS ONE. 2016;11(1): e0147113. https://doi.org/10.1371/journal.pone.0147113.
14. Kita K, Fukuda K, Takahashi H, et al. Patient-derived xenograft models of non-small cell lung cancer for evaluating targeted drug sensitivity and resistance. Cancer Sci. 2019;110(10):3215–24. https://doi.org/10.1111/cas.14171.
15 Choi S Il, Jeon AR, Kim MK, et al. Development of patient-derived preclinical platform for metastatic pancreatic cancer: pdox and a subsequent organoid model system using percutaneous biopsy samples. Front Oncol. 2019;9:875. https://doi.org/10.3389/fonc.2019.00875.
16. Lee HW, Lee J Il, Lee SJ, et al. Patient-derived xenografts from non-small cell lung cancer brain metastases are valuable translational platforms for the development of personalized targeted therapy. Clin Cancer Res. 2015;21(5):1172–82. https://doi.org/10.1158/1078-0432.CCR-14-1589.
17. Kang HN, Choi JW, Shim HS, et al. Establishment of a platform of non-small-cell lung cancer patient-derived xenografts with clinical and genomic annotation. Lung Cancer. 2018;124:168–78. https://doi.org/10.1016/j.lungcan.2018.08.008.
18. Moro M, Bertolini G, Tortoreto M, Pastorino U, Sozzi G, Roz L. Patient-derived xenografts of non small cell lung cancer: resurgence of an old model for investigation of modern concepts of tailored therapy and cancer stem cells. J Biomed Biotechnol. 2012;2012: 568567. https://doi.org/10.1155/2012/568567.
19. Ilie M, Nunes M, Blot L, et al. Setting up a wide panel of patient-derived tumor xenografts of non-small cell lung cancer by improving the pre-analytical steps. Cancer Med. 2015;4(2):201–11. https://doi.org/10.1002/cam4.357.
20. Brown KM, Xue A, Mittal A, Samra JS, Smith R, Hugh TJ. Patient-derived xenograft models of colorectal cancer in preclinical research: a systematic review. Oncotarget. 2016;7(40):66212–25. https://doi.org/10.18632/oncotarget.11184.
21 Pergolini I, Morales-Oyarvide V, Mino-Kenudson M, et al. Tumor engraftment in patient-derived xenografts of pancreatic ductal adenocarcinoma is associated with adverse clinicopathological features and poor survival. PLoS One. 2017;12(8):e0182855. https://doi.org/10.1371/journal.pone.0182855.
22. Hermans E, Van der Merwe SW, Depreeuw J, et al. Successful application of endoscopic ultrasound-guided fine needle biopsy to establish pancreatic patient-derived tumor xenografts: a pilot study. Endoscopy. 2016;48(11):1016–22. https://doi.org/10.1055/s-0042-113597.
23. Wang Z, Fu S, Zhao J, et al. Transbronchoscopic patient biopsy-derived xenografts as a preclinical model to explore chemorefractory-associated pathways and biomarkers for small-cell lung cancer. Cancer Lett. 2019;440–441:180–8. https://doi.org/10.1016/j.canlet.2018.10.014.

24. Lilja-Fischer JK, Ulhøi BP, Alsner J, et al. Characterization and radiosensitivity of HPV-related oropharyngeal squamous cell carcinoma patient-derived xenografts. Acta Oncol. 2019;58(10):1489–94. https://doi.org/10.1080/0284186X.2019.1660802.
25. Kang HN, Kim JH, Park AY, et al. Establishment and characterization of patient-derived xenografts as paraclinical models for head and neck cancer. BMC Cancer. 2020;20(1):316. https://doi.org/10.1186/s12885-020-06786-5.
26. Kang HN, Kim JH, Park AY, et al. Establishment and characterization of patient-derived xenografts as paraclinical models for head and neck cancer. BMC Cancer. 2020;20(1):1–12. https://doi.org/10.1186/s12885-020-06786-5.
27. Facompre ND, Rajagopalan P, Sahu V, et al. Identifying predictors of <scp>HPV</scp> -related head and neck squamous cell carcinoma progression and survival through patient-derived models. Int J Cancer. 2020;147(11):3236–49. https://doi.org/10.1002/ijc.33125.
28. Kimple RJ, Harari PM, Torres AD, et al. Development and characterization of HPV-positive and HPV-negative head and neck squamous cell carcinoma tumorgrafts. Clin Cancer Res. 2013;19(4):855–64. https://doi.org/10.1158/1078-0432.CCR-12-2746.
29. Klinghammer K, Raguse J-D, Plath T, et al. A comprehensively characterized large panel of head and neck cancer patient-derived xenografts identifies the mTOR inhibitor everolimus as potential new treatment option. Int J cancer. 2015;136(12):2940–8. https://doi.org/10.1002/ijc.29344.
30. Ny L, Rizzo LY, Belgrano V, et al. Supporting clinical decision making in advanced melanoma by preclinical testing in personalized immune-humanized xenograft mouse models. Ann Oncol. 2020. https://doi.org/10.1016/j.annonc.2019.11.002.
31. Dong Y, Manley BJ, Becerra MF, et al. Tumor xenografts of human clear cell renal cell carcinoma but not corresponding cell lines recapitulate clinical response to sunitinib: feasibility of using biopsy samples. Eur Urol Focus. 2017;3(6):590–8. https://doi.org/10.1016/j.euf.2016.08.005.
32. Roife D, Kang Y, Wang L, et al. Generation of patient-derived xenografts from fine needle aspirates or core needle biopsy. Surgery. 2017;161(5):1246–54. https://doi.org/10.1016/j.surg.2016.11.020.
33 Linnebacher M, Maletzki C, Ostwald C, et al. Cryopreservation of human colorectal carcinomas prior to xenografting. BMC Cancer. 2010;10:362. https://doi.org/10.1186/1471-2407-10-362.
34. Tanaka R, Kageyama K, Kimura K, et al. Establishment of a liver transplant patient-derived tumor xenograft (PDX) model using cryopreserved pancreatic ductal adenocarcinoma. Anticancer Res. 2020;40(5):2637–44. https://doi.org/10.21873/anticanres.14234.
35. Hernandez MC, Yang L, Leiting JL, et al. Successful secondary engraftment of pancreatic ductal adenocarcinoma and cholangiocarcinoma patient-derived xenografts after previous failed primary engraftment. Transl Oncol. 2019;12(1):69–75. https://doi.org/10.1016/j.tranon.2018.09.008.
36 Guerrera F, Tabbo F, Bessone L, et al. The influence of tissue ischemia time on RNA integrity and patient-derived xenografts (PDX) engraftment rate in a non-small cell lung cancer (NSCLC) Biobank. PLoS One. 2016;11(1):0145100. https://doi.org/10.1371/journal.pone.0145100.
37. Jiang W, Xie S, Liu Y, Zou S, Zhu X. The application of patient-derived xenograft models in gynecologic cancers. J Cancer. 2020;11(18):5478–89. https://doi.org/10.7150/jca.46145.
38 Cho S-Y. Patient-derived xenografts as compatible models for precision oncology. Lab Anim Res. 2020;36(1):14. https://doi.org/10.1186/s42826-020-00045-1.
39. Fujii E, Kato A, Chen YJ, Matsubara K, Ohnishi Y, Suzuki M. The status of donor cancer tissues affects the fate of patient-derived colorectal cancer xenografts in NOG mice. Exp Anim. 2015;64(2):181–90. https://doi.org/10.1538/expanim.14-0080.
40. Maeda R, Ishii G, Neri S, et al. Circulating CD14+CD204+ cells predict postoperative recurrence in non-small-cell lung cancer patients. J Thorac Oncol. 2014. https://doi.org/10.1097/JTO.0000000000000044.
41. Zhang B, Cao M, He Y, et al. Increased circulating M2-like monocytes in patients with breast cancer. Tumor Biol. 2017;39(6):1010428317711571. https://doi.org/10.1177/1010428317711571.
42. Yamamoto K, Makino T, Sato E, et al. Tumor-infiltrating M2 macrophage in pretreatment biopsy sample predicts response to chemotherapy and survival in esophageal cancer. Cancer Sci. 2020;111(4):1103–12. https://doi.org/10.1111/cas.14328.
43. Badr M, Jöhrens K, Allgäuer M, et al. Morphomolecular analysis of the immune tumor microenvironment in human head and neck cancer. Cancer Immunol Immunother. 2019;68(9):1443–54. https://doi.org/10.1007/s00262-019-02378-w.

Publisher's Note

cancers

MDPI

Article

Preclinical Head and Neck Squamous Cell Carcinoma Models for Combined Targeted Therapy Approaches

Nina Schoenwaelder [1], Mareike Krause [1], Thomas Freitag [1], Björn Schneider [2], Sarah Zonnur [2], Annette Zimpfer [2], Anne Sophie Becker [2], Inken Salewski [1], Daniel Fabian Strüder [3], Heiko Lemcke [4,5], Christina Grosse-Thie [1], Christian Junghanss [1] and Claudia Maletzki [1,*]

[1] Hematology, Oncology, Palliative Medicine, Department of Medicine, Clinic III, Rostock University Medical Center, 18057 Rostock, Germany; nina.schoenwaelder@med.uni-rostock.de (N.S.); mareike.krause@med.uni-rostock.de (M.K.); thomas.freitag@uni-rostock.de (T.F.); inken.salewski@med.uni-rostock.de (I.S.); christina.grosse-thie@med.uni-rostock.de (C.G.-T.); christian.junghanss@med.uni-rostock.de (C.J.)
[2] Institute of Pathology, Rostock University Medical Centre, 18057 Rostock, Germany; bjoern.schneider@med.uni-rostock.de (B.S.); sarah.zonnur@med.uni-rostock.de (S.Z.); annette.zimpfer@med.uni-rostock.de (A.Z.); anne-sophie.becker@med.uni-rostock.de (A.S.B.)
[3] Head and Neck Surgery "Otto Koerner", Department of Otorhinolaryngology, Rostock University Medical Centre, 18057 Rostock, Germany; daniel.strueder@med.uni-rostock.de
[4] Department of Cardiac Surgery, Reference and Translation Center for Cardiac Stem Cell Therapy (RTC), Rostock University Medical Center, University of Rostock, 18057 Rostock, Germany; heiko.lemcke@med.uni-rostock.de
[5] Faculty of Interdisciplinary Research, Department Life, Light & Matter, University Rostock, 18057 Rostock, Germany
* Correspondence: claudia.maletzki@med.uni-rostock.de

Simple Summary: Head and neck squamous cell carcinoma are characterized by a high degree of inter- and intratumoral heterogeneity. Well-characterized preclinical models represent the heterogeneity of this disease and enable the development of innovative therapeutic concepts. The present work dealt with the establishment of patient-individual tumor models to explore new treatment approaches for HNSCC patients and to identify suitable biomarkers for predicting treatment response. In this study, tumor specimens from advanced cancers of the oral cavity, hypopharynx, and larynx were used to establish individual tumor models. These novel cell lines were used to apply different combinations of strategies, preclinically, and to overcome intrinsic resistance mechanisms.

Abstract: This study aimed to refine combined targeted approaches on well-characterized, low-passage tumor models. Upon in vivo xenografting in immunodeficient mice, three cell lines from locally advanced or metastatic HNSCC were established. Following quality control and basic characterization, drug response was examined after therapy with 5-FU, Cisplatin, and cyclin-dependent kinase inhibitors (abemaciclib, THZ1). Our cell lines showed different in vitro growth kinetics, morphology, invasive potential, and radiosensitivity. All cell lines were sensitive to 5-FU, Cisplatin, and THZ1. One cell line (HNSCC48 P0 M1) was sensitive to abemaciclib. Here, Cyto-FISH revealed a partial *CDKN2a* deletion, which resulted from a R58* mutation. Moreover, this cell line demonstrated chromosome 12 polysomy, accompanied by an increase in CDK4-specific copy numbers. In HNSCC16 P1 M1, we likewise identified polysomy-associated *CDK4*-gains. Although not sensitive to abemaciclib per se, the cell line showed a G1-arrest, an increased number of acidic organelles, and a swollen structure. Notably, intrinsic resistance was conquered by Cisplatin because of *cMYC* and *IDO-1* downregulation. Additionally, this Cisplatin-CDKI combination induced HLA-ABC and PD-L1 upregulation, which may enhance immunogenicity. Performing functional and molecular analysis on patient-individual HNSCC-models, we identified *CDK4*-gains as a biomarker for abemaciclib response prediction and describe an approach to conquer intrinsic CDKI resistance.

Keywords: cisplatin sensitivity; migration; invasion; phenotype; molecular alterations; preclinical tumor models; combined targeted approaches

Citation: Schoenwaelder, N.; Krause, M.; Freitag, T.; Schneider, B.; Zonnur, S.; Zimpfer, A.; Becker, A.S.; Salewski, I.; Strüder, D.F.; Lemcke, H.; et al. Preclinical Head and Neck Squamous Cell Carcinoma Models for Combined Targeted Therapy Approaches. *Cancers* **2022**, *14*, 2484. https://doi.org/10.3390/cancers14102484

Academic Editors: Maria Flavia Di Renzo and Simona Corso

Received: 25 April 2022
Accepted: 17 May 2022
Published: 18 May 2022

1. Introduction

Representative preclinical models are important tools to improve knowledge on tumor biology and treatment response. An ideal model preserves the phenotype and molecular features of the tumor, but also the complex and heterogeneous tumor microenvironment (TME) including immune and stromal cells. However, no available model covers all these characteristics [1]. Three experimental systems are currently used: long-term cultured cell lines, 2D- and 3D-patient-derived cultures, and xenograft models [1,2]. Each of them has specific advantages and limitations.

More than 800,000 patients per year are diagnosed with head and neck squamous cell cancer (HNSCC) worldwide. The mortality rate is almost 50% and the survivors suffer from massive functional limitations [3]. These tumors differ in location (e.g., oral cavity, pharynx, larynx), pathogenesis (human papillomavirus (HPV)-related vs. unrelated), mutational profiles (e.g., *TP53*-mutated and wild type), immune landscapes (immunologically "hot" vs. "cold"), and clinical prognosis (poor to moderate) [3–6]. The urgent need for biomarkers and effective personalized therapies demands well-characterized models that represent HNSCC's heterogeneity to translate data from bench-to-bedside. Therefore, low-passage cell lines enable the studying of the intratumoral heterogeneity and clonal evolution under therapy pressure [7,8]. While surgery and radiotherapy remain standard in primary therapy, recurrent and metastatic HNSCC are treated with Cisplatin-based (radio-) chemotherapy or immune checkpoint inhibition to restore immune surveillance [9,10]. In HNSCC, implementing immunotherapy has only led to a slight increase in response rates and survival. The major reasons are insufficient biomarkers and resistance development. Preclinical tumor models assist in identifying more effective agents for HNSCC treatment. However, representative preclinical models are rarely available in this tumor entity. Moreover, recurrent and metastatic HNSCC are often treated without surgery and these tumors do not become available for preclinical research. This limitation is a hindrance for testing innovative treatment regimens. Still, there are some agents currently under investigation in early phase clinical trials. Cyclin-dependent kinase inhibitors (CDKIs) are a potential new HNSCC therapy. These agents were specifically designed to interfere with the tumors' cell cycle [11–13]. Three CDK4/6 inhibitors are FDA-approved: palbociclib, ribociclib, and abemaciclib [14]. This latter agent is being used in several clinical trials for HNSCC treatment, either alone or in combination with anti-PD-1 antibodies (clinical trials.gov identifier: NCT03356223, NCT03356587, NCT03292250 NCT04169074, and NCT03356223). To increase the number of preclinical and patient-individual tumor models, we focused here on HNSCC from locally advanced or metastatic tumors. These novel models represent ideal tools for performing molecular analysis and drug screening. By using three individual models from different locations, we identified *CDK4* gains as a biomarker for abemaciclib response. These novel patient-individual HNSCC models represent the diseases' heterogeneity and help to guide combination strategies for upcoming clinical application.

2. Materials and Methods

2.1. Tumor Sample Preparation

HNSCC samples were received fresh from surgery at the University Medical Center as described [15]. Written informed consent from the HNSCC patients was obtained according to the local Ethics Committee (reference number A2018-0003) and the guidelines for the use of human material (Declaration of Helsinki).

2.2. Ethical Statement

2.2.1. In Vivo Study

The German local authority approved all animal experiments: Landesamt für Landwirtschaft, Lebensmittelsicherheit und Fischerei Mecklenburg-Vorpommern (7221.3-1-066/18 and 7221.3-1-032/19-4), under the German animal protection law and the EU Guideline 2010/63/EU. Mice were bred in the animal facility of the University Medical Center in Rostock under specific pathogen-free conditions. All animals received enrichment as

mouse-igloos (ANT Tierhaltungsbedarf, Buxtehude, Germany), nesting material (shredded tissue paper, Verbandmittel GmbH, Frankenberg, Deutschland), paper roles (75 × 38 mm, H 0528–151, ssniff-Spezialdiäten GmbH), and wooden sticks (40 × 16 × 10 mm, Abedd, Vienna, Austria). During the experiment, mice were kept in type III cages (Zoonlab GmbH, Castrop-Rauxel, Germany) at a 12-h dark:light cycle, a temperature of 21 ± 2 °C, and relative humidity of 60 ± 20% with food (pellets, 10 mm, ssniff-Spezialdiäten GmbH, Soest, Germany) and tap water ad libitum.

2.2.2. Patient-Derived Xenograft (PDX) Generation

Six-week-old female NOD.Cg-Prkdc^{scid}Il2rg^{tm1}Wjl (NSG, Charles River Laboratories, Lyon, France) mice were used as recipients. A detailed protocol is described in [15]. The patients' serial numbers were maintained throughout all PDX passages. Cell culture was started after the first or second in vivo passage.

2.2.3. Experimental Protocol

Cell-line derived xenografts were generated by injecting 5 × 10^6 cells of HNSCC16 P1 M1, HNSCC46 P0 M2, and HNSCC48 P0 M2 subcutaneously in the right flank of 6–8 weeks old female NSG mice. Tumor diameters were measured with a caliper every three to four days. Tumor volumes were calculated as (length × width^2)/2. Mice were euthanized before tumors reached 1.5 cm^3. An in vivo therapy approach was carried out with HNSCC16 P1 M1. If the mice were bearing tumors of ~50 mm^3, they were allocated to the control or the treatment group.

2.3. Collagenase Digestion for Ex Vivo Primary Cell Cultures

Collagenase digestion was carried out with minor modifications according to [16]. Vital tumor tissues were cut into small pieces of approximately 2 mm^3 and washed two times with phosphate-buffered saline (PBS). Collagenase (2.5 mg/mL, Nordmark Biochemicals, Uetersen, Germany) was dissolved in 0.5 M tris(hydroxymethyl)aminomethane and 150 mM Calcium chloride. Collagenase digestion was carried out for 1.5–2 h at 37 °C with regular vortexing. Cells were washed with PBS and suspended in medium: DMEM/Hams F12 supplemented with 20% fetal calf serum (FCS), glutamine (2 mmol/L), and antibiotics (medium and antibiotics were from Pan Biotech, Aidenbach, Germany, FCS from Sigma–Aldrich, Darmstadt, Germany and glutamine from Biochrom, Berlin, Germany). Single cells were obtained by using a 100 µm cell strainer. Single cells and remaining tissue were separated into two different 6-wells. Medium was changed regularly. Growing cell cultures were seeded into 25 cm^2 flasks and the serum concentration was serially reduced to 10% (with exception of HNSCC48 P0 M1: final serum concentration 15%).

2.4. Spheroid Formation

A total of 5000 cells were seeded in serum free DMEM/Hams F12 supplemented with 1× NCS21 (50×; Capricorn Scientific, Ebsdorfergrund, Germany), 20 ng/mL recombinant human epidermal growth factor (rhEGF), and 10 ng/mL recombinant human fibroblast growth factor (rhFGF-b) (both from ImmunoTools, Friesoythe, Germany) in ultra-low-attachment (ULA) plates (Greiner Bio-One, Kremsmünster, Austria). Spheroids formed after ~72 h.

2.5. Mycoplasma and Fibroblast Contamination Test

The MycoAlert Mycoplasma Detection Kit (LONZA, Rockland, ME, USA) was used to exclude a mycoplasma contamination. Analysis was carried out following the manufacturer's instruction. To exclude fibroblast contamination, cells were stained with anti-CD90 and anti-CD326 antibodies (both 1:50, BioLegend, San Diego, CA, USA) for 30 min at 4 °C followed by washing and analysis on a FACSVerse Cytometer (BD Pharmingen, Heidelberg, Germany). Data analysis was performed using BD FACSuite software (BD Pharmingen).

2.6. Histology and Immunohistochemistry

The morphology of the patients' tumor tissue and their corresponding PDX was studied by an expert pathologist. Histopathology of primary tumors and PDX followed standard protocols for HNSCC diagnostics including HE staining and immunohistochemistry; antibodies: anti-p16 (clone: G175-405, BD Bioscience, Heidelberg, Germany), anti-Ki-67 (Clone Mib-1, Dako, Glostrup, Denmark), anti-PD-L1 (Clone 22C3, Dako), and anti-p53 (Clone Do7, Dako). Standard immunoperoxidase technique was applied using an automated immunostainer, Autostainer Link48 (DAKO) with diaminobenzidine as chromogen.

2.7. Tumor Microenvironment

A single cell suspension of the patients' tumor was stained with 1 µg of each of the following surface markers: anti-CD3 FITC (clone OKT-3), anti-CD4 PE (clone IT4), anti-CD8 PE (clone MEM-31), anti-CD56 PE (clone MEM-188), anti-CD19 APC (clone LT19), anti-CD14 FITC (clone 63D3), anti-CD163 PECy7 (clone GHI/61), anti-CD169 APC (clone 7-239), anti-CD204 PE (clone 7C9C20), anti-CD274 PECy7 (clone 29E.2A3), anti-CD276 PE (clone DCN.70), anti-CD273 APC (clone 24F.10C12). Antibodies were incubated for 30 min at 4 °C. Finally, cells were washed, suspended in PBS, and analyzed with FACSVerse Cytometer (BD Pharmingen). Data analysis was performed using BD FACSuite software (BD Pharmingen).

2.8. Molecular Pathology

HPV status and genomic alterations were analyzed using the Illumina Cancer Hotspot Panel (Illumina, Berlin, Germany) as described previously [15]. As a quality control, a DNA Fingerprint PCR of matched tumor tissue, PDX, and cell line was carried out as described [17]. To check for gene specific amplifications 30,000 cells per cell line were fixed on a coated cytoslide (THARMAC cellspin, Wiesbaden, Germany) by using the SHANDON cytospin3 centrifuge cell preparation system. Centrifugation was conducted for 10 min at 700 rpm. After 24 h, the gene specific staining of *CDKN2A* and *CDK4* was conducted according to the manufacturer's instructions. The staining kits SPEC CDK4/CEN 12 Dual Color Probe and SPEC CDKN2A/CEN9 Dual Color Probe (ZytoVision, Bremerhaven, Germany) were used.

2.9. In Vitro Growth Kinetics

Population doubling times (PDT) were determined by seeding 500,000 cells into replicate 25 cm^2 (HNSCC46 P0 M2, HNSCC48 P0 M1) or 75 cm^2 flasks (HNSCC16 P1 M1) and counted daily for five days. The doubling time was calculated as follows: $PDT = t \times \ln 2/\ln(N_x/N_0)$, t = incubation time between N_x and N_0, N_x = total amount of cells at the end of the exponential growth and N_0 = total amount of cells at the beginning of the exponential growth.

2.10. Phenotyping

For initial phenotyping, cells were left untreated and stained for 30 min at 4 °C with FITC anti-HLA-ABC antibody (MHC I) (1:50; both from ImmunoTools), PE/Cy7 anti-CD274 (PD-L1), and APC anti-CD279 (PD-1) (1:50; both from BioLegend; blue (488 nm) and red (633 nm) laser). The antibodies were diluted in 2% BSA with 2 mM Ethylenediaminetetraacetic acid disodium salt solution (EDTA) (Sigma–Aldrich, Darmstadt, Germany). Finally, cells were analyzed with FACSVerse Cytometer (BD Pharmingen). Data analysis was performed using BD FACSuite software (BD Pharmingen). Additionally, untreated cells were stained with anti-CD279 (PD-1) (1:50) at 4 °C overnight. Cells were washed and cell nuclei were stained with 4′,6-diamidino-2-phenylindole (DAPI) (AAT Bioquest, Sunnyvale, CA, USA). After, a second washing step analysis was performed on a ZEISS Elyra 7 Confocal Laser Microscope (Zeiss, Jena, Germany). To investigate the effect of the applied test substances on the cell surface markers HLA-ABC and PD-L1, the cells were treated for 2 × 72 h and stained as described for the initial treatment.

2.11. Radiation Response

A total of 5000 cells (HNSCC16 P1 M1, HNSCC48 P0 M1) or 15,000 cells (HNSCC46 P0 M2) were seeded in 100 µL in three technical replicates/cell line in 96-well plates. Irradiation was started after four days with 2 Gy and 14 Gy single radiation dose (Cs-137 γ-irradiation; IBL 637, CIS Bio-International, Codolet, France). Cells were irradiated for five days daily. On the third day of irradiation, 100 µL fresh medium was added. Three days after the last irradiation, a crystal violet assay was carried out.

2.12. Migration and Invasiveness

Migration and invasion was examined as described [18].

2.13. In Vitro Drug Response

Cells were seeded in 96-well plates in three technical replicates and treated after 24 h incubation at 37 °C and 5% CO_2. Cells were treated for 2 × 72 h in monotherapy with the different test substances in varying concentrations ranging from 0.048 µg/mL to 1 mg/mL for approved drugs (Cisplatin, 5-Fluorouracil (5-FU), Cetuximab, pharmacy of the University Hospital Rostock) and 1 nM–1 µM for targeted substances (abemaciclib, dinaciclib, Selleckchem, Munich, Germany, THZ1 Hycultec, Beutelsbach, Germany). The level of 50% inhibition (IC_{50}) was calculated using the IC_{50} calculator from AAT Bioquest (https://www.aatbio.com/tools/ic50-calculator/ (accessed on 1 November 2021)). A combination was carried out in a simultaneous setting for 2 × 72 h hours using the following concentrations: abemaciclib [HNSCC16 P1 M1/HNSCC46 P0 M2: 1 µM, HNSCC48 P0 M1: 0.1 µM], dinaciclib [HNSCC16 P1 M1/HNSCC46 P0 M2: 1 nM, HNSCC48 P0 M1: 5 nM], THZ1 [HNSCC16 P1 M1/HNSCC48 P0 M1: 20 nM, HNSCC46 P0 M2: 10 nM], and Cisplatin [HNSCC16 P1 M1/HNSCC46 P0 M2: 1 µg/mL, HNSCC48 P0 M1: 0.05 µg/mL]. A readout was conducted with crystal violet staining. The Bliss Independence model was used to analyze potential synergistic and additive effects between the substances.

2.14. Cell Death and Cell Cycle

An apoptosis–necrosis assay was carried out after 2 × 72 h of treatment, supplemented by cell cycle analysis after 2 × 72 h treatment as described previously [18].

2.15. Assessment of Viability, Acidic Compartments, Cytoskeleton and ROS

Acidic compartments were visualized as described [19]. Therefore, cells were treated for 2 × 72 h. The influence on cytoskeleton and formation of reactive oxygen species (ROS) were likewise analyzed after 2 × 72 h treatment. Cells were washed with HHBS and stained with ROS Brite 670 (7.5 µM, AAT Bioquest) for 30 min at 37 °C. Subsequently, cells were permeabilized, fixed, and stained with Phalloidin-iFluor 594 conjugate (1:1000, AAT Bioquest) for 30 min at room temperature. Cells were washed and cell nuclei stained with DAPI. After a second washing step analysis was performed on a ZEISS Elyra 7 Confocal Laser Microscope (Zeiss, Jena, Germany).

2.16. RNA Isolation, cDNA Synthesis, and Quantitative Real-Time PCR

RNA Isolation, cDNA Synthesis, and Quantitative Real-Time PCR was carried out as described [20]. Reactions were performed in triplicates and repeated three times. *GAPDH* was self-designed and used as a housekeeping gene (GAPDH forward: TCACCAGGGCTGCTTTTAAC; GAPDH reverse: GGGTGGAATCATATTGGAACA; GAPDH 5′ HEX-3′ BHQ-1 TGCCATCAATGACCCCTTCATTG). *MYC* (Hs00153408_m1), *PDK2* (Hs00176865_m1), *SKP2* (Hs01021864_m1), and *IDO-1* (Hs00984148_m1) were 6-FAM labeled and purchased from ThermoFisher Scientific (Waltham, MA, USA).

2.17. Allogenic Co-Culture

HNSCC48 P0 M1 was stained with 5 µM 5-(and-6)-Carboxyfluorescein diacetate, succinimidyl ester (CMFDA; Biotium, Fremont, California, USA) before seeding. 24 h later,

PBMCs (Peripheral Blood Mononuclear Cells) were isolated by a density gradient centrifugation and added (tumor cell:PBMC ratio: 1:10). PBMCs were stimulated with 100 IU/mL of IL-2 (Novartis, Basel, Switzerland). Abemaciclib [0.1 µM], Pembrolizumab [10 µg/mL] or the combination of both were added simultaneously with the PBMCs. After 1 × 72 h, cells were harvested and collected in FACS tubes. For the readout, 50 µL of 1:35 diluted beads (fluorescent microsphere beads; 1.4×10^4 beads/mL; size 10 µm; Polyscience, Warrington, PE, USA) were added to the 200 µL of cell suspension in the respective FACS tubes. Measurement of the beads and residual tumor cells stopped when 5000 beads were counted.

2.18. Statistics

All values are given as mean ± SD (in vitro analysis) or mean ± SEM (in vivo approach). Statistical evaluation was performed using GraphPad PRISM software, version 8.0.2 (GraphPad Software, San Diego, CA, USA). The criterion for significance was set to $p < 0.05$. After proving the assumption of normality (Shapiro–Wilk test), one-way ANOVA (Dunnett's multiple comparison), two-way ANOVA (Tukey's multiple comparison) or T-test was performed. If the normality test failed, the Kruskal–Wallis or U-Test was performed.

3. Results

3.1. Clinicopathological Patients' Data, and Cell Line Establishment

Three novel HNSCC cell lines HNSCC16 M1 P1, HNSCC46 P0 M2, and HNSCC48 P0 M1 were generated after xenografting in NSG mice. Clinicopathological patients' characteristics are summarized in Table 1.

Table 1. Clinical characteristics.

Cell Line	Age Sex	TNM Grade	Localization	Origin	p16/HPV	Noxes	Treatment	Clinical Follow-Up
HNSCC16 P1 M1	82 m	rpT4a pN0 cM0 G2	Larynx	Recurrence	-/-	non-smoker	surgery 2008, radiation 2015, surgery 2020	alive
HNSCC46 P0 M2	69 m	pT3 pN3b cM0 G2	Hypopharynx	primary tumor	+/-	nicotine, C2	surgery (later adjuvant RCT)	†
HNSCC48 P0 M1	63 m	pT3 pN3b cM0 G2	Lymph node (primary tumor: oral cavity (floor of moth))	metastasis/ recurrence	-/-	non-smoker	RCT (64 Gy, Cisplatin), surgery (later Nivolumab)	†

RCT: Radiochemotherapy; +: positive; -: negative; †: dead

3.2. Histopathology and Tumor Microenvironment of Primary Tumors

The histological pattern of all three cases is that of a moderately differentiated squamous cell carcinoma (Figure 1A). HNSCC48 shows an expression pattern typical for *TP53* mutations; while in the other cases, the p53-expression pattern is not mutation-specific. Because of tissue processing artifacts, the immunohistochemistry data (Ki-67, p53, and PD-L1) for HNSCC46 are not fully exploitable.

The TME was heterogeneous (Figure 1B). The strongest lymphocytic infiltration was detectable in HNSCC16 with $CD3^+CD4^+$/$CD3^+CD8^+$ T cells and $CD19^+$ B cells. $CD16^+CD56^+$ natural killer (NK) cells were found in all cases with the highest abundance in HNSCC46. This tumor case additionally showed the highest number of tumor-associated macrophages (TAM). The infiltrating $CD3^+$ T cells showed a low level of $CD274^+$ (no data available for HNSCC48). Roughly 15% of T cells were $CD273^+$ (=PD-L2) and numbers comparable between the three HNSCC cases, while $CD276^+$ was highest on HNSCC46/HNSCC48 (vs. HNSCC16).

natural killer (NK) cells were found in all cases with the highest abundance in HNSCC46. This tumor case additionally showed the highest number of tumor-associated macrophages (TAM). The infiltrating CD3+ T cells showed a low level of CD274+ (no data available for HNSCC48). Roughly 15% of T cells were CD273+ (=PD-L2) and numbers comparable between the three HNSCC cases, while CD276+ was highest on HNSCC46/HNSCC48 (vs. HNSCC16).

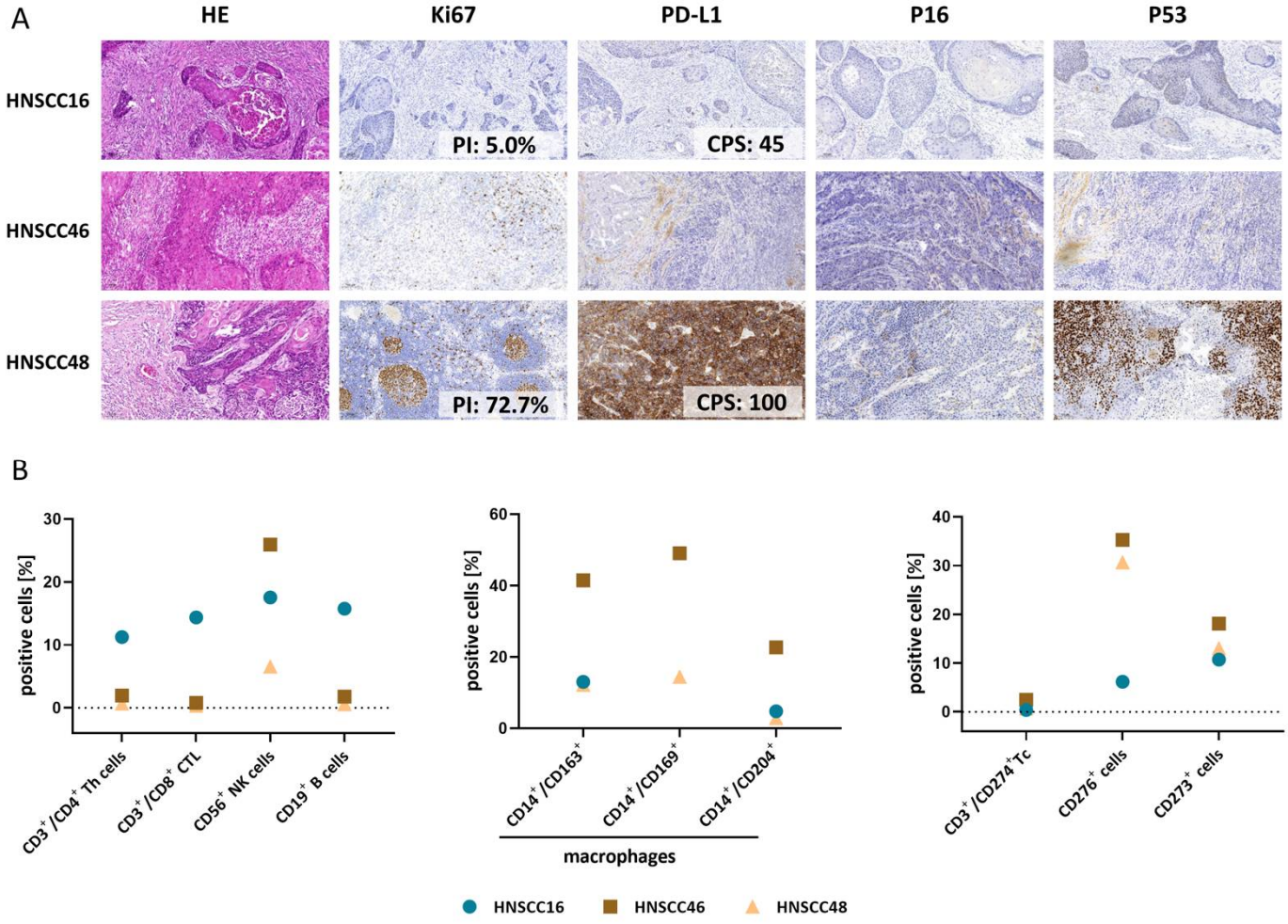

Figure 1. Histopathology and tumor microenvironment of primary tumors. (**A**) HE, Ki67, PD-L1, P16, and P53 staining of the patients' tumors HNSCC16, HNSCC46, and HNSCC48. 10 × magnification. (**B**) Tumor microenvironment of the primary tumors HNSCC16 (turquoise circles), HNSCC46 (brown squares), and HNSCC48 (orange triangles). Relative fractions of lymphocytes (left diagram), TAMs (middle diagram), and selected checkpoints (right diagram) are illustrated.

3.3. Quality Control, Comparative Analysis of the Molecular Profile & Detection of Gene Specific Alteration of CDK4 and CDKN2A

Using fingerprint PCR as quality control, the ancestry of the cell lines with its corresponding PDX and patient's tumor were validated (Supplementary Figure S1). *TP53* hotspot mutations (single or multiple) were detectable in all cases (Table 2). The patient's tumor HNSCC16 harbored an additional p.P27R mutation that was lost during passage. In HNSCC48, the *CDKN2A* mutation p.R58* and the *SMAD4* mutation p.R135* was found. The variant allele frequencies (VAF) of individual mutations revealed higher VAFs in the PDX and cell line compared to the patients' tumors (Table 2). The only exception is HNSCC48.

Gene-specific amplifications of *CDKN2A* (located on 9p21) and *CDK4* were checked as potential biomarkers. All cell lines showed chromosome 9 polysomy with high copy numbers of the respective centromer (Figure 2). In HNSCC16 P1 M1/HNSCC46 P0 M2, *CDKN2A* gains were equal to chromosome 9 copies. In HNSCC48 P0 M1, fewer copies of the *CDKN2A* gene compared to the number of copies of the centromere of chromosome 9 were found (ratio: 3:1), indicative for a gene specific *CDKN2A* deletion and thus confirming sequencing data.

Mutation	HNSCC16			HNSCC46			HNSCC48		
	Patient	PDX	Cell Line	Patient	PDX	Cell Line	Patient	PDX	Cell Line
TP53	p.R306 * VAF 37% p.P72R VAF 32.7%	p.R306 * VAF 100%	p.R306 * VAF 99.5%	p.E294Sfs *51 VAF 64.5% p.P72R VAF 100%	p.E294Sfs *51 VAF 99.3% p.P72R VAF 99.3%	p.E294Sfs *51 VAF 99.9% p.P72R VAF 99.6%	p.R175H VAF 99.4% p.P72R VAF 99.5%	p.R175H VAF 60.5% p.P72R VAF 80.4%	p.R175H VAF 99.8% p.P72R VAF 99.9%
CDKN2A	wt	wt	wt	wt	wt	wt	p.R58 * VAF 99.6%	p.R58 * VAF 55.8%	p.R58 * VAF 99.8%
SMAD4	wt	wt	wt	wt	wt	wt	p.R135 * VAF 99.6%	p.R135 * VAF 48.2%	p.R135 * VAF 100%

Table 2. Comparative analysis of mutational profile between patients' tumor, the corresponding PDX and cell line.

VAF: Variant allele frequency; Wt: Wild type; *: stop codon. The specific mutation loci and the VAF are shown. Analysis was carried out with the Illumina Cancer Hotspot Panel.

Gene-specific amplifications of *CDKN2A* (located on 9p21) and *CDK4* were checked as potential biomarkers. All cell lines showed chromosome 9 polysomy with high copy numbers of the respective centromer (Figure 2). In HNSCC16 P1 M1/HNSCC46 P0 M2, *CDKN2A* gains were equal to chromosome 9 copies. In HNSCC48 P0 M1, fewer copies of the *CDKN2A* gene compared to the number of copies of the centromere of chromosome 9 were found (ratio: 3:1), indicative for a gene specific *CDKN2A* deletion and thus confirming sequencing data.

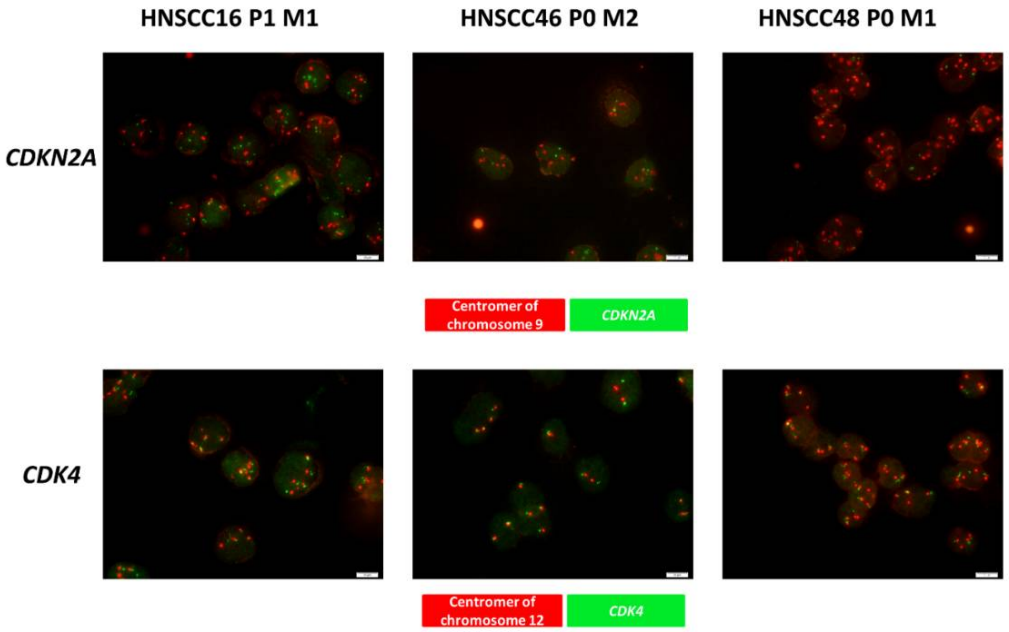

Figure 2. Cyto-FISH for *CDKN2a* and *CDK4*. Cytospins of HNSCC cell lines were stained with the SPEC CDK4/CEN 12 Dual Color Probe or SPEC CDKN2A /CEN9 Dual Color Probe to check for gene specific amplification of *CDKN2A* and *CDK4*. The red spots indicate the centromers and the green spots indicate the specific gene. A readout was carried out with the fluorescence microscope Olympus BX53. Original magnification 1000×.

CDK4 is of high relevance for CDKI treatment. HNSCC16 P1 M1/HNSCC48 P0 M1 demonstrated polysomy of the chromosome 12, with the latter having 4–6 chromosomes/cell (Figure 2). Notably, this was accompanied by an increase in gene-specific copy numbers and was most pronounced in HNSCC48 P0 M1.

3.4. Cell Morphology and Spheroid Formation

All cells reveal tight adherence to the flask bottom with different morphology (Supplementary Figure S2). HNSCC48 P0 M1 changed morphologically during culture and a phenotypically small cell clone dominated at later passages. A fraction of HNSCC16 M1 P1 cells formed spheroidal-like cell clusters spontaneously, which were preserved under spheroid-forming conditions (Supplementary Figure S2A). Fibroblasts were excluded by flow cytometry (CD90/EpCAM (CD326) staining) (Supplementary Figure S2B).

3.5. Cell Line Characterization

The PDT differed among cells (Supplementary Figure S3). Flow cytometric phenotyping revealed HLA-ABC and PD-L1 positivity on a fraction of cells (Figure 3A). For

example, in HNSCC16 P1 M1, approximately one-third of cells was found to be positive for HLA-ABC and three-quarters were positive for PD-L1 (Figure 3A, left panel). Single cells of HNSCC46 P0 M2 were additionally PD-1$^+$ (Figure 3A, right). Immunofluorescence confirmed PD-1 expression on a fraction of cells in this line, while others were completely negative (Figure 3B, middle). The radiation response was quite heterogeneous: HNSCC48 P0 M1 was most radiosensitive. Increasing the total radiation dose to 70 Gy induced a significant decline in all three cell lines (Figure 3B). Assessment of migration potential revealed fast scratch closure in two-thirds of cases (Figure 3C,D). The invasiveness was compared to UT-SCC-15, a cell line with known invasive behavior [18]. HNSCC16 P1 M1/HNSCC46 P0 M2 were more invasive than UT-SCC-15 and HNSCC48 P0 M1, confirming migration results.

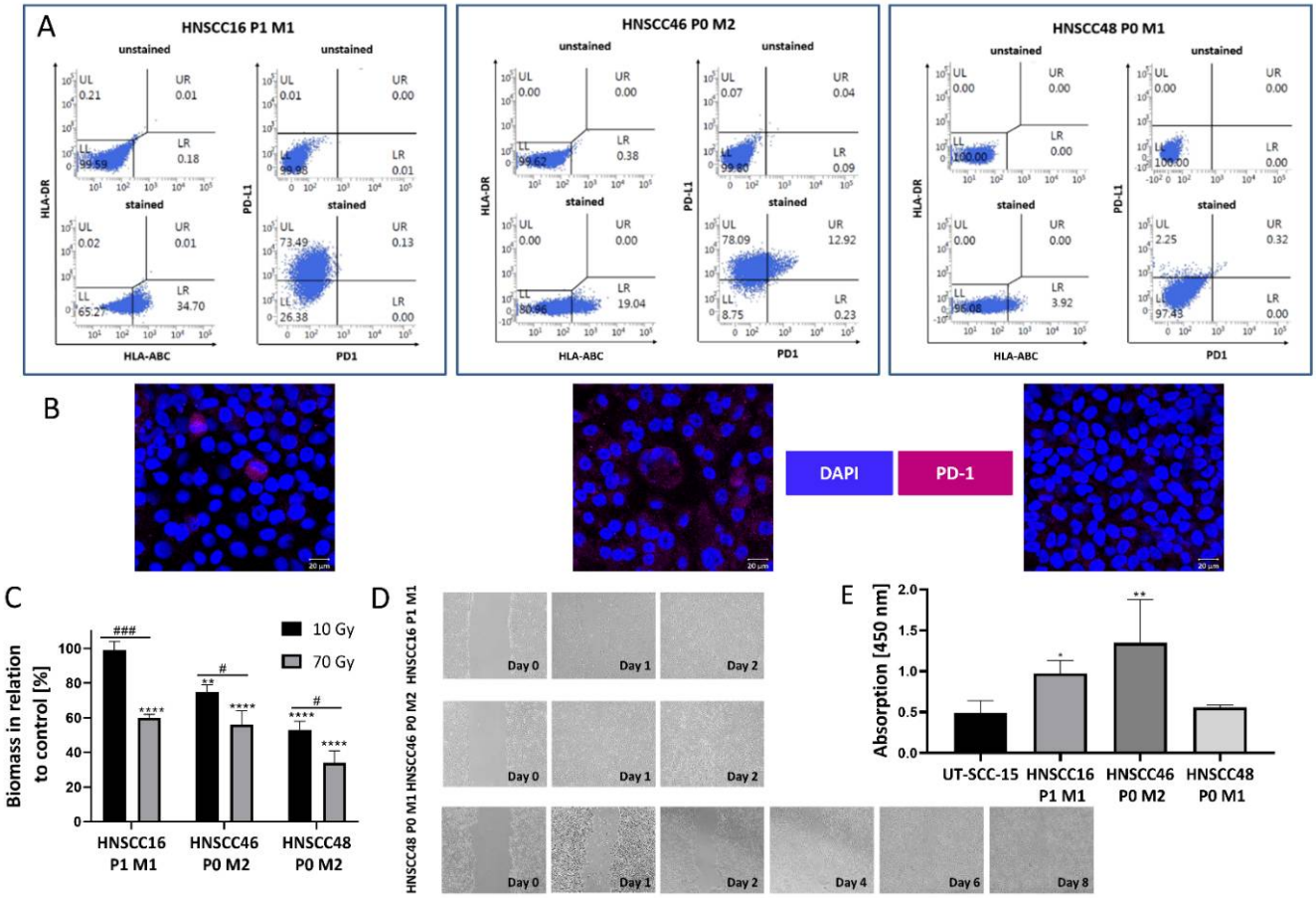

Figure 3. Basal characterization including phenotyping, radiation response, migration, and invasion of untreated HNSCC cell lines. (**A**) FACS-based phenotyping for HLA-ABC, PD-L1 (left) and (**B**) immunofluorescence staining of PD-1 (right) to confirm PD-1 on the surface of HNSCC46 P0 M2. A read out was conducted with the ZEISS Elyra 7 Cyrotical Laser Microscope (Zeiss). Original magnification 400×. (**C**) Radiation response was examined after 5 fractions of 2 Gy and 14 Gy on 5 consecutive days, resulting in a total radiation dose of 10 Gy (black columns) and 70 Gy (grey columns). A readout was conducted by crystal violet staining and biomass quantified in relation to non-irradiated controls. Unpaired *t*-test ($n = 3$ independent experiments) $^{\#}p < 0.05$; $^{\#\#\#}p < 0.001$ vs. 70 Gy; one-way ANOVA ($n = 3$ independent experiments) $^{**}p < 0.01$; $^{****}p < 0.0001$ vs. control (100%). (**D**) Migratory potential was investigated via scratch assay. The scratch was monitored daily by light microscopy (original magnification 100×) until the wound was closed. (**E**) Matrigel invasion assay. Invasive behavior was studied compared to UT-SCC-15, a cell line derived from a nodal HNSCC recurrence. A readout was conducted with WST-1 assay. The absorbance at 450 nm is shown. One-way ANOVA ($n \geq 3$ independent experiments) $^{*}p < 0.05$; $^{**}p < 0.01$ vs. invasion of UT-SCC-15.

3.6. In Vitro and In Vivo Drug Response

Drug response analysis was carried out after two rounds of treatment with each treatment cycle lasting 72 h. The dose–response curves are given in Supplementary Figure S4

3.6. In Vitro and In Vivo Drug Response

Drug response analysis was carried out after two rounds of treatment with each treatment cycle lasting 72 h. The dose–response curves are given in Supplementary Figure S4 and the resulting IC50 values are presented in Table 3.

Table 3. IC_{50} values of test substances as determined by crystal violet staining.

Substance	HNSCC16 P1 M1	HNSCC46 P0 M2	HNSCC48 P0 M1
Cisplatin [µg/mL]	1.43	1.54	0.30
5-FU [µg/mL]	0.31	0.17	0.04
Cetuximab [µg/mL]	not reached	not reached	137.26
dinaciclib [nM]	2.69	1.65	7.33
THZ1 [nM]	49.22	39.47	32.00
abemaciclib [nM]	not reached	not reached	696.65

Cells were treated for 2 × 72 h with the different test substances in varying concentrations between 0.048 µg/mL–1 mg/mL for approved drugs (Cisplatin, 5-FU, and Cetuximab) and 1 nM–1 µM for targeted substances (dinaciclib, abemaciclib, and THZ1). Based on the dose–response curves IC_{50} was calculated using the IC_{50} calculator from AAT Bioquest (https://www.aatbio.com/tools/ic50-calculator/ (accessed on 9 November 2021)). If the highest dose applied did not result in a reduction in biomass compared to the control, this was defined as IC_{50} not reached.

All cell lines were sensitive towards Cisplatin and 5-FU, while an individual response profile was seen for Cetuximab and the CDKIs. On a basis of this initial screening, combination strategies were applied to check for potential synergistic effects. Therefore, the IC_{20} was applied, and functional analysis was carried out to decipher underlying molecular mechanisms. Using a combined chemo-CDKI approach synergistic effects were seen upon Cisplatin and abemaciclib/THZ1 in HNSCC16 P1 M1/HNSCC48 P0 M1 cells (Figure 4A). Vice versa, the respective combinations were antagonistic in HNSCC46 P0 M2, nicely reflecting the HNSCCs heterogeneity. For the latter case, all combinations failed to be synergistic (Figure 4A). In an in vivo trial, drug response against Cisplatin was examined and HNSCC16 M1 P1 was chosen as experimental model, due to the comparably fast and reliable in vivo growth kinetics (Figure 4B). As therapeutic agent, we applied Cisplatin because all cell lines showed high sensitivity in vitro. Also, this drug is still widely applied in the clinic for the treatment of HNSCC patients both in mono- or combination therapy. In this initial study, Cisplatin slightly decelerated growth; still, no significant growth reduction was seen (Figure 4C) and trials were stopped prematurely.

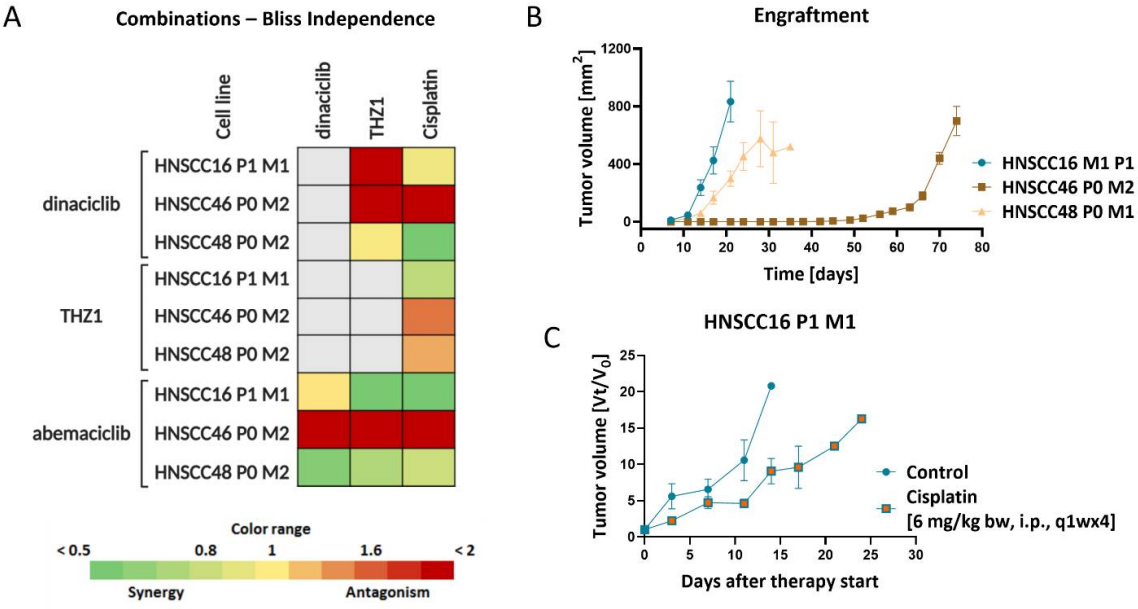

Figure 4. In vitro and in vivo drug response. (**A**) The Bliss Independence model was used to calculate potential synergistic or additive effects. The green color indicates a synergistic and red color indicates an antagonistic effect of the simultaneous combinations. Drug doses were applied for 2 × 72 h as follows: abemaciclib [HNSCC16 P1 M1/HNSCC46 P0 M2: 1 µM, HNSCC48 P0 M1: 0.1 µM], dinaciclib [HNSCC16 P1 M1/HNSCC46 P0 M2: 1 nM, HNSCC48 P0 M1: 5 nM], THZ1 [HNSCC16 P1 M1/HNSCC48 P0 M1: 20 nM, HNSCC46 P0 M2: 10 nM] and Cisplatin [HNSCC16 P1 M1/HNSCC46 P0 M2: 1 µg/mL, HNSCC48 P0 M1: 0.05 µg/mL]. (**B**) Engraftment of the cell lines HNSCC16 P1 M1 (green), HNSC46 P0 M2 (red), and HNSCC48 P0 M1 (blue) in NSG mice. (**C**) Ther-

antagonistic effect of the simultaneous combinations. Drug doses were applied for 2 × 72 h as follows: abemaciclib [HNSCC16 P1 M1/HNSCC46 P0 M2: 1 µM, HNSCC48 P0 M1: 0.1 µM], dinaciclib [HNSCC16 P1 M1/HNSCC46 P0 M2: 1 nM, HNSCC48 P0 M1: 5 nM], THZ1 [HNSCC16 P1 M1/HNSCC48 P0 M1: 20 nM, HNSCC46 P0 M2: 10 nM] and Cisplatin [HNSCC16 P1 M1/HNSCC46 P0 M2: 1 µg/mL, HNSCC48 P0 M1: 0.05 µg/mL]. (**B**) Engraftment of the cell lines HNSCC16 P1 M1 (green), HNSCC46 P0 M2 (red), and HNSCC48 P0 M1 (blue) in NSG mice. (**C**) Therapy approach. Tumor growth curve of HNSCC16 P1 M1. Tumor volume was calculated as tumor volume on day × (Vt) divided through tumor volume at the therapy start (V0).

3.7. Molecular Alterations Predict CDK1 Resistance, Which Is Partially Reversible by Combined Targeted Therapy In Vitro

The applied treatment schedules induced apoptosis and/or necrosis to varying degrees (Figure 5A). Notably, dual CDK inhibition (i.e., abemaciclib + THZ1) was comparably effective as Cisplatin-tailored CDK1 combinations. Autophagy, as indicated by acidic organelles, was additionally seen after Cisplatin and abemaciclib mono- and combination therapy in HNSCC16 P1 M1 (Figure 5B). In HNSCC46 P0 M2, the effect was weaker but still visible. Interestingly, all monotherapies reduced the level of reactive oxygen species (ROS), whereas Cisplatin with THZ1 increased ROS in HNSCC16 P1 M1 (Figure 5C).

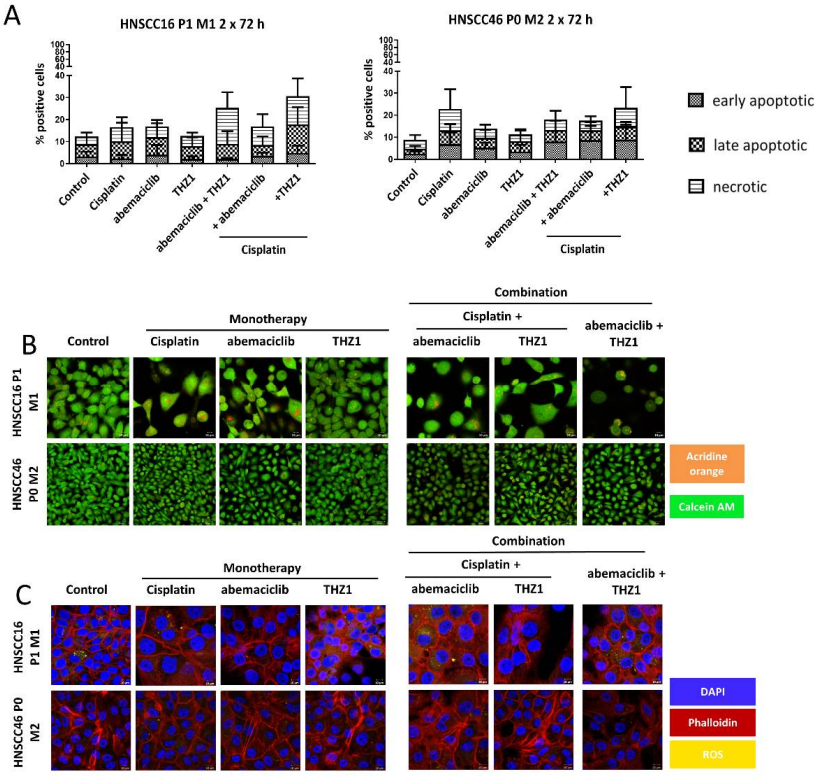

Figure 5. Apoptosis-necrosis assay, detection of acidic components, the cytoskeleton, and reactive oxygen species (ROS). Drug doses were abemaciclib [HNSCC16 P1 M1/HNSCC46 P0 M2: 1 µM], THZ1 [HNSCC16 P1 M1/HNSCC46 P0 M2: 10 nM], and Cisplatin [HNSCC16 P1 M1/HNSCC46 P0 M2: 1 µg/mL]. (**A**) Apoptosis-necrosis assay was studied after 2 × 72 h treatment. Cells were stained with Yo-Pro 1 iodide and PI. Early apoptotic cells were defined as positive for Yo-Pro 1 iodide, late apoptotic cells were defined as positive for Yo-Pro 1 iodide and PI and necrotic cells were defined as positive for PI. Kruskal–Wallis (n = 4 independent experiments) vs. control. (**B**) Semi-quantitative analysis of acidic components and viability of the 2 × 72 h treated cells was carried out with acridine orange and Calcein AM. Representative images are shown. A read out was conducted with the ZEISS Elyra 7 Confocal Laser Microscope (Zeiss). Original magnification 400×. (**C**) Semi-quantitative analysis of the cytoskeleton and ROS of the 2 × 72 h treated cells. A readout was conducted with the ZEISS Elyra 7 Confocal Laser Microscope (Zeiss). Original magnification 630×.

as positive for PI. Kruskal–Wallis (n = 4 independent experiments) vs. control. (**B**) Semi-quantitative analysis of acidic components and viability of the 2 × 72 h treated cells was carried out with acridine orange and Calcein AM. Representative images are shown. A read out was conducted with the ZEISS Elyra 7 Confocal Laser Microscope (Zeiss). Original magnification 400×. (**C**) Semi-quantitative analysis of the cytoskeleton and ROS of the 2 × 72 h treated cells. A readout was conducted with the ZEISS Elyra 7 Confocal Laser Microscope (Zeiss). Original magnification 630×.

Thereafter, resistance-associated genes were examined, because of the promising effects of combined Cisplatin-CDKI application (Figure 6): basal expression levels confirmed an upregulation of *SKP2* and *cMYC*, but not *PDK2* or *IDO-1* compared to normal mucosa (Figure 6A). Cisplatin further induced *SKP2* in two-thirds of cases, while *SKP2* was counter regulated in the combination (Figure 6B). HNSCC46 P0 M2 and HNSCC48 P0 M1 responded with an upregulation of *cMYC* and *IDO-1* upon abemaciclib. In HNSCC46 P0 M2, upregulation was repealed by Cisplatin. *PDK2* was massively induced in HNSCC46 P0 M2 after Cisplatin and abemaciclib monotherapy, but the combination again revoked this effect.

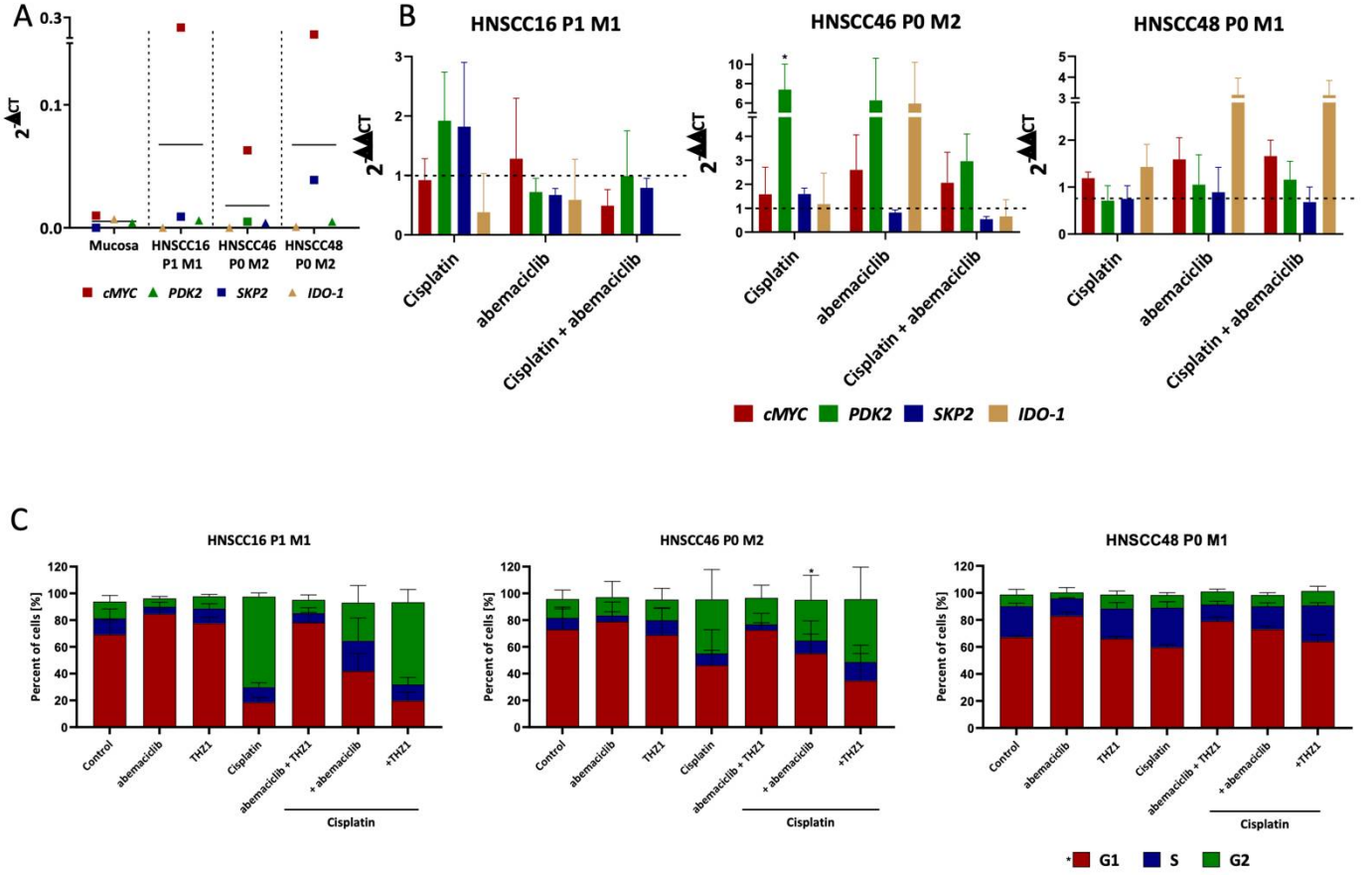

Figure 6. Expression of resistance-associated genes (*SKP2*, *cMYC*, *PDK2*, and *IDO-1*) and cell cycle analysis. (**A**) Quantitative real-time PCR was carried out on untreated HNSCC cell lines compared to benign mucosa. (**B**) Influence of 2 × 72 h treatment on the expression of the resistance associated genes *cMYC*, *PDK2*, *SKP2*, and *IDO-1*. Drug doses were abemaciclib [HNSCC16 P1 M1/HNSCC46 P0 M2: 1 µM, HNSCC48 P0 M1: 0.1 µM], and Cisplatin [HNSCC16 P1 M1/HNSCC46 P0 M2: 1 µg/mL, HNSCC48 P0 M1: 0.05 µg/mL]. Kruskal–Wallis (n = 3 independent experiments) * $p < 0.05$ vs. control. For *PDK2* and *SKP2* genes in HNSCC46 after THZ1- and Cisplatin treatment qPCR could only be performed two times because of poor RNA quality. (**C**) Cell cycle analysis was performed after 2 × 72 h of treatment. Drug doses were: abemaciclib [HNSCC16 P1 M1/HNSCC46 P0 M2: 1 µM, HNSCC48 P0 M1: 0.1 µM], THZ1 [HNSCC16 P1 M1/HNSCC48 P0 M1: 20 nM, HNSCC46 P0 M2: 10 nM], and Cisplatin [HNSCC16 P1 M1/HNSCC46 P0 M2: 1 µg/mL, HNSCC48 P0 M1: 0.05 µg/mL]. Cells were ethanol fixed and stained with PI. Quantitative analysis of the flow cytometry data was performed using using BD FlowJo software. Given are cells in the G1-, S- and G2-phase. Kruskal–Wallis (n ≥ 3 independent experiments) * $p < 0.05$ vs. control.

As the cell cycle is the main target of CDKIs, this was analyzed by flow cytometry (Figure 6C). In HNSCC16 P1 M1 and HNSCC48 P0 M1, abemaciclib and THZ1 induced a G1 phase arrest, which was not enhanced in the combination. Cisplatin led to a G2 phase arrest that was preserved in combination with THZ1. In HNSCC46 P0 M2, effects were

3.8. Enhanced Immunogenicity and Confirmation of Immune-Stimulatory Potential upon Co-Culture with Abemaciclib and Pembrolizumab

The abundance of HLA-ABC increased after abemaciclib monotherapy and in combination with Cisplatin or THZ1 in all three cases (Figure 7A). The highest increase was seen on HNSCC48 P0 M1, in which PD-L1 was additionally upregulated. HNSCC16 P1 M1 showed comparable, though less strong, phenotypic changes. No effect on PD-L1 was recognizable on HNSCC46 P0 M2 cells.

In a final in vivo-like co-culture system HNSCC48 P0 M1 cells were included because of their PD-L1-positivity and abemaciclib sensitivity (Figure 7B). Tumor and immune cells were co-cultured in the presence of abemaciclib, the anti-PD-1 inhibitor Pembrolizumab or a combination of both to test which strategy exerts highest immune-mediated tumor killing. Abemaciclib reduced cell viability to ~50% (vs. control). Pembrolizumab effectivity was donor specific. While residual cells decreased to 39% in Donor B and 83% in donor D PBMC co-culture, the amount of tumor cells remained unchanged for donor A and C. Interestingly, the combination of abemaciclib and Pembrolizumab was most effective and donor independent (donor A 44%, donor B 39%, donor C 45%, donor D 26%).

again weaker and mainly attributable to Cisplatin (Figure 6C). Adding CDKIs to Cisplatin slightly boosted effects of the monotherapy.

3.8. Enhanced Immunogenicity and Confirmation of Immune-Stimulatory Potential upon Co-Culture with Abemaciclib and Pembrolizumab

The abundance of HLA-ABC increased after abemaciclib monotherapy and in combination with Cisplatin or THZ1 in all three cases (Figure 7A). The highest increase was seen on HNSCC48 P0 M1, in which PD-L1 was additionally upregulated. HNSCC16 P1 M1 showed comparable, though less strong, phenotypic changes. No effect on PD-L1 was recognizable on HNSCC46 P0 M2 cells.

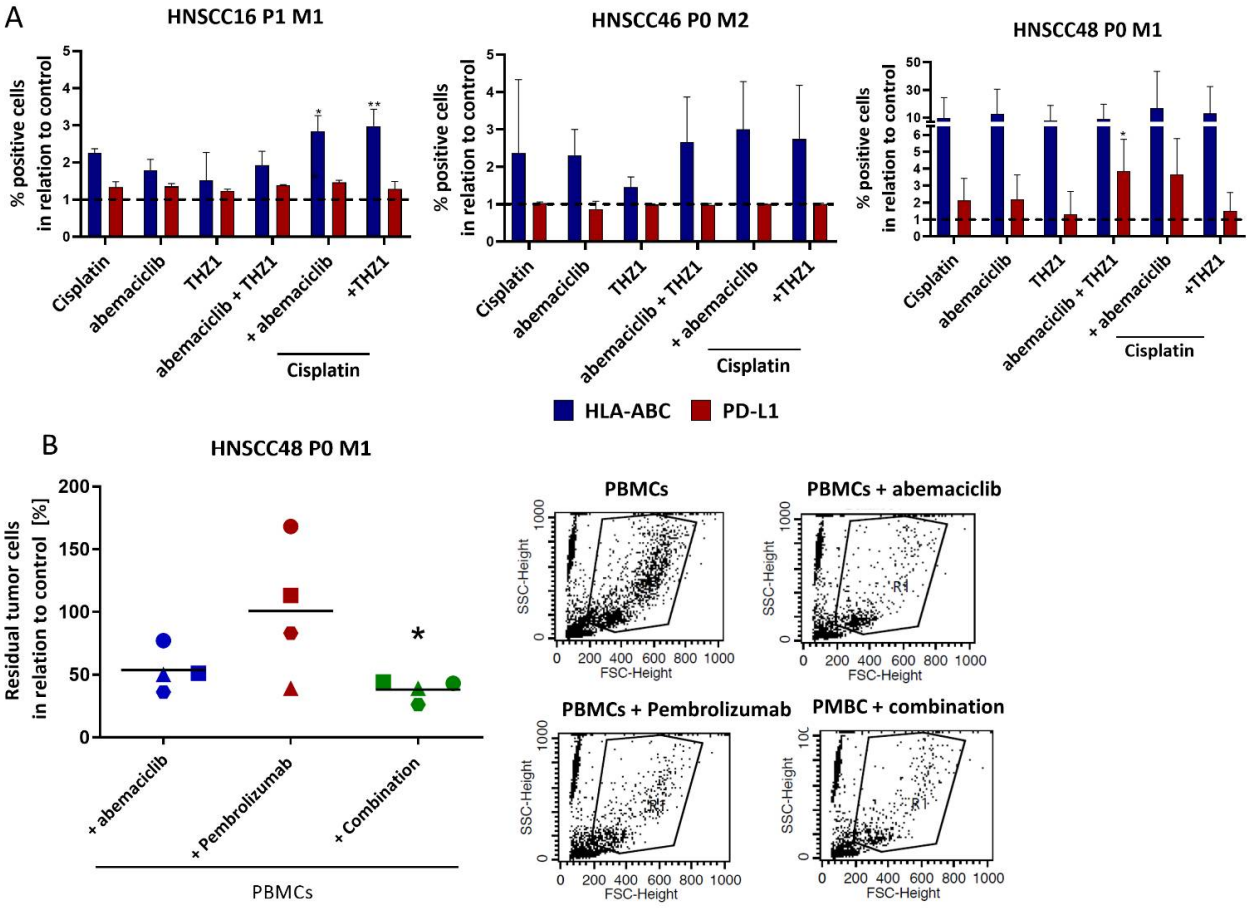

Figure 7. Phenotyping and allogenic co-culture. (**A**) Phenotyping was carried out after 2 × 72 h treatment. Drug doses were: abemaciclib [HNSCC16 P1 M1/HNSCC46 P0 M2: 1 µM, HNSCC48 P0 M1: 0.1 µM], THZ1 [HNSCC16 P1 M1/HNSCC48 P0 M1: 20 nM, HNSCC46 P0 M2: 10 nM], and Cisplatin [HNSCC16 P1 M1/HNSCC46 P0 M2: 1 µg/mL, HNSCC48 P0 M1: 0.05 µg/mL]. Cells were stained with anti-HLA-ABC antibody (MHC I) and anti-CD274 (PD-L1) after 2 × 72 h treatment. Shown are the HLA-ABC and PD-L1 positive cells are illustrated in relation to the control. Kruskal-Wallis (n = 3 independent experiments) * $p < 0.05$ vs. control. (**B**) Allogenic co-culture. The cell line HNSCC48 P0 M1 was simultaneously treated for 1 × 72 h with (1) abemaciclib in combination with PBMCs (blue), (2) Pembrolizumab in combination with PBMCs (red), or (3) abemaciclib with Pembrolizumab and PBMCs (green). Drug doses were: abemaciclib 0,1 µM, Pembrolizumab 10 µg/mL. The ratio of target to effector cells was 1:10. The PBMCs were stimulated with 100 IU/mL IL-2. After 72 h, the residual tumor cells were counted by adding fluorescent beads. A readout was conducted with the FACS. The squares indicate for donor A, the triangle for donor B, the circles for donor C, and the hexagon for donor D. In the right part, representative FACS dot plots of treated cells with PBMCs and PBMCs in combination with abemaciclib are shown. One-way ANOVA (n = 4 independent experiments) * $p < 0.05$ vs. control (100%).

In a final in vivo-like co-culture system HNSCC48 P0 M1 cells were included because of their PD-L1-positivity and abemaciclib sensitivity (Figure 7B). Tumor and immune cells were co-cultured in the presence of abemaciclib, the anti-PD-1 inhibitor Pembrolizumab or a combination of both to test which strategy exerts highest immune-mediated tumor killing. Abemaciclib reduced cell viability to ~50% (vs. control). Pembrolizumab effectivity was donor specific. While residual cells decreased to 39% in Donor B and 83% in donor D PBMC co-culture, the amount of tumor cells remained unchanged for donor A and C. Interestingly, the combination of abemaciclib and Pembrolizumab was most effective and donor independent (donor A: 44%; donor B 39%; donor C 43%; donor D 26%).

4. Discussion

In this study, we established three novel xenograft-derived HNSCC cell lines to address intertumoral heterogeneity. We showed that the TME of the patients' tumors consists of varying numbers of infiltrating lymphocytes, TAMs, and immune checkpoint molecules. All tumors were resected at advanced stages, allowing us to investigate therapies on low-passage models with particular relevance for patients with poor prognoses [4]. In fact, representative well-characterized preclinical HNSCC models are rarely available. This is mainly attributable to the fact that patients with recurrent and metastatic disease are usually treated with systemic therapy, without surgery. The paucity of such HNSCC models precludes preclinical research that can be translated into clinical trials. To fill this gap, novel tumor models from advanced HNSCCs are warranted. This is of particular clinical relevance, knowing that the currently available drugs have limited efficacy in many patients.

To address this issue, we initially tested HNSCC cell line establishment directly from patient tumor samples. Though this was described before [8,21], we failed to generate cell lines because of overgrowing fibroblasts (data not shown). We moved on with the NSG mouse PDX model to generate cell lines from PDX and to exclude fibroblast overgrowth [16]. Using this method, we generated three novel cell lines (and more are being established). All cells were defined as epithelial tumor cells ($EpCAM^+$, $CD90^-$) with a molecular profile reflecting HPV-unrelated HNSCC. This included *TP53* mutations in all cases [22], along with *SMAD4* and *CDKN2A* mutations in HNSCC48 [23]. *CDKN2A* cyto-FISH identified a partial gene deletion accompanied by chromosome 9 polysomy. In the other two cases, *CDKN2A* gains were equal to chromosome 9 copies (HNSCC16, n = 4–5/cell) or remained unchanged with only chromosome 9 polysomy (HNSCC46). Chromosome polysomy is a common characteristic of advanced tumors and was described in p53 dysregulated HNSCC before [24].

The direct comparison between patients' tumors, PDX, and the corresponding cell line revealed preservation of the molecular profile—at least in early passages. This analysis is imperative to guarantee high-quality data generation and to correlate molecular features of the parental tumor with drug response. Rather unexpected were the VAFs of the PDX from HNSCC48. In HNSCC16 and HNSCC46, the VAFs remained stable or increased during transfer, likely because of increasing amounts of mutated cell clones and/or outgrowth of one dominating clone in culture. But in the HNSCC48 case, the VAF transiently decreased during passage, likely because of intratumoral heterogeneity. It can thus be assumed that a subclone in the tissue used for the PDX generation could not adapt to in vitro conditions. This phenomenon shows a limitation of our study and of cell lines in general and can only be vanquished by including different regions of one tumor. Still, this is laborious, time-consuming, and costly and thus hardly realizable. Solid cancers initially originate from one mutated cell clone with sustained proliferation ability and immune evasion capacity. But with disease progression, subclones develop and different genomic alterations occur, as a result of genomic instability. In HNSCC, up to six different subclones were found [6,25]. Hence, cell cultures can only partially reflect the in vivo situation and only about one-third of somatic mutations are ubiquitously detectable in every tumor region [25,26]. By collecting background information via NGS, TME, and comprehensive evaluation of the

drug response, we aimed to overcome such limitations and provide helpful information for follow-up studies.

Our cell lines exhibited various growth kinetics, radiation sensitivity, migration/invasion potential, and only HNSCC46 P0 M1 was positive for PD-1. Two of three cell lines formed solid spheroids in vitro and engrafted rapidly in vivo. HNSCC46 P0 M2 is the only exception, forming loose spheroids and showing slow engraftment rates, thus reflecting the reduced population doubling time in vitro. Still, the fact that two-thirds of cell lines formed spheroids allows further research to be a step closer to the in vivo setting. Such 3D models recapitulate interactions in the TME, transport properties, oxygen, nutrient, and proliferation gradients [27].

Radiosensitivity was classified based on clinical doses [28]. All cell lines were sensitive to cytostatics (5-FU, Cisplatin) and global-acting CDKIs, however, with individual differences. HNSCC48 P0 M1 was additionally vulnerable to abemaciclib and Cetuximab. Cytotoxic effects matched with those described in other entities [29,30]. Whether such cross-sensitivity/-resistance is a unique finding or a general phenomenon, prospective examination on a larger cell line panel is necessary. Notably, however, is the fact that abemaciclib resistance was reversible in HNSCC16 P1 M1 cells by adding Cisplatin. Regarding HNSCC48 P0 M1, we conclude the partial deletion of *CDKN2A* due to a pathogenic R58* mutation may be the most likely molecular correlate for abemaciclib response [31,32]. Vice versa, HNSCC16 P1 M1 harbored wild type *CDKN2A*. We therefore checked for *CDK4* gene amplifications via cyto-FISH because abemaciclib has a higher selectivity for CDK4 than for CDK6 [33]. HNSCC48 P0 M1 cells displayed the expected chromosome 12 polysomy along with *CDK4* gains. Such polysomy-associated *CDK4* gains were also detectable in HNSCC16 P1 M1, but not HNSCC46 P0 M2 cells, which may explain our findings best. This is supported by the observation of morphological changes, such as an increased number of acidic organelles, a swollen cell structure and also the G1 phase arrest upon abemaciclib monotherapy in HNSCC16 P1 M1. We therefore propose *CDK4* gains as a biomarker for response to abemaciclib, additionally to the known *CDKN2A* deletion. This allows us to conclude that polysomy and the associated increased copy number of the *CDK4* gene increases the abemaciclib response (especially when combined with Cisplatin). HNSCC46 P0 M2 was the most chemotherapy resistant and "special". Though, eventually coincidentally, it is worth mentioning that the TME of the patients' tumors harbored a high number of TAMs and NK cells as likely indicators for poor drug response. Such a link between the TME and cellular characteristics has been described for (intrinsic drug-resistant) cancer-stem cells only [34] and demands further investigation.

The challenge to improve the drug response is partially attributed to the upregulation of genes mediating drug resistance. *CMYC* is a prominent marker and was also higher in our cell lines than in adjacent normal mucosa [35]. Abemaciclib-induced upregulation was partially counter regulated by Cisplatin. A previous study reported contrary effects in thyroid cancer, however, at 10–20-fold higher abemaciclib doses [36]. We interpret our finding as an acute stress response, underscored by an upregulation of *IDO-1* after abemaciclib treatment. Future research should address sequential pharmacological inhibition of IDO-1 (Indoximod or Epacadostat) [37] to boost CDKI efficacy. Noteworthy from an immunological point is the upregulation of HLA-ABC/PD-L1 by abemaciclib and its combinations, likely because of CDK4 inhibition. CyclinD-CDK4 is involved in mediating PD-L1 ubiquitination and degradation [38,39]. Given the fact that immune-checkpoint inhibitors are approved as first-line standard treatment for recurrent and metastatic HNSCC patients, abemaciclib may provide a perspective for the majority of patients that do not respond to PD-1 antibodies. Indeed, a very recent study on patients with advanced, refractory solid tumors described clinical benefits in CDKI/immune-checkpoint inhibitor combinations vs. the respective monotherapy [40]. Using an allogenic co-culture system, we demonstrated promising results upon combined abemaciclib and Pembrolizumab therapy, which even exceeded the effects of the monotherapy. However, this must be further investigated in an autologous setting using "tumor-edited" T cells. In our HNSCC biobank [15], we routinely

collect autologous lymphocytes along with tumor samples. Hence, performing such sophisticated analyses on primary tumors and immune cells will help in becoming a step closer to "in vitro immunotherapy".

Summing up our findings, these newly established patient-individual tumor models guide the selection of drugs (combinations) and help in detecting intrinsic or acquired resistance mechanisms. With our complex set of analyses, we not only addressed morphological, molecular, and immunological aspects of advanced HNSCC, but also identified *CDK4* gains as a new "surrogate" marker for abemaciclib response and describe a personalized approach to conquer intrinsic CDKI resistance.

5. Conclusions

This work shows that well-characterized patient-individual tumor models are crucial for identification of effective therapy (combinations) and play an important role in detecting intrinsic resistance mechanisms. However, it also illustrates that in light of the intertumoral heterogeneity of HNSCC, a comprehensive characterization is necessary to draw general conclusions between the cell lines investigated or to explain different results and to identify potential new biomarkers.

Here, we propose CDK4 gains as a biomarker for response to abemaciclib. Of note, abemaciclib resistance was reversible in one case (HNSCC16 P1 M1) by Cisplatin. This highlights the potential for combination therapies, especially in the context of intrinsic resistance towards targeted therapies.

This study provides further evidence for the therapeutic potential of CDKIs and shows that they can be combined with classical chemotherapy. These findings contribute to our understanding of how the treatment of HNSCC can be improved in the future.

Supplementary Materials: The following supporting information can be downloaded at: https://www.mdpi.com/article/10.3390/cancers14102484/s1, Figure S1: Fingerprint PCR of patients' tumor, PDX and cell line of (A) HNSCC16 (B) HNSCC46 and (C) HNSCC48. Figure S2: Establishment of xenograft-derived cell lines. Figure S3: Population doubling times of (A) HNSCC16 M1 P1, (B) HNSCC46 P0 M2, and (C) HNSCC48 P0 M1. Figure S4: Dose–response curve analysis. Tumor cells were treated for 2 × 72 h with the different test substances in varying concentrations ranging between 0.048 µg/mL–1 mg/mL for approved drugs (Cisplatin, 5-FU, and Cetuximab) and 1 nM–1 µM for targeted substances (dinaciclib, abemaciclib, and THZ1). Based on the dose–response curves IC_{50} was calculated as outlined in Table 3. * $p < 0.05$; ** $p < 0.01$; *** $p < 0.001$; **** $p < 0.0001$ vs. control (100%). Two-way ANOVA.

Author Contributions: Conceptualization, C.M. and N.S.; methodology, N.S., M.K., T.F., B.S., S.Z., A.Z., A.S.B., I.S. and H.L.; validation, N.S. and C.M.; formal analysis, N.S.; investigation, N.S. and B.S.; resources, C.M., C.J., C.G.-T. and D.F.S.; data curation, N.S. and M.K.; writing—original draft preparation, N.S.; writing—review and editing, C.M., B.S., C.G.-T. and C.J.; visualization, N.S.; supervision, C.M.; project administration, C.M. All authors have read and agreed to the published version of the manuscript.

Funding: This research received no external funding.

Institutional Review Board Statement: The study was conducted according to the guidelines of the Declaration of Helsinki and approved by the German local authority Ethics Committee (reference number A2018-0003). The German local authority approved all animal experiments: Landesamt für Landwirtschaft, Lebensmittelsicherheit und Fischerei Mecklenburg-Vorpommern, under the German animal protection law and the EU Guideline 2010/63/EU (protocol code: 7221.3-1-066/18 and 7221.3-1-032/19-4).

Informed Consent Statement: Informed consent was obtained from all subjects involved in the study.

Data Availability Statement: The data presented in this study are available in this article (and Supplementary Material).

Acknowledgments: We gratefully thank Chantal von Hörsten for breeding mice at the core facility and Christin Schlie for the assistance with the therapy approach. We also gratefully acknowledge

the excellent assistance from the Core Facility for Cell Sorting & Cell Analysis, Laboratory for Clinical Immunology, University Medical Center Rostock (Michael Müller, Brigitte Mueller-Hilke). Furthermore, we would like to thank Reidar Grénman (Turku University Hospital, Turku, Finland) for providing us with the cell line UT-SCC-15.

Conflicts of Interest: The authors declare no conflict of interest.

References

1. Lum, D.H.; Matsen, C.; Welm, A.L.; Welm, B.E. Overview of Human Primary Tumorgraft Models: Comparisons with Traditional Oncology Preclinical Models and the Clinical Relevance and Utility of Primary Tumorgrafts in Basic and Translational Oncology Research. *Curr. Protoc. Pharmacol.* **2012**, *59*, 14–22. [CrossRef] [PubMed]
2. Białkowska, K.; Komorowski, P.; Bryszewska, M.; Miłowska, K. Spheroids as a Type of Three-Dimensional Cell Cultures—Examples of Methods of Preparation and the Most Important Application. *Int. J. Mol. Sci.* **2020**, *21*, 6225. [CrossRef] [PubMed]
3. Canning, M.; Guo, G.; Yu, M.; Myint, C.; Groves, M.W.; Byrd, J.K.; Cui, Y. Heterogeneity of the Head and Neck Squamous Cell Carcinoma Immune Landscape and Its Impact on Immunotherapy. *Front. Cell Dev. Biol.* **2019**, *7*, 52. [CrossRef] [PubMed]
4. Grünwald, V.; Chirovsky, D.; Cheung, W.Y.; Bertolini, F.; Ahn, M.-J.; Yang, M.-H.; Castro, G.; Berrocal, A.; Sjoquist, K.; Kuyas, H.; et al. Global treatment patterns and outcomes among patients with recurrent and/or metastatic head and neck squamous cell carcinoma: Results of the GLANCE H&N study. *Oral Oncol.* **2020**, *102*, 104526. [CrossRef]
5. Argiris, A.; Karamouzis, M.V.; Raben, D.; Ferris, R.L. Head and neck cancer. *Lancet* **2008**, *371*, 1695–1709. [CrossRef]
6. Morris, L.G.T.; Chandramohan, R.; West, L.; Zehir, A.; Chakravarty, D.; Pfister, D.G.; Wong, R.J.; Lee, N.Y.; Sherman, E.J.; Baxi, S.S.; et al. The Molecular Landscape of Recurrent and Metastatic Head and Neck Cancers: Insights from a precision oncology sequencing platform. *JAMA Oncol.* **2017**, *3*, 244–255. [CrossRef]
7. Niehr, F.; Eder, T.; Pilz, T.; Konschak, R.; Treue, D.; Klauschen, F.; Bockmayr, M.; Türkmen, S.; Jöhrens, K.; Budach, V.; et al. Multilayered Omics-Based Analysis of a Head and Neck Cancer Model of Cisplatin Resistance Reveals Intratumoral Heterogeneity and Treatment-Induced Clonal Selection. *Clin. Cancer Res.* **2017**, *24*, 158–168. [CrossRef]
8. Tinhofer, I.; Braunholz, D.; Klinghammer, K. Preclinical models of head and neck squamous cell carcinoma for a basic understanding of cancer biology and its translation into efficient therapies. *Cancers Head Neck* **2020**, *5*, 9. [CrossRef]
9. Ferris, R.; Gonçalves, A.; Baxi, S.; Martens, U.; Gauthier, H.; Langenberg, M.; Spanos, W.; Leidner, R.; Kang, H.; Russell, J.; et al. An open-label, multicohort, phase 1/2 study in patients with virus-associated cancers (CheckMate 358): Safety and efficacy of neoadjuvant nivolumab in squamous cell carcinoma of the head and neck (SCCHN). *Ann. Oncol.* **2017**, *28*, v628–v629. [CrossRef]
10. Wise-Draper, T.M.; Old, M.O.; Worden, F.P.; O'Brien, P.E.; Cohen, E.E.; Dunlap, N.; Mierzwa, M.L.; Casper, K.; Palackdharry, S.; Hinrichs, B.; et al. Phase II multi-site investigation of neoadjuvant pembrolizumab and adjuvant concurrent radiation and pembrolizumab with or without cisplatin in resected head and neck squamous cell carcinoma. *J. Clin. Oncol.* **2018**, *36*, 6017. [CrossRef]
11. Reinius, M.A.V.; Smyth, E. Anti-cancer therapy with cyclin-dependent kinase inhibitors: Impact and challenges. *Expert Rev. Mol. Med.* **2021**, *23*, e6. [CrossRef] [PubMed]
12. Sánchez-Martínez, C.; Lallena, M.J.; Sanfeliciano, S.G.; de Dios, A. Cyclin dependent kinase (CDK) inhibitors as anticancer drugs: Recent advances (2015–2019). *Bioorg. Med. Chem. Lett.* **2019**, *29*, 126637. [CrossRef] [PubMed]
13. Poratti, M.; Marzaro, G. Third-generation CDK inhibitors: A review on the synthesis and binding modes of Palbociclib, Ribociclib and Abemaciclib. *Eur. J. Med. Chem.* **2019**, *172*, 143–153. [CrossRef] [PubMed]
14. Sobhani, N.; Fassl, A.; Mondani, G.; Generali, D.; Otto, T. Targeting Aberrant FGFR Signaling to Overcome CDK4/6 Inhibitor Resistance in Breast Cancer. *Cells* **2021**, *10*, 293. [CrossRef] [PubMed]
15. Strüder, D.; Momper, T.; Irmscher, N.; Krause, M.; Liese, J.; Schraven, S.; Zimpfer, A.; Zonnur, S.; Burmeister, A.-S.; Schneider, B.; et al. Establishment and characterization of patient-derived head and neck cancer models from surgical specimens and endoscopic biopsies. *J. Exp. Clin. Cancer Res.* **2021**, *40*, 246. [CrossRef] [PubMed]
16. Oppel, F.; Shao, S.; Schürmann, M.; Goon, P.; Albers, A.E.; Sudhoff, H. An Effective Primary Head and Neck Squamous Cell Carcinoma In Vitro Model. *Cells* **2019**, *8*, 555. [CrossRef]
17. Maletzki, C.; Gock, M.; Randow, M.; Klar, E.; Huehns, M.; Prall, F.; Linnebacher, M. Establishment and characterization of cell lines from chromosomal instable colorectal cancer. *World J. Gastroenterol.* **2015**, *21*, 164–176. [CrossRef]
18. Schoenwaelder, N.; Salewski, I.; Engel, N.; Krause, M.; Schneider, B.; Müller, M.; Riess, C.; Lemcke, H.; Skorska, A.; Grosse-Thie, C.; et al. The Individual Effects of Cyclin-Dependent Kinase Inhibitors on Head and Neck Cancer Cells—A Systematic Analysis. *Cancers* **2021**, *13*, 2396. [CrossRef]
19. Maletzki, C.; Rosche, Y.; Riess, C.; Scholz, A.; William, D.; Classen, C.F.; Kreikemeyer, B.; Linnebacher, M.; Fiedler, T. Deciphering molecular mechanisms of arginine deiminase-based therapy—Comparative response analysis in paired human primary and recurrent glioblastomas. *Chem. Interact.* **2017**, *278*, 179–188. [CrossRef]
20. Riess, C.; Schneider, B.; Kehnscherper, H.; Gesche, J.; Irmscher, N.; Shokraie, F.; Classen, C.F.; Wirthgen, E.; Domanska, G.; Zimpfer, A.; et al. Activation of the Kynurenine Pathway in Human Malignancies Can Be Suppressed by the Cyclin-Dependent Kinase Inhibitor Dinaciclib. *Front. Immunol.* **2020**, *11*, 55. [CrossRef]

21. Welkoborsky, H.-J.; Jacob, R.; Riazimand, S.H.; Bernauer, H.S.; Mann, W.J. Molecular Biologic Characteristics of Seven New Cell Lines of Squamous Cell Carcinomas of the Head and Neck and Comparison to Fresh Tumor Tissue. *Oncology* **2003**, *65*, 60–71. [CrossRef] [PubMed]
22. Zhou, G.; Liu, Z.; Myers, J.N. *TP53* Mutations in Head and Neck Squamous Cell Carcinoma and Their Impact on Disease Progression and Treatment Response. *J. Cell. Biochem.* **2016**, *117*, 2682–2692. [CrossRef] [PubMed]
23. Farah, C.S. Molecular landscape of head and neck cancer and implications for therapy. *Ann. Transl. Med.* **2021**, *9*, 915. [CrossRef] [PubMed]
24. Shin, D.M.; Charuruks, N.; Lippman, S.M.; Lee, J.J.; Ro, J.Y.; Hong, W.K.; Hittelman, W.N. p53 protein accumulation and genomic instability in head and neck multistep tumorigenesis. *Cancer Epidemiol. Biomark. Prev.* **2001**, *10*, 603–609.
25. Bs, M.Y.L.; Allen, C.T. Mechanisms of resistance to T cell-based immunotherapy in head and neck cancer. *Head Neck* **2020**, *42*, 2722–2733. [CrossRef]
26. Gerlinger, M.; Rowan, A.J.; Horswell, S.; Math, M.; Larkin, J.; Endesfelder, D.; Gronroos, E.; Martinez, P.; Matthews, N.; Stewart, A.; et al. Intratumor heterogeneity and branched evolution revealed by multiregion sequencing. *N. Engl. J. Med.* **2012**, *366*, 883–892. [CrossRef]
27. Katt, M.E.; Placone, A.L.; Wong, A.D.; Xu, Z.S.; Searson, P.C. In Vitro Tumor Models: Advantages, Disadvantages, Variables, and Selecting the Right Platform. *Front. Bioeng. Biotechnol.* **2016**, *4*, 12. [CrossRef]
28. Van Gestel, D.; Weyngaert, D.V.D.; Schrijvers, D.; Weyler, J.; Vermorken, J.B. Intensity-modulated radiotherapy in patients with head and neck cancer: A European single-centre experience. *Br. J. Radiol.* **2011**, *84*, 367–374. [CrossRef]
29. Hino, H.; Iriyama, N.; Kokuba, H.; Kazama, H.; Moriya, S.; Takano, N.; Hiramoto, M.; Aizawa, S.; Miyazawa, K. Abemaciclib induces atypical cell death in cancer cells characterized by formation of cytoplasmic vacuoles derived from lysosomes. *Cancer Sci.* **2020**, *111*, 2132–2145. [CrossRef]
30. Riess, C.; Koczan, D.; Schneider, B.; Linke, C.; del Moral, K.; Classen, C.F.; Maletzki, C. Cyclin-dependent kinase inhibitors exert distinct effects on patient-derived 2D and 3D glioblastoma cell culture models. *Cell Death Discov.* **2021**, *7*, 54. [CrossRef]
31. Billard-Sandu, C.; Tao, Y.G.; Sablin, M.P.; Dumitrescu, G.; Billard, D.; Deutsch, E. CDK4/6 Inhibitors in P16/HPV16-Negative Squamous Cell Carcinoma of the Head and Neck. *Eur. Arch. Oto-Rhino Laryngol.* **2020**, *277*, 1273–1280. [CrossRef] [PubMed]
32. Karamboulas, C.; Bruce, J.P.; Hope, A.J.; Meens, J.; Huang, S.H.; Erdmann, N.; Hyatt, E.; Pereira, K.; Goldstein, D.P.; Weinreb, I.; et al. Patient-Derived Xenografts for Prognostication and Personalized Treatment for Head and Neck Squamous Cell Carcinoma. *Cell Rep.* **2018**, *25*, 1318–1331.e4. [CrossRef] [PubMed]
33. Corona, S.P.; Generali, D. Abemaciclib: A CDK4/6 inhibitor for the treatment of HR+/HER2– advanced breast cancer. *Drug Des. Dev. Ther.* **2018**, *12*, 321–330. [CrossRef] [PubMed]
34. Gomez, K.E.; Wu, F.; Keysar, S.B.; Morton, J.J.; Miller, B.; Chimed, T.-S.; Le, P.N.; Nieto, C.; Chowdhury, F.N.; Tyagi, A.; et al. Cancer cell CD44 mediates macrophage/monocyte-driven regulation of head and neck cancer stem cells. *Cancer Res.* **2020**, *80*, 4185–4198. [CrossRef] [PubMed]
35. Alexa-Stratulat, T.; Pešić, M.; Gašparović, A.Č.; Trougakos, I.P.; Riganti, C. What sustains the multidrug resistance phenotype beyond ABC efflux transporters? Looking beyond the tip of the iceberg. *Drug Resist. Updates* **2019**, *46*, 100643. [CrossRef] [PubMed]
36. Abutorabi, E.S.; Irani, S.; Yaghmaie, M.; Ghaffari, S.H. Abemaciclib (CDK4/6 Inhibitor) Blockade Induces Cytotoxicity in Human Anaplastic Thyroid Carcinoma Cells. *Rep. Biochem. Mol. Biol.* **2020**, *8*, 438.
37. Le Naour, J.; Galluzzi, L.; Zitvogel, L.; Kroemer, G.; Vacchelli, E. Trial watch: IDO inhibitors in cancer therapy. *OncoImmunology* **2020**, *9*, 1777625. [CrossRef]
38. Zhang, J.; Bu, X.; Wang, H.; Zhu, Y.; Geng, Y.; Nihira, N.T.; Tan, Y.; Ci, Y.; Wu, F.; Dai, X.; et al. Cyclin D–CDK4 kinase destabilizes PD-L1 via cullin 3–SPOP to control cancer immune surveillance. *Nature* **2018**, *553*, 91–95. [CrossRef]
39. He, X.; Xu, C. Immune checkpoint signaling and cancer immunotherapy. *Cell Res.* **2020**, *30*, 660–669. [CrossRef]
40. Patnaik, A.; Yap, T.A.; Chung, H.C.; de Miguel, M.J.; Bang, Y.-J.; Lin, C.-C.; Su, W.-C.; Italiano, A.; Chow, K.H.; Szpurka, A.M.; et al. Safety and Clinical Activity of a New Anti-PD-L1 Antibody as Monotherapy or Combined with Targeted Therapy in Advanced Solid Tumors: The PACT Phase Ia/Ib Trial. *Clin. Cancer Res.* **2020**, *27*, 1267–1277. [CrossRef]

9. Anhang

9.1 Ergänzende Abbildungen

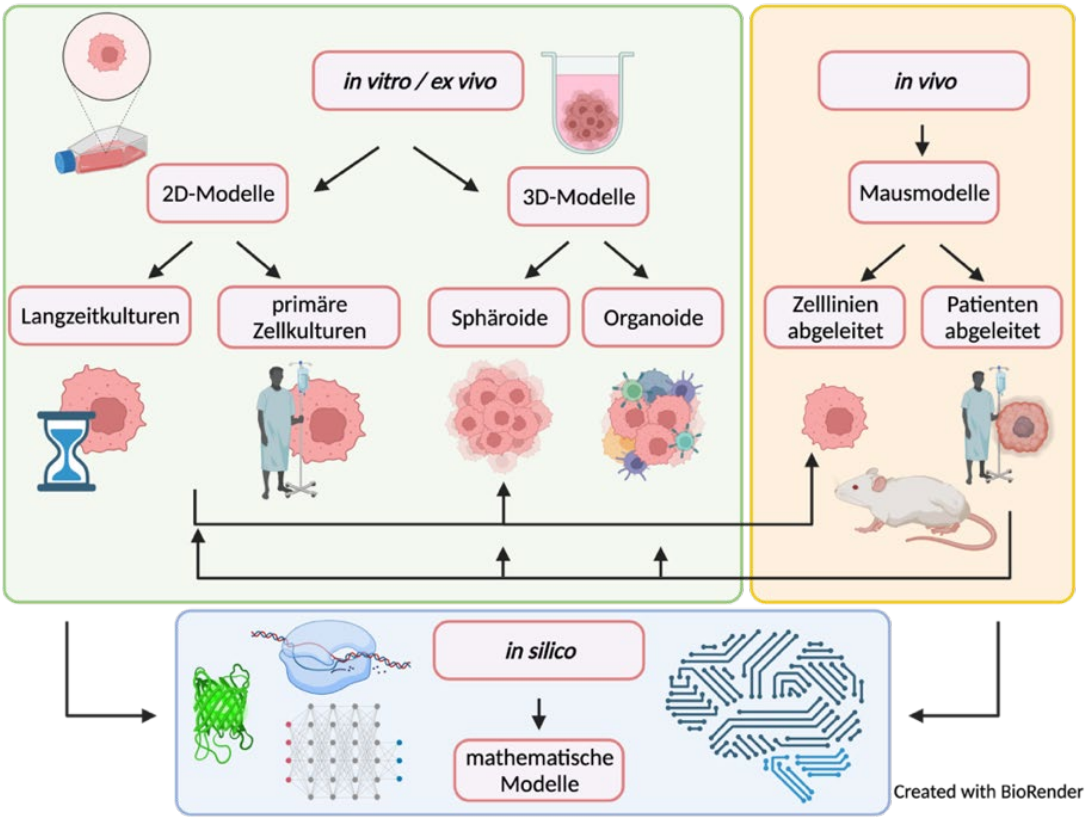

Abbildung 3: Ausgewählte präklinische Tumormodelle.

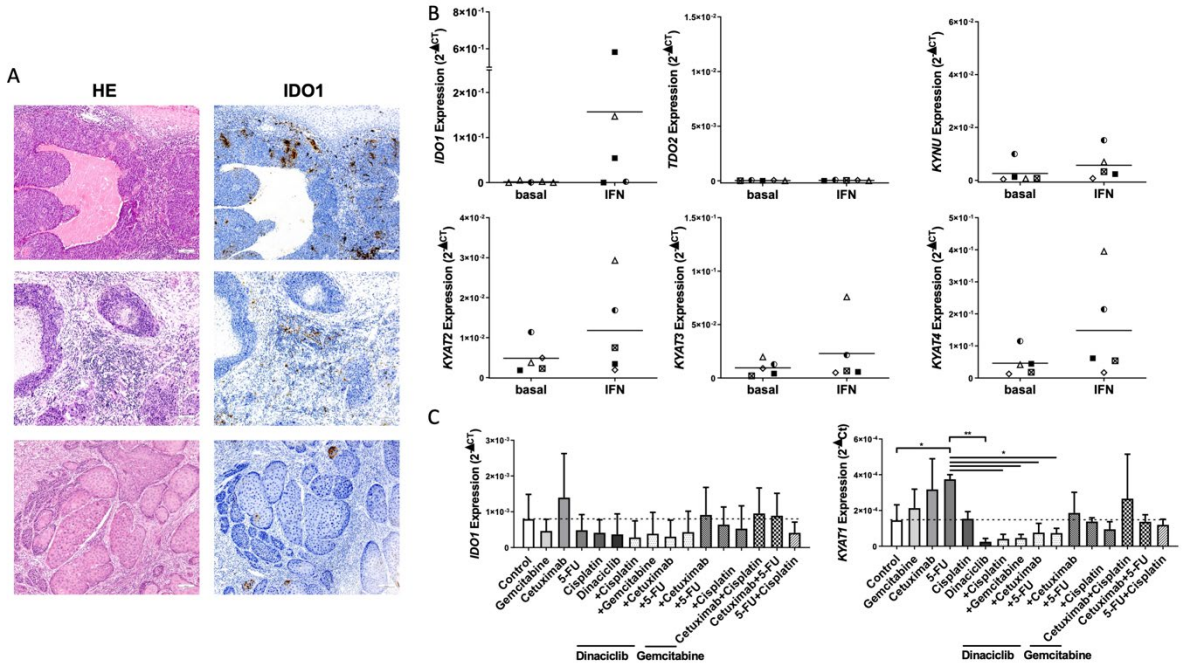

Abbildung 4: Analyse des Kynureninstoffwechsels in HNSCC-Zellen.(A) IDO1 Immunhistochemie. Repräsentative Bilder der HNSCC Proben HNSCC06 (Mandeln, HPV-positiv), HNSCC02 (Mundboden, HPV-negativ, Rezidiv) und HNSCC01 (Kehlkopf, HPV-negativ). Linke Bildhälfte: Routine HE-Färbung. Rechte Bildhälfte: Fokale IDO1 Expression auf auf tumorinfiltrierenden Lymphozyten. Vergrößerung 10x bzw. 20x. (B) basale und mit IFNγ induzierte relative mRNA-Expression von *IDO1, TDO2, KYNU, KYAT2, KYAT3* und *KYAT4* normalisiert auf *GAPDH* in HNSCC-Zelllinien. (C) relative mRNA-Expression von *IDO1* und *KYAT1* unter dem Einfluss von Zytostatika und zielgerichteter Therapie in HNSCC-Zellen normalisiert auf *GAPDH.* One-way ANOVA (n=3 unabhängige Experimente) *p < 0.05; **p < 0.01.

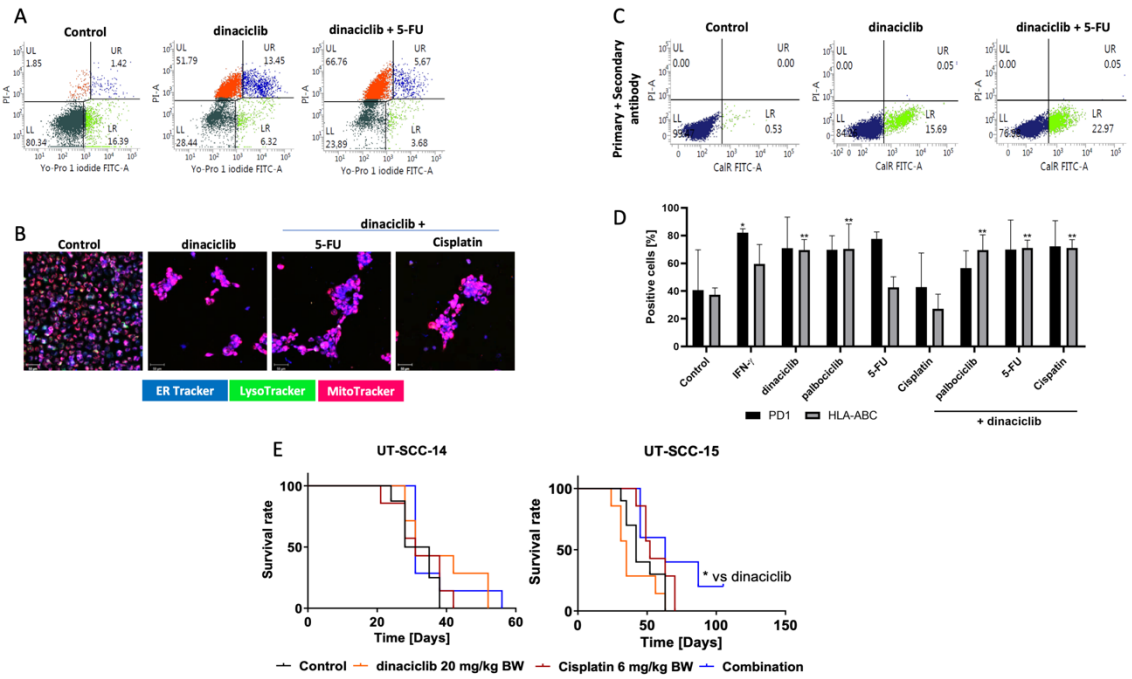

Abbildung 5: Kombinationstherapie von CDKi und Zytostatika zeigt verstärkte Effekte.(A) Repräsentative FACS-Diagramme des Apoptose-Nekrose-Assays. Zellen wurden nach Behandlung mit Yo-Pro-1-Iodid und PI angefärbt. Zellen, die positiv für Yo-Pro-1-Iodid waren, wurden als früh apoptotisch definiert, Zellen, die positiv für PI waren, wurden als nekrotisch definiert, und doppelt positive Zellen wurden als spät apoptotisch definiert. (B) Repräsentative Bilder der Untersuchung der Wirkung der Testsubstanzen auf UT-SCC-14 Zellen auf die mitochondriale Aktivität (rot), die Lysosomen (grün) und das ER (blau). (C) Repräsentative FACS-Diagramme nach Färbung des immunogenen Moleküls CalR auf der Oberfläche von UT-SCC-14 Zellen. (D) Anteil PD1- und HLA-ABC-positiver UT-SCC-14 Zellen nach Behandlung. One-way ANOVA (n ≥ 3 unabhängige Experimente) * $p < 0,05$, ** $p < 0,01$, vs. Kontrolle. (E) *In vivo* Therapieversuch. Kaplan-Meier-Überlebenskurve und Log-rank-Test (Mantel-Cox). UT-SCC-14: Kontrolle (n = 8 Mäuse); Cisplatin/Dinaciclib/Kombination (n = 7 Mäuse/Gruppe); UT-SCC-15: Kontrolle (n = 10 Mäuse); Cisplatin/Dinaciclib (n = 7 Mäuse/Gruppe); Kombination (n = 5 Mäuse); * $p < 0,05$ vs. Dinaciclib.

Anhang

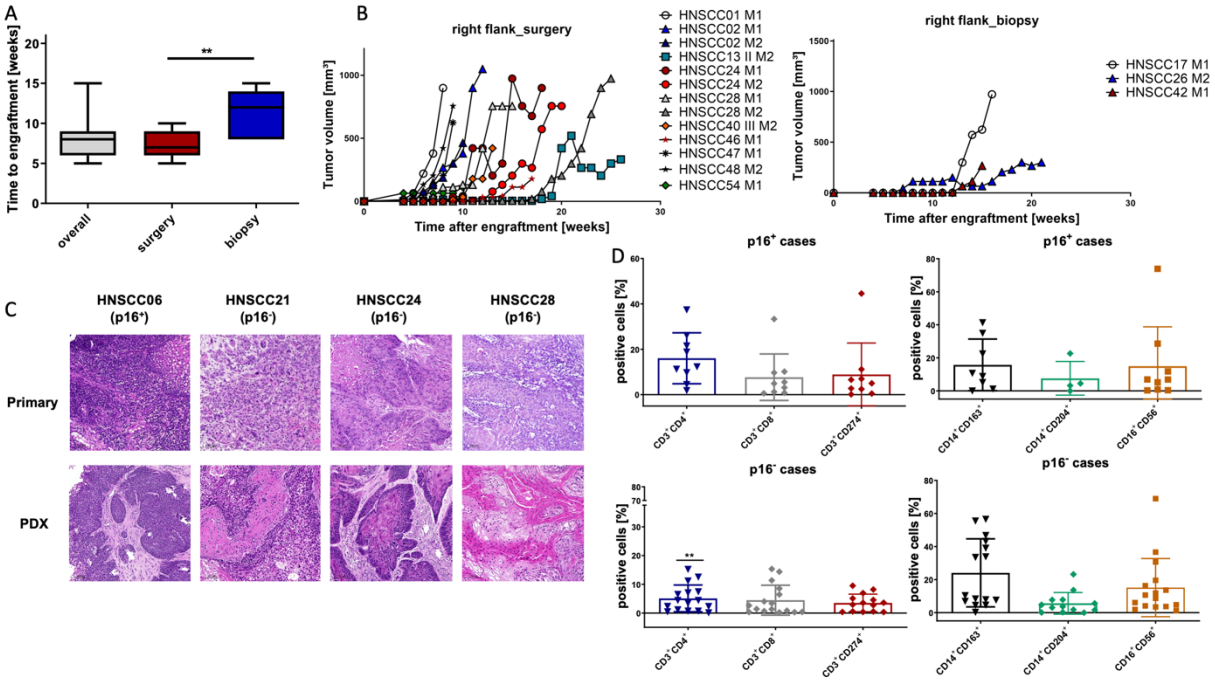

Abbildung 6: Etablierung von PDX aus OP-Resektaten und Biopsien bei Erhaltung der Histomorphologie möglich.(A) Boxplots, die die Zeit von der Implantation bis zum Auftreten eines tastbaren Tumors aller Proben, der OP-Resektate und der Biospien darstellen. Ungepaarter T-Test (zweiseitig) **p < 0,01. (B) Wachstumskurven der einzelnen PDX aufgeschlüsselt nach OP-Resektat (links) und Biopsien (rechts). (C) Histologie von zugehörigen Primärtumoren und PDX-Modellen. Die HE-Histologie zeigt die Beibehaltung der Morphologie des HNSCC-Tumors nach Xenotransplantation. (D) Durchflusszytometrische Phänotypisierung des Tumormikromilieu von $p16^+$ und $p16^-$ HNSCC Tumoren.

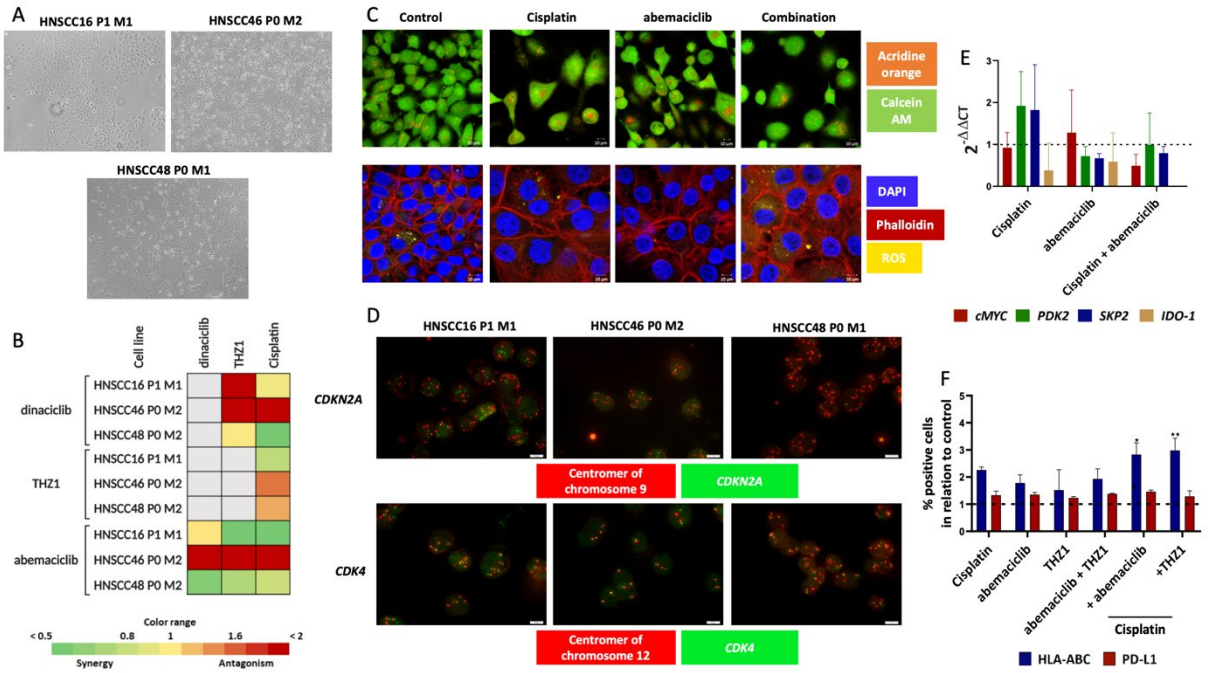

Abbildung 7: Identifizierung von *CDK4*-Zugewinnen als potenziellen Biomarker für die Vorhersage des Ansprechens auf Abemaciclib an in niedriger Passage-gehaltener eigens etablierter Zelllinien. (A) Repräsentative lichtmikroskopische Aufnahme der mittels Kollagenaseverdaus etablierten Zelllinien HNSCC16 P1 M1 (Larynx, Rezidiv), HNSCC46 P0 M2 (Hypopharynx, Primärtumor) und HNSCC48 P0 M1 (Lymphknoten, Metastase). (B) Das *Bliss Independence model* wurde zur Berechnung potenzieller synergistischer oder additiver Effekte verwendet. Die grüne Farbe weist auf eine synergistische und die rote Farbe auf eine antagonistische Wirkung der simultanen Kombinationen hin. (C) Repräsentative Bilder der Immunfluoreszenzfärbung von HNSCC16 P1 M1 zur Detektion saurer Kompartimente (Acridinorange), der Viabilität (Calcein AM, grün), der Aktinfilamente (Phalloidin, rot) und reaktiver Sauerstoffspezies (gelb). Zellkerne wurden mit DAPI gefärbt (blau). (D) Cyto-FISH für *CDKN2a* und *CDK4.* Zytospins der etablierten HNSCC-Zelllinien wurden mit der SPEC CDK4/CEN 12 Dual Color Probe oder SPEC CDKN2A /CEN9 Dual Color Probe angefärbt, um die genspezifische Amplifikation von *CDKN2A* und *CDK4* zu überprüfen. Die roten Punkte zeigen die Zentromere und die grünen Punkte das spezifische Gen an. (E) Expression der Resistenz-assoziierten Gene *SKP2, cMYC, PDK2* und *IDO1* der Zelllinie HNSCC16 P1 M1 unter Behandlung in Relation zur unbehandelten Kontrolle. Kruskal-Wallis (n=3 unabhängige Experimente) vs. Kontrolle. (F) Anteil HLA-ABC- und PD-L1- positiver HNSCC16 P1 M1 Zellen in Relation zur Kontrolle nach Behandlung. Kruskal-Wallis (n=3 unabhängige Experimente) * $p < 0,05$ ** $p < 0,01$ vs. Kontrolle.

9.2 Anmerkung

In dieser Arbeit wird zur leichteren Verständlichkeit in der Regel das generische Maskulinum verwendet. Hiermit weise ich darauf hin, dass dabei auch feminine sowie non binäre Personen gemeint sind.

9.3 Eigenanteil an den Publikationen

Publikation 1: Durchführung von Experimenten und Datenanalyse

Publikation 2: Konzeptentwicklung, Methodik, Validierung, Durchführung von Experimenten, formale Analyse, Datenanalyse und Visualisierung, Schreiben und Erstellen des Erstentwurfes des Manuskriptes

Publikation 3: Durchführung von Experimenten und Datenanalyse

Publikation 4: Konzeptentwicklung, Methodik, Validierung, Durchführung von Experimenten, formale Analyse, Datenanalyse und Visualisierung, Schreiben und Erstellen des Erstentwurfes des Manuskriptes

9.4 Lebenslauf

Persönliche Angaben

Name:	M. Sc. Schönwälder, geb. Irmscher
Vorname:	Nina
Geburtsdatum:	28.09.1995
Nationalität:	deutsch
Familienstand:	verheiratet

Ausbildung

Seit 10/2019	Naturwissenschaftliche Doktorandin / Wissenschaftlicher Mitarbeiter, Zentrum für Innere Medizin Medizinische Klinik III Hämatologie, Onkologie, Palliativmedizin Universitätsmedizin Rostock
10/2017 – 09/2019	Master of Science – Universität Rostock: Mikrobiologie und Biochemie Masterarbeit: Stressantwort von Glioblastoma multiforme nach ADI-basiertem Argininentzug
10/2014 – 09/2017	Bachelor of Science - Universität Bielefeld: Molekulare Biotechnologie Bachelorarbeit: Einfluss eines Aggregationspheromons auf eine ATTRACT-and-KILL Formulierung zur Bekämpfung von *Ixodes ricinus* Nymphen
08/2006 – 06/2014	Gymnasium am Waldhof, Bielefeld

9.5 Vollständige Publikationsliste

9.5.1 Originalarbeiten

Riess, C, Schneider, B, Kehnscherper, H, Gesche, J, **Irmscher, N**, Shokraie, F, Classen, C F, Wirthgen, E, Domanska, G, Zimpfer, A, Strüder, D, Junghanss, C, & Maletzki, C (2020). Activation of the Kynurenine Pathway in Human Malignancies Can Be Suppressed by the Cyclin-Dependent Kinase Inhibitor Dinaciclib. *Frontiers in immunology*, 11, 55.
(IF 2020 5,085)

Salewski, I, Gladbach, Y S, Kuntoff, S, **Irmscher, N**, Hahn, O, Junghanss, C, & Maletzki, C (2020). In vivo vaccination with cell line-derived whole tumor lysates: neoantigen quality, not quantity matters. *Journal of translational medicine*, 18(1), 402.
(IF 4,206)

Schoenwaelder, N, Salewski, I, Engel, N, Krause, M, Schneider, B, Müller, M, Riess, C, Lemcke, H, Skorska, A, Grosse-Thie, C, Junghanss, C, & Maletzki, C (2021). The Individual Effects of Cyclin-Dependent Kinase Inhibitors on Head and Neck Cancer Cells-A Systematic Analysis. *Cancers*, 13(10), 2396.
(IF 2021 6,639)

Strüder, D, Momper, T, **Irmscher, N**, Krause, M, Liese, J, Schraven, S, Zimpfer, A, Zonnur, S, Burmeister, A S, Schneider, B, Frerich, B, Mlynski, R, Große-Thie, C, Junghanss, C, & Maletzki, C (2021). Establishment and characterization of patient-derived head and neck cancer models from surgical specimens and endoscopic biopsies. *Journal of experimental & clinical cancer research*, 40(1), 246.
(IF 2021 11,161)

Schwarz R, Zitzow E, Fiebig A, Hering S, Humboldt Y, **Schoenwaelder N**, Kämpfer N, Volkmar K, Hinz B, Kreikemeyer B, Maletzki C, Fiedler T (2022). PEGylation increases antitumoral activity of arginine deiminase of Streptococcus pyogenes. *Appl Microbiol Biotechnol.*106(1):261-271.
(IF 2021 4,831)

Schoenwaelder N, Krause M, Freitag T, Schneider B, Zonnur S, Zimpfer A, Becker AS, Salewski I, Strüder DF, Lemcke H, Grosse-Thie C, Junghanss C, Maletzki C. (2022). Preclinical Head and Neck Squamous Cell Carcinoma Models for Combined Targeted Therapy Approaches. *Cancers*, 18;14(10):2484.
(IF 2022 6,639)

9.5.2 Übersichtsartikel

Riess, C*, **Irmscher, N***, Salewski, I, Strüder, D, Classen, C F, Große-Thie, C, Junghanss, C, & Maletzki, C (2021). Cyclin-dependent kinase inhibitors in head and neck cancer and glioblastoma-backbone or add-on in immune-oncology?. *Cancer metastasis reviews*, 40(1), 153–171. * both authors contributed equally
(IF 2020 9,26)

Richter, A, **Schoenwaelder, N**, Sender, S, Junghanss, C, & Maletzki, C (2021). Cyclin-Dependent Kinase Inhibitors in Hematological Malignancies-Current Understanding, (Pre-)Clinical Application and Promising Approaches. *Cancers*, 13(10), 2497.
(IF 2021 6,639)

9.6 Konferenzbeiträge

Der präsentierende Autor ist unterstrichen.

9.6.1 Vorträge

Irmscher N, Momper T, Strüder D, Liese J, Schraven S, Zimpfer A, Schneider B , Frerich B, Mlynski R, Junghanss C, Große-Thie C, Maletzki C, Establishment of a head and neck cancer biobank and patient-derived xenografts for preclinical research – comparative analysis of engraftment efficacy between surgical specimens and endoscopic biopsies. *DGHO* virtuell, 09.-11. Oktober 2020

Irmscher N, Krause M, Schneider B, Strueder D, Maletzki C, Establishment, characterization and drug response of individual patient-derived head and neck squamous cell carcinoma models. *DGHO* hybrid, 01.-04. Oktober 2021

Krause M, **Irmscher N**, Strüder D, Momper T, Zimpfer A, Zonnur S, Schneider B, Mlynski R, Große-Thie C, Junghanss C, Maletzki C, Characterization & preclinical drug response analysis of patient-derived head and neck cancer models from surgical specimens and endoscopic biopsies. *DGHO* hybrid, 01.-04. Oktober 2021

9.6.2 Posterbeiträge

Strüder D, **Irmscher N**, Kehnscherper H, Junghanss C, Mlynski R, Maletzki C, Cyclin-dependent kinase inhibitors enhance chemotherapy, immunogenic cell death and radiosensitivity in head and neck cancer– a comprehensive in vitro analysis. *Meeting on Experimental and Translational Research in Head and Neck Cancer,* Köln, 17.-18. Januar 2020

Irmscher N, Volkmar K, Maletzki C, Kreikemeyer B, Schwarz R, Fiedler T, PEGylation increases stability and pharmacokinetic properties of arginine deiminase of Streptococcus pyogenes. *6th Joint Conference of the DGHM & VAAM*, Leipzig, 08.-11. März 2020

Schoenwaelder N, Schneider B, Freitag T, Krause M, Strueder D, Grosse-Thie C, Junghanss C, Maletzki C, Preclinical head and neck squamous cell carcinoma models for combined targeted therapy approaches. *3rd International Symposium on Tumor-Host Interaction in Head and Neck Cancer,* Essen, 28.-29. Januar 2022

9.7 Danksagung

Zunächst möchte ich mich bei Prof. Dr. Christian Junghanß für die Vergabe des Promotionsthemas und die Aufnahme in seine Abteilung bedanken.
Mein ganz besonderer Dank gilt PD Dr. Claudia Maletzki für die exzellente Betreuung und jegliche Unterstützung während der gesamten Zeit. Neben dem ganzen Alltagsstress hatte sie immer ein offenes Ohr und teilte ihre umfassende Erfahrung und ihr Sachverständnis mit einem. Ebenfalls ein riesiges Dankeschön an PD. Dr. Annette Zimpfer, für die tolle Zusammenarbeit und ihren Einsatz bei gemeinsamen Projekten.
Großer Dank gilt auch sämtlichen Kooperationspartnern der Arbeit aus dem Institut für Pathologie, der Klinik und Poliklinik für Hals-Nasen-Ohrenheilkunde, Kopf- und Halschirurgie und dem Rudolf-Zenker-Institut für Experimentelle Chirurgie/ Core Facility Zentrale Versuchstierhaltung ohne die diese Arbeit nicht möglich gewesen wäre. Dabei sind besonders Dr. Daniel Strüder, Dr. Sarah Zonnur sowie Dr. Björn Schneider zu erwähnen, der immer Zeit fand einem bei sämtlichen molekularpathologischen Fragestellungen zu unterstützen.
Ein großes Dankeschön geht auch an die gesamte Arbeitsgruppe der Hämatologie und Onkologie heraus, für die vielen gemeinsam verbrachten Stunden im Labor, die Grillfeste, Ausflüge im Sommer und Weihnachtsfeiern. Es war eine schöne Zeit an die ich mich gerne zurückerinnere. Dabei möchte ich mich besonders bei Inken Salewski bedanken, die mir in dieser Zeit auch eine Freundin geworden ist und einem im Alltag einfach immer mit Rat und Tat zur Seite gestanden hat.

Abschließend möchte ich mich noch bei meinem Mann und meiner Familie bedanken. Ihr habt immer an mich geglaubt und euer Rückhalt und Grundvertrauen in mich hat es mir ermöglicht, diese wunderbare Zeit zu erleben.